MYOCARDIAL APPLICATIONS OF CARDIOVASCULAR X-RAY COMPUTED TOMOGRAPHY

James Elliott Stirrup

CertPhys BSc MBBS MRCP

National Heart and Lung Institute

Imperial College, London

A thesis submitted for the Degree of Doctor of Medicine (Research)

July 2012

BRIEF ABSTRACT

This thesis evaluated the role of cardiovascular computed tomography (CCT) in assessing the left ventricular (LV) myocardium. The technical and clinical performance of single-slice CT for attenuation correction (CTAC) of SPECT myocardial perfusion scintigraphy (MPS) was evaluated. Early and delayed multi-slice CT (eCCT and dCCT respectively) myocardial enhancement patterns were validated against SPECT MPS (single-source CCT) and cardiovascular magnetic resonance imaging (CMR, dual-source CCT) for detection of chronic myocardial infarction (MI), as were CCT measures of segmental LV wall thickness and global and regional LV function. Impact of cardiac phase and reconstruction kernel on agreement with SPECT MPS was also measured. The following results were shown: CTAC showed no benefits on MPS report or reporter confidence when studied in a way that reflects clinical practice; dCCT best identifies segmental MI, showing good agreement and high specificity, negative predictive value and accuracy compared with SPECT MPS and CMR; choice of smooth or medium-smooth reconstruction kernel appears relatively unimportant; dual-energy dCCT may be more sensitive for segmental MI on CMR; CCT end-systolic wall thickness is a better predictor of myocardial scarring on MPS and CMR than end-diastolic wall thickness; CCT overestimates end-systolic and end-diastolic volumes on MPS but LV ejection fraction is equivalent; CCT shows no systematic differences in measures of global LV function when compared to CMR; measures of regional ventricular function on CCT show excellent and good agreement with MPS and CMR respectively; inter- and intraobserver agreement for dCCT myocardial enhancement patterns and regional LV function is excellent.

SUMMARY OF ORIGINAL FINDINGS

SECTION ONE CLINICAL UTILITY OF X-RAY COMPUTED TOMOGRAPHY ATTENUATION CORRECTION OF SPECT MYOCARDIAL PERFUSION SCINTIGRAPHY

1. Attenuation correction (AC) using either X-ray computed tomography (CTAC) or gadolinium-153 line sources (GdAC) reduces fixed perfusion defects on myocardial perfusion scintigraphy (MPS), predominantly inferiorly but also, for CTAC, laterally.
2. Both AC methods create apparent anteroapical abnormalities that are reversible on GdAC and fixed on CTAC.
3. Both AC methods show unpredictable effects on clinically-informed reports.
4. AC has no effect on the number of reports indicating an element of myocardial infarction (MI); CTAC changes normal reports to those suggesting inducible ischaemia and vice versa; despite increasing apparent anteroapical reversibility, GdAC results in fewer reports of inducible ischaemia.
5. CTAC and GdAC improve reporter confidence and interobserver agreement when blind to clinical information. Once this is known, benefits of AC are abolished.
6. Overall, there are no demonstrable benefits of CTAC over GdAC, nor of AC in general, when studied in a way that reflects clinical reporting as performed in the real world.

SECTION TWO ASSESSMENT OF MYOCARDIAL SCARRING BY 64-SLICE CARDIAC CT: COMPARISON WITH SPECT MPS

Visual Analysis

1. Delayed enhancement on delayed cardiac CT (dCCT) is best appreciated using a slow-flow iodinated contrast infusion after the main contrast bolus and by reducing X-ray tube voltage to 80kV. Tube current should be increased to compensate.
2. dCCT summed scarring scores demonstrate a better linear relationship with MPS summed rest scores than those measured by early CCT (eCCT).
3. dCCT is consistently more sensitive at patient level than eCCT for detecting MI on SPECT MPS and is probably more accurate at detecting patients with transmural MI.
4. Compared with eCCT, dCCT shows better overall segmental agreement with MPS resting tracer uptake scores and better performance at detecting segments with normal resting tracer uptake and transmural MI.
5. CCT measures of MI show differential agreement across typical coronary artery territories. dCCT significantly improves agreement in all 3 territories compared to eCCT, but agreement is poorest in the RCA territory. This may be related to the effects of inferior attenuation artefact on MPS, as shown in Section 1.

Quantitative Analysis

1. Segmental wall intensity (SWI) is a poor discriminator of resting MPS uptake categories.
2. The ratio of early and delayed SWI – the delayed enhancement ratio (DER) – is a better measure that is significantly different across nearly all MPS uptake categories (the exception being distinguishing severely reduced from absent tracer uptake).

3. Only delayed SWI and DER are able to discriminate normal myocardium, non-transmural and transmural MI.
4. DER provides the highest accuracy for discriminating normal and infarcted myocardial segments, although this is still only fair (74%). Sensitivity and PPV are particularly low (55% and 63% respectively), but specificity and NPV are reasonable (85% and 80% respectively).
5. DER provides the highest accuracy (82%) for discriminating non-transmural and transmural MI. PPV is poor (44%) and sensitivity only moderate (71%), but specificity and NPV are reasonable (81% and 93% respectively).
6. Overall, DER provides the best quantitative statistic for identifying MI, but performance is not good enough to replace expert visual scoring at this stage.

Effects of Phase of Cardiac Cycle

1. At patient level, end-systolic and end-diastolic phases show similar sensitivity and PPV for detection of patients with reduced resting MPS tracer uptake, with the latter >90% in all cases. Specificity and NPV are poor, although end-systole is superior to end-diastole.
2. Overall correlation between CT summed scarring score and MPS summed rest score is similar for both phases, with values on dCCT higher than on eCCT.
3. Overall segmental agreement is similar for both phases, with dCCT showing higher values than eCCT. No difference in overall accuracy was identified between phases for discrimination of normal from abnormal myocardial segments and non-transmural from transmural MI.

4. Heart rates >65bpm significantly reduce overall segmental agreement. The best segmental agreement is seen in end-diastole on dCCT with heart rates <65bpm.
5. DE ratios were higher on end-systolic images. The optimal DER cut-off for the end-systolic phase had marginally higher specificity and PPV than that of the end-diastolic phase. Overall, there were no differences in accuracy of DER for discriminating normal segments or those with transmural MI.
6. Whilst the overall differences between the phases are relatively marginal, the excellent (and significantly higher) segmental agreement seen on end-diastolic dCCT in patients with heart rates <65bpm suggest that these are the most important factors in accurately identifying MI on CCT.

Effects of Reconstruction Kernel

1. At patient level, smooth kernels offer better specificity and accuracy, but negative predictive value remains relatively modest.
2. The use of smooth or medium-smooth kernels has no effect on the excellent linear relationship between CT summed scarring scores and MPS summed resting scores, overall segmental agreement or visual discrimination of either normal from abnormal myocardium or transmural from non-transmural MI.
3. Medium-smooth kernels lead to a small but significant increase in the accuracy of DER for discriminating normal from abnormal myocardium. Neither kernel increases accuracy of DER for distinguishing transmural from non-transmural MI.

CCT Myocardial Wall Thickness as a Predictor of Myocardial Infarction on MPS

1. End-systolic wall thickness (ESWT) is a better differentiator of MPS resting uptake scores than end-diastolic wall thickness (EDWT).
2. Although both ESWT and EDWT vary with infarct transmurality, absolute differences between normal, non-transmural and transmural categories are larger for ESWT, suggesting that it discriminates between these categories more effectively.
3. ESWT has all round better performance for discrimination of normal from abnormal myocardium and transmural from non-transmural MI.
4. Although ESWT shows good accuracy, it suffers from poor sensitivity and PPV, rendering it more useful for ruling out MI when used as a single marker.
5. ESWT >9mm excludes segmental transmural MI on MPS in 95% of cases.

Comparison of CCT and MPS Measures of Global and Regional Function

1. CCT systematically overestimates end-systolic and end-diastolic volumes compared with SPECT MPS, although there is no difference in calculated LV ejection fractions.
2. There were no proportional differences or deviations from linearity between CCT and MPS measures of global LV function, suggesting that CCT can be used reliably provided systematic errors are accounted for by defining normal reference ranges.
3. No patient with LVEDV <160mL on CCT had a dilated LV on MPS.
4. Qualitative measures of regional LV function on CCT (segmental wall motion and thickening) demonstrate excellent agreement with similar measures on MPS.
5. Moderate or greater reductions in segmental wall motion and thickening carry a 96-97% negative predictive value for transmural MI in that segment. Positive predictive value is poorer, however (64-71%).

6. Segmental wall thickening on CCT appears better than wall motion at discriminating normal from abnormal myocardium and non-transmural from transmural MI.
7. Quantitative measures of regional LV function on CCT (segmental EF and percentage wall thickening) are less accurate than qualitative measures and should not replace expert visual scoring.

SECTION THREE ASSESSMENT OF MYOCARDIAL SCARRING BY DUAL SOURCE CARDIAC CT: COMPARISON WITH CARDIAC MAGNETIC RESONANCE IMAGING

Visual Analysis

1. Single-energy (SE-) and dual-energy (DE-) dCCT result in higher summed scarring scores when compared to eCCT. SE-dCCT scores show the strongest linear relationship with CMR LGE scores.
2. SE-dCCT is most accurate at identifying patients with LGE on CMR, whilst both SE-dCCT and DE-dCCT show perfect accuracy for determining patients with ≥50% LGE in at least one segment. Small patient numbers limits the significance of this result.
3. SE-dCCT and DE-dCCT perform equally well at segment level, with excellent overall agreement with CMR and accuracy for discriminating patients with any LGE or ≥50% LGE on CMR. DE-dCCT may be more sensitive but both are superior to eCCT.
4. Inter- and intraobserver agreement for visual analysis of DE-dCCT is excellent.
5. Results suggest that, despite the small number of patients studied, DE-dCCT reproducibly identifies partial- and full-thickness myocardial scarring on CMR.

Dual-Source CCT Segmental Wall Thickness as a Predictor of Myocardial Infarction on CMR

1. EDWT on CCT differed from CMR values by less than 1mm on average. However, limits of agreement were wide and EDWT on CCT and CMR were non-linearly related, possibly as a result of small sample size.
2. ESWT is superior to EDWT at discriminating normal myocardium, non-transmural and transmural MI on both dCCT and CMR.
3. Although ESWT shows good accuracy, it suffers from poor sensitivity and PPV, rendering it more useful for ruling out MI.
4. ESWT >9mm excludes ≥50% segmental LGE on CMR in 92% of cases.

Comparison of Dual-Source CCT and CMR Measures of Global and Regional Function

1. On Bland-Altman analysis, CCT shows ~5% underestimation of LVEF compared to CMR; this is mediated by ~10mL overestimation of LVESV. EDV is not significantly different between the techniques.
2. Passing and Bablok regression yields no systematic or proportional differences between techniques for any measure of global LV function.
3. Although sample size was too small to allow estimation for women, no man with LVEDV <126mL (BSA-indexed 69mL) has a dilated LV on CMR.
4. Agreement between CCT and CMR for measures of regional LV function is good.
5. CCT segmental wall motion and thickening shows good accuracy for detection of segments with absent or ≥50% LGE on CMR.
6. Inter- and intraobserver agreement for CCT segmental wall motion and thickening are excellent.

STATEMENT OF CANDIDATE

The following thesis describes research undertaken by the candidate over 3 years using single-slice and multi-slice cardiovascular computed tomography (CCT). Single-slice CCT is in use clinically for attenuation correction of myocardial perfusion scintigrams, whilst myocardial characterisation using multi-slice CCT remains a research application. Discussions of pertinent published research reflect current thinking, although the presented data should be interpreted with reference to accepted wisdom at the time of collection. All imaging studies were performed between April 2008 and January 2011 in the departments of radiology, nuclear cardiology and cardiovascular magnetic resonance imaging at the Royal Brompton Hospital. All studies were approved by a local Research Ethics Committee and patients gave written informed consent prior to enrolment. Studies were supported by the Royal Brompton Hospital Research and Development Office and Imperial College Clinical Research Office. Research images were analysed by the candidate and, where necessary and indicated, by colleagues in relevant departments. All imaging undertaken for clinical indications was analysed by the relevant clinicians as part of standard clinical care. Data analysis, including statistical evaluation, was performed by the candidate, except where stated explicitly. The thesis was prepared and produced wholly by the candidate. The copyright of this thesis rests with the author and is made available under a Creative Commons Attribution Non-Commercial No Derivatives licence. Researchers are free to copy, distribute or transmit the thesis on the condition that they attribute it, that they do not use it for commercial purposes and that they do not alter, transform or build upon it. For any reuse or redistribution, researchers must make clear to others the licence terms of this work.

TABLE OF CONTENTS

TITLE PAGE 1

BRIEF ABSTRACT 2

SUMMARY OF ORIGINAL FINDINGS 3

STATEMENT OF CANDIDATE 10

TABLE OF CONTENTS 11

LIST OF FIGURES 17

LIST OF TABLES 21

ACKNOWLEDGEMENTS 30

CHAPTER 1 INTRODUCTION

1.1 Introduction 32

1.2 Fundamentals of X-ray computed tomography

1.2.1 Image acquisition 32

1.2.2 The X-ray tube 34

1.2.3 Effects of varying tube current and voltage 35

1.2.4 Image processing 36

1.3 Cardiac X-ray computed tomography 37

1.4 Applications of single-slice CT

1.4.1 Principles of myocardial perfusion scintigraphy 41

1.4.2 Attenuation correction

1.4.2.1 Radionuclide attenuation correction 42

1.4.2.2 X-ray attenuation correction 42

1.4.3 Clinical value of attenuation correction 45

1.4.4 Gaps in research 47

1.5 Applications of multi-slice CT

1.5.1 Background 48

1.5.2 Contrast kinetics of iodinated contrast media 50

1.5.3 Clinical value of delayed enhancement of myocardial scarring 53

1.5.4 Gaps in research 54

1.6 Aims of thesis 55

CHAPTER 2 GENERAL METHODS

2.1 Introduction 58

2.2 Standardised segmentation of the left ventricle 58

2.3 Myocardial perfusion scintigraphy

2.3.1 Stress protocol 61

2.3.2 Image acquisition parameters 62

2.3.3 Attenuation correction methods

2.3.3.1 Computed tomography attenuation correction 62

2.3.3.2 ^{153}Gd line source attenuation correction 63

2.3.4 Reporting protocol 63

2.3.5 Reporting summed perfusion images 63

2.3.6 Summary clinical reports 67

2.3.7 Reporting gated images 67

2.4 Multislice cardiovascular computed tomography

2.4.1 Patient preparation 70

2.4.2 Acquisition parameters 70

2.4.3 Contrast protocols 71

2.4.4 Acquisition timing 71

2.4.5 Image reconstruction 72

2.5 Cardiovascular magnetic resonance imaging 74

2.6 Assessment of global and regional left ventricular systolic function

2.6.1 Cardiovascular computed tomography 74

2.6.2 Myocardial perfusion scintigraphy 76

2.6.3 Cardiovascular magnetic resonance imaging 77

2.7 Quantification of myocardial scarring

2.7.1 Cardiovascular computed tomography 78

2.7.2 Myocardial perfusion scintigraphy 80

2.7.3 Cardiovascular magnetic resonance imaging 81

2.8 Statistics

2.8.1 Testing data for normality 82

2.8.2 Comparison of parametric and non-parametric data 82

2.8.3 Agreement 83

2.8.4 Regression 84

2.8.5 Receiver operator characteristic analysis 85

SECTION 1 CLINICAL UTILITY OF X-RAY COMPUTED TOMOGRAPHY ATTENUATION CORRECTION OF SPECT MYOCARDIAL PERFUSION SCINTIGRAPHY

CHAPTER 3 EFFECTS OF X-RAY COMPUTED TOMOGRAPHY AND GADOLINIUM-153 ATTENUATION CORRECTION ON QUALITATIVE TRACER UPTAKE SCORES ON SPECT MPS

3.1 Introduction 88
3.2 Methods 89
3.3 Results 93
3.4 Discussion 99
3.5 Limitations 100
3.6 Summary of findings 101

CHAPTER 4 EFFECTS OF X-RAY COMPUTED TOMOGRAPHY AND GADOLINIUM-153 ATTENUATION CORRECTION ON CLINICAL REPORT AND REPORTER CONFIDENCE

4.1 Introduction 102
4.2 Methods 103
4.3 Results 106
4.4 Discussion 121
4.5 Limitations 125
4.6 Summary of findings 125

SECTION 2 ASSESSMENT OF MYOCARDIAL SCARRING BY 64-SLICE CARDIAC COMPUTED TOMOGRAPHY: COMPARISON WITH SPECT MYOCARDIAL PERFUSION SCINTIGRAPHY

CHAPTER 5 PILOT COMPARISON WITH SPECT MYOCARDIAL PERFUSION SCINTIGRAPHY

5.1 Introduction 128
5.2 Methods 128
5.3 Results 132
5.4 Discussion 135
5.5 Summary of findings 136

CHAPTER 6 VISUAL SCORING OF SEGMENTAL MYOCARDIAL ENHANCEMENT ON CARDIAC CT IN PATIENTS WITH PREVIOUS MYOCARDIAL INFARCTION

6.1 Introduction 137
6.2 Methods 138
6.3 Results 141
6.4 Discussion 151
6.5 Limitations 154
6.6 Summary of findings 154

CHAPTER 7 QUANTITATIVE ANALYSIS OF SEGMENTAL MYOCARDIAL ENHANCEMENT ON CARDIAC CT IN PATIENTS WITH PREVIOUS MYOCARDIAL INFARCTION

7.1 Introduction 155
7.2 Methods 156
7.3 Results 158
7.4 Discussion 164
7.5 Limitations 166
7.6 Summary of findings 166

CHAPTER 8 COMPARATIVE ACCURACY OF END-SYSTOLIC AND END-DIASTOLIC PHASES ON CARDIAC CT FOR DETECTION OF MYOCARDIAL SCARRING ON SPECT MPS

8.1 Introduction 168
8.2 Methods 169
8.3 Results 171
8.4 Discussion 183
8.5 Limitations 185
8.6 Summary of findings 186

CHAPTER 9 EFFECT OF CARDIAC CT RECONSTRUCTION KERNEL ON AGREEMENT WITH SPECT MPS

9.1 Introduction 187
9.2 Methods 189
9.3 & 4 Results 190
9.5 Discussion 199
9.6 Limitations 201
9.7 Summary of findings 201

CHAPTER 10 SEGMENTAL MYOCARDIAL THICKNESS ON CARDIAC CT AS A PREDICTOR OF MYOCARDIAL INFARCTION ON SPECT MPS

10.1 Introduction 202
10.2 Methods 203
10.3 Results 204
10.4 Discussion 210
10.5 Limitations 212
10.6 Summary of findings 212

CHAPTER 11 ASSESSMENT OF GLOBAL AND REGIONAL LEFT VENTRICULAR FUNCTION BY CARDIAC CT IN PATIENTS WITH PREVIOUS MYOCARDIAL INFARCTION: COMPARISON WITH SPECT MPS

11.1 Introduction 213
11.2 Methods 214
11.3 Results 216
11.4 Discussion 231
11.5 Limitations 233
11.6 Summary of findings 233

SECTION 3 ASSESSMENT OF MYOCARDIAL SCARRING BY DUAL SOURCE CARDIAC COMPUTED TOMOGRAPHY: COMPARISON WITH CARDIAC MAGNETIC RESONANCE IMAGING

CHAPTER 12 DELAYED DUAL SOURCE CARDIAC CT IN PATIENTS WITH PREVIOUS MYOCARDIAL INFARCTION: COMPARISON WITH CMR

12.1 Introduction 235
12.2 Methods 236
12.3 Results 238
12.4 Discussion 245
12.5 Limitations 247
12.6 Summary of findings 247

CHAPTER 13 SEGMENTAL MYOCARDIAL THICKNESS ON DUAL SOURCE CARDIAC CT AS A PREDICTOR OF MYOCARDIAL INFARCTION ON CMR

13.1 Introduction 248
13.2 Methods 249
13.3 Results 251
13.4 Discussion 257
13.5 Limitations 258
13.6 Summary of findings 259

CHAPTER 14 ASSESSMENT OF LEFT VENTRICULAR FUNCTION BY DUAL SOURCE CARDIAC CT IN PATIENTS WITH PREVIOUS MYOCARDIAL INFARCTION: COMPARISON WITH CMR

14.1 Introduction 260
14.2 Methods 261
14.3 Results 263
14.4 Discussion 274
14.5 Limitations 276
14.6 Summary of findings 276

CHAPTER 15 FINAL CONCLUSIONS

15.1 General comments 278
15.2 Review of findings 279
15.3 Areas for further study 281

CHAPTER 16 REFERENCES 283

APPENDIX 1 PUBLICATIONS 297

LIST OF FIGURES

Figure 1.1	Cross section of an X-ray CT scanner	33
Figure 1.2	Single slice CT	34
Figure 1.3	Simplified components of an X-ray tube	35
Figure 1.4	Components of an axial image slice	37
Figure 1.5	Multi-slice CT	40
Figure 1.6	Attenuation maps derived from gadolinium-153 radionuclide transmission and X-ray computed tomography	44
Figure 1.7	Misregistration of perfusion images and CT attenuation map	45
Figure 1.8	Two compartment model of contrast distribution	51
Figure 2.1	American Heart Association 17-segment model of the human heart	59
Figure 2.2	Typical coronary territories over the AHA 17-segment model of the human heart, assuming right coronary artery dominance	60
Figure 2.3	Regionalisation of the AHA 17-segment model into myocardial walls	61
Figure 2.4	Representation of myocardial tracer uptake	64
Figure 2.5	Myocardial perfusion images presented in splash format	64
Figure 2.6	Classification of myocardial perfusion abnormalities	66
Figure 2.7	Gated SPECT myocardial perfusion scintigraphy.	69
Figure 2.8	Test bolus method for contrast timing	73
Figure 2.9	Calculation of left ventricular volume on cardiac CT (CCT)	75
Figure 2.10	Epicardial and endocardial contours on CCT	77
Figure 2.11	Visual analysis of enhancement patterns of myocardial scarring on early and delayed imaging	79

Figure 2.12 Polar plots of mean segmental wall intensity on early CCT image and delayed CCT images, with comparative resting MPS polar plot 81

Figure 3.1 MPS imaging protocol with variation of assignment to gamma camera 91

Figure 3.2 Attenuation correction of the inferior wall 97

Figure 4.1 Reporting strategy for non-corrected (Session 1), gadolinium-corrected and CT-corrected MPS images (Sessions 2 & 3). 105

Figure 5.1 Contrast protocols 131

Figure 5.2 Effect of contrast protocol on delayed enhancement of MI 133

Figure 5.3 Effect of X-ray tube voltage and current on delayed enhancement of MI 134

Figure 7.1 Comparison of early and delayed segmental wall intensity (HU) and delayed enhancement ratio (DER) ROC curves for detection of any segmental myocardial infarction (MI) 162

Figure 7.2 Comparison of early and delayed segmental wall intensity (HU) and DER ROC curves for discrimination of non-transmural and transmural (MI) 163

Figure 8.1 Comparison of DER between end-systolic and end-diastolic phases according to transmurality of segmental MI 179

Figure 8.2 Comparison of ROC curves for detection of any MI on end-systolic and end-diastolic CCT 180

Figure 8.3 Comparison of ROC curves for detection of transmural MI on end-systolic and end-diastolic CCT 182

Figure 9.1 Comparison of ROC curves of smooth and medium-smooth kernels for discrimination of normal and abnormal myocardial segments 197

Figure 9.2 Comparison of ROC curves of segment-level accuracy of smooth and medium-smooth kernels for discrimination of non-transmural and transmural MI 198

Figure 10.1 ROC curves showing accuracy of end-systolic and end-diastolic segmental wall thickness (ESWT and EDWT respectively) for detection of any MI on MPS 208

Figure 10.2 ROC curves showing accuracy of ESWT and EDWT for detection of transmural MI on MPS 209

Figure 11.1 Bland-Altman plots showing the relationship between cardiac CT and MPS for measures of LV ejection fraction (EF), end-diastolic volume (EDV) and end-systolic volume (ESV) 219

Figure 11.2 Comparison of CCT and MPS LVEF, with regression line and residuals plot 220

Figure 11.3 Comparison of CCT and MPS LVEDV, with regression line and residuals plot 221

Figure 11.4 Comparison of CCT and MPS LVESV, with regression line and residuals plot 222

Figure 11.5 ROC curve showing good accuracy of EDV on CCT for predicting left ventricular dilatation on MPS 223

Figure 11.6 ROC curves showing accuracy of quantitative CT segmental EF and thickening for discriminating normal and abnormal myocardium 229

Figure 11.7 ROC curves showing accuracy of quantitative CT segmental EF and thickening for discriminating non-transmural and transmural MI 230

Figure 13.1 Bland-Altman plot of CCT and CMR EDWT 252

Figure 13.2 ROC curves showing accuracy of ESWT and EDWT for detection of any LGE on CMR 255

Figure 13.3 ROC curves showing accuracy of ESWT and EDWT for detection of ≥50% late gadolinium enhancement on CMR 256

Figure 14.1 Bland-Altman plots showing the relationship between CCT and CMR for measures of LVEF, EDV and ESV 266

Figure 14.2 Comparison of CCT and CMR LVEF, with regression line and residuals plot 267

Figure 14.3 Comparison of CCT and CMR LVEDV, with regression line and residuals plot 268

Figure 14.4 Comparison of CCT and CMR LVESV, with regression line and residuals plot 269

LIST OF TABLES

Table 3.1	Patient demographics	90
Table 3.2	Intervals between stress/resting injections and subsequent imaging	92
Table 3.3	Summed perfusion scores, presented as median (IQR), on both cameras with and without attenuation correction (AC)	93
Table 3.4	Median summed perfusion scores according to coronary territory	95
Table 3.5	Median summed perfusion scores according to myocardial wall	98
Table 4.1	Comparison of provisional reports using NC and CTAC strategies	107
Table 4.2	Comparison of number of scans reported provisionally as normal or as having evidence of MI (fixed/mixed) or inducible ischaemia (reversible/mixed) for NC and CTAC strategies.	107
Table 4.3	Comparison of provisional reports using NC and GdAC strategies	108
Table 4.4	Comparison of number of scans reported provisionally as normal or as having evidence of MI (fixed/mixed) or inducible ischaemia (reversible/mixed) for NC and GdAC strategies.	108
Table 4.5	Comparison of final clinical reports using NC and CTAC strategies	109
Table 4.6	Comparison of number of scans reported finally as normal or as having evidence of MI (fixed/mixed) or inducible ischaemia (reversible/mixed) for NC and CTAC strategies.	110
Table 4.7	Comparison of final clinical reports using NC and GdAC strategies	111
Table 4.8	Comparison of number of scans reported finally as normal or as having evidence of MI (fixed/mixed) or inducible ischaemia (reversible/mixed) for NC and GdAC strategies.	111

Table 4.9	Comparison of updated and provisional reports for the CTAC strategy	112
Table 4.10	Comparison of updated and provisional reports for the GdAC strategy	113
Table 4.11	Comparison of provisional and final clinical reports for the CTAC strategy	114
Table 4.12	Comparison of provisional and final clinical reports for the GdAC strategy	115
Table 4.13	Summary of impact of CTAC and GdAC on number of normal clinical reports and those showing any fixed and reversible component.	116
Table 4.14	Between group effects on confidence with each stage	118
Table 4.15	Variation in clinical confidence at each stage of reporting	118
Table 4.16	Interobserver agreement for clinical reports before and after clinical information	119
Table 4.17	Intraobserver agreement for initial and updated reports	120
Table 4.18	Intraobserver agreement in clinical confidence in initial and updated reports	120
Table 5.1	Myocardial segments demonstrating <50% tracer uptake on myocardial perfusion scintigraphy (MPS) and delayed enhancement on cardiac computed tomography (CCT) for different X-ray tube settings and contrast protocols	132
Table 6.1	Proportions of segmental MI on MPS according to coronary artery territory	142

Table 6.2	Proportions of segmental MI on eCCT according to coronary artery territory	142
Table 6.3	Proportions of segmental MI on dCCT according to coronary artery territory	143
Table 6.4	Analysis of CCT for patient-level sensitivity, specificity, positive predictive value (PPV), negative predictive value (NPV) and accuracy for detection of ≥1 segment of myocardial infarction (MI) on MPS	145
Table 6.5	Analysis of CCT for patient-level sensitivity, specificity, PPV, NPV and accuracy for detection of patients with at least one segment of transmural MI on MPS	145
Table 6.6	Correlation between MPS summed rest scores and CCT summed scarring scores for both eCCT and dCCT	146
Table 6.7	Segment-level agreement for the presence of transmural and non-transmural MI and normal myocardium	146
Table 6.8	Analysis of CCT for segment-level agreement, sensitivity, specificity, PPV, NPV and accuracy for detection of any MI on MPS	148
Table 6.9	Analysis of CCT for segment-level agreement, sensitivity, specificity, PPV, NPV and accuracy for discrimination of transmural and non-transmural MI on MPS	148
Table 6.10	Segmental agreement between MPS and eCCT and dCCT separated according to typical coronary artery territory	149
Table 6.11	Mean relative segmental uptake scores on MPS according to classification of MI on CCT	150

Table 7.1	Early and delayed segmental wall intensities and delayed enhancement ratios for each category of resting MPS segmental tracer uptake	159
Table 7.2	Early and delayed segmental wall intensities and delayed enhancement ratios according to transmurality of MI on MPS	160
Table 7.3	Accuracy of early and delayed segmental wall intensity and delayed enhancement ratio (DER) for discrimination of normal and infarcted myocardium	162
Table 7.4	Accuracy of early and delayed segmental wall intensity and delayed enhancement ratio (DER) for detection of transmural MI	163
Table 8.1	Analysis of CCT for patient-level sensitivity, specificity, PPV, NPV and accuracy for detection of at least one segment of MI on MPS	172
Table 8.2	Correlation between MPS summed rest scores and end-systolic and end-diastolic CCT summed scarring scores for both early and late pass images	172
Table 8.3	Segmental agreement for discrimination of normal myocardium, transmural and non-transmural MI at end-systole and end-diastole	173
Table 8.4	Analysis of CCT for segment-level agreement, sensitivity, specificity, PPV, NPV and accuracy for discrimination of normal and abnormal myocardium on MPS in end-systolic and end-diastolic phases	175
Table 8.5	Analysis of CCT for segment-level agreement, sensitivity, specificity, PPV, NPV and accuracy for detection of at least one segment of transmural MI on MPS in end-systolic and end-diastolic phases	176

Table 8.6	Segmental agreement for discrimination of normal myocardium, transmural and non-transmural MI at end-systole and end-diastole according to heart rate at time of scan	177
Table 8.7	Delayed enhancement ratios according to transmurality of MI for end-systolic and end-diastolic phases of the cardiac cycle	179
Table 8.8	Accuracy of end-systolic and end-diastolic DER for detection of MI	180
Table 8.9	Accuracy of DE ratios for detection of transmural MI in end-systole and end-diastole	182
Table 9.1	Analysis of CCT for patient-level sensitivity, specificity, PPV and NPV for detection of at least one segment of MI on MPS	191
Table 9.2	Correlation between MPS summed rest scores and CCT summed scarring scores for both reconstruction kernels	190
Table 9.3	Comparison of segmental agreement for both reconstruction kernels	192
Table 9.4	Segmental agreement between delayed CCT and MPS for normal and abnormal myocardial segments for each reconstruction kernel	192
Table 9.5	Segmental agreement between delayed CCT and MPS for non-transmural and transmural MI for each reconstruction kernel	193
Table 9.6	Analysis of CCT for segment-level sensitivity, specificity, PPV and NPV for detection of normal segments and those demonstrating transmural MI	194
Table 9.7	Comparison of delayed enhancement ratios across MPS categories for both reconstruction kernels	195

Table 9.8	DER values for normal myocardium and non-transmural and transmural MI after reconstruction using smooth and medium-smooth kernels	196
Table 9.9	Accuracy of DER for each reconstruction kernel for discrimination of normal and abnormal myocardial segments	197
Table 9.10	Accuracy of DER for each reconstruction kernel for discrimination of non-transmural and transmural MI	198
Table 10.1	Variation in end-systolic and end-diastolic segmental wall thickness (ESWT and EDWT respectively) according to resting MPS uptake categories	206
Table 10.2	ESWT and EDWT in segments with normal tracer uptake, non-transmural MI and transmural MI on resting MPS	206
Table 10.3	Accuracy of ESWT and EDWT for detection of any MI on MPS	208
Table 10.4	Accuracy of ESWT and EDWT for detection of transmural MI on MPS	209
Table 11.1	Distribution of segmental wall motion and thickening on MPS and CCT	216
Table 11.2	Global left ventricular (LV) function parameters for MPS and CCT	218
Table 11.3	Comparison of CCT and MPS indices of global LV function using Passing and Bablok regression	218
Table 11.4	Threshold values for end-diastolic volume on CCT to predict a dilated ventricle on MPS	223
Table 11.5	Agreement between CCT and MPS regional wall motion and thickening	224

Table 11.6	Analysis of CCT segmental wall motion and thickening for sensitivity, specificity, PPV, NPV and accuracy for detection of any MI on MPS	225
Table 11.7	Analysis of CCT segmental wall motion and thickening for sensitivity, specificity, PPV, NPV and accuracy for discrimination of transmural and non-transmural MI on MPS	225
Table 11.8	Variation in CCT segmental ejection fraction (EF) across MPS wall motion categories	227
Table 11.9	Segmental ejection fraction according to transmurality of MI on MPS	227
Table 11.10	CCT segmental wall thickening across MPS wall motion categories	228
Table 11.11	ROC analysis for CCT segmental EF and thickening for discriminating normal and abnormal myocardium	229
Table 11.12	ROC analysis for CCT segmental EF and thickening for discriminating non-transmural and transmural MI	230
Table 12.1	Analysis of CCT for patient-level sensitivity, specificity, PPV, NPV and accuracy for detection of patients with any segmental late gadolinium enhancement (LGE) on CMR	240
Table 12.2	Analysis of CCT for patient-level sensitivity, specificity, PPV, NPV and accuracy for detection of patients with ≥1 segment of ≥50% LGE on CMR	240
Table 12.3	Correlation between CMR summed rest scores and CCT summed scarring scores	241
Table 12.4	Segment-level agreement between CCT and CMR for the presence of normal myocardium, non-transmural and transmural MI	241

Table 12.5	Analysis of CCT for segment-level sensitivity, specificity, PPV, NPV and accuracy for detection of any LGE on CMR	243
Table 12.6	Analysis of CCT for segment-level sensitivity, specificity, PPV, NPV and accuracy for detection of ≥50% LGE on CMR	243
Table 12.7	Interobserver and intraobserver agreement for DE-dCCT detection of normal myocardium, non-transmural and transmural MI	244
Table 13.1	Comparison of EDWT on CCT and CMR	252
Table 13.2	ESWT and EDWT according to transmurality of LGE on CMR	253
Table 13.3	Accuracy of ESWT and EDWT for detection of any LGE on CMR	255
Table 13.4	Accuracy of ESWT and EDWT for detection of ≥50% LGE on CMR	256
Table 14.1	Distribution of segmental wall motion and thickening on CMR and CCT	263
Table 14.2	Indices of global LV function for CMR and CCT	265
Table 14.3	Comparison of CCT and CMR indices of global LV function using Passing and Bablok regression	265
Table 14.4	Male threshold values for CCT end-diastolic volume to predict a dilated LV on CMR	265
Table 14.5	Agreement between CCT and CMR regional wall motion and thickening	270
Table 14.6	Analysis of CCT segmental wall motion and thickening for sensitivity, specificity, PPV, NPV and accuracy for detection of any LGE on CMR	271
Table 14.7	Analysis of CCT segmental wall motion and thickening for sensitivity, specificity, PPV, NPV and accuracy for ≥50% LGE on CMR	271

Table 14.8 Interobserver agreement for CCT regional wall motion and thickening 272

Table 14.9 Intraobserver agreement for CCT regional wall motion and thickening 273

ACKNOWLEDGMENTS

The following thesis has taken time and effort. That it exists at all is testament to the contributions and guidance from others, coupled with, perhaps above all, their patience. First, I thank Professor Richard Underwood, who has guided me through the process from start to finish. My time at the Royal Brompton Hospital has been (and will be forevermore) career defining. I remember approaching Professor Underwood via email to enquire about research opportunities in cardiac imaging. I was fresh out of SHO jobs with a crisp MRCP diploma in hand but no research experience save for a BSc project in retinal physiology some 7 years earlier. Our discussions resulted in a job description and then a research post that I was fortunate to be allowed to fill. For the gamble taken and, ultimately, the remarkable patience shown whilst waiting for me to see the following studies through to write up, I am grateful beyond measure. By the same token, I am equally grateful to Dr Ed Nicol, with whom I was fortunate to work whilst his MD was in progress. I am indebted for the many opportunities that have arisen as a result of our meeting. Collaborating on his work validating computed tomography (CT) coronary angiography early in its clinical life afforded me the time and training opportunity to develop the skills that I have now put to use in my own work. My feeling is that we bring complimentary skills to clinical research and I hope therefore that we will continue to work together in the years that lie ahead. Within the field of cardiac CT, I also extend my deep gratitude to Dr Michael Rubens and Dr Simon Padley, whose convivial attitude towards having a second cardiologist interfering in the Radiology department and patience with my initial (and still slight) obliviousness to axial imaging was refreshing and rewarding in equal measure.

Many others have been crucial to the development and production of this work. In particular, I thank Dr Eliana Reyes for keeping a cheery demeanour whilst slogging through yet another dreary MPS reporting session, reporting the cardiovascular magnetic resonance images and, most of all, her friendship during my time at the Royal Brompton Hospital. Thanks also to Katherine Standbridge, without whom I doubt a single patient would have been recruited to any of the following studies, and Jim Bailey, Trupti Patel, Brad Park and Sally Copperwaite, who helped me find time in otherwise busy clinical imaging lists to fit in research patients. For helping me with the physical aspects of this research, I thank Dr Isabel Castellano in the Department of Medical Physics at the Royal Marsden Hospital.

Most importantly of all, I thank my family. My wife Helen has been a rock during the preparation of this work. Whilst I have been sitting at a desk typing, she has been doing the real work, initially with our first daughter, Freya, in tow and subsequently, 13 months ago, following the birth of our twin daughters, Phoebe and Emily. The twins' prematurity required a stay on Neonatal Intensive Care; this and subsequent demands meant that thesis writing took a backseat for some months but they are now healthy. All 3 children are waiting for me to finish typing so that I can play with them. In the last 18 months we have moved house 3 times and so, in addition to Helen for her efforts, I am also grateful to her parents, Alan and Jackie, for all the assistance they have provided, including more childcare than should ever be reasonably expected of grandparents. Finally, I thank my parents – for giving me the best start in life and all the encouragement and support I needed thereafter. I wouldn't be here without them.

CHAPTER 1 GENERAL INTRODUCTION

1.1 INTRODUCTION

X-ray computed tomography (CT) represents the culmination of work by Sir Godfrey Hounsfield, an electrical engineer at EMI Laboratories, and, independently, Allan Cormack, a South African-born physicist working at Tufts University, Massachusetts. Cormack published the mathematical basis for CT in 1963, providing the foundation for development of the first CT scanner (EMI Mark 1) at EMI Laboratories in 1971 by Sir Godfrey Hounsfield. The impact of CT on medical practice was recognised by the Nobel Committee, who awarded Hounsfield and Cormack the Prize for Physiology or Medicine in 1979.

1.2 FUNDAMENTALS OF X-RAY COMPUTED TOMOGRAPHY

Despite excellent spatial resolution, conventional plain film radiography suffers from the conversion of 3-dimensional data into a 2-dimensional image, leading to superposition of adjacent structures. CT overcomes this limitation by providing a series of axial slices which may be reconstructed into a 3-dimensional dataset.

1.2.1 Image Acquisition

X-rays are emitted through the patient in the transverse plane (Figure 1.1). Interaction with body tissue reduces the energy of the X-ray photons, a process known as attenuation. Upon reaching the detectors (Figure 1.1B), X-ray photon energy is recorded. The X-ray tube is then rotated (Figure 1.1C) and the process repeated. Acquisition of ~1000 – 2000 recordings over an ~180° arc provides

sufficient data to allow reconstruction of an axial image. The X-ray tube is then translated in the z-axis and acquisition of a new slice begins (Figure 1.2). The thickness of each slice is determined by the z-axis dimension of the detector elements; z-axis translation continues until enough slices have been acquired to cover fully the area of interest.

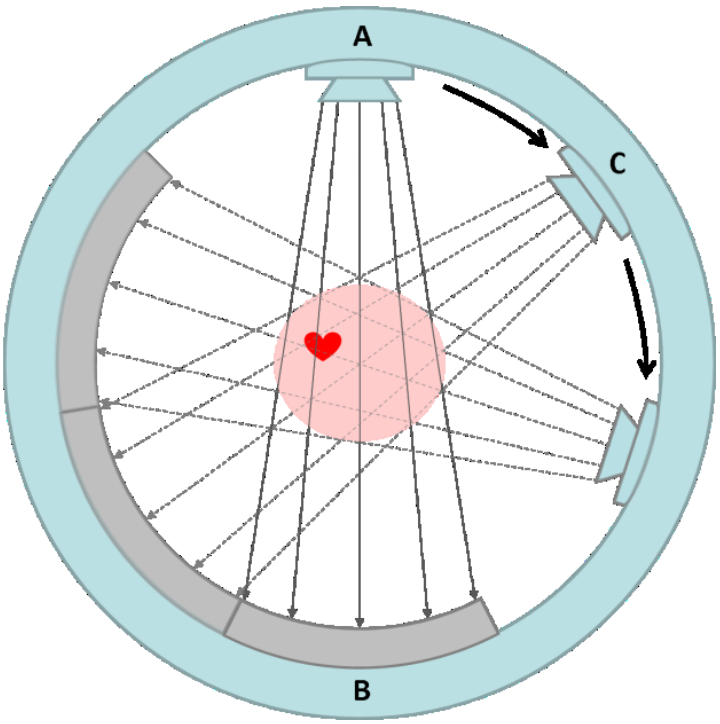


Figure 1.1 *Cross section of an X-ray CT scanner. The patient lies in the centre of a circular gantry on which a rotating X-ray tube (A) and detector array (B) are mounted. X-rays are transmitted through the patient and their remaining energy after transit recorded by the detectors. The X-ray tube/detector assembly rotates (C) and the process repeated. Slice acquisition requires ~180° rotation.*

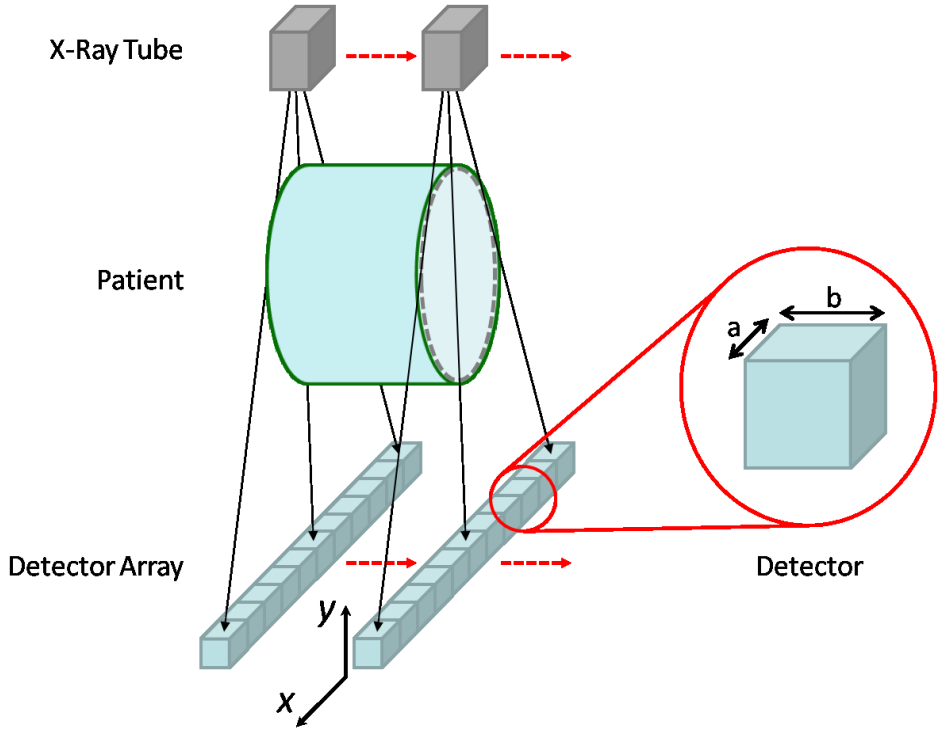


Figure 1.2 *Single slice CT. After data has been acquired over a 180° arc, the gantry is translated in the z-axis (red arrows) and a new axial slice acquired. Detector element width (b) determines slice thickness and thus magnitude of z-axis translation required. Spatial resolution of the axial slice in the (x,y) plane is determined in part by the detector width (a).*

1.2.2 The X-ray tube

The X-ray tube comprises a cathode that emits a beam of electrons towards a rotating tungsten anode (Figure 1.3). The shape of the anode is such that X-ray photons are emitted – the primary beam – through a hole in the side of the X-ray tube housing. This hole can be adjusted using filters and collimators to alter the shape or energy composition of the X-ray beam. The beam itself is composed of a heterogeneous spectrum of X-ray energies. Lower energy photons are easily

absorbed by tissues in the path of the X-ray beam and therefore contribute to total dose but not final image. By design, lower energy X-rays are removed from the primary beam by filtration, usually by the X-ray tube housing. The generated X-ray spectrum demonstrates several peaks (Figure 1.3), which represent electron transition energies. Beam intensity describes the quantity of X-ray photons within the primary beam, whilst beam energy describes the spectrum of their energies, often summarised as either the mean or peak X-ray energy.

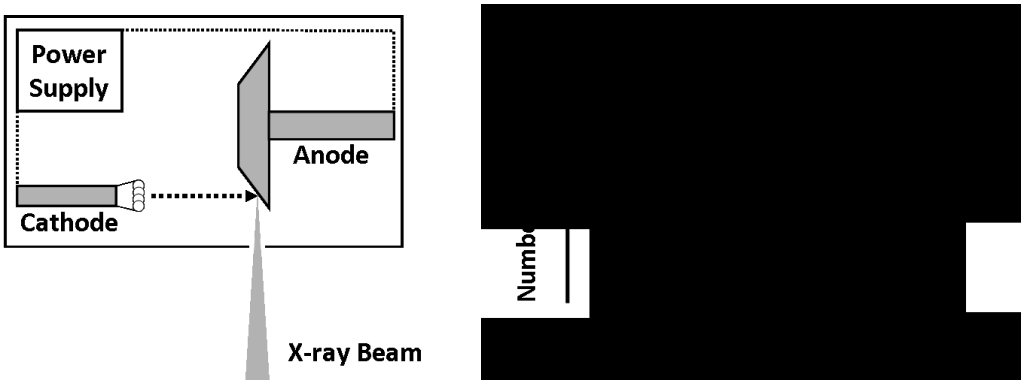


Figure 1.3 *Simplified components of an X-ray tube (left), with an electron beam (dashed arrow) travelling from cathode to rotating tungsten anode. The emitted X-ray spectrum (right) is heterogeneous, with peaks corresponding to electron transition energies.*

1.2.3 Effects of varying X-ray tube current and voltage

X-ray tube current determines beam intensity but has no effect on beam energy. Tube voltage is the potential energy difference between cathode and anode and therefore determines beam energy and, to a lesser extent, beam intensity. Increasing tube voltage produces an X-ray spectrum with a higher mean energy.

Changes to either X-ray tube current or voltage have implications for CT imaging. Final image quality is determined by the signal to noise ratio. Any intervention that increases beam intensity will increase the number of photons arriving at the detectors – the primary signal. Image noise is related first to the number of scattered photons incorrectly assigned as primary signal and second to quantum variations within the detectors (quantum mottling). The latter is a fairly fixed property of the system, whilst the number of scattered photons is proportional to the beam intensity. Increasing beam intensity therefore has the effect of minimising the effects of quantum mottle and therefore increasing signal to noise ratio. Increasing beam energy leads to more energetic X-ray photons that are less attenuated by any given tissue (see Section 5.4). Increasing tube voltage therefore affects the imaging characteristics of the tissue under investigation. For the multi-slice CT investigations in this thesis, lower tube voltages are used as this exacerbates the differences between tissues with small relative differences in enhancement after injection of iodinated contrast.

1.2.4 Image Processing

X-ray photons are attenuated according to the density and depth of tissue through which they pass. This may be summarised simply by the following equation:

$$I = I_o e^{-\mu x}$$

where I_o is the initial intensity of the X-ray photon, I the intensity after travelling distance x and μ the mean attenuation coefficient of the material through which the photon has passed. The equation can be rearranged:

$$\mu \propto \ln(I_o/I)$$

such that μ is proportional to the natural logarithm of the ratio of initial and final X-ray energies. By measuring attenuation coefficients at multiple angles, it is possible to reconstruct axial images using filtered back-projection. Images are made up of volume picture elements (voxels) which are assigned a grey-scale value according to the calculated mean attenuation coefficient of that volume (Figure 1.4).

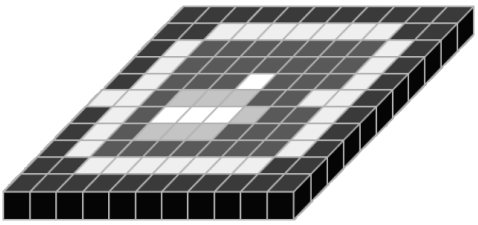


Figure 1.4 *Components of an axial image. Each cube is a voxel which represents the mean attenuation coefficient for that volume of tissue represented on a gray scale.*

1.3 CARDIAC X-RAY COMPUTED TOMOGRAPHY

Although in use for nearly 40 years, it is only since the advent of multi-slice CT (MSCT) that CT has been applied to cardiac imaging. Since invention, CT contrast resolution has been superior to conventional radiography but the spatial resolution somewhat poorer. Spatial resolution represents the smallest distance two points may be separated and still be resolved as individual objects. The in-plane (*x,* y) resolution of a CT image is determined by detector width (Figure 1.2), X-ray beam focal spot size, scanner geometry and sampling frequency. In-plane spatial resolution of 64-slice CT is around 20 line pairs/cm, a figure substantially higher than single-

slice (SSCT) used for attenuation correction (3 lp/cm) but still 2-3 fold lower than for conventional coronary angiography (40 lp/cm). The longitudinal (z-axis) resolution is more difficult to compute in helical MSCT and relates to detector width as well as the spiral interpolation algorithm. Both are affected by reconstruction algorithm, with sharper algorithms resulting in noisier images of higher spatial resolution. Whilst the original EMI Mark 1 scanner had a longitudinal spatial resolution of around 3mm, subsequent improvements in detector technology have increased this to ~0.4mm, allowing accurate assessment of the distal coronary arteries.

The main obstacle limiting the initial feasibility of cardiac CT (CCT) was cardiac motion, as poor temporal resolution (the ability to resolve two points in time as individual events) led to blurred cardiac images. CT temporal resolution is determined mainly by the time taken to acquire a single axial image – i.e. ~180° gantry rotation (Figure 1.1C). It is only relatively recently that this time has been reduced to <1 cardiac cycle. Further determinants of temporal resolution include scan pitch (table feed per gantry rotation divided by X-ray beam collimation) and patient heart rate. 64-slice CT scanners require strict control of heart rate to minimise the effects of cardiac motion, although advances such as dual-source technology may render this unnecessary.

Images may also be blurred as a result of respiratory motion. Breath-holding is therefore mandatory during acquisition. The EMI Mark 1 scanner required 4.5 minutes to acquire an image, a duration which made breath-holding unfeasible. SSCT requires ~60s to cover the whole heart due to the multiple z-axis translations

required. The addition of multiple detector arrays to the gantry allows acquisition of multiple slices during a single gantry rotation (Figure 1.5), decreasing the amount of time required to cover the thorax to just a few seconds. This makes breath-holding feasible and allows minimisation of respiratory motion artefact.

Improvements in temporal resolution and the addition of multiple detector arrays have allowed CCT to evolve into a reliable clinical imaging modality. 64-slice CT is the accepted minimum standard for all CCT applications. Although this has reduced the use of SSCT as a standalone diagnostic tool, new applications have been developed in nuclear medicine, particularly in the correction of radionuclide myocardial perfusion images to improve distinction of attenuation artefacts from true perfusion abnormalities. The value of attenuation correction is debated and the role of SSCT in cardiac imaging is by no means secure. MSCT coronary angiography is well validated but the role of CCT in evaluating myocardial scarring is uncertain.

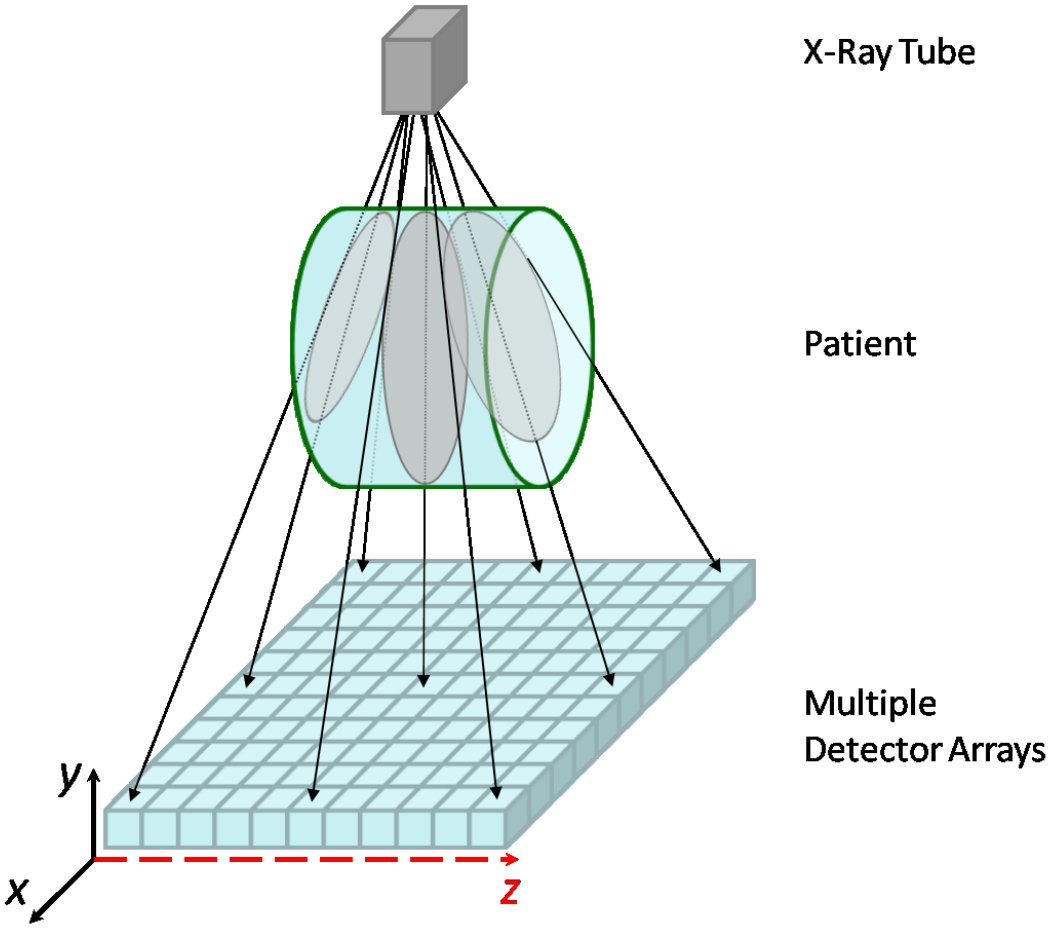


Figure 1.5 *Multislice CT. Although acquisition still requires ~180° arc, multiple detector arrays increase z-axis coverage (red arrow) over a single gantry rotation and fewer translations are required to achieve full coverage.*

1.4 APPLICATIONS OF SINGLE SLICE X-RAY COMPUTED TOMOGRAPHY

In order to investigate the role of SSCT in nuclear cardiology, it is necessary first to review some principles of myocardial perfusion scintigraphy (MPS).

1.4.1 Principles of Myocardial Perfusion Scintigraphy

MPS involves intravenous injection of a radiopharmaceutical which accumulates in the heart in proportion to myocardial perfusion and viability and decays to release gamma photons of specific energy. The latter may be detected by a gamma camera, which registers counts whenever photons of appropriate energy are detected. Interaction with soft tissue along the photon path attenuates photon energy such that they are no longer registered. As the human body is non-uniform, certain photon paths are affected more than others. In females, photons leaving the anterior surface of the heart must pass through breast tissue to reach the gamma camera whereas those leaving the lateral wall do not. As the former are attenuated more than the latter, the camera registers fewer counts anteriorly than laterally, even though the true number of emitted photons may be identical. This is known as *attenuation artefact*, and is typically caused by the breast in females and the diaphragm in males. Such artefacts may be mistaken for true perfusion abnormalities, suggesting that methods to correct tracer distribution patterns for attenuation may be clinically useful.

1.4.2 Attenuation Correction

It is possible to ‘correct’ perfusion images by proportionally adjusting detected counts according to the magnitude of regional attenuation. These coefficients are

derived from an 'attenuation map' created using the standard principles of CT described above. Any photon source may be used to generate the map as long as initial photon energy is known. Clinically, attenuation correction (AC) is performed using sources that emit either gamma photons or X-rays.

Radionuclide attenuation correction

Typically, gadolinium-153 sources are used (Figure 1.6), which have the advantage of allowing simultaneous acquisition of AC (transmission scan) and MPS (emission scan) images as both require the detection of gamma photons. The transmission scan contributes relatively little extra radiation exposure to the study (~10μSv) and simultaneous acquisition reduces the impact on departmental throughput. However, there are technical issues that require consideration. The transmission and emission radionuclides must have similar energies in order for the calculated attenuation coefficients to be valid. Attenuation of transmission photons may alter their energy such that they are recorded in the emission scan energy window, a process called downscattering. Therefore, the transmission radionuclide must emit photons of lower energy to prevent contamination of the emission scan and reduction in test accuracy. However, downscatter of emission photons into the transmission scan energy window may reduce the accuracy of the attenuation map[1]. Furthermore, transmission radionuclide decay necessitates regular replacement.

X-ray CT attenuation correction

X-ray CT attenuation correction (CTAC) is theoretically advantageous because, unlike gamma photons, X-ray photon energy can be modified according to the size of the

patient, improving signal to noise ratio and accuracy of the resulting attenuation map (Figure 1.6). As a dedicated CT scanner is required, the transmission and emission scans must be performed separately. Although this removes the possibility of contamination of the emission scan by transmission photons, patient movement between MPS and AC acquisitions may lead to misregistration of the two images sets and thus application of AC values to non-corresponding regions of the MPS image (Figure 1.7). This issue may affect as many as 40% of studies[2], so checking and manual adjustment of image registration is mandatory[3]. Second, CTAC has a relatively high spatial resolution (Figure 1.6) and errors may arise when it is used to correct low resolution MPS. Similarly, CTAC acquisition time is shorter than that of MPS. The latter takes around 20 minutes, during which the patient is breathing freely. MPS images thus represent heart position averaged over many respiratory cycles. CTAC acquisitions are performed during comfortable free breathing so that respiratory blurring on the attenuation map is matched as closely as possible to that on the MPS images. Nonetheless, any differences may lead to inaccurate AC. Finally, CTAC carries a higher radiation exposure than radionuclide transmission methods (~1mSv).

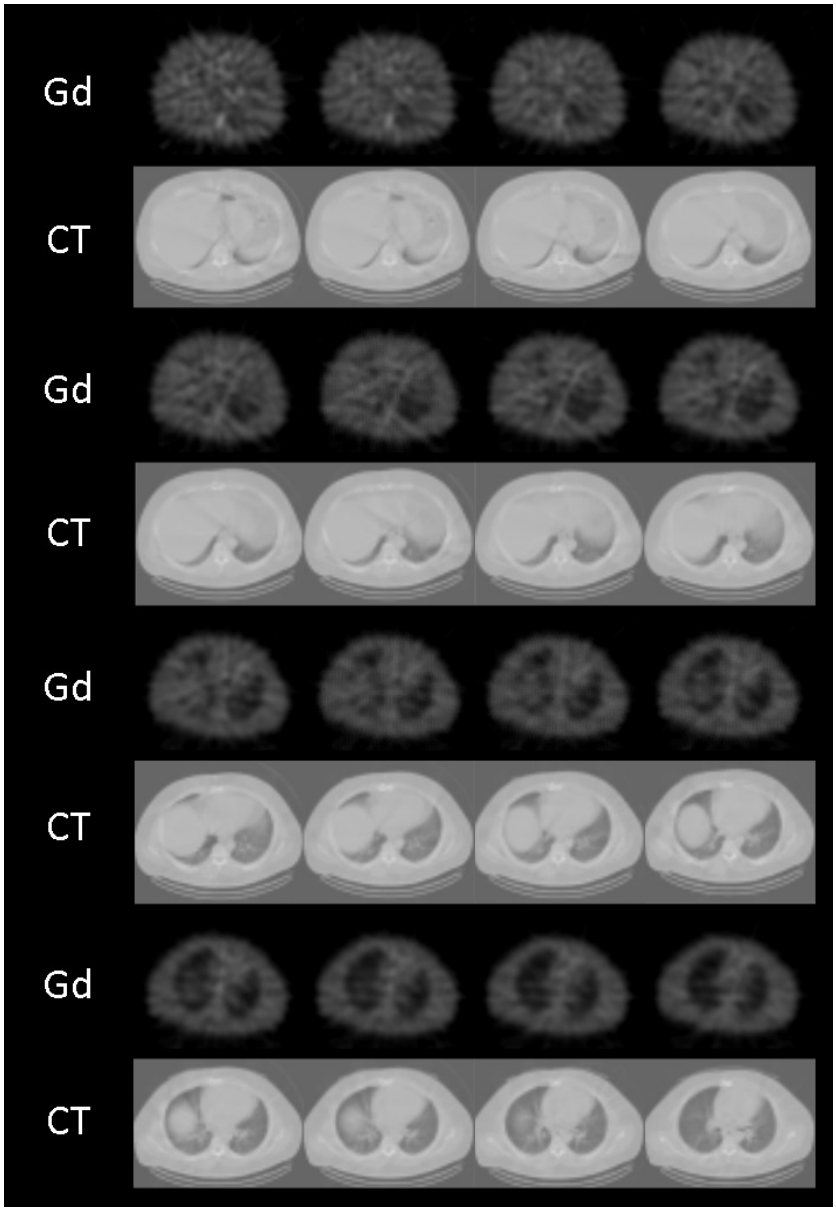


Figure 1.6 *Attenuation maps derived from gadolinium-153 radionuclide AC (Gd) and X-ray computed tomography (CT). Slices are presented in order from the level of the diaphragm (top left) to the superior aspect of the left ventricle (bottom right). The poorer spatial resolution of the radionuclide AC map is apparent, although it is much closer to that of MPS.*

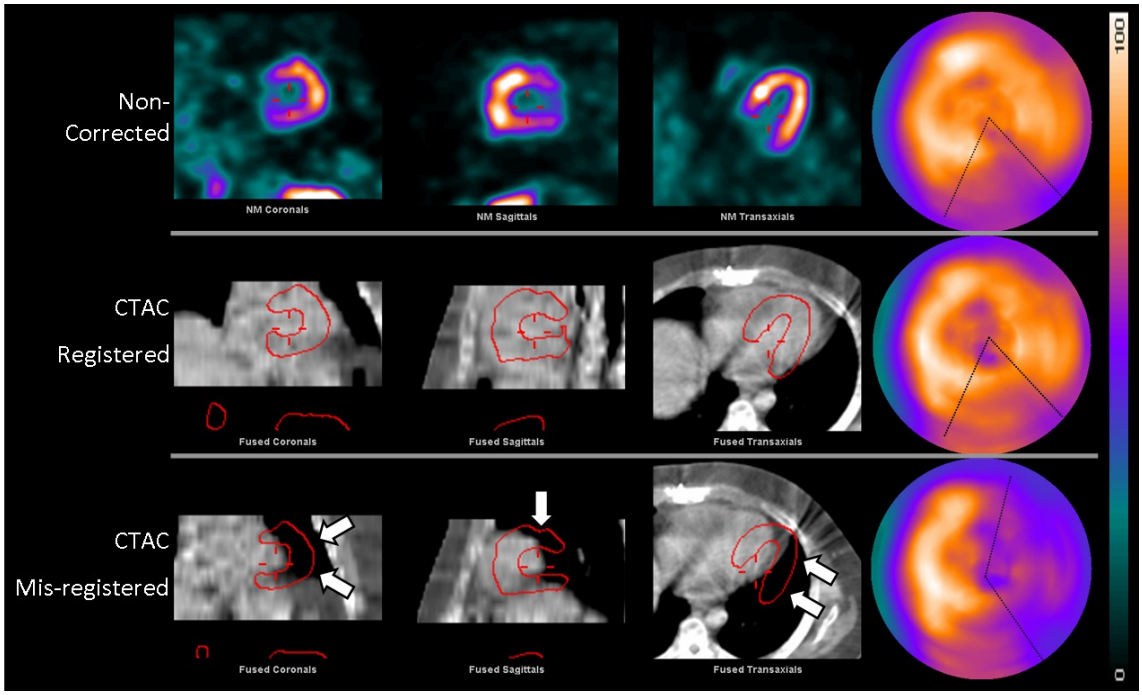


Figure 1.7 *Misregistration of perfusion images and CT attenuation map. The non-corrected data (top row) demonstrates a mild reduction in counts inferiorly (top right, black lines) in a distribution typical for diaphragmatic attenuation artefact. When properly registered with the CT attenuation map (middle row), counts in the inferior wall return to within normal limits (middle right, black lines). When the MPS and CT data are misregistered (bottom row), the lateral wall on the nuclear image (arrows) lies within the lung field rather than over the heart. This leads to inappropriate correction of the lateral wall on the perfusion images (bottom right, black lines) and creates the appearance of a moderate perfusion abnormality.*

1.4.3 Clinical Value of Attenuation Correction

The use of AC in MPS has been validated in both single-[4-11] and multi-centre[12-17] trials. The majority of early trials studied radionuclide AC[4-9, 12-15, 17] and demonstrated an improvement in diagnostic accuracy by reducing soft tissue

artefact and thus false-positives. Specificity and normalcy (the number of normal scans in patients at low risk of coronary artery disease [CAD]) were the most commonly improved parameters[18]. AC has also been shown to improve the detection of myocardial viability[8, 19]. The American Society of Nuclear Cardiology and the Society of Nuclear Medicine issued a joint statement in 2004 recommending the use of AC when available and technically feasible[20]. Since this time, the number of studies evaluating AC has increased[10, 11, 16, 21-23], although X-ray CT attenuation correction (CTAC) has become the predominant focus[11, 16, 21, 22].

More recently, the true value of AC in MPS has been questioned. In a study comprised of men and women of low and high BMI, no difference was observed in sensitivity, specificity or normalcy for detection of significant CAD when using AC[24]. This result is part of conflicting data that both supports[10, 17] and refutes[6] the use of AC in those with high BMI. Studies in women, in whom breast attenuation artefact is likely to be a significant issue, have suggested little or no improvement in either specificity or normalcy using AC[21, 25, 26]. The multi-centre SPAG study showed that AC improved specificity in overweight men but not in other groups; sensitivity was frequently reduced[27]. Even in studies reporting overall benefit of AC, subanalysis suggests that although normalcy improves, the ability to detect multi-vessel CAD declines[12]. It is possible that improvements in non-corrected reconstruction algorithms as well as the use of normal reference databases have rendered AC less important. The experience of the reader also plays an important part in the value of AC. Those with less experience are more likely to mistake attenuation artefact for real perfusion abnormalities and thus have more to gain from algorithms which

correct these artefacts to normal[16]. Those who have substantial experience in reading around attenuation artefacts show little improvement in normalcy when viewing AC images[16]. AC may only be useful, therefore, as a training tool to improve awareness of inexperienced reporters. AC may have a role in patients in whom attenuation artefact on stress imaging mandates rest imaging in order to exclude real disease. AC and subsequent normalisation of the stress images may negate the need for rest imaging, improving the efficiency of the nuclear imaging service whilst also reducing radiation dose to the patient[28-30].

1.4.4 Gaps in Research

Head-to-head comparisons of AC methods are lacking, with most studies limited to comparison of the chosen AC technique against non-corrected images. These comparisons have often been performed blind to clinical information, which is necessarily disadvantageous to the identification of artefact on non-corrected images. CTAC is theoretically best as X-ray energy can be tailored to the patient, image quality is not degraded by downscattering and there is no need to regularly replace the AC photon source. However, the possibility of misregistration of emission and transmission scans remains a concern. Further, CTAC radiation exposure, although small in relation to the MPS study, is around 50 times greater than that received from radionuclide AC. Finally, although either AC technique may technically improve images, the ultimate effect on report and reporter confidence may be negligible, indicating little clinical utility. There remains, therefore, a pressing need for a prospective, clinically-informed comparison of CTAC and radionuclide AC methods.

1.5 APPLICATIONS OF MULTISLICE X-RAY COMPUTED TOMOGRAPHY

1.5.1 Background

MSCT is now used widely for non-invasive coronary angiography (CTA). Initial data suggested good agreement between CTA and invasive coronary angiography for the assessment of obstructive CAD[31-33]. More recent data has shown that the ability of CTA to classify the severity of CAD when present is rather more limited than first appreciated[34, 35], reinforcing the notion of CTA as a rule-out test. Ironically, this shift in attitude reflects effects of improved scanner technology on CTA image quality. Early publications demonstrated high sensitivity and specificity for detection of significant CAD but based their results on data excluding 'unassessable' segments, reflecting the relatively poor temporal resolution of 16-slice MSCT. One such study excluded 24% of coronary segments from analysis[36]. Furthermore, limited spatial resolution led to outright exclusion of coronary artery segments below 1.5-2mm in diameter. Published performance therefore reflected the ability of CTA to assess large coronary arteries on high quality images only. As detector-row numbers have increased, there has been a concomitant increase in image quality stemming from improved spatial and temporal resolutions, resulting in both fewer unassessable segments and assessment of the entire coronary tree regardless of diameter. Recent data therefore offers a more realistic evaluation of CTA as a diagnostic test, with meta-analysis suggesting sensitivity and specificity of 81% and 93% respectively for detection of significant CAD by CTA and positive and negative predictive values of 68% and 97% respectively[37]. Very recent data using 320-slice CTA has suggested

maintained sensitivity and specificity (78% and 98% respectively at segment-level) but with significantly reduced effective radiation exposure[38].

The standard CTA dataset contains more than just coronary artery data. The use of additional parameters, such as functional ventricular assessment, has been shown to improve sensitivity of tests such as MPS[39] and it is likely that this concept applies equally to CTA. Assessment of global and regional left ventricular (LV) function is possible using CTA data and compares well with other techniques[40, 41]. At present, ventriculography is possible only using retrospective ECG gating. In this mode, the timing of each count registered by the detectors is compared with a simultaneously recorded surface ECG. By separating the acquired data in this way, it is possible to evaluate cardiac images in different phases of the cardiac cycle and thus assess regional and global LV function. As CTA requires only a portion of the cardiac cycle (usually end-diastole), prospectively triggered scans have become more commonplace in order to limit patient exposure. As the X-ray beam is active for only a portion of the cardiac cycle, ventriculography is not possible except on newer high-specification scanners.

Beyond ventriculography, CCT has the capacity to detect myocardial scarring and, by implication, quantify myocardial viability. The extent of myocardial scarring is an important indicator of prognosis[42-45]. Many techniques may be used to demonstrate myocardial viability, including cardiovascular magnetic resonance (CMR) and SPECT MPS, but the role for CCT in this setting remains undefined. Recent work has demonstrated that conventional iodinated X-ray contrast media show delayed

uptake into areas of myocardial scar[46-48]. If such a phenomenon were found consistently, it may be possible to perform coronary angiography and assess myocardial viability during the same scan session.

1.5.2 Contrast Kinetics of Intravenous Iodinated Contrast Media

Iodinated X-ray contrast agents are water soluble, do not undergo metabolism and are excreted unchanged by the kidneys[49]. The small size of the contrast molecule (~770Da for Iomeprol), coupled with its water solubility, permits free distribution of contrast across the vascular endothelium and thus between the intravascular extracellular space (blood pool) and the extravascular extracellular space (interstitium). It does not accumulate within intact cells. Contrast distribution may be described simply according to the two-compartment model (Figure 1.8).

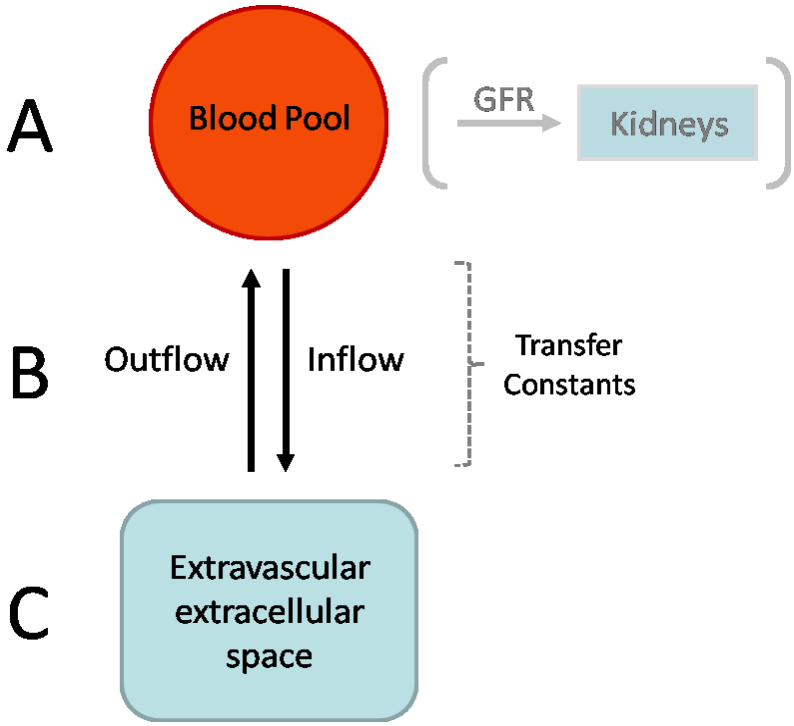


Figure 1.8 *Two compartment model of contrast distribution. Contrast diffuses freely between blood pool (A) and extravascular extracellular space (C) according to concentration gradient and inflow/outflow transfer constants (B). Concentration gradient across (A) and (C) increases with administered contrast volume, leading to greater accumulation of contrast in (C). Assuming normal renal function, there is constant reduction in blood pool contrast concentration proportional to glomerular filtration rate (GFR). The transfer constants (B) are dependent on factors such as microvascular function and functional capillary density. Adapted from* [49].

After myocardial infarction (MI), alterations in inflow and outflow constants (Figure 1.8B) and the extravascular extracellular space (Figure 1.8C) may be exploited for the purposes of imaging. Acute MI is characterised by microvascular plugging, myocyte membrane rupture and interstitial oedema. These characteristics are present in variable proportions and extent depending on the delay in institution and adequacy of reperfusion therapy. Regardless, microvascular dysfunction may be present in 30-60% of patients even after successful restoration of perfusion[50]. Microvascular plugging and dysfunction lead to impairment of contrast exchange between the blood pool and extravascular extracellular space such that both inflow and outflow of contrast (Figure 1.8B) is delayed. There is therefore an initial delay in contrast enhancement, followed by hyperenhancement as the contrast is retained in the extravascular extracellular space[48]. Myocyte membrane rupture exposes the previously intracellular space to the extracellular environment, effectively increasing volume of extravascular extracellular space into which contrast can distribute. Interstitial oedema swells the extravascular extracellular space further still, increasing volume of contrast distribution and promoting accumulation within the zone of myocardial necrosis.

Maturation of the myocardial infarct is characterised by resolution of interstitial oedema and replacement of ruptured myocytes by collagenous scar. The extracellular space within collagenous scar remains expanded but the affected territory contracts, reducing myocardial thickness. The lack of viable myocardium leads to a dramatic fall in functional capillary density, which in turn delays inflow and outflow of contrast. Contrast kinetics within acute and chronic MI are therefore

similar (early hypoenhancement, delayed hyperenhancement), although the underlying microvascular and ultrastructural changes are different.

Delayed enhancement of myocardial scarring in animal models typically occurs around 5 minutes after contrast injection and persists for around 40 minutes[51, 52]. In humans, delayed-pass images have successfully demonstrated enhancement when performed 7 to 10 minutes after contrast bolus administration[47, 52]. Delayed enhancement in the animal model is optimal when a slow-flow infusion of contrast is given after the main bolus injection[53]. This protocol does not yet have demonstrated utility in humans.

1.5.3 Clinical Value of Delayed Enhancement of Myocardial Scarring

The clinical importance of delayed enhancement has been described mainly with gadolinium-enhanced CMR. Delayed enhancement on CMR correlates with histopathologically-defined MI[54], non-viability defined by SPECT MPS and dobutamine stress echocardiography[55] and with clinical indices of acute MI[56]. Larger areas of early hypoenhancement and delayed hyperenhancement in patients after acute MI correlate with higher rates of short and medium term adverse cardiovascular events and a higher likelihood of adverse left ventricular remodelling[57, 58]. In the chronic setting, delayed hyperenhancement implies myocardial scarring and thus irreversible dysfunction, whilst absence correlates with viability on SPECT MPS[55] and, in the presence of impaired contractile function, predicts the likelihood of functional recovery after coronary revascularisation[59, 60].

Assessment of delayed enhancement has the potential to go beyond simply predicting prognosis in general or predicting benefit from revascularisation. Delayed enhancement on gadolinium CMR may be used to plan optimal LV lead placement during cardiac resynchronisation therapy, with CMR-guided placement to areas without transmural myocardial scarring associated with fewer hospitalisations for heart failure and episodes of sudden cardiac death[61]. Similar findings have been demonstrated using MPS[62] and there is every reason to suppose that delayed CCT (dCCT) may offer similar benefits.

1.5.4 Gaps in Research

Although the evidence for the utility of delayed hyperenhancement has been obtained using gadolinium-enhanced CMR, the similarities in contrast kinetics between iodinated and gadolinium based contrast media have been confirmed[52]. Delayed CCT has been investigated in the setting of acute MI, usually after contrast administration in the cardiac catheterisation laboratory, with promising results[63, 64]. However, the real value of quantifying myocardial scarring is in the chronic setting to determine of likelihood of functional recovery of the myocardium after revascularisation. There is a paucity of data comparing delayed-pass CCT prospectively against established techniques for detection and quantitation of chronic myocardial scarring.

The advent of dual-energy dCCT (DE-dCCT) has led to potential improvement in detection of myocardial scarring[65-67]. Available only on higher-specification CT scanners, DE-dCCT exploits the dependence of the mean attenuation coefficient of

tissue on X-ray beam energy. Two X-ray beams are emitted simultaneously, each with different beam energy. Low- and high-density structures, such as normal and contrast-enhanced tissue respectively, respond differently to the 2 beam energies. Responses are measured at the detectors and allow image reconstruction using attenuation coefficients derived from the two X-ray beams in isolation and combined. This enables selective enhancement of tissues with, for example, high iodine density. This benefits tissues that are contrast-enhanced, particularly when contrast resolution is small compared with unenhanced tissue, as is the case with delayed enhancement of myocardial scarring. The technique has research value only at present, but is promising.

1.6 AIMS OF THESIS

The aim of this thesis is to investigate the usefulness of CCT in evaluating the LV myocardium. The thesis is split into 3 sections. In Section One (chapters 3-4), single slice X-ray CT is evaluated as a method for correcting SPECT MPS for attenuation artefact and compared with reporting strategies that use either no AC or an alternative form of commercially available AC (gadolinium-153 line source AC). In Section Two (chapters 5-11), 64-slice CT is used to quantify myocardial scarring and LV function and compared with SPECT MPS for common myocardial parameters, as outlined below. Section Three (chapters 12-14) looks at preliminary data for the comparison of DE-dCCT and CMR for quantification of myocardial scarring.

Specific aims are as follows:

- To assess the effects of CT and gadolinium-153 line source AC on summed stress and resting MPS scores **(Chapter 3)**
- To compare reporter confidence in SPECT MPS without AC and after X-ray computed tomography (CTAC) and gadolinium-153 (GdAC) attenuation correction **(Chapter 4)**
- To compare final clinical report and interobserver agreement between reporting strategies using CTAC, GdAC and no AC **(Chapter 4)**
- To evaluate a small pilot study using different contrast protocols and X-ray tube settings for 64-slice CT evaluation of chronic MI in comparison to SPECT MPS **(Chapter 5)**
- To compare visual analysis of early and delayed myocardial enhancement patterns on CCT with SPECT MPS in patients with previous MI **(Chapter 6)**
- To quantify early and delayed segmental myocardial intensity in patients with previous MI and evaluate the usefulness of their ratio (delayed enhancement ratio, DER) as a measure of chronic MI on SPECT MPS **(Chapter 7)**
- To compare end-systolic and end-diastolic phase CCT for accuracy at detecting chronic MI on MPS **(Chapter 8)**
- To evaluate the accuracy of images reconstructed with medium-smooth and smooth reconstruction kernels for detecting chronic MI on MPS **(Chapter 9)**
- To quantify segmental myocardial thickness on CCT as a marker of transmurality of MI on MPS **(Chapter 10)**
- To compare global and regional LV functional parameters between CCT and SPECT MPS **(Chapter 11)**

- To evaluate visual analysis of DE-dCCT images for the diagnosis of chronic MI on CMR in patients with previous MI **(Chapter 12)**
- To estimate inter- and intraobserver agreement for visual analysis of DE-dCCT **(Chapter 12)**
- To quantify segmental myocardial thickness on dual-source CCT as a marker of scar transmurality on CMR **(Chapter 13)**
- To compare global and regional LV functional parameters between dual-source CCT and CMR **(Chapter 14)**
- To estimate inter- and intraobserver agreement for regional LV function on dual-source CCT **(Chapter 14)**

CHAPTER 2 GENERAL METHODS

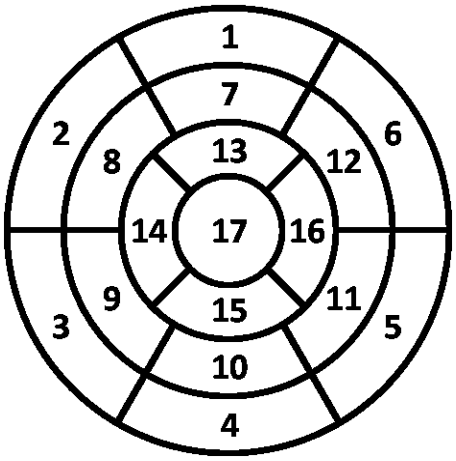
2.1 INTRODUCTION

The following chapter outlines standard principles and protocols for imaging investigations used in succeeding parts of this thesis. Where relevant, certain sections in succeeding chapters will refer back to this chapter to avoid repetition.

2.2 STANDARDISED SEGMENTATION OF THE LEFT VENTRICLE

The American Heart Association (AHA) 17-segment model provides a standardised reporting scheme that can be used across cardiac imaging modalities[68]. The left ventricular (LV) myocardium is divided into 6 basal, 6 mid and 4 apical ventricular segments, as well as a single segment representing the LV apex (Figure 2.1). This scheme is used for assessment of segmental perfusion, enhancement and function, as described below.

Despite its usefulness for inter-test and inter/intraobserver comparisons, the AHA model is cumbersome clinically. Reporting individual segments is only necessary for small abnormalities requiring accurate localisation. It is often more practical to report abnormalities according to correspondence to typical coronary artery territories as this allows direction of subsequent treatment. For example, inducible ischaemia might be reported as affecting 'much of the right coronary artery territory' rather than according to specific segments. This indicates functional significance, allows the referrer to plan appropriate treatment and is the essence of clinically relevant reporting.



Basal		Mid		Apical	
1	Anterior	**7**	Anterior	**13**	Anterior
2	Anteroseptal	**8**	Anteroseptal	**14**	Septal
3	Inferoseptal	**9**	Inferoseptal	**15**	Inferior
4	Inferior	**10**	Inferior	**16**	Lateral
5	Inferolateral	**11**	Inferolateral	**17**	Apex
6	Anterolateral	**12**	Anterolateral		

Figure 2.1 *American Heart Association 17-segment model of the human heart.*

The 17-segment model is arranged according to typical coronary territories as shown in Figure 2.2. There is variation of coronary distribution, most importantly in the vessel that supplies the inferior wall (the 'dominant' coronary artery), which, in 85% of individuals, is the right coronary artery (RCA). For the large majority of the remaining 15% of individuals, the left circumflex artery (LCx) supplies this territory; in a small proportion, both right coronary and left circumflex arteries supply this area (co-dominance). Despite this uncertainty, summing individual segments into coronary territories improves clinical relevance as described and allows better correlation of imaging findings across techniques. In this thesis, RCA dominance was assumed.

A second strategy for combining segments in image analysis involves segmentation of the LV myocardium into anteroapical, septal, inferior and lateral myocardial walls (Figure 2.3). This is relevant for distinguishing attenuation artefacts from real perfusion abnormalities. The combination on MPS of reduced counts inferiorly with normal wall motion and thickening is the hallmark of diaphragmatic attenuation artefact. This is similarly true of the anteroapical wall in breast attenuation artefact. Apparent inducible perfusion abnormalities may be seen in the septum in patients with severe obstructive airways disease stressed with dobutamine. Whether this represents an artefact or a true inducible abnormality remains a matter for debate, but its location is typical and presence understood to be unrepresentative of obstructive CAD. Regionalising segments into myocardial walls therefore has value for clinical reporting.

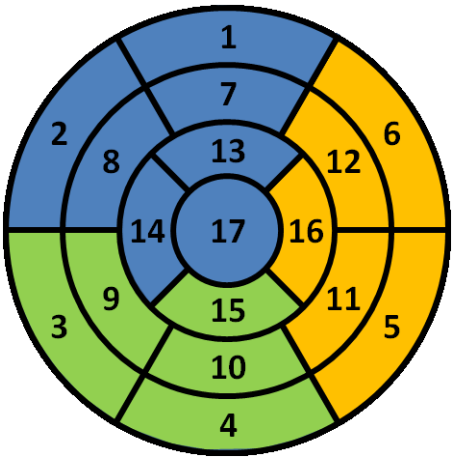


Figure 2.2 *Typical coronary artery territories over the AHA 17-segment model, assuming RCA dominance. The left anterior descending territory (blue area) consists of segments 1, 2, 7, 8, 13, 14 and 17; LCx territory (yellow area) segments 5, 6, 11, 12 and 16; and RCA territory (green area) segments 3, 4, 9, 10 and 15.*

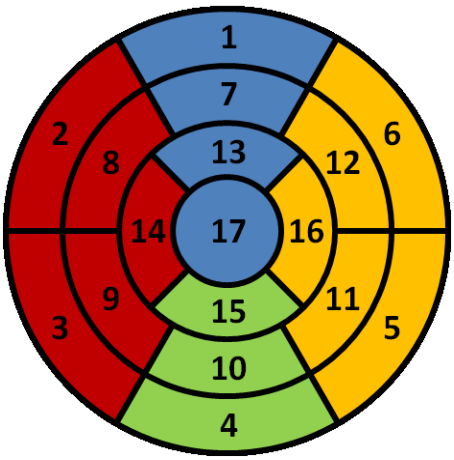


Figure 2.3 *Regionalisation of the American Heart Association 17-segment model into myocardial walls, defined as follows: anteroapical wall (blue area) segments 1, 7, 13, 17; septum (red area) segments 2, 3, 8, 9, 14; inferior wall (green area) segments 4, 10, 15; and lateral wall (yellow wall) segments 5, 6, 11, 12, 16.*

2.3 MYOCARDIAL PERFUSION SCINTIGRAPHY

2.3.1 Stress protocol

All patients underwent pharmacological vasodilator stress using adenosine infused at 140mcg/kg/min for 6 minutes, with injection of radiotracer after 3 minutes to ensure maximum myocardial hyperaemia. During infusion, low level bicycle exercise up to 75W was undertaken. This increases sympathetic vascular tone and limits the effects of adenosine-mediated peripheral vasodilatation[69]. In addition, it reduces splanchnic blood flow and hence hepatobiliary excretion of technetium-99m[69], minimising extracardiac activity and improving MPS image quality.

2.3.2 Image acquisition parameters

Stress-rest/reinjection protocol using technetium-99m tetrofosmin was used in all cases, with radionuclide dose dependent on patient weight. Stress and resting doses were 250MBq/750MBq respectively for patients <100kg and 350MBq/1050MBq respectively otherwise. Image were acquired ~40 minutes after respective tracer injections, with allocation of camera order as appropriate (Chapters 3 and 4). Median interval between stress and resting tracer injections was 120 minutes (IQR 119-124 minutes). MPS images were acquired using single photon emission computed tomography (SPECT) – 64 planar projections of ~30 seconds each, each reconstructed using iterative reconstruction. SPECT reconstructions were manually aligned along the axis of the left ventricle to produce vertical and horizontal long axis and short axis tomograms for both summed perfusion and gated data. Raw data and sinograms were reviewed for motion artefact and corrected as necessary.

2.3.3 Attenuation Correction Methods

<u>Computed Tomography Attenuation Correction</u>

Clinical scans were performed on a general purpose gamma camera (Infinia Hawkeye, General Electric Medical Systems). CTAC images were acquired (2 rotations/minute, 40 slices, 10mm thickness) immediately after MPS acquisition within the same scan period. Tube voltage and current were 140kV and 2.5mA respectively, resulting in an effective radiation exposure of 1mSv. All studies were checked after acquisition to ensure proper registration of perfusion images and

attenuation map. Misregistration was corrected by manual realignment in 3 dimensions as required (see Figure 1.7).

^{153}Gadolinium Line Source Attenuation Correction

Research scans were performed on a general purpose gamma camera (ADAC Forte Vantage, Philips Medical Systems) equipped with two ^{153}Gd line sources (1.94GBq total). Quality control images were acquired for each patient to ensure adequate transmission radionuclide activity. Transmission scans consisted of 32 frames each acquired for either 44 seconds (stress) or 59 seconds (rest). Simultaneous transmission and emission acquisition negated the need for registration correction. Total research exposure was <0.02mSv, representing an excess risk of fatal cancer induction of $1x10^{-6}$.

2.3.4 Reporting protocol

MPS images were reported in standard order (see Figure 4.1). Raw data was reviewed to confirm the presence or absence of artefact (motion, breast, diaphragmatic, extracardiac), followed by stress and rest summed perfusion images, uncorrected or corrected for motion as necessary. If relevant to the study, AC images were reviewed next, followed finally by gated images.

2.3.5 Reporting summed perfusion images

Raw data was reconstructed as above and presented as both polar plots and splash images, which show contiguous cuts in the horizontal long axis, vertical long axis and short axis (Figures 2.4 and 2.5).

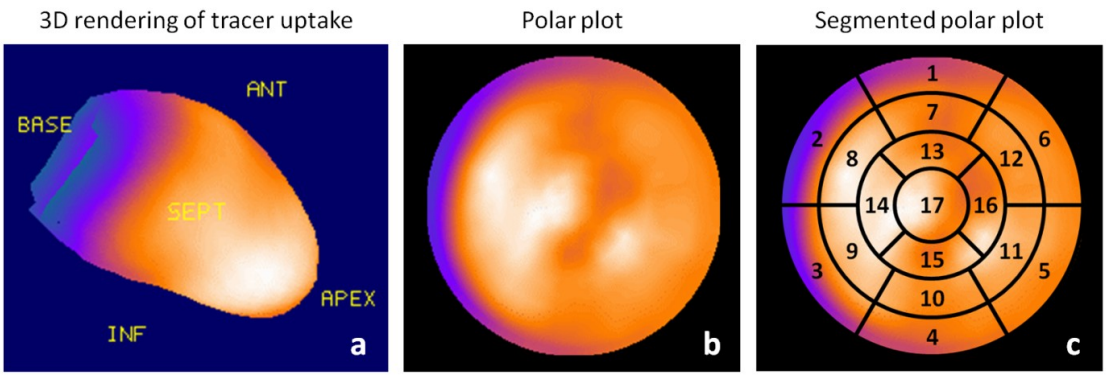


Figure 2.4 *Representation of myocardial tracer uptake (a) as a polar plot (b), which shows the apex in the centre, basal segments outermost and mid segments in between. The 17-segment AHA model is overlaid in panel (c).*

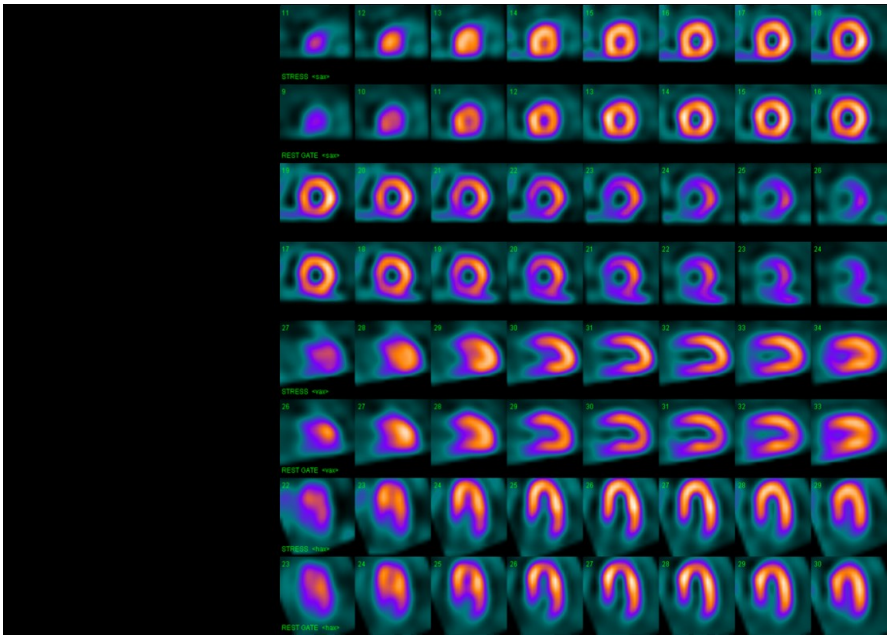


Figure 2.5 *Myocardial perfusion images presented in splash format. Short and long axis views are generated by defining a centreline through the LV cavity from mitral valve level down to apex. Stress images are represented in the 1st, 3rd, 5th and 7th rows, whilst the remaining rows show resting images.*

Tracer uptake was scored visually, semi-quantitatively and qualitatively. Visual tracer uptake scores were either normal, mildly reduced, moderately reduced, severely reduced or absent. Uptake categories were assigned numerical values to allow calculation of summed scores for stress and resting images, which provide a global measure of severity and extent of tracer uptake abnormalities. In this thesis, variation in departmental preferences for scoring uptake resulted in two systems, each using a 5 point scale from 0 to 4. For data presented in Section One, segments with normal uptake were assigned a value of 4, mildly reduced uptake 3 and so on, with those segments showing absent uptake scoring 0. A normal study would therefore score 68. In Sections Two and Three, segments were scored in the opposite order – normal uptake scoring 0, mildly reduced uptake 1 and so on up to absent uptake scoring 4. A normal study would therefore score 0. Segments considered to have artefactually altered tracer uptake had scores adjusted up or down depending on the perceived impact of the artefact – e.g. apparently reduced tracer uptake considered to be wholly artefactual was scored as normal. Semi-quantitative scoring was calculated according to proportional segmental uptake compared to the maximum pixel value within the LV contours defined during reconstruction. This value may be displayed according to a variable colour scale where typically white is 100% maximum uptake and black is absent uptake, with colours in between representing proportions within this range (Figure 2.6). This process – 'normalisation' – assumes that at least one pixel within the LV myocardium has normal tracer uptake to which all other areas may be scaled. Mean uptake scores can be compared on a segmental basis. This scale can be converted into a qualitative scale according to the following scheme: >70% uptake – normal; 50-69%

uptake – mild reduction; 30-49% uptake – moderate reduction: 10-29% - severe reduction; and <10% - absent uptake.

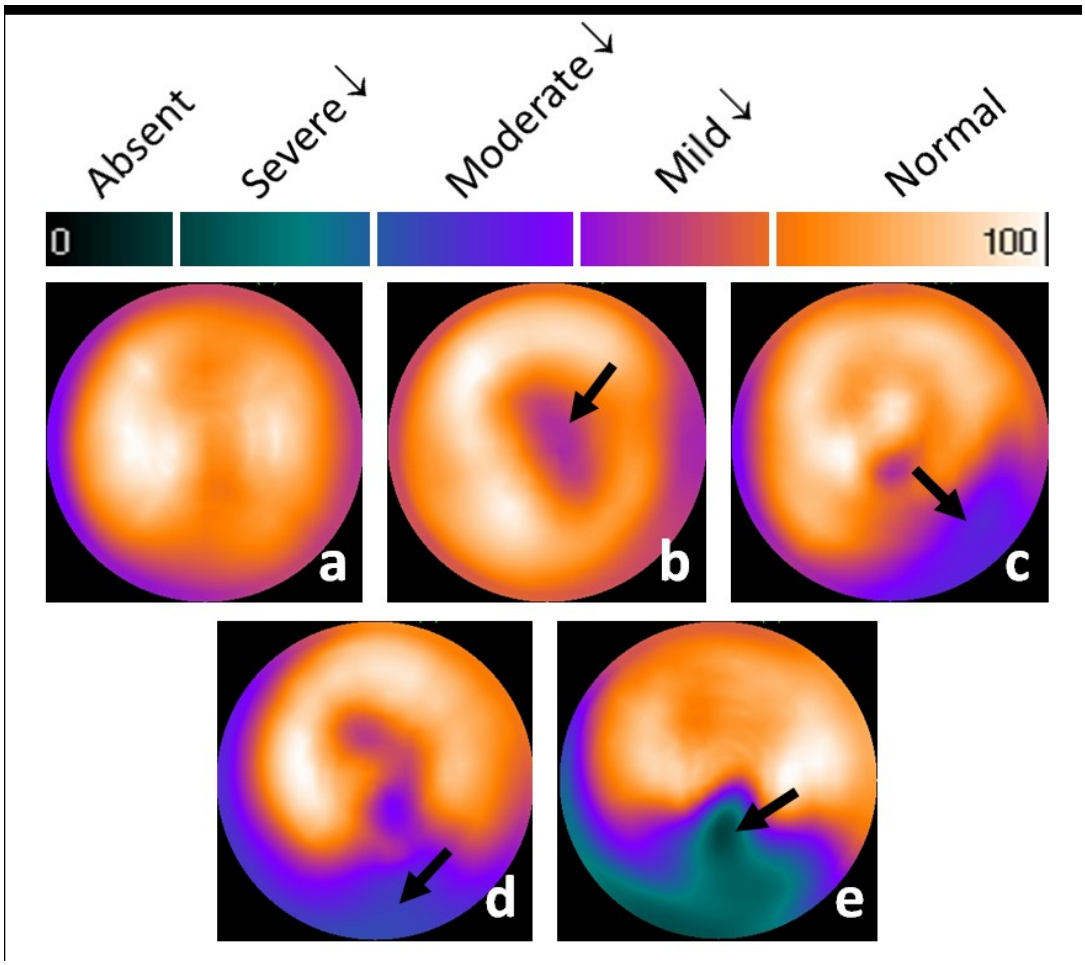


Figure 2.6 *Classification of myocardial perfusion abnormalities. (Top) Normalised colour scale with divisions for qualitative tracer uptake categories. (a) Normal. (b-d) Mild, moderate and severe reductions (arrows). (e) Absent uptake (arrows).*

2.3.6 Summary clinical report of perfusion images

2 categorical systems for reporting MPS images were defined and used as appropriate to the study.

Chapters 3-4: Attenuation correction studies

4 categories of study report were used: pure ischaemia, pure MI, mixed ischaemia/infarction and normal. Apparently reduced tracer uptake considered to be artefactual was dealt with as above. Pure ischaemia was defined as ≥1 segment with inducible perfusion abnormalities and absence of resting abnormalities. Pure MI was defined as ≥1 segment of abnormal resting perfusion and no inducible abnormalities. Mixed ischaemia/infarction consisted of any combination of ischaemia and MI, whilst a normal report required absence of true tracer uptake abnormalities.

Chapters 5-11: Assessment of myocardial scarring

Segments were categorised on resting MPS as either normal or showing mildly reduced, moderately reduced, severely reduced or absent tracer uptake. Segments with mildly reduced tracer uptake were classified as showing non-transmural MI. Those with at best moderately reduced uptake (i.e. <50% resting tracer uptake) were classified as showing transmural MI, in line with accepted definitions of non-viable myocardium on SPECT MPS[70].

2.3.7 Reporting gated images

MPS data is acquired in combination with a surface electrocardiogram, with counts assigned to one of 16 phases of the cardiac cycle. Summed perfusion images

represent the combination of all 16 datasets, providing an image of myocardial perfusion averaged over the cardiac cycle. Any of the 16 individual datasets can be viewed in isolation. It is assumed that the brightest counts are in the mid-myocardium, and various models are used to generate epicardial and endocardial contours from the derived mid-myocardial contour. As an endocardial surface is generated, it is possible to calculate LV volumes provided the level of the mitral valve annulus is defined. When applied to all 16 frames, the highest and lowest volumes represent end-diastolic and end-systolic volumes respectively, enabling calculation of LV ejection fraction. Regional movement of the endocardial surface (Figure 2.7) is representative of regional myocardial wall motion, which can be evaluated according to the 17-segment model, as described above. When frames are viewed in series, mid-myocardial counts vary across the cardiac cycle and are proportional to LV wall thickness. Changes therefore represent regional LV wall thickening. Regional wall motion and thickening were scored qualitatively as being either normal; mildly, moderately or severely reduced; or absent. Dyskinetic wall motion, defined as motion in the opposite direction to normal, was also scored.

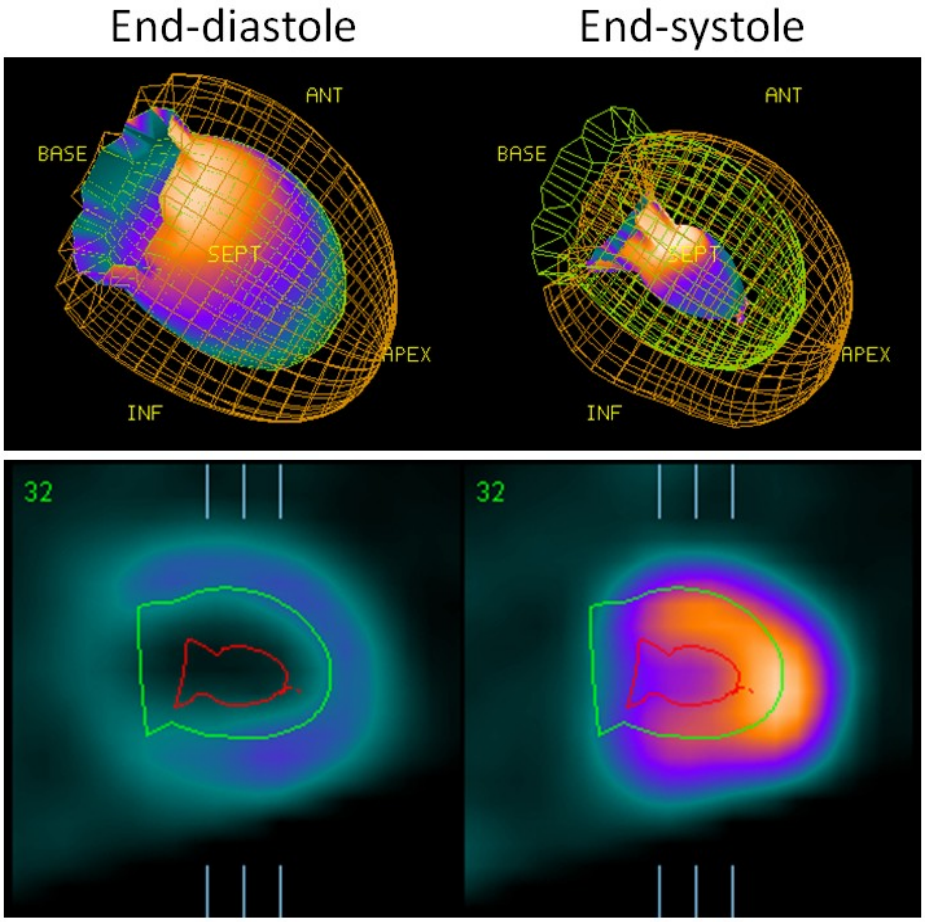


Figure 2.7 *Gated SPECT myocardial perfusion scintigraphy. The left and right columns show end-diastolic and end-systolic frames respectively, with the calculated endocardial surface (top left and right) allowing calculation of end-diastolic and end-systolic volumes respectively. The vertical long-axis slices (bottom) allow analysis of regional wall motion, which can be analysed semi-quantitatively by comparing end-diastolic and end-systolic contours (green and red lines respectively). Comparison of counts between images also allows assessment of wall thickening; there is a clear increase in counts between frames, indicating normal wall thickening.*

2.4 MULTISLICE CARDIOVASCULAR COMPUTED TOMOGRAPHY

2.4.1 Patient preparation

All patients signed written informed consent prior to undertaking research scans. Patients were scanned either in between the stress and resting stages of MPS (Chapters 5 – 11) or immediately after cardiovascular magnetic resonance imaging (CMR, Chapters 12 – 14). All patients were taking beta-blockers for secondary prevention of MI. Patients were weighed and cannulated via an antecubital vein (20G minimum).

2.4.2 Acquisition parameters

CCT images were acquired early after contrast injection and again 7 minutes later. Acquisition parameters were dependent on CT scanner. All scans were acquired during comfortable held inspiration.

64-slice CCT

Scans were performed on a 64-slice CT scanner with oscillating z-axis focal spot (Somatom Sensation 64, Siemens Medical Systems). Early and delayed acquisitions were performed using identical parameters: retrospective ECG gating, 32x0.6mm beam collimation, 0.33s rotation time, 0.2 pitch and CareDose 4D on. Tube current and voltage were varied for the pilot study (80kVp, 825 reference effective mAs; 100kVp, 460 reference effective mAs; 120kVp, 250 reference effective mAs), with the best combination taken forward for later studies. Dose constraints were dose-length product (DLP) 600mGycm and effective radiation dose 15mSv.

Dual-source CCT

Scans were performed on a dual-source 128-slice CT scanner with oscillating z-axis focal spot (Somatom Definition Flash, Siemens Medical Systems). Early acquisitions used identical parameters for each X-ray source, as follows: retrospective ECG gating, tube voltage 100kVp, tube current 120 quality reference mAs/rot, 128x0.6 mm collimation, 0.28s rotation time, pitch 0.23 for 60 bpm, and CareDose 4D on. Delayed acquisitions used a dual-energy technique: Tube A: 100kVp, 120 quality reference mAs/rot; Tube B: 140kVp with Sn filter, 102 quality reference mAs/rot). They were otherwise unchanged from early acquisitions. Dose constraints were DLP 900mGycm and effective radiation dose 18mSv.

2.4.3 Contrast protocols

Identical intravenous iodinated contrast medium was used for all CCT acquisitions (Ultravist 370, Bayer Healthcare Pharmaceuticals Inc). Patient weight was used to determine the required volume of contrast (see Chapter 5).

2.4.4 Acquisition timing

Early acquisitons were timed using a test bolus method (Figure 2.8). 15mL intravenous iodinated contrast is injected, followed by 10mL normal saline. Up to thirty 10mm-thick slices are acquired through the level of the carina at 1s intervals, with a region of interest placed in the ascending aorta. Scanning continues whilst the ascending aorta is observed for first enhancement and then washout of contrast. The scan is terminated as soon as initial washout is observed. Sequential contrast values in the ascending aorta are then graphed to calculate the time of peak aortic

enhancement. Three seconds are added to this time to account for the difference between ascending aortic and distal coronary artery enhancement. This interval is then used for the main acquisition. All delayed acquisitions were performed 7 minutes after main contrast bolus injection.

2.4.5 Image reconstruction

Raw data were reconstructed at the scanner console using proprietary software and two different reconstruction kernels. Kernels are mathematical functions that selectively enhance or smooth object boundaries during image reconstruction. Sharp kernels allow better edge detection at the expense of increased image noise. Smoother kernels blur object boundaries and reduce image noise but at the expense of spatial resolution. Different kernels therefore offer a trade-off between image noise and spatial resolution. In this thesis, two kernels are used, with the appropriate descriptor according to Siemens terminology provided in parentheses: medium-smooth (b35f) and smooth (b10f). The former is used for most CCT applications. However, reduction in tube current to maximise differential enhancement of myocardial scarring and normal myocardium increases image noise, implying that a reconstruction kernel that reduces image noise might be preferable.

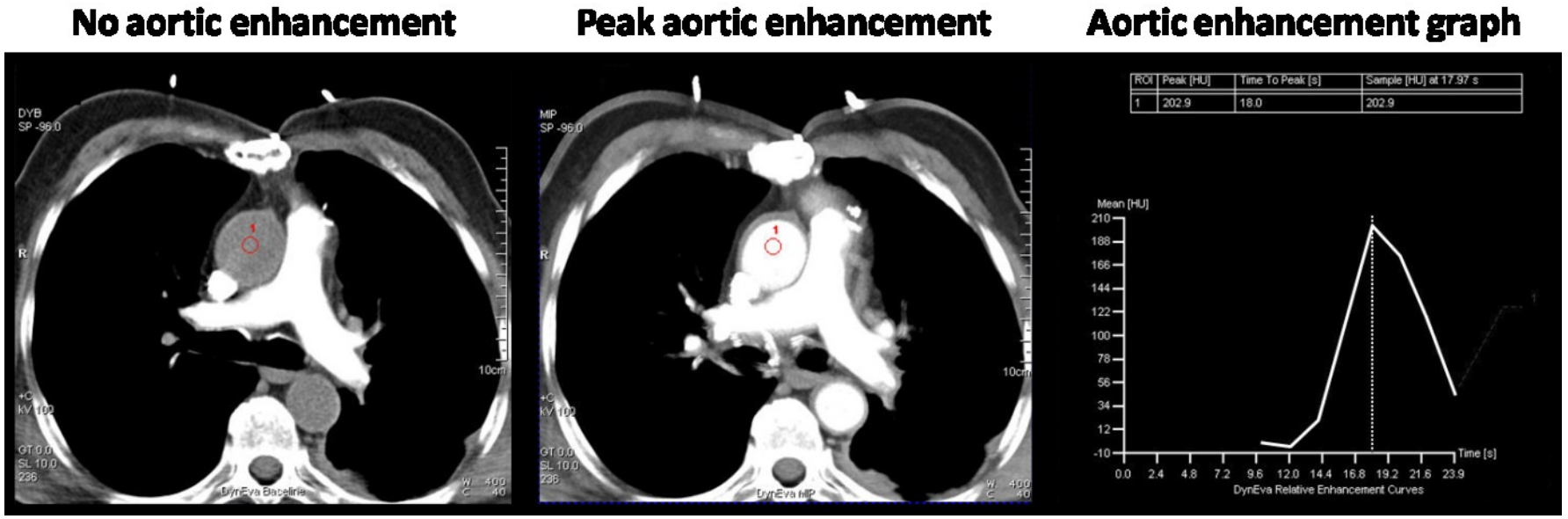


Figure 2.8 *Test bolus method for contrast timing. A region of interest is placed in the ascending aorta (red circle) and enhancement observed by the operator. The scan is terminated once contrast begins to wash out of the ascending aorta after peak enhancement. The time of peak aortic enhancement is derived by charting aortic enhancement against time, which is then used to determine the scan delay required for the main acquisition.*

2.5 CARDIOVASCULAR MAGNETIC RESONANCE IMAGING

All patients underwent clinical cardiovascular magnetic resonance imaging (CMR) using a 1.5T Siemens Sonata system (Siemens Medical Systems, Erlangen, Germany) according to published departmental protocols.[71] In brief, fast imaging with steady-state precession sequential short axis cines (8mm slice thickness, 2mm gap) was performed. An intravenous bolus of gadolinium-DTPA (Gd-DTPA, 0.1 mmol/kg) was injected and enhanced images acquired after at least 10 minutes using a segmented inversion-recovery sequence during diastole. Inversion times were optimized to null normal myocardium with images repeated in 2 separate phase-encoding directions to exclude artefact.[72] Image analysis is described in Sections 2.6.3 and 2.7.3.

2.6 ASSESSMENT OF GLOBAL AND REGIONAL LV SYSTOLIC FUNCTION

2.6.1 Cardiovascular CT

CT images were analysed by an investigator with >5 years experience in CCT using proprietary post-processing software (Aquarius Intuition, Terarecon Inc, San Mateo, USA). Eight phases were reconstructed at 10% increments from 25-95% of the R-R interval and loaded into a volumetric analysis software program (Time Volume Analysis, Intuition, TeraRecon Inc). The mitral and aortic valve planes were identified as boundaries of LV inflow and outflow respectively. A semi-automated thresholding algorithm was used to select voxels representing the LV blood pool, with manual adjustments as deemed appropriate (Figure 2.9). For any given phase, LV volume was calculated from the number of voxels above the threshold for LV blood pool,

with the largest and smallest representing the end-diastolic and end-systolic volumes respectively. Segmental myocardial wall motion and thickening were analysed qualitatively as described above for MPS.

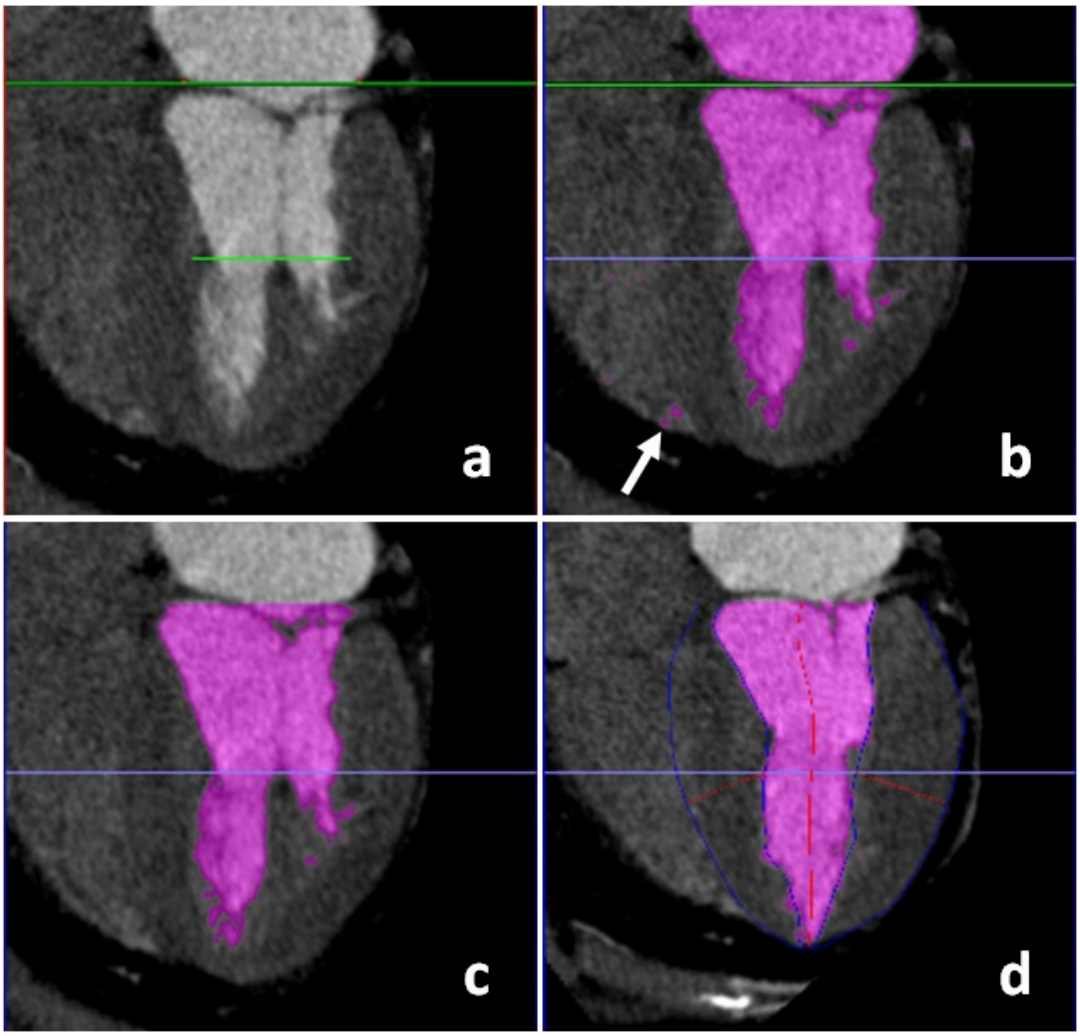


Figure 2.9 *Calculation of LV volumes on CCT. (a) The mitral valve plane is identified. (b) All voxels below the mitral valve plane with intensities greater than the threshold value are highlighted. The threshold can be manually adjusted to ensure optimal selection of the LV blood pool, although this may also lead to selection of non-LV*

voxels (arrow). (c) Any voxels not located within the LV are excluded. (d) Endocardial and epicardial contours are defined.

Quantitative regional analysis was also performed (Figure 2.10). The outer boundary of the thresholded volume represented the endocardial surface by definition. The epicardial surface was defined by manually tracing the outer LV surface at its boundary with epicardial fat. The distance between the epicardial and endocardial surfaces represents the myocardial thickness, which may be averaged over an individual myocardial segment to give mean segmental thickness. End-diastolic and end-systolic thickness (Th_{ED} and Th_{ES} respectively) may be compared to give percentage segmental thickening according to the following equation:

$$\frac{(Th_{ES} - Th_{ED})}{Th_{ED}} \times 100$$

Inward movement of the endocardial surface during myocardial contraction may also be used to calculate segmental ejection fraction, a quantitative measure of segmental myocardial wall motion.

2.6.2 Myocardial perfusion scintigraphy

This is described in section 2.3.7.

2.6.3 Cardiovascular magnetic resonance imaging

CMR images were analysed using proprietary software (CMR Tools, Cardiovascular Imaging Solutions) by an experienced observer blind to CT data according to standard clinical protocols. Epi- and endocardial contours were defined semi-automatically in end-systole and end-diastole on all short-axis slices, allowing calculation of LV volumes, global function and, by analysing according to the 17-segment model, regional LV function and segmental wall thickness. Regional function was scored in the same way as for CCT (Section 2.6.1).

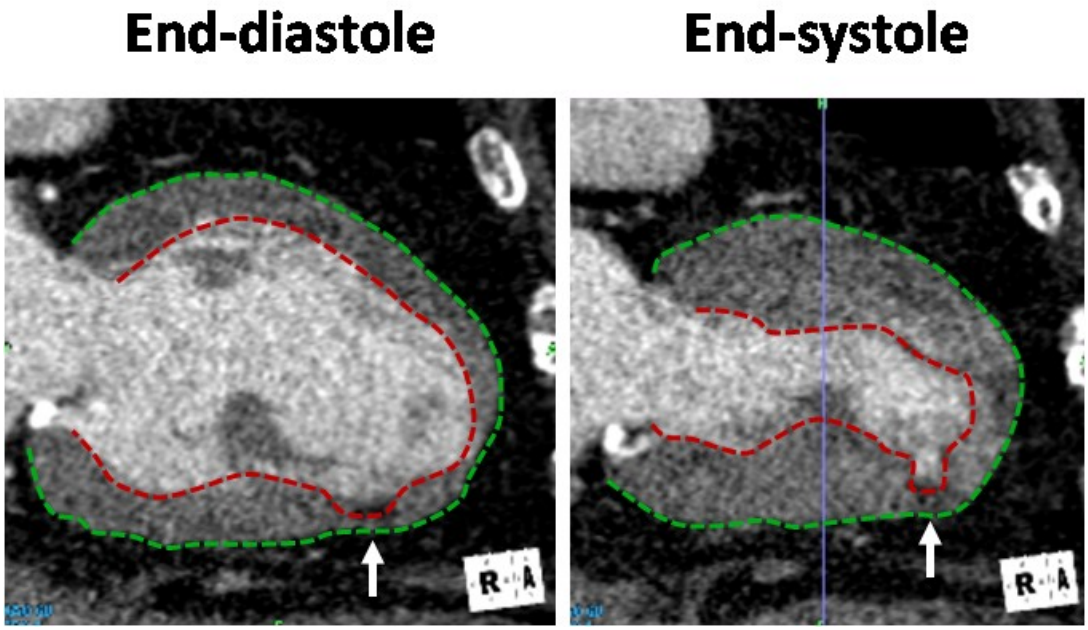


Figure 2.10 *Epicardial and endocardial contours on cardiac CT (green and red lines respectively). A small segment of full-thickness myocardial scarring can be seen in the apical inferior wall (arrow).*

2.7 QUANTIFICATION OF MYOCARDIAL SCARRING

2.7.1 Cardiovascular CT

Phases were reconstructed at 10% increments from 25-95% of the R-R interval. Both early and delayed datasets were analysed using proprietary cardiac software (Intuition, TeraRecon Inc, USA) as 5mm thick multiplanar reformatted images oriented into horizontal long, vertical long and short axis views. Delayed images were viewed using a window width and level of 150 Hounsfield units with manual adjustments as required. Where appropriate to the study (Chapters 12 – 14), single-energy and dual-energy CCT images were analysed in separate sessions and scored using the same technique.

Myocardial segments were defined according to the 17-segment model and scored qualitatively as iso-, hypo-, or hyper-enhanced on early and delayed images (Figure 2.11). Hypo- or hyperenhanced segments were scored as normal (score=0, absent), non-transmural (score=1, <50% transmural) or transmural (score=2, ≥50% transmural). Segmental scores were summed to give a CT summed scarring score (normal=0, maximum=34).

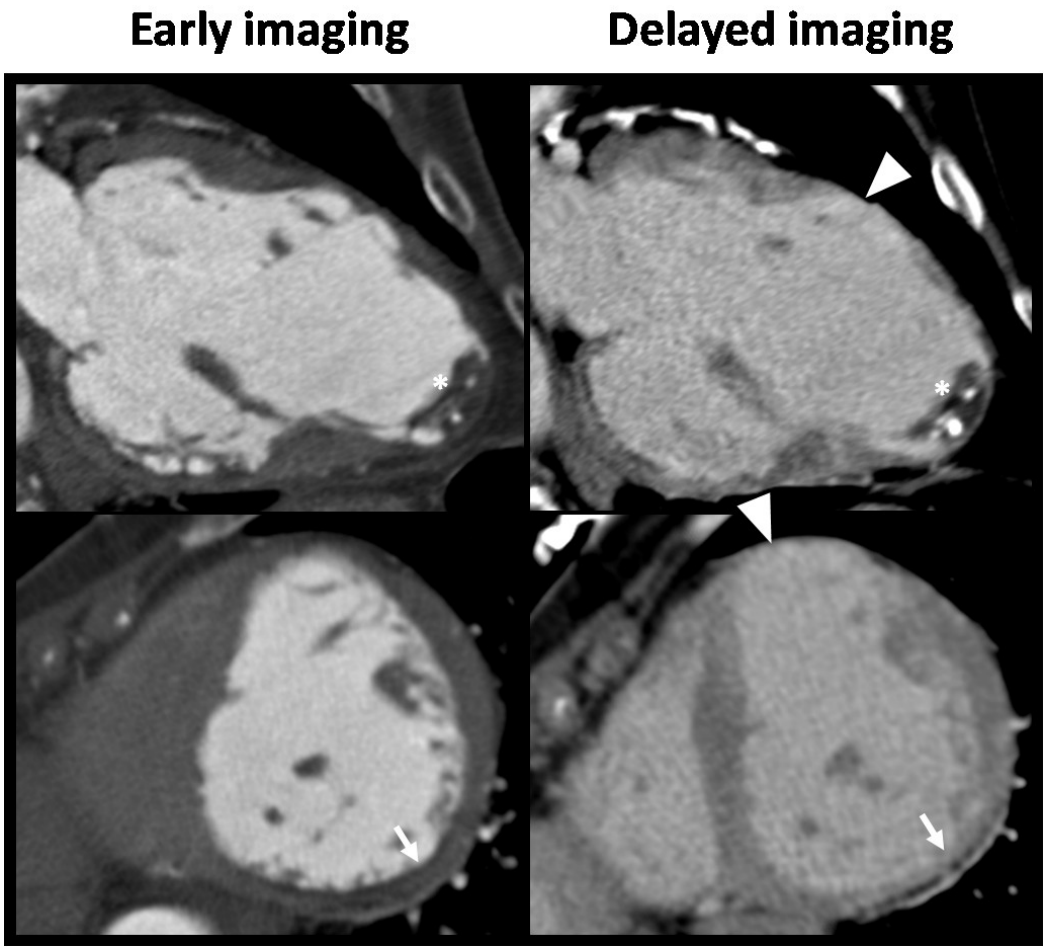


Figure 2.11 *Visual analysis of enhancement patterns of myocardial scarring on early (left) and delayed (right) imaging. Subendocardial hypo- and hyperenhancement is seen inferolaterally on early and delayed imaging respectively (arrows). In addition, there is transmural hyperenhancement in the mid and distal anterior wall on delayed imaging (arrowheads). Both images demonstrate apical thrombus (asterisk).*

For quantitative analysis, epicardial and endocardial contours were identified as in Section 2.5.1 and the resulting myocardial volume fitted to a 17-segment polar plot (Figure 2.12). Each segment was categorised according to mean segmental wall intensity (SWI, average HU value of all voxels within that segment) and myocardial thickness (see above). Identification of epicardial contours was straightforward on early and delayed images as contrast between myocardium and epicardial fat remained high for both. The endocardial contour was more difficult to identify on delayed imaging due to poorer LV blood pool enhancement and delayed myocardial enhancement. After initial processing, segmental myocardial thickness on delayed images was compared to that of the early images and delayed endocardial contour adjusted as necessary. Overall, there was no significant difference in segmental wall thickness between the early and delayed datasets (7.55±2.14mm vs. 7.64±2.11mm respectively, p=0.09), with an absolute mean difference of ~1.5 voxels (1.07mm [0.99 – 1.14mm]).

Early and delayed segmental wall intensities were recorded as absolute values. The ratio of the values was also calculated ([Delayed HU]÷[Early HU]) to give a delayed enhancement ratio (DER). This value is conceptually more appropriate than absolute values as it is self-adjusted for body mass index and image noise.

2.7.2 Myocardial perfusion scintigraphy

This is described in section 2.3.5 – 2.3.6.

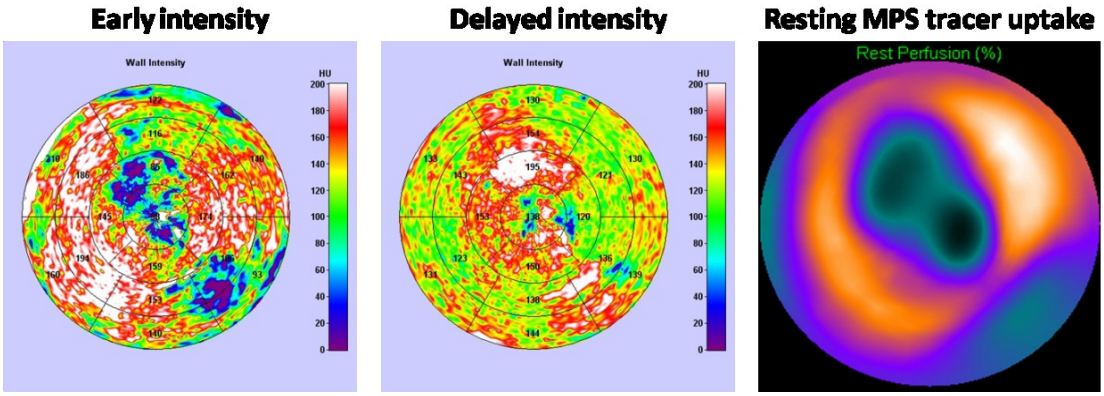


Figure 2.12 *Polar plots of mean segmental wall intensity (SWI) on early CCT (eCCT, left) and delayed CCT (dCCT, middle), with comparative resting MPS polar plot (right). On eCCT, myocardial scarring is hypoenhanced and shows as areas of low SWI (purple areas). The opposite is true on delayed imaging (white/red areas). The affected areas are identical to the areas of reduced tracer uptake on MPS.*

2.7.3 Cardiovascular magnetic resonance imaging

CMR images were acquired at least 10 minutes after Gd-DTPA injection and reconstructed in the end-diastolic phase. LGE patterns were segmented according to the AHA 17-segment model and scored according to transmural segmental involvement as follows: 4=normal; 3=<25%; 2=25-49%; 1=50-74%; and 0=>75%. Segmental scores were summed to give a CMR LGE summed score. Segments were further classified as showing non-transmural myocardial scarring if LGE showed <50% transmurality; those with >50% transmural LGE were classified as demonstrating transmural scarring.

2.8 STATISTICS

All data were analysed using MedCalc statistical software (version 12.2.1.0, MedCalc Software). Unless otherwise specified, $p<0.05$ was considered significant. Exceptions include Bonferroni correction for multiple testing where necessary: $p<(0.05/n)$ where n indicates the number of pair-wise tests performed.

2.8.1 Testing data for normality

Comparisons of parametric (normal) and non-parametric data require different tests. Application of statistical tests that assume normality to non-parametric data lead to unreliable p-values and thus erroneous interpretation of results. Certain data, such as any categorical classification, are obviously non-parametric. Recognition of distribution for continuous datasets is less straightforward and requires formal testing. In this thesis, continuous datasets were tested for goodness of fit to normal using the D'Agostino-Pearson test, which requires no pre-specification of mean or variance of the sample distribution. The test measures skewness and kurtosis and allows acceptance of the null hypothesis that the distribution is significantly different from normal if $p>0.05$. Where this is the case, non-parametric testing is required.

2.8.2 Comparison of parametric and non-parametric data

For normal data, Students t-test and analysis of variance (ANOVA) were used to test hypotheses. The former was used for individual group comparisons, using either paired or unpaired versions of the test as appropriate. ANOVA was used to compare multiple groups and, where significant differences in variance were found, post-hoc testing was used to identify group differences.

Non-parametric data were analysed using Mann-Whitney and Wilcoxon sign-rank tests for unpaired and paired comparisons respectively. Multiple groups were analysed using the Kruskal-Wallis (unpaired data) or Friedman (paired data) tests. Binary non-parametric outcomes were analysed using McNemar's test.

2.8.3 Agreement

For normal data, agreement may be demonstrated using Bland-Altman plots[73]. These plot the absolute difference between two methods measuring the same parameter against the average of the same values. Tests that agree well will show a small mean absolute difference in measured values and narrow limits of agreement (i.e. the spread of all absolute differences is small). Furthermore, the data points on a Bland-Altman plot should be evenly spread across the whole graph, indicating that the technique under investigation agrees well with the gold standard technique across a range of values[74]. Bland-Altman analysis is superior to the use of correlation coefficients as techniques may correlate perfectly whilst disagreeing significantly, provided there are the same proportional differences across the range of measurements. Although no 'p-value' is generated by Bland-Altman analysis, it does provide clinically relevant analysis. For example, a new measure of LV ejection fraction that showed a mean difference of 10% consistently above that measured by the gold standard would be considered to significantly disagree, whilst a measure consistently within 1% would not.

Agreement for categorical data is calculated using Cohen's kappa statistic. This compares observed proportions in a k x k table and compares them to expected

proportions. This generates values between 0 and 1, indicating no agreement and perfect agreement respectively. Kappa is a better measure than reporting percentage agreement as it accounts for chance agreement. Kappa values may be divided arbitrarily into categories indicating strength of agreement, as follows:

Kappa value	Suggested level of agreement
0.80 – 1.0	Excellent
0.60 – 0.79	Good
0.40 – 0.59	Moderate
0.20 – 0.39	Fair
0 – 0.19	Slight

The chances of disagreement rise with *k*. For nominal categorical data, all categorical disagreements carry equal weight and have similar effects on kappa. For ordinal categorical data, a disagreement of a single category may be less important than a difference of ≥2 categories. Quadratic weighted kappa is more appropriate here[75]. In this thesis, both standard and quadratic kappa values are calculated, as appropriate.

2.8.4 Regression

Differences detected between techniques measuring the same parameter may come from several sources. Much of the data in the following thesis is non-paramterically distributed, rendering linear regression models invalid. A non-parametric alternative, Passing and Bablok regression, is used instead. Strengths of this method include non-reliance on data distribution and relative robustness to outliers. Investigating a population of patients with previous MI (Chapters 5 – 14) is likely to yield extreme

measurements and so this method is preferred. The only requirement for validity is that the two tests are linearly related, a criterion tested as part of the analysis. This form of regression generates estimates of systematic, proportional and random differences between techniques. Of these three categories of disagreement, systematic errors are the easiest to deal with as they can be accounted for by adjusting test results by the appropriate value once the magnitude of the systematic difference is known. Proportional differences are more difficult to account for as their magnitude varies according to the measured values. For example, disagreements might be larger for higher measured values than lower ones. Random differences clearly cannot be accounted for. All parameters are demonstrated graphically with regression equations.

2.8.5 Receiver operator characteristic analysis

Receiver operator characteristic (ROC) analysis is used to evaluate the accuracy of a technique across a range of cut-off values for predicting disease presence or absence[76]. Graphically, this is represented by plotting true-positive rate (sensitivity) against false-positive rate (1-specificity) for different cut-off values. The final result is a curve, the area under which represents overall test accuracy. The closer the area under the curve (AUC) is to 1, the more accurate the test. AUC values may be (arbitrarily) categorised as follows: 0.90 – 1.00: excellent; 0.80 – 0.89: good; 0.70 – 0.79: fair; 0.60 – 0.69: poor. Statistically, AUC represents the probability that a random pair of patients, one with disease and one without, will be correctly discriminated by the test. AUC from different tests may be compared statistically to find the test with the highest accuracy.

ROC analysis may also be used to calculate the variation in test sensitivity and specificity across a range of cut-off values. If disease prevalence is known, it is also possible to calculate positive and negative predictive values[77]. The most appropriate cut-off may be determined as the value that offers the best balance between sensitivity and specificity. This is sometimes summarised as the Youden statistic, calculated as (sensitivity + specificity − 1). A perfect test with sensitivity and specificity of 1.0 (i.e. 100%) will have a Youden value of 1, a property almost unheard of for diagnostic tests in clinical practice. Nonetheless, ROC analysis allows selection of the 'best' cut-off as the one with the highest Youden statistic. Alternatively, any diagnostic test strikes a balance between the clinical importance of false-positive and false-negative results. If the consequences of missing a diagnosis are disastrous, a cut-off that minimises false-negatives should be chosen – i.e. sensitivity should be maximised at the expense of specificity. The converse may also be true. The optimal cut-off is not necessarily therefore the one with the highest Youden statistic, but the one that leads to the most clinically acceptable outcomes[78]. In this thesis, equal importance is assigned to false-positive and false-negative results. The Youden statistic is therefore used to judge optimal cut-off values. As useful information is lost when a diagnostic test is summarised by a single dichotomous cut-off, a combination of AUC and sensitivities/specificities are used to judge performance.

SECTION ONE

CHAPTER 3 EFFECTS OF X-RAY COMPUTED TOMOGRAPHY AND GADOLINIUM-153 ATTENUATION CORRECTION ON QUALITATIVE TRACER UPTAKE SCORES ON SPECT MPS

3.1 INTRODUCTION

Susceptibility to attenuation artefact remains a perceived weakness of SPECT myocardial perfusion scintigraphy (MPS). Measured counts underestimate true tracer uptake in affected areas as a result of attenuation of emitted photons by intervening soft tissue. Attenuation correction (AC) techniques generate maps that can be used to measure differential tissue attenuation of MPS emission data and correct images to reflect better true tracer uptake. The two most common methods for generating attenuation maps use either radionuclide line sources (typically gadolinium-153) or X-ray computed tomography (CT). AC has been shown consistently to increase summed stress and rest scores on SPECT MPS[4-17, 27, 79].

This study assesses the effects of CT and gadolinium-153 line source AC (CTAC and GdAC respectively) on stress and resting MPS. This is a necessary step before assessing the clinical effects of the techniques as, should AC have no measurable effect on the images, it is unlikely that effects on report or reporter confidence will be observed. Further, comparison of the clinical effects of AC with existing published data will be valid only if the technical effects on apparent tracer uptake are similar.

3.2 METHODS

52 patients (31 male, 65±8years) referred for clinical one-day stress/rest technetium-99m Tetrofosmin SPECT MPS were recruited (Table 3.1). Patients were excluded if they were unable to lie flat for one hour or had contraindications to adenosine vasodilator stress (bradyarrhythmia without functioning pacemaker, persistent asthma etc.). All patients underwent pharmacological stress and MPS imaging as outlined in section 2.3. The median time between stress and resting injection was 2 hours (IQR 119 – 124 minutes).

3.2.1 Assignment of camera order

For each imaging period, patients underwent MPS on separate gamma cameras equipped with either CTAC or GdAC. Immediately following the completion of MPS on the first camera, patients crossed to the other for repeat MPS using the alternative AC technique. Camera order was varied on a session-by-session basis to reduce the effects of time delay on tracer distribution as a confounding variable (Figure 3.1). In total, 24/52 patients (46%) went in the order ADAC Forte – Infinia Hawkeye (i.e. CTAC before GdAC) and 28/52 (54%) in the reverse order. Mean times from stress and resting injections to imaging are given in Table 3.2. There were significant differences in intervals between the groups, although none were clinically meaningful. The maximum mean difference was 7 minutes, an interval too short to significantly affect image quality or tracer uptake patterns – technetium-99m has a half life of 6 hours and tetrofosmin fixes within myocytes without clinically meaningful redistribution over 7 minutes.

	TOTAL	%
F	21	40%
M	31	60%

	TOTAL	SD
Age	64	8.4
Weight	77	15.8
BMI	27	5.0
BMI >30	13	

	TOTAL	%
Angina	13	25%
Atypical chest pain	18	35%
Non-Cardiac chest pain	4	8%
SOB only	8	15%
Asymptomatic	9	17%

Diagnostic study	28	54%
Known CAD	24	46%
MI	12	23%
>2 risk Factors	35	67%

Table 3.1 *Patient demographics*

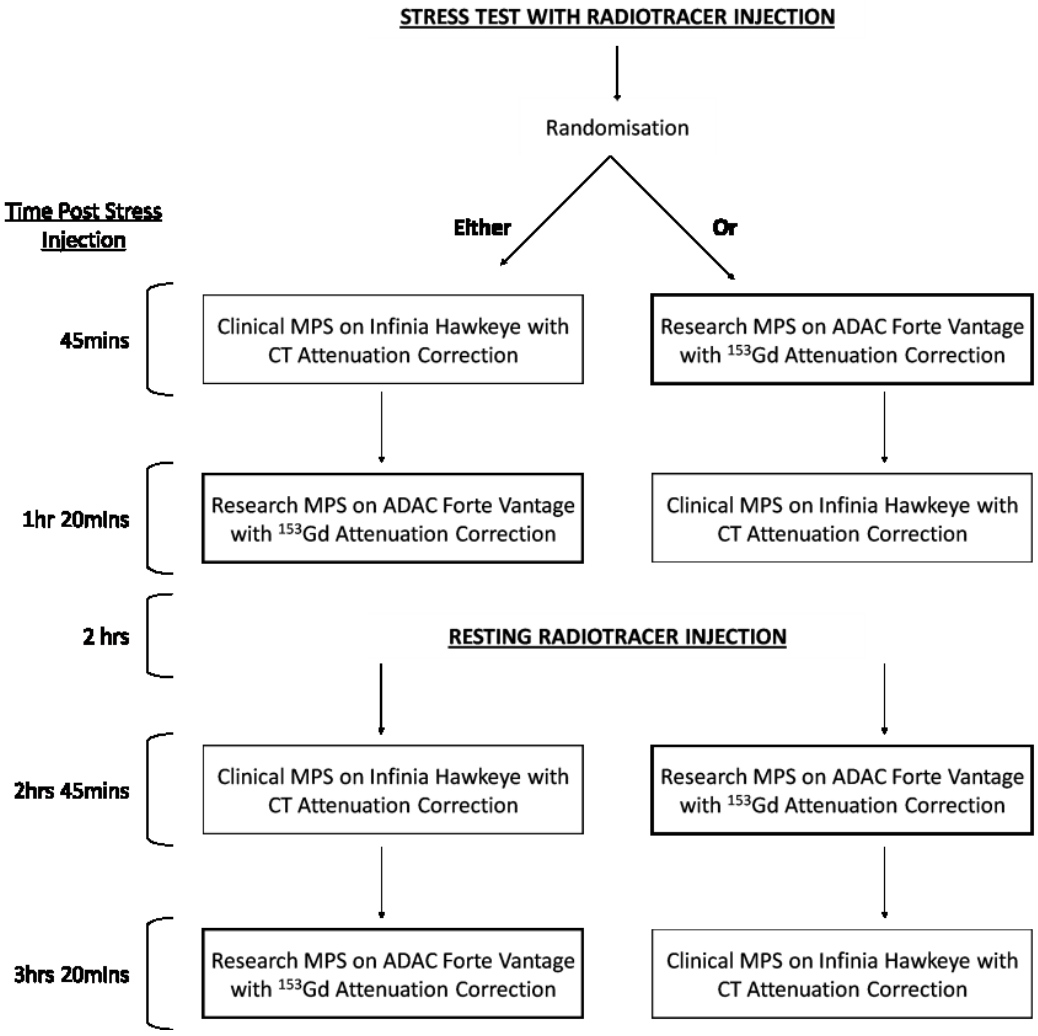


Figure 3.1 *MPS imaging protocol with variation of assignment to gamma camera.*

	First camera	Time/minutes	p-value
Stress MPS	Infinia ADAC	39.4±3.96 44.4±2.86	<0.0001
Rest MPS	Infinia ADAC	44.1±8.02 51.1±12.7	<0.0001
	Second camera	**Time/minutes**	**p-value**
Stress MPS	Infinia ADAC	63.0±3.13 67.5±4.02	<0.0001
Rest MPS	Infinia ADAC	78.3±15.78 79.0±10.96	0.21

Table 3.2 *Intervals between stress and resting injections and subsequent imaging (mean±SD).*

3.2.2 Image Analysis

Images were analysed using QPS/QGS software (Hermes Medical Systems). Non-corrected (NC), CTAC and GdAC scans were scored by an experienced observer (Level 3 trained, CBNC certified) at separate sessions. Segmental uptake was scored according to the AHA 17-segment model using the QPS/QGS normal reference database. Tracer uptake was scored as described in Section 2.3.5. Summed stress (SSS) and rest (SRS) scores were calculated (normal=68), as was the difference between the two (summed difference score [SDS]). Summed scores were also calculated for each coronary artery territory and myocardial wall (as described in Section 2.2).

3.2.3 Statistics

SSS, SRS and SDS are presented as median (interquartile range) and compared using the Wilcoxon sign-rank test, with $p<0.05$ considered significant. Subanalysis of coronary territories and myocardial walls were similarly analysed, although significance level was adjusted by Bonferroni correction ($p<0.006$ and 0.004 respectively).

3.3 RESULTS

3.3.1 Comparison of summed scores

Results are summarised in Table 3.3. Both CTAC and GdAC increased SSS ($p=0.0006$ and 0.0009 respectively) and SRS ($p=0.0002$ and $p<0.0001$ respectively). No differences were seen between AC techniques for either SSS or SRS ($p=0.60$ and 0.57 respectively). CTAC resulted in no difference in SDS compared with uncorrected images ($p=0.39$). In contrast, GdAC resulted in lower SDS ($p=0.03$).

		Non-corrected	AC	p-value
Summed Stress Score	Infinia (CT)	65 (62 – 67)	66 (64.5 – 67)	0.0006
	ADAC (Gd)	65 (62.5 – 62)	67 (65 – 68)	0.0009
Summed Rest Score	Infinia (CT)	66 (64 – 68)	68 (66 – 68)	0.0002
	ADAC (Gd)	66 (63 – 68)	67.5 (67 – 68)	<0.0001
Summed Difference Score	Infinia (CT)	67 (66 – 68)	67 (66 – 68)	0.39
	ADAC (Gd)	68 (67 – 68)	67 (66 – 68)	0.03

Table 3.3 *Summed perfusion scores, presented as median (IQR), on both cameras with and without AC.*

3.3.2 Comparison of summed scores according to coronary territory

Results are summarised in Table 3.4.

Summed stress scores

Both AC methods increased SSS in the RCA territory ($p<0.0001$). CTAC also increased SSS in the left circumflex territory ($p=0.002$). GdAC significantly reduced SSS in the LAD territory ($p=0.002$), whilst changes in this territory following CTAC did not reach significance ($p=0.06$). There were no differences in SSS between AC techniques.

Summed rest scores

Both AC methods increased SRS in the RCA territory ($p<0.0001$ for both CTAC and GdAC). CTAC also increased SRS in the left circumflex territory ($p=0.002$). There were no differences between AC and NC images in any other coronary territory. No differences in SRS were seen between AC techniques.

Summed difference scores

GdAC resulted in a decrease in SDS in the LAD territory ($p=0.005$). No differences were observed in SDS for either AC technique in any other coronary territory. No differences in SDS were observed between AC techniques.

Left anterior descending coronary artery

		Non-corrected	AC	p-value
Summed Stress Score	Infinia (CT)	68 (67 – 68)	67 (66 – 68)	0.06
	ADAC (Gd)	68 (67 – 68)	67 (67 – 68)	0.002
Summed Rest Score	Infinia (CT)	68 (68 – 68)	68 (67 – 68)	0.02
	ADAC (Gd)	68 (67 – 68)	68 (67 – 68)	0.46
Summed Difference Score	Infinia (CT)	68 (67 – 68)	68 (67 – 68)	0.99
	ADAC (Gd)	68 (68 – 68)	68 (67 – 68)	0.005

Left circumflex coronary artery

		Non-corrected	AC	p-value
Summed Stress Score	Infinia (CT)	68 (67 – 68)	68 (68 – 68)	0.002
	ADAC (Gd)	68 (67 – 68)	68 (67 – 68)	0.11
Summed Rest Score	Infinia (CT)	68 (67 – 68)	68 (68 – 68)	0.002
	ADAC (Gd)	68 (67 – 68)	68 (68 – 68)	0.17
Summed Difference Score	Infinia (CT)	68 (68 – 68)	68 (68 – 68)	1.0
	ADAC (Gd)	68 (68 – 68)	68 (68 – 68)	1.0

Right coronary artery

		Non-corrected	AC	p-value
Summed Stress Score	Infinia (CT)	66 (64 – 68)	68 (67 – 68)	<0.0001
	ADAC (Gd)	66 (64 – 68)	68 (67 – 68)	<0.0001
Summed Rest Score	Infinia (CT)	67 (65 – 68)	68 (68 – 68)	<0.0001
	ADAC (Gd)	67 (64.5 – 68)	68 (68 – 68)	<0.0001
Summed Difference Score	Infinia (CT)	68 (67 – 68)	68 (67.5 – 68)	0.45
	ADAC (Gd)	68 (68 – 68)	68 (67.5 – 68)	0.55

Table 3.4 *Median summed perfusion scores according to coronary territory on both cameras with and without AC. Both forms of AC increase SSS and SRS in the right coronary artery territory. CTAC increases SSS and SRS scores in the LCx territory, whilst GdAC decreases SSS and SDS in the LAD territory. Note significance level p<0.006.*

3.3.3 Comparison of summed scores according to myocardial wall

Results are summarised in Table 3.5.

Summed stress scores

Both AC methods increased SSS inferiorly ($p<0.0001$, see Figure 3.2). CTAC also increased SSS laterally ($p=0.002$). GdAC reduced SSS anteroapically ($p<0.0001$) but CTAC did not ($p=0.03$). There were no differences in SSS between AC techniques.

Summed rest scores

Both AC methods increased SRS inferiorly ($p<0.0001$ for both CTAC and GdAC, see Figure 3.2). CTAC also increased SRS laterally ($p=0.002$) and decreased SRS anteroapically ($p=0.003$). These changes were not seen after GdAC. There were no other differences between AC and NC images in any myocardial wall, nor any differences in SRS between AC techniques.

Summed difference scores

No differences were observed in SDS for either AC technique in any myocardial wall at the level of significance defined by the Bonferroni correction given above, although there was a trend towards the creation of apparent inducible perfusion abnormalities anteroapically by GdAC ($p=0.006$). This was not seen with CTAC. No differences were observed between AC techniques.

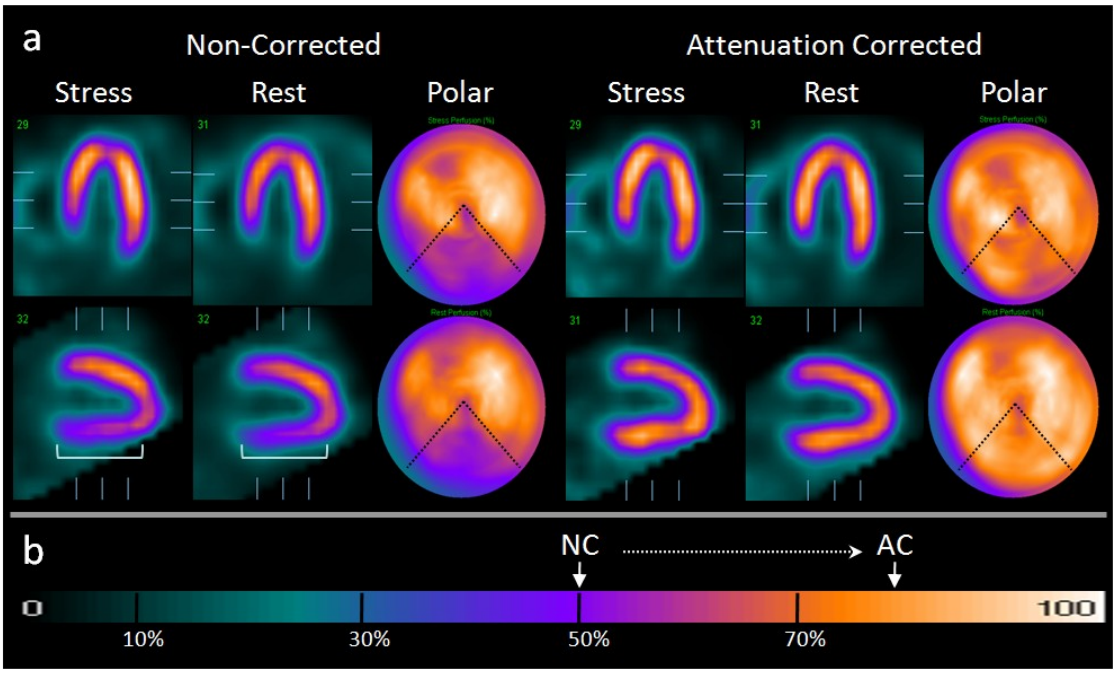


Figure 3.2 *Attenuation correction of the inferior wall. Stress and rest long axis slices are presented for both non-corrected and CT attenuation corrected datasets. Polar plots are also included (stress (top), rest (bottom)). Non-corrected images (a, left) demonstrate mild to moderate reduction in counts inferiorly (white brackets, black lines) in both stress and rest acquisitions, suggesting either diaphragmatic attenuation artefact or partial thickness myocardial infarction. After attenuation correction (AC; a, right), counts inferiorly (black lines) are normal. The change in counts is demonstrated on the colour scale (b), with non-corrected counts (NC) lying at ~50% maximum uptake whilst, after AC, counts are normal (>70%).*

Anteroapical wall

		Non-corrected	AC	p-value
Summed Stress Score	Infinia (CT)	68 (67 – 68)	67 (66 – 68)	0.03
	ADAC (Gd)	68 (67 – 68)	67 (67 – 68)	<0.0001
Summed Rest Score	Infinia (CT)	68 (68 – 68)	68 (67 – 68)	0.003
	ADAC (Gd)	68 (67.5 – 68)	68 (67 – 68)	0.28
Summed Difference Score	Infinia (CT)	68 (67 – 68)	68 (67 – 68)	0.85
	ADAC (Gd)	68 (68 – 68)	68 (67 – 68)	0.006

Septum

		Non-corrected	AC	p-value
Summed Stress Score	Infinia (CT)	68 (68 – 68)	68 (68 – 68)	0.16
	ADAC (Gd)	68 (67.5 – 68)	68 (68 – 68)	0.01
Summed Rest Score	Infinia (CT)	68 (67 – 68)	68 (68 – 68)	0.13
	ADAC (Gd)	68 (67 – 68)	68 (68 – 68)	0.009
Summed Difference Score	Infinia (CT)	68 (68 – 68)	68 (68 – 68)	-
	ADAC (Gd)	68 (68 – 68)	68 (68 – 68)	0.84

Inferior wall

		Non-corrected	AC	p-value
Summed Stress Score	Infinia (CT)	66 (64 – 68)	68 (67 – 68)	<0.0001
	ADAC (Gd)	67 (65 – 68)	68 (67 – 68)	<0.0001
Summed Rest Score	Infinia (CT)	67 (65.5 – 68)	68 (68 – 68)	<0.0001
	ADAC (Gd)	67 (65 – 68)	68 (68 – 68)	<0.0001
Summed Difference Score	Infinia (CT)	68 (67 – 68)	68 (68 – 68)	0.51
	ADAC (Gd)	68 (68 – 68)	68 (68 – 68)	0.30

Lateral wall

		Non-corrected	AC	p-value
Summed Stress Score	Infinia (CT)	68 (67 – 68)	68 (68 – 68)	0.002
	ADAC (Gd)	68 (67 – 68)	68 (67 – 68)	0.11
Summed Rest Score	Infinia (CT)	68 (67 – 68)	68 (68 – 68)	0.002
	ADAC (Gd)	68 (67 – 68)	68 (68 – 68)	0.17
Summed Difference Score	Infinia (CT)	68 (68 – 68)	68 (68 – 68)	1.0
	ADAC (Gd)	68 (68 – 68)	68 (68 – 68)	1.0

Table 3.5 *Median summed perfusion scores according to myocardial wall on both cameras with and without attenuation correction. Both forms of AC increase SSS and SRS inferiorly. CTAC increases SSS and SRS laterally, whilst GdAC decreases SSS anteroapically. Note significance level p<0.004.*

3.4 DISCUSSION

It is clear that both AC techniques increase equally the summed stress and rest scores both generally and specifically in the inferior wall without any differences in SDS. CTAC also increases summed stress and rest scores laterally, again without affecting SDS. SDS reflects the extent and severity of observed inducible perfusion abnormalities and its invariance inferiorly (and laterally for CTAC) implies therefore reduction or elimination of fixed abnormalities on the AC images. These findings are in line with previous studies[11, 80-82]. There was no significant increase in summed scores anteroapically, suggesting either that breast attenuation was not a significant contributor to artefact in this cohort (there were only 2 women under 60 years of age in the sample) or that the AC software was unable to effect significant improvements in apparent counts where breast attenuation was present. As discussed below, AC techniques showed variable effects anteroapically, but in all cases, led to decreases in summed scores, suggesting creation of abnormalities rather than improvement.

AC methods should not change summed difference scores, a measure only of the extent and severity of observed inducible perfusion abnormalities. Nonetheless, there is evidence to suggest that AC methods may generate a new set of artefacts, one of which is the creation of apparent inducible perfusion abnormalities in the anterior wall and apex, particularly in women[25, 82, 83]. In the present analysis, GdAC appears to increase the overall extent and severity of inducible perfusion abnormalities, whilst CTAC does not. This is mediated by an increase in SDS in the LAD territory, mostly in the anteroapical region. It seems, therefore, that GdAC

creates the appearance of inducible ischaemia in the LAD territory. CTAC images do not seem to be affected by this problem, although there was a trend to decreasing apparent anteroapical tracer uptake on both stress and resting images, suggesting that CTAC may create fixed anteroapical abnormalities. The lack of significance may be the result of an excessively conservative Bonferroni correction, but it is interesting that GdAC creates apparent LAD territory ischaemia whilst CTAC suggests infarction in the same territory. It would seem, therefore, that anteroapical changes are common on AC images, potentially trading one artefact on non-corrected images for another after AC.

Putting these results into perspective, the data show that both AC techniques increase apparent counts inferiorly, in line with previous studies[11, 84]. GdAC increases apparent inducible perfusion abnormalities in the LAD territory, whilst CTAC shows a trend towards the creation of fixed defects in this territory. These issues have been raised in previous studies[82, 84]. As the technical effects of AC in this study are broadly in line with effects observed elsewhere, the techniques can be taken forward for assessment of impact on clinical report and reporter confidence.

3.5 LIMITATIONS

The numbers recruited to this study were small, although the observed effects of AC were significant. It is likely that the correction for multiple testing is highly conservative, resulting in inappropriate acceptance of the null hypothesis in some cases. Regardless, the results are similar to other published data, suggesting that no important effects have been missed.

3.6 SUMMARY FINDINGS

1. Both CTAC and GdAC reduce fixed perfusion defects on MPS tomograms, predominantly in the inferior wall but also, for CTAC, laterally.
2. GdAC increases apparent inducible myocardial ischaemia anteroapically. Although this was not demonstrated with CTAC, there was a trend towards the creation of fixed defects in this territory.
3. These findings are consistent with previously published data, implying equivalent technical performance of AC in our department.

CHAPTER 4 EFFECTS OF X-RAY COMPUTED TOMOGRAPHY AND GADOLINIUM-153 ATTENUATION CORRECTION ON CLINICAL REPORT AND REPORTER CONFIDENCE

4.1 INTRODUCTION

As demonstrated in Chapter 3 and elsewhere, attenuation correction (AC) increases summed stress and resting scores on myocardial perfusion scintigraphy (MPS)[4-6, 9, 11, 16]. This has been shown to improve MPS specificity, particularly in the territory typical for the right coronary artery, and normalcy by eliminating fixed artefacts in areas of normal perfusion that might otherwise be mistaken for myocardial infarction (MI)[12]. AC has therefore been recommended by some as a mandatory component of standard MPS protocol[20, 85]. Although intuitively appealing, things may not be this straightforward. The technical effects of AC on MPS images are beyond doubt but the improvements in specificity and normalcy have been disputed[6, 24, 25, 86]. A recent multicentre study demonstrated improvements in the specificity for detection of right coronary artery disease in overweight men but not in any other groups[27]. The reasons for these conflicting data are likely to be manifold. First, the potential benefits of AC presume an inability on the part of the reporting clinician to recognise attenuation artefact. Inferior wall attenuation artefact is such a common problem in MPS that this is rarely the case for the experienced reader. Second, in virtually all cases, MPS images in published studies are reported blind to clinical information[23]. Patient history is fundamental to clinically relevant reporting. A fixed

defect in an asymptomatic 30 year old woman is far more likely to be artefactual than in a 70 year old diabetic man with angina. Blinding therefore necessarily hampers diagnostic interpretation of uncorrected MPS images by removing crucial information, potentially exaggerating the benefits of AC. It also renders study results inapplicable to real-world practice. Third, initial data supporting the use of AC came from studies using radionuclide AC over a decade ago. Since this time, scatter correction methods have improved and the use of normal databases to improve recognition of potential attenuation aretfacts has become commonplace. Finally, X-ray computed tomography AC (CTAC) has become more predominant, a technique that carries different spatial and temporal resolutions to radionuclide AC. There are no head-to-head comparisons of these techniques. Given these variables, it is not surprising that there are disagreements about the clinical usefulness of AC of MPS in practice.

The aims of this study are therefore to compare clinical report, reporter confidence and interobserver agreement in SPECT MPS before and after X-ray computed tomography (CTAC) and gadolinium-153 (GdAC) AC.

4.2 METHODS

52 patients (31 male, 65±8years) referred for clinical one-day stress/rest technetium-99m tetrofosmin SPECT MPS were recruited as described in Section 3.2. MPS protocols are described in section 2.3. Camera order was randomised for each session as described previously (Section 3.2.1, Figure 3.1).

4.2.1 Image Analysis

Images were analysed using QPS/QGS software (Hermes Medical Systems). Non-corrected (NC), CTAC and GdAC scans were reported at separate sessions (NC Strategy, CTAC Strategy and GdAC Strategy respectively). Each study was assessed independently by 2 observers, each with >5 years MPS experience and blinded to AC method. Studies were reported as described in Section 2.3.4, with clinical information withheld until all images had been reviewed. Interim reports and confidences were recorded at each stage (Figure 4.1). Final clinical report and confidence were recorded after provision of clinical information. Studies were reported as either normal or showing pure inducible ischaemia ('reversible'), pure MI ('fixed') or a combination of the two ('mixed'), as described in section 2.3.5. Reporter confidence was recorded as very high, high, moderate, low or very low.

4.2.2 Statistics

Differences in the number of normal cases, those that demonstrated any reversibility (i.e. reported as either 'reversible' or 'mixed') and those with any fixed abnormality (i.e. reported as either 'fixed or 'mixed') were compared using McNemar's test. Comparison of body mass index (BMI) between groups was performed using Student's t-test. Differences in reporter confidence were assessed using Friedman's test, with Wilcoxon sign-rank testing as appropriate. Inter- and intraobserer agreement was measured using Cohen's kappa. Sample size was estimated with the help of a professional statistician and based on a paired t-test calculation with correction for non-parametric data. To detect a one-category difference in report or report confidence, 50 patients were needed to achieve 90% power.

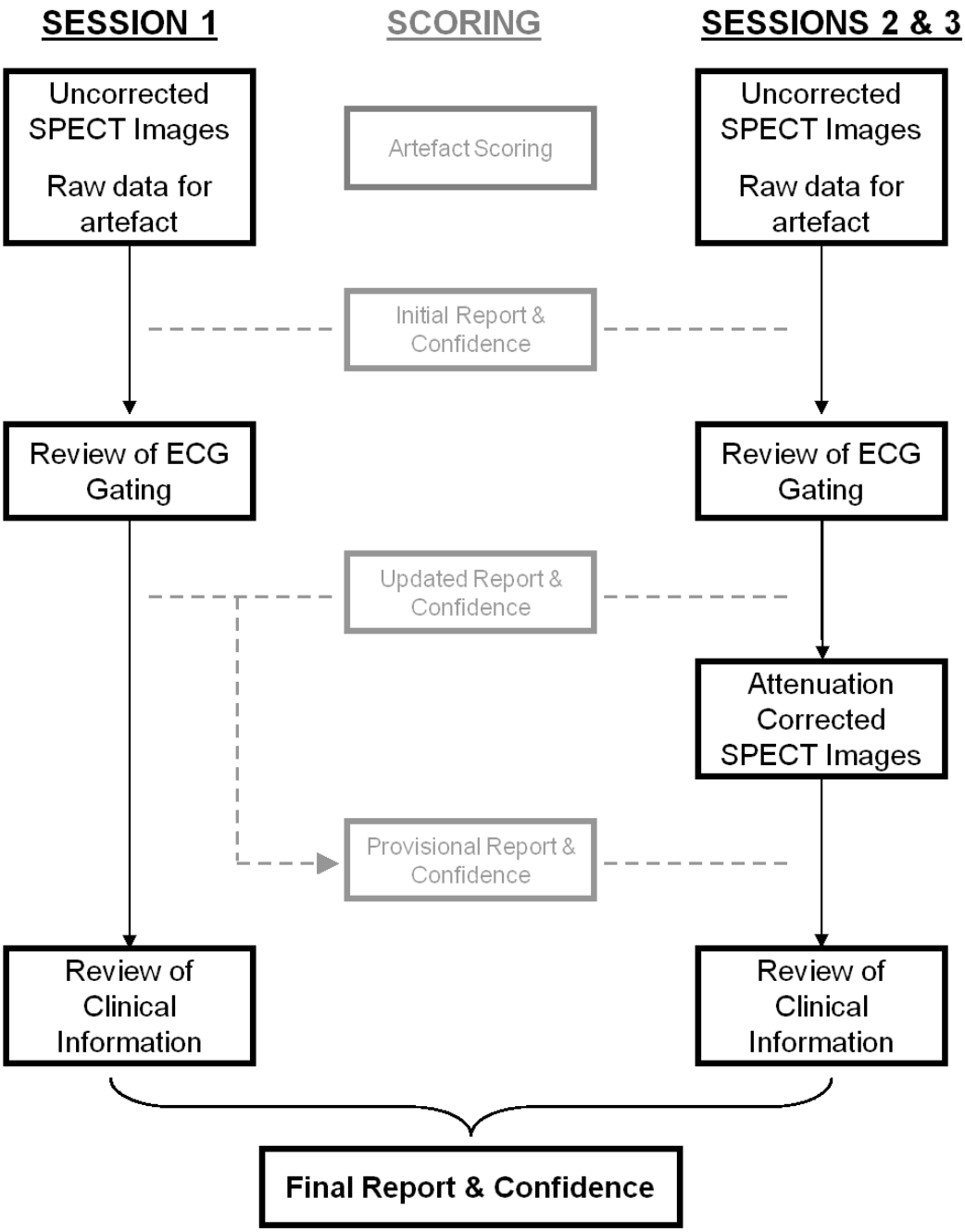


Figure 4.1 *Reporting strategy for non-corrected (Session 1), GdAC and CTAC myocardial perfusion images (Sessions 2 and 3).*

4.3 RESULTS

4.3.1 Effects of AC on provisional clinical report

CTAC

Results are summarised in Tables 4.1 and 4.2. Prior to provision of clinical information, CTAC and NC reports were identical in 71% of cases, with moderate overall agreement (κ=0.54). No difference in the number of normal reports was observed between groups (p=0.77). Report differed in 15/52 (29%) cases, with normalisation of the report in 5/25 (20%) cases considered abnormal on NC images. CTAC abolished reports of reversibility in 5/23 cases (22%), whilst these were created in 7/30 cases (23%). There was no net change in the number of cases reported with any inducible ischaemia (p=0.77). In cases with a fixed component on NC images, only 2/13 (15%) were abolished by CTAC, with no difference overall (p=0.69). There was no difference in BMI between cases where CT and NC reports agreed or disagreed (27.4 vs 25.7, p=0.25).

		CT Attenuation Corrected				
		Normal	Fixed	Mixed	Reversible	
Non-Corrected	Normal	21	1	2	4	28 (53.8%)
	Fixed	0	1	1	0	2 (3.8%)
	Mixed	1	0	8	1	11 (19.2%)
	Reversible	4	0	1	7	12 (23.1%)
		26 (50.0%)	2 (3.8%)	12 (23.1%)	12 (23.1%)	52

Table 4.1 *Comparison of provisional reports using NC and CTAC reporting strategies.*

	Normal		Fixed/Mixed		Reversible/Mixed	
	Number (%)	**p-value**	**Number (%)**	**p-value**	**Number (%)**	**p-value**
NC	28 (53.9)	0.77	12 (23.1)	0.69	22 (42.3)	0.77
CTAC	26 (50.0)		14 (26.9)		24 (46.2)	

Table 4.2 *Comparison of number of scans reported provisionally as normal or as having evidence of MI (fixed/mixed) or inducible ischaemia (reversible/mixed) for NC and CTAC strategies.*

GdAC

Results are summarised in Tables 4.3 and 4.4. GdAC and NC reports were identical in 58% of cases, with only fair agreement (κ=0.32). No difference in the number of normal cases was observed between groups (p=0.77). Provisional clinical report was altered in 22/52 (42%) cases, with normalisation of the report in 7/24 (29%) cases considered abnormal when assessed without AC. In 10/22 (45%) cases, GdAC reports no longer reflected an ischaemic component to the scan, whilst, in 5/30 (17%) cases,

GdAC reports reflected reversibility not considered present after review of initial perfusion and gating images. Overall, this led to no net change in the number of cases reported with any inducible ischaemia (p=0.30). In cases with a fixed component on NC images, only 2/12 (17%) were abolished by GdAC, with no difference overall (p=0.07). There was no difference in BMI between cases where GdAC and NC reports agreed or disagreed (26.3 vs 27.8, p=0.27).

		^{153}Gd Attenuation Corrected				
		Normal	Fixed	Mixed	Reversible	
Non-Corrected	Normal	23	1	1	3	28 (53.8%)
	Fixed	0	1	1	0	2 (3.8%)
	Mixed	2	2	6	0	10 (19.2%)
	Reversible	5	1	6	0	12 (23.1%)
		30 (57.7%)	5 (9.6%)	14 (26.9%)	3 (5.8%)	52

Table 4.3 *Comparison of provisional reports using NC and GdAC reporting strategies.*

	Normal		**Fixed/Mixed**		**Reversible/Mixed**	
	Number (%)	**p-value**	**Number (%)**	**p-value**	**Number (%)**	**p-value**
NC	28 (53.9)	0.77	12 (23.1)	0.07	22 (42.3)	0.30
GdAC	30 (57.7)		19 (36.5)		17 (32.7)	

Table 4.4 *Comparison of number of scans reported provisionally as normal or as having evidence of MI (fixed/mixed) or inducible ischaemia (reversible/mixed) for NC and GdAC strategies.*

4.3.1 Effects of AC on final clinical report

CTAC

Results are summarised in Tables 4.5 and 4.6. CTAC and NC reports were identical in 75% of cases, with overall good agreement (κ=0.63). No difference in the number of normal cases was observed between groups (p=0.75). Final clinical report was different in 13/52 (25%) cases, with normalisation of the report in 6/31 (19%) cases considered abnormal on NC images. CTAC abolished inducible perfusion abnormalities in 6/28 cases (21%) and created them in 6/24 cases (25%). Overall, this led to no net change in the number of cases reported with any inducible ischaemia (p=1.0). In cases with a fixed component on NC images, only 1/13 (8%) was abolished by CTAC, with no differences overall (p=1.0). There was no difference in BMI between cases where CT and NC reports agreed or disagreed (26.8 vs 27.2, p=0.85).

		CT Attenuation Corrected				
		Normal	Fixed	Mixed	Reversible	
Non-Corrected	Normal	17	0	0	4	21 (40.4%)
	Fixed	0	1	2	0	3 (5.8%)
	Mixed	1	0	9	0	10 (19.2%)
	Reversible	5	0	1	12	18 (34.6%)
		23 (44.2%)	1 (1.9%)	12 (23.1%)	16 (30.8%)	52

Table 4.5 *Comparison of final clinical reports using NC and CTAC reporting strategies.*

	Normal		Fixed/Mixed		Reversible/Mixed	
	Number (%)	**p-value**	**Number (%)**	**p-value**	**Number (%)**	**p-value**
NC	21 (40.4)	0.75	13 (25.0)	1.0	28 (53.9)	1.0
CTAC	23 (44.2)		13 (25.0)		28 (53.9)	

Table 4.6 *Comparison of number of scans reported finally as normal or as having evidence of MI (fixed/mixed) or inducible ischaemia (reversible/mixed) for NC and CTAC strategies.*

GdAC

Results are summarised in Tables 4.7 and 4.8. GdAC and NC reports were identical in 63% of cases, with overall moderate agreement (κ=0.47). No difference in the number of normal cases was observed between groups (p=0.11). Final clinical report was altered in 19/52 (37%) cases, with normalisation of the report in 8/31 (26%) cases considered abnormal on NC images. GdAC abolished inducible perfusion abnormalities in 11/28 (39%) cases and created them in 3/24 (13%) cases. Overall, this led to no net change in the number of cases reported with any inducible ischaemia (p=0.06). In cases with a fixed component on NC images, only 2/13 (15%) were abolished by GdAC, with no differences overall (p=0.45). There was no difference in BMI between cases where GdAC and NC reports agreed or disagreed (26.2 vs 28.2, p=0.18).

		^{153}Gd Attenuation Corrected				
		Normal	Fixed	Mixed	Reversible	
Non-Corrected	Normal	19	0	0	2	21 (40.4%)
	Fixed	0	2	1	0	3 (5.8%)
	Mixed	1	2	6	1	10 (19.2%)
	Reversible	7	1	4	6	18 (34.6%)
		27 (51.9%)	5 (9.6%)	11 (21.2%)	9 (17.3%)	52

Table 4.7 *Comparison of final clinical reports using NC and GdAC reporting strategies.*

	Normal		**Fixed/Mixed**		**Reversible/Mixed**	
	Number (%)	**p-value**	**Number (%)**	**p-value**	**Number (%)**	**p-value**
NC	21 (40.4)	0.11	13 (25.0)	0.45	28 (53.9)	0.06
GdAC	27 (51.9)		16 (30.8)		20 (38.5)	

Table 4.8 *Comparison of number of scans reported finally as normal or as having evidence of MI (fixed/mixed) or inducible ischaemia (reversible/mixed) for NC and GdAC strategies.*

4.3.2 Does clinical impression change immediately after reviewing AC images?

CTAC

Results are summarised in Table 4.9. CTAC changed the report in only 6/52 (12%) cases, with excellent agreement between the updated and provisional reports (κ=0.80). In 3 cases, fixed abnormalities became mixed, whereas in the other 3 reversible (2) and mixed (1) were reported as normal. CTAC did not materially change the number of normal reports at this stage (p=0.25).

		Provisional Report				
		Normal	Fixed	Mixed	Reversible	
Updated Report	Normal	23	0	0	0	23 (44.2%)
	Fixed	0	2	3	0	5 (9.6%)
	Mixed	1	0	9	1	11 (21.2%)
	Reversible	2	0	0	11	13 (25.0%)
		26 (50.0%)	2 (3.8%)	12 (23.1%)	12 (23.1%)	52

Table 4.9 *Comparison of updated and provisional reports for the CTAC strategy.*

GdAC

Results are summarised in Table 4.10. GdAC changed the report in 3/52 (5.8%) cases, with excellent agreement between the updated and provisional reports (κ=0.90). 2 reversible abnormalities were reinterpreted as normal after GdAC, whilst 1 normal study was reinterpreted as showing reversibility. GdAC had no impact on the number of normal reports at this stage (p=1.0).

		Provisional Report				
		Normal	Fixed	Mixed	Reversible	
Updated Report	Normal	28	0	0	1	29 (55.8%)
	Fixed	0	5	0	0	5 (9.6%)
	Mixed	0	0	14	0	14 (26.9%)
	Reversible	2	0	0	2	4 (7.7%)
		30 (57.7%)	5 (9.6%)	14 (26.9%)	3 (5.8%)	52

Table 4.10 *Comparison of updated and provisional reports for the GdAC strategy.*

CTAC vs. GdAC

Neither AC technique resulted in more changes to the provisional report (p=0.34).

4.3.3 Is the final report altered by clinical information?

CTAC

Results are summarised in Table 4.11. Clinical details changed the final report in 8/52 (15%) cases, with very good agreement between the provisional and final reports (κ=0.77). 7/8 (88%) changes in report occurred in studies where no change in report had yet been made i.e. they were not reversing changes made as a result of CTAC. Clinical details normalised the report in 4 cases; the remaining changes were each different, as seen in Table 4.11. Clinical information did not materially change the number of normal reports (p=0.45).

		Provisional Report				
		Normal	Fixed	Mixed	Reversible	
Final Clinical Report	Normal	21	1	0	1	23 (44.2%)
	Fixed	0	1	0	0	1 (1.9%)
	Mixed	1	0	11	0	11 (21.2%)
	Reversible	4	0	1	11	13 (25.0%)
		26 (50.0%)	2 (3.8%)	12 (23.1%)	12 (23.1%)	52

Table 4.11 *Comparison of provisional and final clinical reports in the CTAC strategy.*

GdAC

Results are summarised in Table 4.12. Clinical details changed the final report in 8/52 (15%) cases, with very good agreement between the provisional and final reports (κ=0.75). As for CTAC, 7/8 (88%) changes in report occurred in studies where no change in report had yet been made i.e. they were not reversing changes made as a result of GdAC. Three reversible abnormalities were reinterpreted as normal after clinical details, whilst 3 were reinterpreted as showing a mixed picture. Clinical information had no impact on the number of normal reports (p=0.25).

		Provisional Report				
		Normal	Fixed	Mixed	Reversible	
Final Clinical Report	Normal	27	0	0	0	27 (51.9%)
	Fixed	0	4	1	0	5 (9.6%)
	Mixed	0	1	10	0	11 (21.2%)
	Reversible	3	0	3	3	4 (7.7%)
		30 (57.7%)	5 (9.6%)	14 (26.9%)	3 (5.8%)	52

Table 4.12 *Comparison of provisional and final clinical reports for the GdAC strategy.*

Comparison across all 3 reporting strategies

No strategy resulted in more changes in final clinical report after provision of clinical information (p=0.48).

Normal Studies		Number (%)	p-value
Provisional Report	No AC	28 (53.9)	
	CTAC	26 (50.0)	0.77
	GdAC	30 (57.7)	0.77
Final Clinical Report	No AC	21 (40.4)	
	CTAC	23 (44.2)	0.75
	GdAC	27 (51.9)	0.11

Any fixed component		Number (%)	p-value
Provisional Report	No AC	12 (23.1)	
	CTAC	14 (26.9)	0.69
	GdAC	19 (36.5)	0.07
Final Clinical Report	No AC	13 (25.0)	
	CTAC	13 (25.0)	1.0
	GdAC	16 (30.8)	0.45

Any ischaemic component		Number (%)	p-value
Provisional Report	No AC	22 (42.3)	
	CTAC	24 (46.2)	0.77
	GdAC	17 (32.7)	0.30
Final Clinical Report	No AC	28 (53.9)	
	CTAC	28 (53.9)	1.0
	GdAC	20 (38.5)	0.06

Table 4.13 *Summary of impact of CTAC and GdAC on the number of normal clinical reports and those showing any fixed and reversible component.*

4.3.4 Effects on reporter confidence

Results are summarised in Table 4.14 – 4.15.

Initial and Updated Reports

No differences were seen in reporter confidence for initial and updated reports (p=0.22 and 0.97 respectively).

Provisional Report

A significant difference in confidence was observed between the 3 groups (p=0.03) at the provisional report stage. Both CTAC and GdAC strategies allowed higher confidence in the provisional report than for the NC strategy (both median confidences: high, p=0.03 and 0.01 respectively). No differences in confidence were seen between AC techniques (p=0.62).

Final Clinical Report

Once clinical information was known, no between-group differences in confidence were seen, indicating that no strategy resulted in a higher confidence in the final clinical report (median confidence for all strategies: high; p=0.17).

Variation in confidence during the reporting process

Each new piece of information increased confidence in the report for every reporting strategy (Table 4.15). Provision of gating, attenuation correction (where appropriate) and clinical information all increased confidence in report at each stage in all 3 reporting strategies (p<0.001).

		Median (IQR)	p-value
Initial Report	Infinia	2.5 (2 – 3)	0.22
	ADAC	3 (2 – 3.5)	
Updated Report	Infinia	3 (3 – 4)	0.97
	ADAC	3 (3 – 3.5)	
Attenuation Correction	Infinia	4 (3 – 4)	0.62
	ADAC	4 (3 – 4)	
Provisional Report	NC	3 (3 – 4)	0.03*
	CTAC	4 (3 – 4)	
	GdAC	4 (3 – 4)	
Final Clinical Report	NC	4 (3 – 5)	0.66
	CTAC	4 (3.5 – 5)	
	GdAC	4 (3 – 5)	

Table 4.14 *Between group effects on confidence with each stage. *Post hoc analysis: NC vs CTAC p=0.03 ; NC vs GdAC p=0.01*

		Median (IQR)	p-value
Non-Corrected	Initial Report	3 (2 – 3)	<0.001*
	Updated/Provisional Report	3 (3 – 4)	
	Final Clinical Report	4 (3 – 5)	
CT Attenuation Correction	Initial Report	2.5 (2 – 3)	<0.001*
	Updated Report	3 (3 – 4)	
	Provisional Report	4 (3 – 4)	
	Final Clinical Report	4 (3.5 – 5)	
^{153}Gd Attenuation Correction	Initial Report	3 (2 – 3.5)	<0.001*
	Updated Report	3 (3 – 3.5)	
	Provisional Report	4 (3 – 4)	
	Final Clinical Report	4 (3 – 5)	

Table 4.15 *Variation in clinical confidence at each stage of the reporting process. *Post hoc analysis, all within group differences p<0.001*

4.3.5 Interobserver agreement

Results are summarised in Table 4.16.

At the provisional reporting stage, interobserver agreement was higher for the CTAC strategy (moderate, κ=0.59), than for the strategy without AC (moderate, κ=0.48). The GdAC strategy showed the poorest agreement at the provisional reporting stage (fair, κ=0.33).

Interobserver agreement for final clinical report was similar for both the CTAC strategy and the strategy without AC (both moderate; κ=0.52 and 0.53 respectively). Although GdAC agreement improved after provision of clinical information, it still remained lower than for the other reporting strategies (κ=0.44)

		Kappa	**95% CI**
Provisional Report	No AC	0.48	0.30 – 0.67
	CTAC	0.59	0.42 – 0.77
	GdAC	0.33	0.16 – 0.50
Final Clinical Report	No AC	0.53	0.34 – 0.71
	CTAC	0.52	0.34 – 0.70
	GdAC	0.44	0.26 – 0.62

Table 4.16 *Interobserver agreement for clinical reports before and after clinical information*

4.3.6 Intraobserver agreement

Intraobserver agreement for initial and updated reports was moderate (Observer 1: κ=0.51 an 0.50 respectively; Observer 2: κ=0.55 and 0.56 respectively; Table 4.17).

There were no significant differences in median confidences in the initial and updated reports (Table 4.18). Intraobserver agreement for reporter confidence was generally moderate (κ=0.44 – 0.50), although Observer 2 showed only slight agreement for the updated report, suggesting significant variability in confidence at this stage.

	Kappa	
	Observer 1	**Observer 2**
Initial Report	0.51	0.55
Updated Report	0.50	0.56

Table 4.17 I*ntraobserver agreement for initial and updated reports.*

Observer 1	**Median (IQR)**	**p-value**	**Kappa**
Initial Report	3 (2 – 3)	0.43	0.50
	3 (2 – 3.5)		
Updated Report	3 (3 - 4)	0.87	0.44
	3 (3 - 4)		
Observer 2			
Initial Report	3 (2- 3)	0.98	0.49
	2.5 (2 – 3)		
Updated Report	3 (3 – 4)	0.79	0.14
	3 (3 – 4)		

Table 4.18 *Intraobserver agreement for clinical confidence in initial and updated reports.*

4.4 DISCUSSION

These results demonstrate that neither AC technique predictably affects the pattern of reporting, both improve confidence when clinical information is unknown but no difference is observed once clinical information is known. The CTAC strategy resulted in a difference in final clinical reports compared to the non-corrected strategy (NC) in a quarter of cases, whilst this was true 37% of the time for the GdAC strategy. On no occasion did the CTAC strategy result in change from a fixed or mixed report to a normal or reversible study respectively, whilst this occurred in only 2 cases by the GdAC strategy. These findings are surprising given the highly significant increase in apparent counts inferiorly on both AC images, as demonstrated in Chapter 3. They suggest that AC methods correct artefacts that are easy to recognise on non-corrected images, offering nothing further beyond expert visual scoring. This concept was summarised elegantly in the EANM/ESC 2005 procedural guidelines for MPS: "A major factor to be considered when incorporating AC data into clinical practice is that many trained physicians mentally perform an internal AC."[69]

The differences in final report that *are* seen suggest that the main intervention AC offers is to alter the reporting of reversibility. Whether AC images represent true perfusion better in this regard was not the subject of this study. Of the differences in final report between CTAC and NC, half were reported as reversible using the CTAC strategy but normal with the NC strategy and the other half vice versa. The two main contributors to disagreement between the GdAC and NC strategies were differences in reports suggesting reversibility on NC images but either normal (7/19, 37%) or mixed reports (4/19, 21%) after GdAC. Again, it is difficult to reconcile the results

with the technical effects on the images presented in Chapter 3. The summed difference scores in the LAD territory on GdAC images were lower, which leads to the expectation of more reporting of reversibility via the GdAC strategy. Although there were no overall differences, the GdAC strategy led to fewer reversible reports than the CTAC and NC strategies (9 vs. 16 vs. 18 respectively). This suggests that either the GdAC images are ignored with respect to reporting reversibility or that the propensity of GdAC to 'create' reversibility leads to adjustment of reporting (and thus overcorrection) to account for it. In the former case, it may be that the effects of AC are only considered in the area of interest –the inferior wall in a man, for example – whilst other areas are ignored. In this way, the appearance of anteroapical reversibility on GdAC images has no effect on reporting as it is not accounted for in the analysis by the observer. Given our results, it seems more likely that 'overcorrection' is more likely. It is possible that the creation of apparent inducible LAD territory defects on GdAC imaging leads to presumption of artefact in cases of true reversibility, with a consequent under-reporting of reversible abnormalities. Whichever is the case, it can be seen from these data that AC has a far greater impact on the reporting of reversibility than on fixed defects and there seems to be no meaningful differences between the AC techniques in terms of their effects on report once clinical information is known.

Reporter confidence is higher when AC is used but clinical information blinded. This tallies with several previous studies that have used an essentially combined reporting score reflecting both confidence and nature of report – for example: definitely normal, probably normal, equivocal, probably abnormal or definitely

abnormal[29, 87, 88]. GdAC reduces the number of probably normal/abnormal and equivocal results in stress-only MPS, implying improved confidence in the report with AC[29]. The same group demonstrated similar results when validating a new method of AC for a small-field-of-view cardiac SPECT camera system[89]. Others have also shown equivalent reductions in the number of borderline reports[21, 87]. Our data show a one-category improvement in confidence when clinical information is unknown, with no significant difference between the AC strategies.

Once clinical information is known, there is no difference in reporter confidence for any of the 3 reporting strategies. Images were reported over the course of several months, with no case presented twice within the same or successive reporting sessions. It is highly unlikely therefore that familiarity with the cases is the explanation for this. Indeed, none contained any particularly memorable information – all were conventional cases referred for standard clinical indications. No comparative data from the literature could be found that assessed AC in a clinically open fashion. The 2010 EANM/ESCR/ECNC joint position statement on hybrid cardiac imaging states that AC improves final reporter confidence in MPS images but provides no reference to support this[90]. All data in the aforementioned studies were obtained by image analysis blind to clinical information. The data presented here show clearly that differences in confidence disappear when clinical information is known. Confidence alone cannot therefore be used to justify the use of AC in clinical practice. SPECT MPS should never be reported blind to clinical information as it risks failing to answer the clinical question that generated the referral and renders the patient's pre-test likelihood of significant CAD unknown. This second point is

important as disease prevalence influences positive and negative predictive value. In patient groups with a very low prevalence of ischaemic heart disease (e.g. asymptomatic 30 year old women), mild fixed inferior wall defects are far more likely to represent artefact than in patient groups with a high prevalence (men over 65 with angina). Equally, a history of prior MI renders the same defect far more likely to represent scarring than artefact. Disallowing clinical information when comparing strategies with and without AC disadvantages the non-corrected strategy. When clinical information is known, as would be the case in clinical practice, the benefits of AC on reporter confidence disappear.

Interobserver agreement in final clinical report is higher following the CTAC strategy when clinical information is unknown. This difference again disappears when clinical information is known. The absolute kappa values for agreement remain in the moderate range, probably due to the high prevalence of normal reports. Regardless, comparison of values before and after provision of clinical information is useful. This shows again that clinical information equalises the advantage AC strategies have over non-AC strategies when blind to clinical information.

Use of AC is by no means universal[91], despite the evidence to date, expert recommendations[85] and position statements from learned bodies[20]. This is counter-intuitive unless the true clinical usefulness of AC is perceived to be lower than demonstrated in blinded studies. AC is now being put forward for new indications, for which it is likely to have a much more necessary role. These include stress-only SPECT imaging[30, 92], where AC improves recognition of artefact and negates the need

for a resting acquisition, and absolute quantitation of myocardial perfusion, traditionally a parameter within the domain of PET only. None of the presented data is meant to suggest that AC has no clinical role – only that attenuation artefacts can be read around by experienced observers in possession of full clinical details. Whether the effects of AC on reporting of reversibility carry clinical implications remains to be seen.

4.5 LIMITATIONS

This is a small, single centre study and may be underpowered to detect differences between the strategies. However, differences were found in certain areas in line with previous studies (e.g. reporter confidence), so differences elsewhere ought to have been seen if they existed. It is not possible from our data to confirm which strategy results in the 'truth', as there is no gold standard with which to compare. This was not the purpose of this study, however. Instead the rationale was to measure any changes resulting from AC and their persistence after provision of clinical information.

4.6 SUMMARY FINDINGS

1. Despite the technical effects demonstrated in Chapter 3, clinically-informed reporting strategies using AC do not reduce the number of reported fixed abnormalities.

2. When compared to a non-corrected strategy, a strategy using CTAC is as likely to change a normal report to one indicating reversible ischaemia as it is to do the opposite, whilst GdAC is less likely to result in a report indicating reversibility.
3. Both CTAC and GdAC improve confidence in the clinical report and interoberver agreement when reporters are blind to clinical information. Once clinical information is known, these differences disappear.
4. Overall, clinically-informed reporting strategies using AC have unpredictable effects on final clinical report but no effect on final reporter confidence or interobserver agreement.

SECTION TWO

CHAPTER 5 ASSESSMENT OF MYOCARDIAL SCARRING USING CARDIAC COMPUTED TOMOGRAPHY: PILOT COMPARISON WITH SPECT MYOCARDIAL PERFUSION SCINTIGRAPHY

5.1 INTRODUCTION

Intravenous iodinated and gadolinium contrast agents show similar behaviour in myocardial scarring when compared to normal myocardium[93]. Gadolinium enhancement on delayed cardiovascular magnetic resonance imaging (CMR) has been validated extensively for the evaluation of extent and transmurality of myocardial scarring[59, 60, 94, 95]. Delayed contrast enhancement on cardiovascular computed tomography (CCT) has been demonstrated also, most strikingly in the minutes and hours after acute myocardial infarction (MI) [63, 64, 96]. The aim of the following pilot study was to verify assumed CCT parameters for detection of chronic myocardial scarring in patients with known previous MI, with the intention of taking these parameters forward into a formal prospective study.

5.2 METHODS

10 patients (9 male, mean age 60±15years) with known transmural myocardial infarction on SPECT myocardial perfusion scintigraphy (MPS), defined as ≥50% reduction of tracer uptake in ≥1 myocardial segments according to the AHA 17-segment model, were recruited between June and November 2008 to undergo CCT

with delayed acquisition (dCCT). Patients were excluded if they had any of the following: NYHA class IV symptoms; contraindication to negative chronotropic agents; maximum heart rate >70bpm (including after pharmacologic treatment); severe renal dysfunction (creatinine>150μmol/L); pregnancy or childbearing potential; allergy or previous intolerance of iodinated contrast. All patients were on oral beta-blockade and had resting heart rates of <70 beats per minute. The study was approved by the local research ethics committee and all patients gave written informed consent.

5.2.1 CCT Acquisition Protocol

Images were acquired using 64-slice CT (Sensation 64, Siemens AG Medical Solutions, Erlangen) using retrospective ECG-gating, 32x0.6mm beam collimation, 0.33s rotation time and beam pitch 0.2. Three protocols were used for tube voltage and current respectively: 120kV and 250mAs; 100kV and 460mAs; and 80kV and 825mAs. Two acquisitions were performed for each patient: an initial arterial phase study and subsequent delayed acquisition 7 minutes later. Each protocol maintained a dose-length product of ≤600mGycm.

5.2.2 Contrast Protocol

A test bolus technique was used to time scan delay, as described in Section 2.4.4. Two contrast protocols were assessed (Figure 5.1). In protocol A, 80mL iodinated contrast (Ultravist 370, Bayer Healthcare Pharmaceuticals Inc) was injected at 5mL/s followed immediately by 60mL normal saline/contrast (in 50:50 proportion) at 4mL/s and finally a 25mL normal saline flush at 2.5mL/s. In protocol B, the total contrast

volume required was calculated as 1.5 x patient body weight (BW) in kilograms. 30mL were removed from this volume, leaving an initial contrast volume of (1.5BW-30)mL. This was injected as a 5mL/s bolus and followed by 40mL normal saline at 5mL/s. Immediately thereafter, the remaining 30mL of contrast was administered as an infusion at 0.1mL/s over 5 minutes.

5.2.3 Image Reconstruction and Analysis

Simultaneous ECG recording allowed assignment of images to respective phases of the cardiac cycle. Phases were reconstructed in contiguous 2mm slices at 10% increments from 25-95% of the R-R interval. Both early and delayed datasets were analysed using a custom cardiac software package (TeraRecon Inc) as 5mm multiplanar reformatted images oriented into horizontal long, vertical long and short axis views. Delayed images were viewed using a window width and level of 150 Hounsfield units with manual adjustments as required. Myocardial segments were defined as iso-, hypo-, or hyper-enhanced on early and delayed images. Areas of hypo- and hyperenhancement were characterised as transmural if involving ≥50% of the left ventricular (LV) wall. Segmental LV enhancement patterns were compared between CCT and MPS studies.

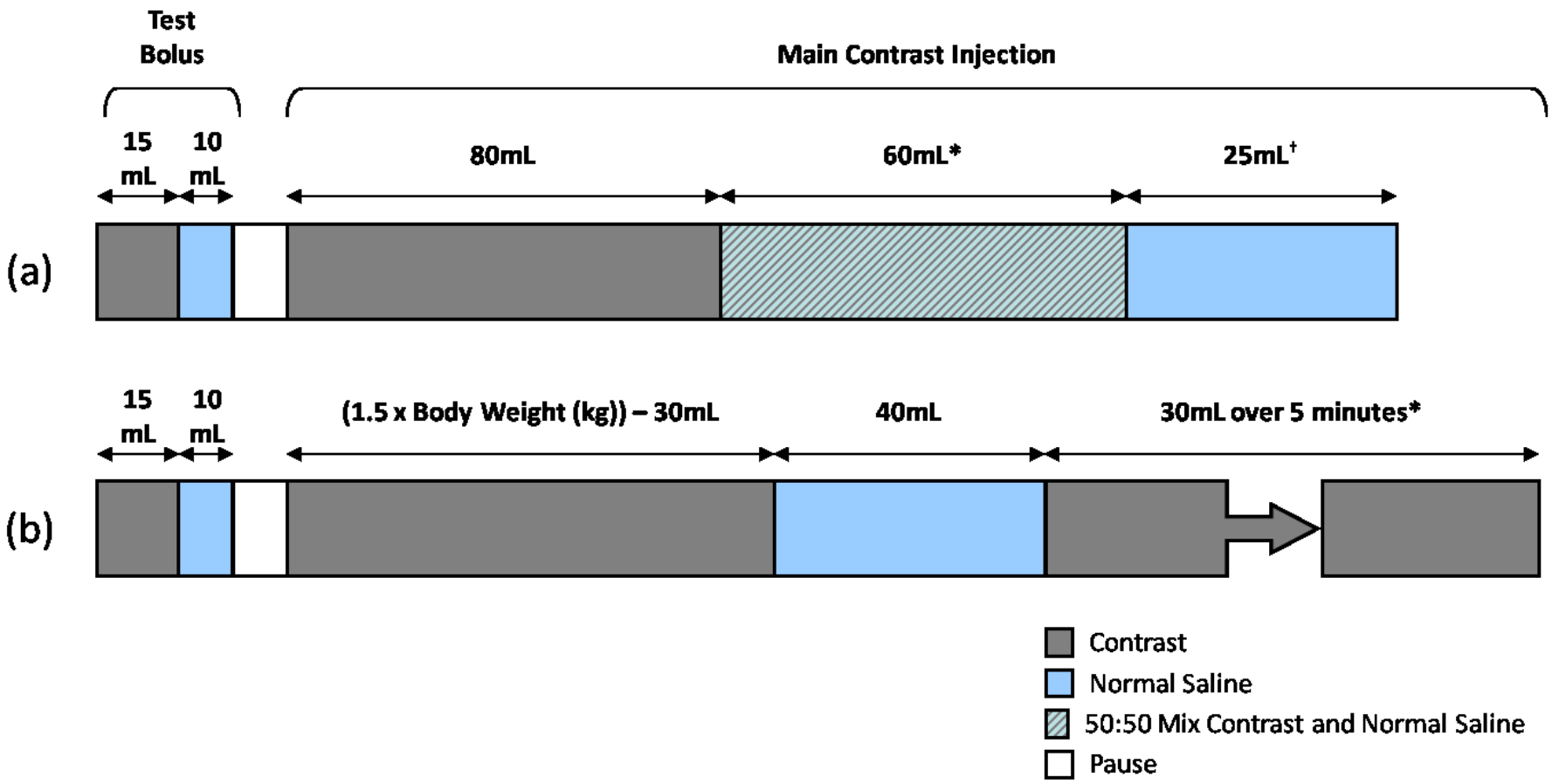


Figure 5.1 *(a) Contrast Protocol A. Injection rate 5mL/s except (*) 4mL/s and (†) 2.5mL/s. (b) Contrast Protocol B. Injection rate 5mL/s except (*) 0.1mL/s.*

5.3 RESULTS

Results are summarised in Table 5.1 and illustrated in Figures 5.2 – 5.3. A total of 44/170 (26%) myocardial segments showed ≥50% reduction of tracer uptake on MPS. The visual extent of myocardial enhancement on dCCT showed better agreement using contrast protocol B than contrast protocol A (24/25 (96%) and 11/19 (58%) segments respectively). dCCT showed the best agreement with MPS when acquired using the 80kV/825mAs acquisition protocol (20/24 (83%) segments vs. 14/18 (78%) and 1/2 (50%) segments for 100kV/460mAs and 120kV/250mAs acquisitions respectively).

Tube Voltage (kV)	Tube Current (mAs)	Contrast Protocol	MPS Transmural MI (% total)	CCT Delayed Enhancement	Percentage Agreement
120	250	A	2 (12%)	1	50%
100	460	A	12 (24%)	8	75%
100	460	B	6 (35%)	6	100%
80	825	A	5 (29%)	2	40%
80	825	B	19 (28%)	18	95%

Table 5.1 *Myocardial segments demonstrating transmural myocardial infarction (MI) on myocardial perfusion scintigraphy (MPS) and delayed enhancement on cardiac computed tomography (CCT) for different X-ray tube settings and contrast protocols.*

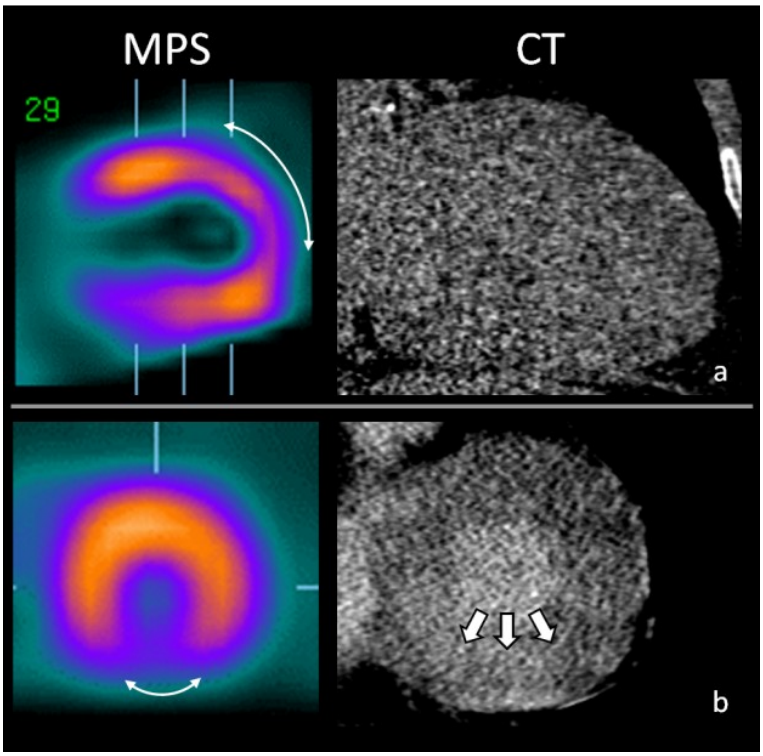


Figure 5.2 *Effect of contrast protocol on delayed enhancement of myocardial scarring. (a) Contrast Protocol A. There is mild to moderate scarring in the anterior wall and apex on the resting MPS images (arrow). There is no delayed enhancement on CCT. (b) Contrast Protocol B. There is moderate inferior scarring on MPS images (arrow). Delayed enhancement is seen in the same area on CCT (arrows).*

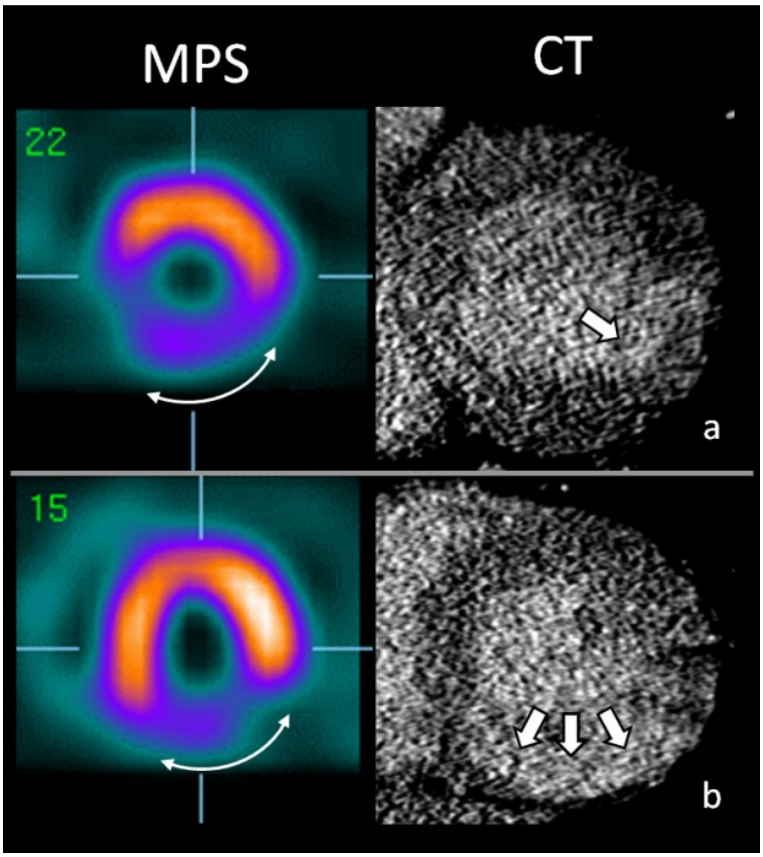


Figure 5.3 *Effect of X-ray tube voltage and current on delayed enhancement of myocardial scarring. (a) Tube voltage 100kV and current 460 effective mAs. There is moderate partial thickness damage inferiorly and inferolaterally on the myocardial perfusion images (double arrow). On CCT, there is subendocardial delayed enhancement inferolaterally only (arrow). (b) Tube voltage 80kV and current 825 effective mAs. There is almost full thickness infarction inferolaterally with moderate partial thickness extension inferiorly (double-head arrow). The pattern of delayed enhancement on CCT is identical (arrows).*

5.4 DISCUSSION

This pilot study demonstrates that the detection of MI by dCCT is feasible. The numbers studied are small and no statistical comparison of contrast protocols or X-ray tube settings is intended. Nonetheless, the data highlight some important points for the main study method moving forward. Delayed enhancement was seen most readily using contrast protocol B. This protocol is likely to have been successful for a number of reasons. First, the contrast dose is tailored to the body weight of the patient. The standard dose of 110mL in use for clinical CT coronary angiography is suitable for the average 80kg patient and facilitates the planning of adequate stock within the department. However, the dose will exceed requirements for patients under 80kg and be inadequate for those above. This may be particularly important in the latter case where the presumed circulating volume is higher, leading to dilution of contrast within the intravascular space, diminution of the contrast gradient into the extravascular extracellular space and thus poorer distribution of contrast within areas of MI. Additionally, the use of a continuous low-flow contrast infusion after main bolus injection allows better delineation of MI. Although validated in the animal model[53], it has found little use in recent human studies looking at delayed enhancement of infarcted myocardium on CCT. This is likely to be due to the almost universal study of delayed enhancement after acute MI. Contrast retention is probably more profound in acute infarction due to associated microvascular plugging and interstitial oedema. Although the volume of contrast distribution remains high in chronic MI, the absence of the features of acute infarction may necessitate a more exotic contrast protocol to encourage retention. It is likely that continuation of a slow-flow contrast infusion after the main contrast bolus improves accumulation and retention of contrast within chronic scarring due to extended maintenance of the contrast gradient.

Delayed enhancement of the myocardium was viewed optimally when the X-ray tube voltage was 80kV. Reducing the tube voltage to 80kV has the effect of lowering the peak energy of the emitted X-rays, resulting in greater attenuation by contrast enhanced structures. It is expected, therefore, that this setting seems optimal for identifying delayed myocardial enhancement. Reducing tube voltage has the negative effect of lowering signal to noise ratio, which can be partly offset by increasing the tube current to increase beam intensity (see Section 1.2.3). When tube voltage and current are set at 80kV and 825mAs respectively, image quality is reasonable and total radiation dose remains within the limit approved by the Research Ethics Committee.

5.5 SUMMARY FINDINGS

1. Identification of MI by dCCT is feasible. Delayed enhancement is best appreciated using a continuous slow flow iodinated contrast infusion after the main bolus and reducing X-ray tube voltage to 80kV. Tube current should be increased to 825mAs to compensate. These settings will be carried over to the main studies for formal prospective assessment of the technique.

CHAPTER 6 ASSESSMENT OF MYOCARDIAL SCARRING USING CARDIAC COMPUTED TOMOGRAPHY: COMPARISON OF VISUAL SCORING WITH SPECT MYOCARDIAL PERFUSION SCINTIGRAPHY

6.1 INTRODUCTION

Extent and depth of myocardial scarring predicts prognosis[97-101] and its quantification allows prediction of segmental recovery after revascularisation[102, 103]. Myocardial scarring in patients without history of myocardial infarction (MI) carries high risk for subsequent cardiac events and is incremental to clinical, angiographic and functional predictors[104]. Several techniques are available for quantification of myocardial scarring, the most common being SPECT myocardial perfusion scintigraphy (MPS) and cardiovascular magnetic resonance imaging (CMR). Both techniques are validated in this domain and, when combined with quantification of myocardial ischaemia, predict segmental recovery after revascularisation[59, 60, 94, 105]. Echocardiography may also be used to evaluate regional myocardial function at rest and during stress; resting regional myocardial dysfunction that fails to improve after low-dose dobutamine stress implies transmural MI that is highly unlikely to recover function after revascularisation[106]. However, it is still possible to have myocardial scarring in the presence of normal wall motion and identification of scar in this setting remains the strongest predictor of adverse cardiovascular events[95]. As such, techniques that image myocardial scarring (or viability) directly, such as MPS and CMR, are theoretically more advantageous.

Cardiac computed tomography (CT) is a validated technique for non-invasive evaluation of the coronary arteries[107, 108] and is recommended by the current NICE guidelines for patients with stable chest pain at low to intermediate pre-test likelihood of significant coronary artery disease[109]. The left ventricular myocardium is imaged as part of the standard CTA dataset and MI may be seen as areas of hypoenhancement. This is due to impairment of iodinated contrast handling in scarred myocardium that results from reduction in functional capillary density and increased volume of contrast distribution in collagenous scar[110]. In this way, iodinated contrast media behave similarly to gadolinium contrast used in CMR[111]. Early hypoenhancement of MI on CCT is a specific but relatively insensitive finding[112, 113]. Delayed hyperenhancement on gadolinium-enhanced CMR is used clinically to determine depth and extent of myocardial scarring. Similar results have been demonstrated in CCT in the setting of acute MI[63, 64, 96] but demonstration of utility in the chronic setting has been more limited[114-116]. It is possible that delayed hyperenhancement on CCT offers better sensitivity for detection of myocardial scarring compared to standard arterial phase CCT acquisitions used for CTA.

The aim of this study was to compare visual quantification of early and delayed CCT (eCCT and dCCT respectively) enhancement patterns in patients with previous MI and assess agreement with resting tracer uptake on MPS.

6.2 METHODS

50 patients (39 male, mean age 66±8.8 years) with previous MI referred for clinical stress/rest SPECT MPS were recruited. Time since MI was 10±9.0 years (min 62 days, max 30 years). Eleven (22%) patients underwent primary percutaneous coronary intervention at the time of MI. Patients were excluded if they had any of the following: NYHA class IV

symptoms; contraindication to negative chronotropic agents; maximum heart rate >70bpm (including after beta-blockade); severe renal dysfunction (creatinine >150µmol/L); pregnancy or childbearing potential; allergy or previous intolerance of iodinated contrast. All patients were taking beta-blockers. The study was approved by a local research ethics committee and all patients gave written informed consent.

6.2.1 SPECT Myocardial Perfusion Scintigraphy

Patients underwent pharmacological stress and rest MPS imaging as outlined in Section 2.3. MPS images were analysed using QPS/QGS software (Hermes Medical Systems). Segmental uptake scores were obtained according to the AHA 17-segment model of the heart using the QPS/QGS normal reference database. Segmental resting tracer uptake was classified as normal, mildly/moderately/severely reduced or absent. Segments were also categorised as showing no evidence of MI (normal resting tracer uptake), non-transmural MI (mildly reduced resting tracer uptake) and transmural infarction (≥moderately reduced resting tracer uptake). Segmental resting scores were summed to give a summed rest score (SRS, normal=0, maximum 68).

6.2.2 Cardiac Computed Tomography

Images were acquired using 64-slice CT (Sensation 64, Siemens AG Medical Solutions, Erlangen) using retrospective ECG-gating, tube voltage 80kV, tube current 825mAs, 32x0.6mm beam collimation, 0.33s rotation time and beam pitch 0.2. Intravenous iodinated contrast (Ultravist 370, Bayer Healthcare Pharmaceuticals Inc) was administered in a triphasic protocol as described in Chapter 5.2.2, with a continuous slow-flow contrast infusion after the main bolus. A test bolus technique was used to time scan delay, as described in Section 2.4.4. Patients underwent arterial phase and delayed-pass

acquisitions, with the latter performed 7 minutes after main contrast bolus injection. Median dose-length product was 596mGycm (IQR 553 – 635 mGycm). This was calculated during original ethics application to equate to a maximum effective dose of 15mSv using a thoracic conversion coefficient of 0.014. Subsequent evidence suggests that this coefficient underestimates CCT doses, being somewhat closer to 0.028[117]. Using this corrected coefficient, median effective radiation exposure for cardiac CT was 16.7mSv (IQR 15.5 – 17.8mSv). All patients had heart rates <70 beats per minute (bpm) and required no beta-blockade. Median heart rates were lower during eCCT (60bpm [IQR 54 – 63bpm]) compared with dCCT (63bpm [IQR 56 – 66bpm], p=0.007).

6.2.3 Image Analysis

Phases were reconstructed according to position within the R-R interval, at 10% increments from 25-95% of the R-R interval. For this study, the end-diastolic phase (75% R-R interval) was chosen for analysis. Both eCCT and dCCT images were analysed using proprietary cardiac software (TeraRecon Inc) as 5mm thick multiplanar reformatted images oriented into horizontal long, vertical long and short axis views. The left ventricular myocardium was divided into 17 segments as described in Section 2.2. Delayed images were viewed using a window width and level of 150HU with manual adjustments as required. Myocardial segments were defined as iso-, hypo-, or hyper-enhanced compared to surrounding segments. Areas of abnormal enhancement were characterised as transmural if involving ≥50% of segmental myocardial thickness and non-transmural otherwise. Segmental scores were summed to give a CCT summed scarring score (normal=0, maximum score 34).

6.2.4 Statistics

All statistics were calculated using MedCalc statistical software (version 12.2.1.0, MedCalc Software). Data are presented as mean±SD or median (interquartile range) as appropriate. Patient and segment-level agreement were compared using Cohen's kappa. Where appropriate, sensitivities, specificities, positive and negative predictive values were calculated. MPS summed rest scores and CCT summed scarring scores were correlated using Spearman's rank correlation. Differences in mean segmental relative uptake scores within CCT scarring categories were assessed by one-way ANOVA.

Study power calculations were based on the work of Buderer[118] and performed with the assistance of a professional statistician. Previous data have suggested that CCT may have around 90% sensitivity and 80% specificity for detection of MI. In a population with clinically-defined previous MI, MPS and CMR abnormalities would be expected in 75-80% of patients. Allowing a 10% confidence interval for sensitivity and specificity, 50 patients need to be recruited (β=0.8, α=0.05) to detect an effect.

6.3 RESULTS

6.3.1 Myocardial Perfusion Scintigraphy

43/50 (86%) patients showed evidence of previous MI. Median summed rest score was 7.5 (3 – 18). Of 850 segments, 579 (68%) were normal, while 123 (15%), 67 (8%), 44 (5%) and 37 (4%) showed mild, moderate or severe reduction or absent uptake respectively. These were grouped into 579 (68%), 123 (15%) and 148 (17%) segments showing either no MI,

non-transmural or transmural MI respectively. Distribution according to coronary artery territory is shown in Table 6.1.

Coronary Territory	No infarction	Non-transmural	Transmural	% Infarction
LAD	242	45	63	31
LCx	191	29	30	24
RCA	146	49	55	42
Total	**579 (68%)**	**123 (15%)**	**148 (17%)**	**32**

Table 6.1 *Proportions of segmental MI on MPS according to coronary artery territory.*

6.3.2 Computed Tomography

Early CCT

38/50 (76%) patients demonstrated MI. Median summed scarring score was 3.5 (1 – 9). Of 850 segments, 657 (77%) were considered normal, whilst 119 (14%) and 74 (9%) showed non-transmural or transmural MI respectively. Distribution according to coronary artery territory is shown in Table 6.2.

Coronary Territory	No infarction	Non-transmural	Transmural	% Infarction
LAD	231	70	49	34
LCx	219	21	10	12
RCA	207	28	15	17
Total	**657 (77%)**	**119 (14%)**	**74 (9%)**	**24**

Table 6.2 *Proportions of segmental MI on eCCT according to coronary artery territory.*

Delayed CCT

43/50 (86%) patients demonstrated MI, of which 32 (74%) had at least one segment of transmural scarring. Median summed scarring score was 5.5 (1 – 11). Of 850 segments, 620 (73%) were considered normal, whilst 112 (13%) and 118 (14%) showed non-transmural or transmural MI respectively. Distribution according to coronary artery territory is shown in Table 6.3.

Coronary Territory	No infarction	Non-transmural	Transmural	% Infarction
LAD	247	48	55	29
LCx	194	31	25	22
RCA	179	33	38	28
Total	**620 (73%)**	**112 (13%)**	**118 (14%)**	**27**

Table 6.3 *Proportions of segmental MI on dCCT according to coronary artery territory.*

6.3.3 Patient-level agreement between MPS and CCT

Discrimination of normal and abnormal myocardium

Results are summarised in Table 6.4. eCCT agreed with MPS in 37/50 (74%) cases. Sensitivity, specificity, positive and negative predictive values were 79%, 43%, 90% and 25% respectively. eCCT was false positive and false negative at patient level in 4/38 (11%) and 9/12 (75%) cases respectively. Overall accuracy was poor (AUC 0.61).

dCCT agreed with MPS in 42/50 (84%) cases. Sensitivity, specificity, positive and negative predictive values were 91%, 43%, 91% and 43% respectively. dCCT was false positive in 4/43 (9%) cases, whilst 4/7 (57%) negative scans were false negative. Overall accuracy was poor (AUC 0.67), with no differences in accuracy between eCCT and dCCT (p=0.70).

Discrimination of non-transmural and transmural myocardial infarction

Results are summarised in Table 6.5. eCCT agreed with MPS in 38/50 (76%) cases. Sensitivity, specificity, positive and negative predictive values were 64%, 100%, 100% and 59% respectively. eCCT was false positive and false negative at patient level in 0/21 (0%) and 12/29 (41%) cases respectively. Overall accuracy was good (AUC 0.82).

dCCT agreed with MPS in 47/50 (94%) cases. Sensitivity, specificity, positive and negative predictive values were 94%, 94%, 97% and 89% respectively. CCT was false positive in 1/32 (3%) cases, whilst 2/18 (11%) negative scans were false negative. Overall accuracy was excellent (AUC 0.94), with no differences in accuracy between eCCT and dCCT (p=0.07).

	Sensitivity	Specificity	PPV	NPV	AUC	p-value
Early	79 (64 – 90)	43 (10 – 82)	90 (75 – 97)	25 (6 – 57)	0.61 (0.46 – 0.74)	0.70
Delayed	91 (78 – 97)	43 (10 – 82)	91 (78 – 98)	43 (10 – 82)	0.67 (0.52 – 0.80)	

Table 6.4 *Analysis of CCT for patient-level sensitivity, specificity, positive predictive value (PPV), negative predictive value (NPV) and accuracy (AUC, area under the curve) for detection of patients with any evidence of myocardial infarction on MPS.*

	Sensitivity	Specificity	PPV	NPV	AUC	p-value
Early	64 (45 – 80)	100 (81 – 100)	100 (84 – 100)	59 (39 – 77)	0.82 (0.68 – 0.91)	0.07
Delayed	94 (80 – 99)	94 (71 – 100)	97 (84 – 100)	89 (64 – 99)	0.94 (0.84 – 0.99)	

Table 6.5 *Analysis of CCT for patient-level sensitivity, specificity, positive predictive value (PPV), negative predictive value (NPV) and accuracy (AUC, area under the curve) for detection of patients with at least one segment of transmural myocardial infarction on MPS.*

Correlation between CCT and MPS summed scores

Correlation between MPS summed rest scores and CCT summed scaring scores were good (r=0.66) and excellent (r=0.92) for eCCT and dCCT images respectively (Table 6.6).

	Spearman's rank correlation	95% Confidence Interval
Early	0.66	0.47 – 0.79
Delayed	0.92	0.86 – 0.95

Table 6.6 *Correlation between MPS summed rest scores and CCT summed scarring scores for both eCCT and dCCT.*

6.3.4 Segment-level agreement between MPS and CCT

Results for overall segmental agreement are shown in Table 6.7. eCCT showed moderate agreement (614/850 (72%) segments , κ=0.53), whilst on delayed images it was good (714/850 (84%) segments, κ=0.79).

	Kappa	95% Confidence Interval
Early	0.53	0.47 – 0.60
Delayed	0.79	0.75 – 0.83

Table 6.7 *Segment-level agreement for the presence of transmural and non-transmural myocardial infarction and normal myocardium.*

For detection of any segmental MI, sensitivity, specificity, positive and negative predictive values were 49%, 89%, 68% and 79% respectively for eCCT and 75%, 95%, 88% and 89% respectively for dCCT (Table 6.8). Agreement was moderate (650/850 (76%) segments, κ=0.41) and good (753/850 (89%) segments, κ=0.73) for eCCT and dCCT respectively. Overall accuracy was fair for eCCT (AUC 0.69) and good for dCCT (AUC 0.85), with the latter significantly higher than the former ($p<0.0001$).

For discrimination of segments with transmural MI, sensitivity, specificity, positive and negative predictive values were 44%, 99%, 88% and 89% respectively for eCCT and 70%, 98%, 87% and 94% respectively for dCCT (Table 6.9). Agreement was moderate (758/850 (89%) segments, κ=0.53) and good (790/850 (93%) segments, κ=0.73) for eCCT and dCCT respectively. Overall accuracy was fair for eCCT (AUC 0.71) and good for dCCT (AUC 0.84), with the latter significantly higher than the former ($p=0.0001$).

	Agreement	Sensitivity	Specificity	PPV	NPV	AUC	p-value
Early	0.41 (0.35 – 0.48)	49 (43 – 55)	89 (87 – 92)	68 (61 – 75)	79 (76 – 82)	0.69 (0.66 – 0.72)	<0.0001
Delayed	0.73 (0.68 – 0.78)	75 (69 – 80)	95 (93 – 97)	88 (83 – 92)	89 (86 – 91)	0.85 (0.82 – 0.87)	

Table 6.8 *Analysis of CCT for segment-level agreement (κ), sensitivity, specificity, positive predictive value (PPV), negative predictive value (NPV) and accuracy (AUC, area under the curve) for detection of any myocardial infarction on MPS.*

	Agreement	Sensitivity	Specificity	PPV	NPV	AUC	p-value
Early	0.53 (0.45 – 0.61)	44 (36 – 52)	99 (98 – 99)	88 (78 – 94)	89 (87 – 91)	0.71 (0.68 – 0.74)	0.0001
Delayed	0.73 (0.67 – 0.80)	70 (62 – 77)	98 (96 – 99)	87 (80 – 93)	94 (92 – 96)	0.84 (0.81 – 0.86)	

Table 6.9 *Analysis of CCT for segment-level agreement (κ), sensitivity, specificity, positive predictive value (PPV), negative predictive value (NPV) and accuracy (AUC, area under the curve) for discrimination of transmural and non-transmural myocardial infarction on MPS*

6.3.5 Agreement by coronary territory

Results are summarised in Table 6.10.

eCCT showed good agreement in the LAD territory (264/350 (75%) segments, κ=0.70) but only fair to moderate agreement in the LCx and RCA territories (188/250 (75%) segments, κ=0.36; and 162/250 (65%) segments, κ=0.40 respectively).

dCCT showed excellent agreement in the LAD territory (308/350 (88%) segments, κ=0.86) and good agreement in the LCx and RCA territories (216/250 (86%) segments, κ=0.79; and 190/250 (76%) segments, κ=0.70 respectively).

	Territory	Kappa	95% Confidence Interval
Early	LAD	0.70	0.62 – 0.78
	LCx	0.36	0.21 – 0.51
	RCA	0.40	0.29 – 0.52
Delayed	LAD	0.86	0.81 – 0.91
	LCx	0.79	0.71 – 0.88
	RCA	0.70	0.61 – 0.78

Table 6.10 *Segmental agreement between MPS and eCCT and dCCT separated according to typical coronary artery territory.*

6.3.6 Transmurality of myocardial scarring on CCT compared with relative percentage segmental uptake on MPS

Results are summarised in Table 6.11. Median relative uptake scores in segments classified as normal on eCCT and dCCT were 72 and 74 respectively. In segments classified as non-transmural and transmural infarction on CT, median relative uptake scores were 67 and 62; and 39 and 41 for eCCT and dCCT respectively. No differences were seen between eCCT and dCCT, but within group differences were significant across all categories.

	Normal	**Non-transmural**	**Transmural**	**p-value**
Early	72 (61 – 81)	67 (55 – 77)	39 (29 – 53)	<0.001*
Delayed	74 (64 – 83)	62 (53.5 – 68.5)	41 (31 – 53)	<0.001*

Table 6.11 *Mean relative segmental uptake scores on MPS according to classification of myocardial scarring on CCT. *All within group differences significant (p<0.05 for all when adjusted for post-hoc analysis).*

6.4 DISCUSSION

The results demonstrate that MI can be identified on both eCCT and dCCT, although the latter clearly performs best. dCCT summed scarring scores correlate highly with MPS summed rest scores (r=0.92) and suggest a better linear relationship compared to eCCT (r=0.66). At patient level, dCCT is more sensitive than eCCT (94% vs 64%) for detection of patients with transmural MI and overall accuracy is excellent (AUC 0.94). Overall segmental agreement is also higher with dCCT (κ=0.79 vs 0.53 on eCCT), as is agreement for the distinction of normal from infarcted myocardium (κ=0.73 vs 0.41 on eCCT) and non-transmural from transmural MI (κ=0.73 vs 0.53 on eCCT). Segmental agreement between dCCT and MPS is therefore consistently good, with specificities, PPV and NPV of 95-98%, 87-88% and 89-94% respectively for detection of MI. Sensitivity of dCCT remains modest (70-75%) but is again consistently higher than on eCCT. The modest sensitivity might possibly relate to an imperfect gold-standard, as discussed below – attenuation artefact on MPS interpreted as true disease but not seen on CCT. Overall segmental accuracy is very good for dCCT (AUC 0.84-0.85) and significantly higher than that seen by eCCT.

Hypoattenuation on eCCT in areas of MI has been studied before and was seen even in the single slice CT era in patients scanned within a month of acute MI[119]. Since this time, studies have focussed on CT imaging of acute MI[63, 64, 120, 121], a setting in which CT performs better when compared with chronic MI[111]. When performed within an hour of primary percutaneous coronary intervention, dCCT has a patient-level sensitivity, specificity, positive and negative predictive value of 92%, 100%, 100% and 85% respectively[64]. The majority of this study population (94%) was imaged

following ST-elevation MI – data were therefore enriched by acute transmural MI – and those with previous infarction were excluded. Our study demonstrates roughly equivalent values for detection of transmural MI in the chronic setting by dCCT (94%, 94%, 97% and 89% respectively). Patient-level parameters for detection of MI of any depth or extent (as opposed to transmural scarring alone) were poorer (91%, 43%, 91% and 43% respectively), which probably reflects the greater pathophysiological disturbance in acutely infarcted myocardium, namely myocardial oedema and availability of intramyocellular space for contrast distribution. These parameters fade when acute infarction matures into chronic, collagenous scar. Segment-level sensitivity, specificity, PPV, NPV and accuracy of dCCT shortly after acute MI for predicting lack of contractile reserve on dobutamine stress echocardiography (i.e. transmural MI) have been shown to be 98%, 94%, 99%, 79% and 97%[64]. In the chronic setting, eCCT has sensitivity, specificity, PPV and NPV of 75%, 98%, 68% and 99% for segmental MI on SPECT MPS[122]. Values for the present study using dCCT are similar to this (70%, 98%, 87%, 94% respectively), although we have shown a better positive predictive value. Reasons for poorer sensitivity compared with imaging of acute MI are discussed below; PPV and NPV remain good in the present study, and the variation with results from the AMI setting may be the result of prevalence of segmental transmural MI in the study populations (17.4% in this study, 9.2% in [23]).

It is interesting that there is differential agreement across coronary artery territories. This may in part explain the modest sensitivity offered by dCCT. Agreement in all coronary territories is improved on dCCT, but RCA territory agreement is poorer on both eCCT and dCCT. The number of infarcted segments in the RCA territory was

greater on MPS than on eCCT and dCCT (42% vs. 18% vs. 28% respectively, p<0.0001 for MPS vs. eCCT/dCCT). Median end-diastolic segmental wall thickness in the RCA territory, calculated on eCCT as part of another study (Chapter 10), was greater than that seen in the LAD (8mm [IQR 6 – 9mm] vs 7mm (6 – 9mm], p=0.01), suggesting that disagreement is unlikely to be related to lower spatial resolution or partial volume artefact on MPS. As seen in Chapter 3, MPS is significantly affected by inferior attenuation artefact and it may be that areas of artefactually reduced tracer uptake were instead reported as MI. Excluding RCA segments from analysis does not materially increase sensitivity and accuracy of dCCT for detecting transmural MI (74% vs. 70% and 86% vs. 84% respectively, 95% confidence intervals for both significantly overlap). However, these values are probably higher when discriminating normal and abnormal segments (83% vs. 75% and AUC 0.89 vs. 0.85 respectively, 95% confidence intervals only just overlap), suggesting possible misinterpretation of inferior wall attenuation artefact as mild partial thickness MI. Regardless, MPS is the gold-standard in this study and overall segment-level analysis must be interpreted on this basis. The issue of MPS as an imperfect gold-standard could only be addressed by comparing CCT and MPS to a third standard, such as cardiovascular magnetic resonance imaging. The value of CCT is in its ability to predict the presence or absence of MI. In this regard, dCCT offers superior segmental PPV and NPV in the region of 90% (NPV ~95% if the RCA territory is excluded), suggesting that it is an acceptable method for evaluating MI.

6.5 LIMITATIONS

This is a small, single centre study evaluating patients with known previous MI, so the results may not be applicable to other populations with a lower segmental prevalence of MI. Patient-level values in particular manifest wide 95% confidence intervals, probably due to the small sample size. This limits interpretation as the significance of patient-level results that seem intuitively different may be underestimated (e.g. patient-level accuracy for detecting transmural MI 94% on dCCT and 82% on eCCT but p=0.07). Image noise on dCCT images seemed high and may have affected results. Improved software techniques for displaying dCCT images may improve visual evaluation of myocardial enhancement patterns.

6.6 SUMMARY FINDINGS

1. dCCT summed scarring scores demonstrate a better linear relationship with MPS summed rest scores than those measured by eCCT.
2. dCCT is consistently more sensitive at patient level than eCCT for detecting MI on SPECT MPS and is probably more accurate at detecting patients with transmural MI.
3. Compared with eCCT, dCCT shows better overall segmental agreement with MPS resting tracer uptake scores and better performance at detecting segments with normal resting tracer uptake and transmural MI.
4. CCT measures of MI show differential agreement across typical coronary artery territories. dCCT significantly improves agreement in all 3 territories compared to eCCT, but agreement is poorest in the RCA territory. This may be related to the effects of inferior attenuation artefact on MPS, as shown in Section 1.

CHAPTER 7 QUANTITATIVE ANALYSIS OF SEGMENTAL MYOCARDIAL ENHANCEMENT ON CARDIAC CT IN PATIENTS WITH PREVIOUS MYOCARDIAL INFARCTION

7.1 INTRODUCTION

Visual assessment of segmental myocardial enhancement patterns on delayed cardiac CT (dCCT) is highly specific for chronic myocardial infarction (MI) and carries positive and negative predictive values in the region of 90%, as demonstrated in Chapter 6. Although visual identification of delayed myocardial enhancement is clearly possible, objective quantification carries theoretical advantages, particularly for potential reproducibility and detection of subtle enhancement that is difficult to distinguish by the naked eye. These advantages have been demonstrated for SPECT myocardial perfusion scintigraphy (MPS)[123]. dCCT using CT parameters stated in the previous chapter is subject to reasonable image noise and so it is also possible that this is accounted for better by the experienced observer rather than software, with higher accuracy for identification of MI visually than by objective measurements.

The aim of this study is to quantify mean segmental wall intensity (SWI), the average Hounsfield value of all voxels included within a myocardial segment, on early (eCCT) and delayed (dCCT) cardiac CT images and compare this with segmental resting tracer uptake on MPS. Accuracy in discriminating normal from abnormal myocardium and non-transmural from transmural MI will also be assessed.

7.2 METHODS

50 patients (39 male, mean age 66±8.8 years) with previous MI referred for clinical stress/rest SPECT MPS were recruited. Full demographics and recruitment criteria are described in Section 6.2. The study was approved by the local research ethics committee and all patients gave written informed consent. Cardiac CT protocol, including contrast regime, is described in Sections 2.4, 5.2.2 and 6.2.2. SPECT MPS was performed and analysed as described in Sections 2.3 and 6.2.1.

7.2.1 Cardiac CT image analysis

The end-diastolic phase (75% R-R interval) was reconstructed using a medium-smooth kernel. Early and delayed datasets were analysed using proprietary cardiac software (TeraRecon Inc). The 75% phase of the early dataset was loaded into a density threshold program (Time Volume Analysis) and the LV blood pool identified in semi-automated fashion, as described in Sections 2.5 and 2.6. The outer edge of the LV blood pool was defined as the endocardial contour, with manual adjustments made as necessary. The epicardial contour was defined as the boundary between the myocardial surface and epicardial fat. The endo- and epicardial contours defined the myocardial volume, which was then fitted to the AHA 17-segment model and displayed on a polar plot, as described in Section 2.6. Each segment was categorised according to mean wall intensity (average HU value of all voxels included in that segment) and myocardial thickness (see Sections 2.5.1 and 2.6.1). The same process was repeated for the 75% phase of the delayed dataset. Epicardial contour remained straightforward to identify on delayed images as contrast between myocardium and epicardial fat remained high. The endocardial contour was more difficult to identify

due to similar enhancement of LV blood pool and scarred myocardium, where present. After initial processing, segmental myocardial thickness on dCCT was compared to that on eCCT and delayed endocardial contour adjusted as necessary. Overall, there was no significant difference in segmental wall thickness between the eCCT and dCCT (7.55±2.14mm vs. 7.64±2.11mm respectively, p=0.09).

Early and delayed SWI were recorded as absolute Hounsfield unit (HU) values. The ratio of the values was also calculated ([Delayed HU]÷[Early HU]) to give a delayed enhancement ratio (DER). This value is conceptually more appropriate than absolute values as it self-adjusts for patient BMI and image noise.

7.2.2 Statistics

Data were analysed using MedCalc statistics software (version 12.2.1.0, MedCalc Software). Early SWI, delayed SWI and DER were compared across MPS categories using Kruskal-Wallis testing with pairwise comparisons adjusted for multiple testing if indicated. Sensitivity, specificity, positive and negative predictive values (PPV/NPV respectively) of CCT for discriminating normal segments from those with non-transmural or transmural MI were calculated. ROC analysis was used to find the method with highest accuracy, as measured by areas under the curve (AUC).

7.3 RESULTS

7.3.1 Comparison of segmental wall intensity across MPS categories

Results are summarised in Table 7.1.

Early CCT

Differences in SWI were seen across MPS categories ($p<0.0001$), although normal and mildly reduced resting tracer uptake (125HU vs. 122HU respectively, $p=0.19$) and severely reduced and absent uptake (105.5HU vs. 84HU, $p=0.08$) were not distinguished. Segments with moderately reduced tracer uptake showed lower and higher SWI than those with mildly or severely reduced tracer uptake respectively (110HU vs. 122HU, $p=0.01$; 110HU vs. 105HU, $p=0.02$ respectively).

Delayed CCT

Differences in SWI were seen across MPS categories ($p<0.0001$). Normal segments were significantly different from abnormal segments but no discrimination was otherwise possible (102HU vs. 110.5HU [mild reduction], $p<0.0001$).

Delayed enhancement ratio

Differences in DER were seen across MPS categories ($p<0.0001$). DER was no different in segments showing severe reduction in or absent resting tracer uptake (1.17 vs. 1.36, $p=0.18$), but all other comparisons were significant. In particular, DER differed between segments with normal tracer uptake and those with mild reduction (0.81 vs. 0.90, $p<0.0001$) and between those with mild and moderate reductions (0.90 vs. 1.03, $p=0.003$) on MPS.

	eCCT	dCCT	DER
Normal	125 (107 – 149)†	102 (96 – 110)	0.81 (0.71 – 0.95)
Mild ↓	122 (106 – 138)†	110.5 (98 – 128.5)*	0.90 (0.76 – 1.12)
Moderate ↓	110 (95.25 – 132.75)	114.5 (103 – 130)*	1.03 (0.86 – 1.28)
Severe ↓	105.5 (74.5 – 114.5)*	119 (105.5 – 138)*	1.17 (1.03 – 1.53)*
Absent	84 (59.5 – 110)*	129.5 (108.5 – 148)*	1.36 (1.16 – 2.14)*
p-value	<0.0001	<0.0001	<0.0001

Table 7.1 *Early and delayed segmental wall intensities and delayed enhancement ratios (DER) for each category of resting MPS segmental tracer uptake. *no significant differences for these within-group comparisons.*

7.3.2 Comparison according to transmurality of myocardial infarction on MPS

Results are summarised in Table 7.2.

Early CCT

Segments with transmural MI showed lower SWI than those with non-transmural MI (104HU vs. 122HU, p<0.001) or no evidence of infarction (104HU vs. 125HU, p<0.001). No differences were seen between segments with non-transmural MI and normal segments on MPS (122HU vs. 125HU, p=0.57).

Delayed CCT

Segments with transmural MI showed higher SWI than those with non-transmural MI (119HU vs. 110.5HU, p=0.04) or normal resting tracer uptake (119HU vs. 102HU,

p<0.001). Segments with non-transmural MI had higher SWI than normal segments (110.5HU vs. 102HU, p<0.0001).

Delayed enhancement ratio

Segments with transmural MI showed higher DER than those with non-transmural MI (1.16 vs. 0.90, p<0.0001) or normal resting tracer uptake (1.16 vs. 0.81, p<0.001). Segments with non-transmural MI had higher DER than normal segments (0.90 vs. 0.81, p<0.0001).

	eCCT	dCCT	DER
Normal	125 (107 – 149)*	102 (96 – 110)	0.81 (0.71 – 0.95)
Non-transmural	122 (106 – 138)*	110.5 (98 – 128.5)	0.90 (0.76 – 1.12)
Transmural	104 (78.5 – 121.5)	119 (105 – 135)	1.16 (0.97 – 1.49)
p-value	<0.0001	<0.0001†	<0.0001†

Table 7.2 *Early and delayed segmental wall intensities and delayed enhancement ratios according to transmurality of myocardial infarction on MPS. *no differences between highlighted categories; †all pairwise comparisons significant.*

7.3.3 Discrimination of normal and abnormal resting MPS uptake

Results are summarised in Table 7.3. Using a threshold of 110HU for discriminating normal and abnormal myocardial segments, eCCT showed sensitivity, specificity, PPV and NPV of 49%, 71%, 44% and 75% respectively, with AUC 0.64 (95% CI: 0.61 – 0.67). With a similar cut-off (113HU), values on dCCT were 53%, 81%, 57% and 79% respectively, with AUC 0.70 (95% CI: 0.67 – 0.74). DER showed the best accuracy (cut-off 1.01), with sensitivity, specificity, PPV and NPV of 55%, 85%, 63% and 80%

respectively, generating an AUC of 0.74 (95% CI: 0.71 – 0.77). Comparison of ROC curves (Figure 7.1) showed better accuracy of DER compared to eCCT and dCCT for discriminating normal segments on MPS ($p<0.0001$ and 0.05 respectively).

7.3.4 Detection of transmural myocardial infarction

Results are summarised in Table 7.4. Using a threshold of 110HU for discriminating segmental non-transmural and transmural MI, eCCT showed sensitivity, specificity, PPV and NPV of 62%, 70%, 30% and 90% respectively, with AUC 0.72 (95% CI: 0.68 – 0.75). With a similar cut-off (113HU), values on dCCT were 60%, 77%, 35% and 90% respectively, with AUC 0.72 (95% CI: 0.69 – 0.75). DER showed the best accuracy (cut-off 1.01), with sensitivity, specificity, PPV and NPV of 71%, 81%, 44% and 93% respectively, and AUC 0.82 (95% CI: 0.79 – 0.85). Comparison of ROC curves (Figure 7.2) showed better accuracy for DER compared to eCCT and dCCT for detecting segments with transmural MI on MPS ($p<0.0001$ and 0.0002 respectively).

	eCCT	dCCT	DER
Threshold	110HU	113HU	1.01
Sensitivity	49 (43 – 55)	53 (47 – 60)	55 (49 – 62)
Specificity	71 (67 – 74)	81 (78 – 85)	85 (82 – 88)
PPV	44 (38 – 50)	57 (51 – 64)	63 (56 – 69)
NPV	75 (71 – 78)	79 (75 – 82)	80 (77 – 83)
AUC	0.64 (0.61 – 0.67)	0.70 (0.67 – 0.74)	0.74 (0.71 – 0.77)

Table 7.3 *Accuracy of early and delayed segmental wall intensity and delayed enhancement ratio (DER) for detection of any segmental MI (prevalence 31.9%).*

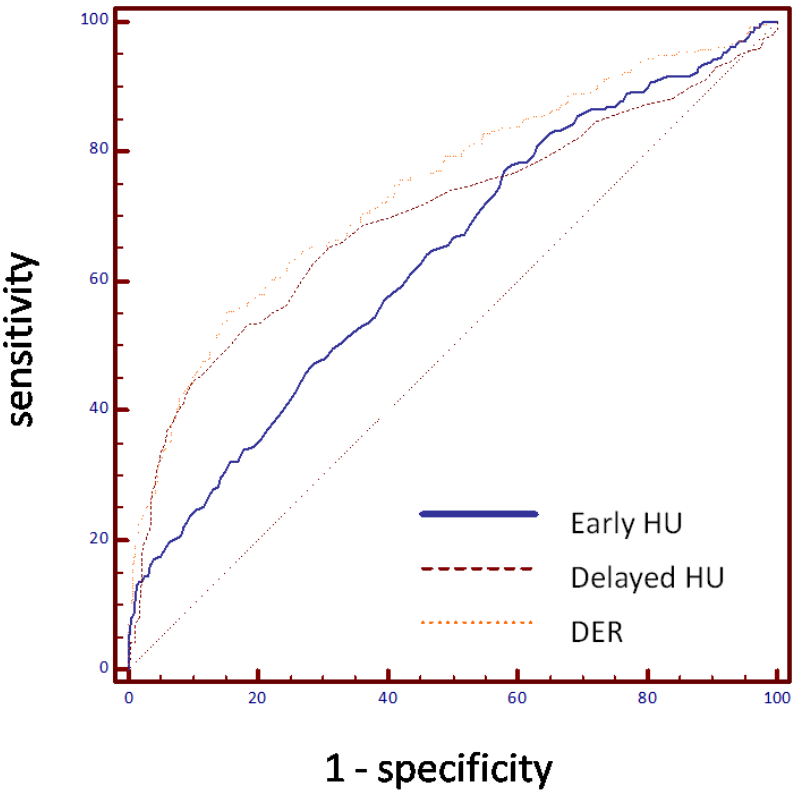


Figure 7.1 *Comparison of early and delayed segmental wall intensity (HU) and delayed enhancement ratio (DER) ROC curves for detection of any segmental MI.*

	eCCT	dCCT	DER
Threshold	110HU	113HU	1.01
Sensitivity	62 (54 – 70)	60 (51 – 68)	71 (63 – 78)
Specificity	70 (66 – 73)	77 (73 – 80)	81 (78 – 84)
PPV	30 (25 – 36)	35 (29 – 41)	44 (38 – 51)
NPV	90 (87 – 92)	90 (87 – 92)	93 (91 – 95)
AUC	0.72 (0.68 – 0.75)	0.72 (0.69 – 0.75)	0.82 (0.79 – 0.85)

Table 7.4 *Accuracy of early and delayed segmental wall intensity and delayed enhancement ratio (DER) for detection of transmural MI (prevalence 17.4%).*

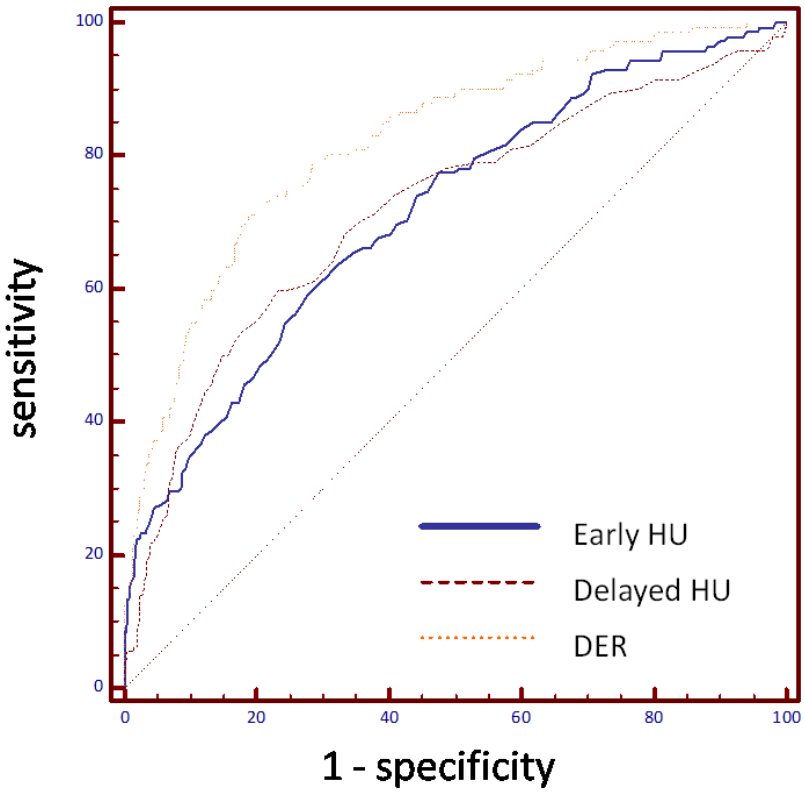


Figure 7.2 *Comparison of early and delayed segmental wall intensity (HU) and delayed enhancement ratio (DER) ROC curves for detection of transmural MI.*

7.4 DISCUSSION

These results show that quantitative measurement of SWI can discriminate between normal and infarcted myocardium but less accurately than by expert visual scoring. Taken on their own, early and delayed SWI show only fair accuracy for discriminating normal myocardium from non-transmural and transmural MI. This result may well be, in part, technical. SWI is the consequence of not just myocardial characteristics but also patient factors such as body weight. Hence a normal segment may show different wall intensity for different patients. Combining values from different patients and finding the median for the group incorporates this patient specific variation, broadens the interquartile range and lowers the chances of finding meaningful differences. Furthermore, the differences in group median SWI are rather small. For example, the difference in delayed SWI between normal myocardial segments and those affected by non-transmural scarring is only 8HU. Combining early and delayed mean SWI into a ratio, DER, has the effect of correcting the values for patient size and image noise and thus allows comparison between patients without these confounding factors. It is therefore unsurprising that DER provides the best statistic for quantitative analysis.

Segmental non-transmural scarring proves more difficult to assess quantitatively. Segments that demonstrate transmural MI are enhanced for the majority of their thickness compared to normal segments; the difference in mean SWI is therefore relatively great. Segments with non-transmural MI contain a smaller proportion of myocardial scarring and so the mean SWI is much closer to that of a normal segment. Further, on eCCT, segments with non-transmural MI show

hypoenhancement in the area of scarring and arterial-phase enhancement in the normal subsegment. This pattern reverses on dCCT, with the net effect of no change in mean SWI when DER is derived. This explains why median DER in segments with non-transmural MI are ~1, whilst values for normal segments and those with transmural MI are lower and higher respectively.

Although there are differences in DER between normal myocardium, non-transmural and transmural MI, the 'best' thresholds (i.e. the ones that carry the highest Youden index; see Section 2.7.6) for discriminating normal from abnormal myocardium and transmural from non-transmural MI are identical. In essence, DER<1.01 has an 80% NPV for any MI and a 93% NPV for transmural MI. Clinically, the latter is probably most relevant for imaging, as the absence of transmural MI (defined in this study as <50% resting segmental tracer uptake on SPECT MPS) implies segmental viability. A segment with DER<1.01 therefore has a 93% chance of being viable. The problem for quantitative scoring on this analysis is the very poor positive predictive value. DER>1.01 has 63% PPV for any MI and only 44% PPV for transmural MI. With respect to viability, this means that over 50% of segments with DER>1.01 are in fact viable. Part of the power of ROC analysis is that a threshold can be adjusted to achieve the most clinically acceptable outcome (see Section 2.7.6). Adjusting the threshold to DER>2 leads to a PPV of 95% and NPV of 84% - but sensitivity in this case drops to just 13%, implying that only 1 in 8 segments with transmural MI will have DER>2. These values should not therefore be expected often. However, a single threshold may not be useful or possible on quantitative analysis. It may be better to have a two DER thresholds above and below which segments are virtually always non-viable and

viable respectively; all values in between would require further testing to guide clinical decision making. Analysis of the presented data reveals that DER<0.9 carries 95% NPV for transmural MI (with 61% of normal segments meeting this criterion in this study) whilst DER>2 carries 95% PPV for the same. The interval between these values is rather large and so, for now, it seems unlikely that quantitative analysis will replace expert visual scoring.

7.5 LIMITATIONS

Endocardial definition on delayed imaging proved difficult., with contour accepted if segmental thickness on eCCT and dCCT were equivalent . This may have introduced error into measured SWI as end-diastolic intervals on eCCT and dCCT may have been slightly different. Differences in heart rate between early and delayed acquisitions were small (see Section 6.2.2) so this potential error should have been minimised. Image noise was relatively high given the low tube voltage. Although this allowed better visual interpretation (Chapter 5), it may have generated a large spread of HU values within each segment, potentially reducing accuracy of mean SWI overall. Further studies are required to assess whether higher X-ray tube voltages reduce image noise enough to improve quantitative myocardial parameters on dCCT without sacrificing visual conspicuity of segmental enhancement.

7.6 SUMMARY FINDINGS

1. SWI on both eCCT and dCCT is a poor discriminator of resting MPS uptake categories.

2. The ratio of early and delayed SWI – the delayed enhancement ratio (DER) – is a better measure that is significantly different across nearly all MPS uptake categories (the exception being distinguishing severely reduced from absent tracer uptake).
3. Only delayed SWI and DER are able to discriminate normal myocardial segments, non-transmural MI and transmural MI on MPS.
4. DER provides the highest accuracy for discriminating normal and infarcted myocardial segments, although this is still only fair (74%). Sensitivity and PPV are particularly low (55% and 63% respectively), but specificity and NPV are reasonable (85% and 80% respectively).
5. DER provides the highest accuracy (82%) for discriminating non-transmural and transmural MI. PPV is poor (44%) and sensitivity moderate (71%), but specificity and NPV are reasonable (81% and 93% respectively).
6. Overall, DER provides the best quantitative statistic for identifying MI, but performance is not good enough to replace expert visual scoring at this stage.

CHAPTER 8 COMPARATIVE ACCURACY OF END-SYSTOLIC AND END-DIASTOLIC PHASES ON CARDIAC COMPUTED TOMOGRAPHY FOR DETECTION OF MYOCARDIAL SCARRING ON SPECT MYOCARDIAL PERFUSION SCINTIGRAPHY

8.1 INTRODUCTION

The end-diastolic phase is used typically in cardiovascular magnetic resonance imaging (CMR) to quantify late gadolinium enhancement in areas of myocardial scarring. Although the measured extent of scar transmurality on CMR may not be equivalent in end-diastolic and end-systolic phases[124], the latter may be more accurate for patients with heart rates over 75 beats per minute (bpm)[125]. This may be due to preferential shortening of the end-diastolic rather than end-systolic interval of minimum cardiac motion at higher heart rates. Control of heart rate is essential for good quality images on cardiac computed tomography (CCT), with beta-blockade often used to ensure heart rates <65bpm. Heart rates above this are associated with image artefacts on 64-slice CT coronary angiography[126]. Iodinated contrast shows similar pharmacokinetic behaviour to gadolinium contrast in normal and abnormal myocardium[111] and therefore allows identification of delayed hyperenhancement of myocardial scarring on CCT, as shown in Chapters 5-7 and elsewhere[63, 64, 96, 112-116]. Injection of iodinated contrast media itself may increase heart rate by up to 5±9bpm[127]. 64-slice CCT has lower temporal resolution than CMR and so shortening of the end-diastolic interval of minimum cardiac motion might

have an even greater effect on conspicuity of enhancement of myocardial scarring on CCT. Use of a sustained low-flow contrast infusion may also have effects on heart rate that affect the optimum phase for assessment. It is therefore prudent to analyse whether end-diastole is the most accurate phase for detecting myocardial scarring on CCT.

The aim of this study was to assess visual and quantitative (delayed enhancement ratios, DER) measures of contrast enhancement on early and delayed CCT (eCCT and dCCT respectively) in end-systole and end-diastole and compare them with resting tracer uptake on SPECT myocardial perfusion scintigraphy (MPS) for accuracy at discriminating normal myocardium and myocardial infarction (MI).

8.2 METHODS

50 patients (39 male, mean age 66±8.8 years) with previous MI referred for clinical stress/rest SPECT MPS were recruited. Full demographics and recruitment criteria are described in Section 6.2. The study was approved by the local research ethics committee and all patients gave written informed consent. Cardiac CT protocol, including contrast regime, is described in Sections 2.4, 5.2.2 and 6.2.2. SPECT MPS was performed and analysed as described in Sections 2.3 and 6.2.1. Median heart rates were 60bpm (IQR 54 – 63bpm) and 63bpm (IQR 56 – 66bpm) during eCCT and dCCT respectively. Heart rate was significantly higher on dCCT ($p=0.007$). Heart rate was >65bpm in 7/50 (14%) and 15/50 (30%) patients during eCCT and dCCT respectively.

8.2.1 Cardiac CT image analysis

End-systolic (25% R-R interval) and end-diastolic phases (75% R-R interval) were reconstructed from both early and delayed datasets. Images were analysed and scored using proprietary cardiac software (TeraRecon Inc) in the same manner as described in Sections 2.5, 2.6 and 7.2.1.

8.2.2 Statistics

Data were analysed using MedCalc statistics software (version 12.2.1.0, MedCalc Software). Heart rates are presented as median (interquartile range). Paired values for eCCT and dCCT were compared using the Wilcoxon sign-rank test. Sensitivity, specificity, positive and negative predictive values (PPV and NPV respectively), accuracy and agreement for discrimination of normal myocardium, non-transmural MI and transmural MI on visual analysis were calculated using ROC analysis and Cohen's kappa statistic. CT summed scarring score and MPS summed rest scores were compared using Spearman's rank correlation. DERs were compared across MPS categories for each phase using the Kruskal-Wallis test and optimal thresholds for discriminating non-transmural and transmural MI calculated using ROC analysis.

8.3 RESULTS

8.3.1 Visual analysis

Patient level

Results are summarised in Table 8.1. 95% confidence intervals for all parameters were wide. There was disagreement between end-systolic and end-diastolic phases for detection of MI in 1/50 (2%) and 3/50 (6%) cases on eCCT and dCCT respectively. End-systolic and end-diastolic phases showed similar sensitivity and PPV on both eCCT and dCCT but specificity and NPV were higher for the end-systolic phase, particularly on dCCT (71% vs. 43%; and 50% vs. 43% respectively). Accuracy was numerically but not significantly higher in the end-systolic phase (AUC: Early 0.68 vs. 0.61, p=0.27; Delayed 0.80 vs. 0.67, p=0.16).

Comparison of summed scores

Results are summarised in Table 8.2. Correlation between MPS summed rest scores and CT summed scarring scores on eCCT was higher for end-systole (0.74 vs. 0.66 (end-diastole)). No difference was seen on dCCT but correlation was higher for both phases compared to eCCT (0.93 vs. 0.92 (end-diastole)).

		Sensitivity	Specificity	PPV	NPV	AUC	p-value
eCCT	End-systole	79 (64 – 90)	57 (18 – 90)	92 (78 – 98)	31 (9 – 61)	0.68 (0.53 – 0.81)	0.27
	End-diastole	79 (64 – 90)	43 (10 – 82)	90 (75 – 97)	25 (6 – 57)	0.61 (0.46 – 0.74)	
dCCT	End-systole	88 (75 – 96)	71 (29 – 96)	95 (83 – 99)	50 (19 – 81)	0.80 (0.66 – 0.90)	0.16
	End-diastole	91 (78 – 97)	43 (10 – 82)	91 (78 – 98)	43 (10 – 82)	0.67 (0.52 – 0.80)	

Table 8.1 *Analysis of CT for patient-level sensitivity, specificity, positive predictive value (PPV), negative predictive value (NPV) and accuracy (AUC, area under the curve) for detection of at least one segment of myocardial infarction on MPS.*

		Spearman's rank correlation	95% Confidence Interval
eCCT	End-systole	0.74	0.58 – 0.85
	End-diastole	0.66	0.47 – 0.79
dCCT	End-systole	0.93	0.87 – 0.96
	End-diastole	0.92	0.86 – 0.95

Table 8.2 *Correlation between MPS summed rest scores and end-systolic and end-diastolic CT summed scarring scores for both early and delayed pass images.*

Segment level

Results are summarised in Table 8.3. Agreement for discrimination of normal myocardium, non-transmural and transmural MI on eCCT was moderate on both end-systolic (630/850 (74%), κ=0.59) and end-diastolic (614/850 (72%), κ=0.53) phases, with no significant differences between them. Agreement was good on dCCT, with no significant differences observed between phases (end systole: 706/850 (83%), κ=0.76; end-diastole: 714/850 (84%), κ=0.79).

		Agreement (κ)	**95% Confidence Interval**
eCCT	End-systole	0.59	0.53 – 0.65
	End-diastole	0.53	0.47 – 0.60
dCCT	End-systole	0.76	0.72 – 0.81
	End-diastole	0.79	0.75 – 0.83

Table 8.3 *Segmental agreement for discrimination of normal myocardium, transmural and non-transmural myocardial infarction at end-systole and end-diastole.*

Discrimination of normal and abnormal myocardium

On eCCT, agreement was better for the end-systolic phase (Table 8.4), but nonetheless still moderate (κ=0.49 vs. 0.41 for end-diastole). The end-systolic phase was also slightly more sensitive (56% vs. 49% for end-diastole). Specificity, PPV and NPV were similar. Overall accuracy was fair for both phases (AUC 0.73 and 0.69 for

end-systole and end-diastole respectively) but higher for the end-systolic phase (p=0.003).

On dCCT, agreement was similar for end-systolic and end-diastolic phases (good; κ=0.69 and 0.73 respectively). The end-diastolic phase was slightly more sensitive (75% vs. 70% vs. end-systole) but had similar specificity, PPV and NPV. Overall accuracy was good for both phases (AUC 0.83 and 0.85 for end-systole and end-diastole respectively) with no differences between them (p=0.10).

Discrimination of non-transmural and transmural MI

On eCCT, agreement was similar for both end-systolic and end-diastolic phases (moderate; κ=0.54 and 0.53 respectively, Table 8.5). Both phases showed poor sensitivity (46% and 45% respectively), but excellent specificity, positive and negative predictive values (end-systole: 98%, 86% and 90% respectively; end-diastole: 99%, 88% and 89% respectively). Overall accuracy was fair for both phases (AUC 0.72 and 0.69 for end-systole and end-diastole respectively, p=0.67).

On dCCT, agreement (good; κ=0.71 and 0.73 for end-systole and end-diastole respectively), sensitivity, specificity, PPV and NPV were similar for both phases and significantly higher than those seen on eCCT. Overall accuracy was good for both phases (AUC 0.82 and 0.84 for end-systole and end-diastole respectively, p=0.37).

		Agreement (κ)	Sensitivity	Specificity	PPV	NPV	AUC	p-value
eCCT	End-systole	0.49 (0.43 – 0.56)	56 (50 – 62)	90 (87 – 92)	73 (66 – 78)	82 (78 – 85)	0.73 (0.70 – 0.76)	0.003
	End-diastole	0.41 (0.35 – 0.48)	49 (43 – 55)	89 (87 – 92)	68 (61 – 75)	79 (76 – 82)	0.69 (0.66 – 0.72)	
dCCT	End-systole	0.69 (0.64 – 0.75)	70 (64 – 75)	96 (94 – 97)	88 (83 – 92)	87 (84 – 90)	0.83 (0.80 – 0.85)	0.10
	End-diastole	0.73 (0.68 – 0.78)	75 (69 – 80)	95 (93 – 97)	88 (83 – 92)	89 (86 – 91)	0.85 (0.82 – 0.87)	

Table 8.4 *Analysis of CT for segment-level agreement (κ), sensitivity, specificity, positive predictive value (PPV), negative predictive value (NPV) and accuracy (AUC, area under the curve) for discrimination of normal and abnormal myocardium on MPS in end-systolic and end-diastolic phases.*

		Agreement	Sensitivity	Specificity	PPV	NPV	AUC	p-value
eCCT	End-systole	0.54 (0.46 – 0.62)	46 (38 – 54)	98 (97 – 99)	86 (77 – 93)	90 (87 – 92)	0.72 (0.69 – 0.75)	0.67
	End-diastole	0.53 (0.45 – 0.61)	44 (36 – 52)	99 (98 – 99)	88 (78 – 94)	89 (87 – 91)	0.71 (0.68 – 0.74)	
dCCT	End-systole	0.71 (0.65 – 0.78)	66 (58 – 74)	98 (97 – 99)	81 (80 – 94)	93 (91 – 95)	0.82 (0.79 – 0.85)	0.37
	End-diastole	0.73 (0.67 – 0.80)	70 (62 – 77)	98 (96 – 99)	87 (80 – 93)	94 (92 – 96)	0.84 (0.81 – 0.86)	

Table 8.5 *Analysis of CT for segment-level agreement (κ), sensitivity, specificity, positive predictive value (PPV), negative predictive value (NPV) and accuracy (AUC, area under the curve) for detection of at least one segment of transmural myocardial infarction on MPS in end-systolic and end-diastolic phases.*

Effect of heart rate on segmental agreement

Results are summarised in Table 8.6.

For all datasets, segmental agreement was higher with heart rates <65bpm. 95% confidence intervals for agreement were wide, but for heart rates <65bpm, there appeared to be higher segmental agreement for end-systolic images on eCCT and end-diastolic images on dCCT. However, there were no differences in segmental agreement between phases when heart rate was >65bpm. Overall the best agreement was seen on dCCT in the end-diastolic phase with heart rates <65bpm (κ=0.84).

		Agreement (κ)	
		Heart rate <65bpm	**Heart rate >65bpm**
eCCT	End-systole	0.60 (0.52 – 0.67)	0.49 (0.35 – 0.63)
	End-diastole	0.54 (0.46 – 0.61)	0.45 (0.30 – 0.59)
dCCT	End-systole	0.77 (0.72 – 0.82)	0.70 (0.61 – 0.79)
	End-diastole	0.84 (0.79 – 0.88)	0.72 (0.64 – 0.81)

Table 8.6 *Segmental agreement for discrimination of normal myocardium, transmural and non-transmural myocardial infarction at end-systole and end-diastole according to heart rate at time of scan.*

8.3.2 Quantitative analysis

Delayed enhancement ratios and scar transmurality

Differences in DER were seen across categories of segmental scar transmurality for both end-systolic and end-diastolic phases ($p<0.0001$ for both, Table 8.7). All within group comparisons were significant. Median end-systolic DERs were significantly higher than those in end-diastole (Figure 8.1).

Discrimination of normal from abnormal myocardial segments

Results are summarised in Table 8.8. Cut-off values for optimal diagnostic accuracy of DER were different (1.16 vs. 1.01 for end-systolic and end-diastolic phases respectively). The end-systolic phase showed higher specificity and PPV (90% vs. 85% and 71% vs. 63% respectively), slightly poorer sensitivity (51% vs. 55% respectively) and identical NPV (80% for both). Overall, DER showed similar accuracy in both end-systolic and end-diastolic phases, with areas under the curve of 0.75 (95% CI: 0.71 – 0.78) and 0.74 (95% CI: 0.71 – 0.77) respectively. Comparison of ROC curves showed no significant difference in accuracy ($p=0.78$, Figure 8.2).

	End-systole	End-diastole
Normal	0.84 (0.71 – 0.99)	0.81 (0.71 – 0.95)
Non-transmural	0.98 (0.81 – 1.23)	0.90 (0.76 – 1.12)
Transmural	1.29 (1.02 – 1.65)	1.16 (0.97 – 1.49)
p-value	<0.0001	<0.0001

Table 8.7 *End-systolic and end-diastolic delayed enhancement ratios according to MI transmurality on MPS.*

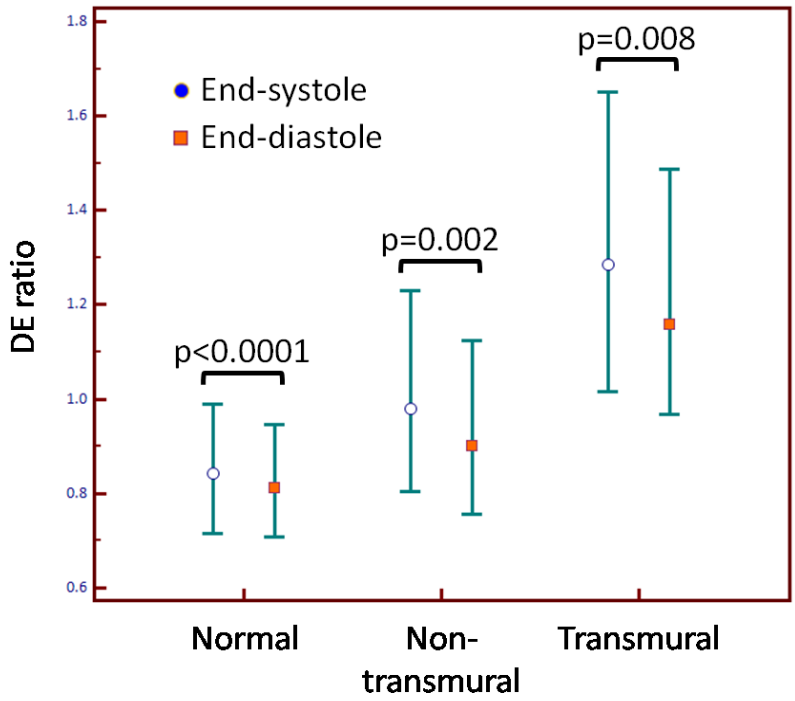


Figure 8.1 *Comparison of delayed enhancement ratios between end-systolic and end-diastolic phases according to transmurality of segmental MI.*

	End-systole	End-diastole
Criterion	1.16	1.01
Sensitivity	51 (44 – 57)	55 (49 – 62)
Specificity	90 (88 – 93)	85 (82 – 88)
PPV	71 (64 – 78)	63 (56 – 69)
NPV	80 (76 – 83)	80 (77 – 83)
AUC	0.75 (0.71 – 0.78)	0.74 (0.71 – 0.77)

Table 8.8 *Accuracy of end-systolic and end-diastolic DE ratios for detection of any segmental MI on MPS (prevalence 31.9%)*

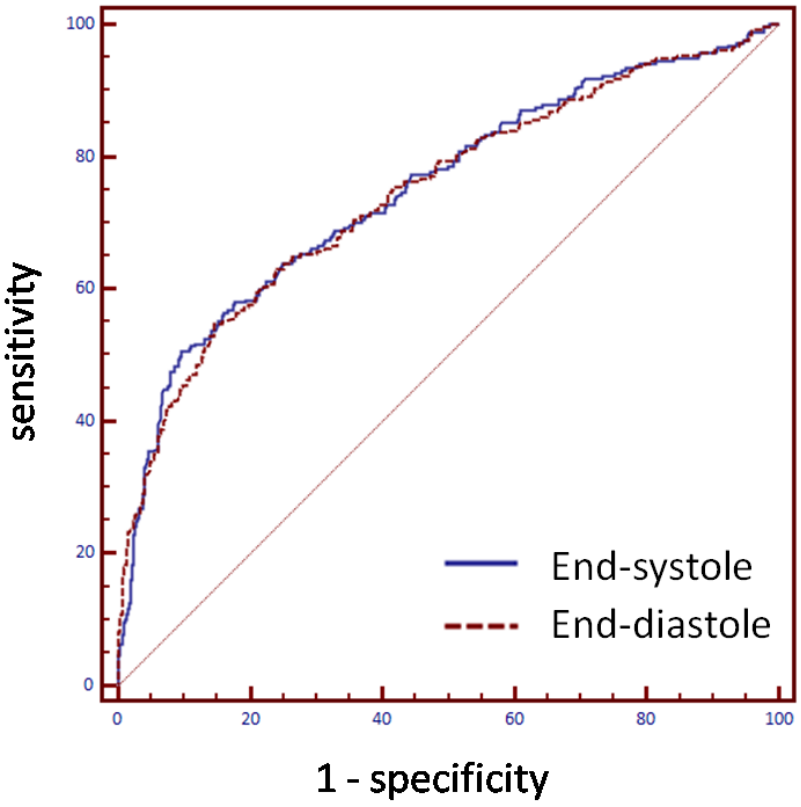


Figure 8.2 *Comparison of ROC curves for detection of any myocardial scarring in end-systole and end-diastole. There were no significant differences in AUC (p=0.78).*

Detection of segmental transmural myocardial infarction

Results are summarised in Table 8.9. Cut-off values for optimal diagnostic accuracy of DER were different (1.16 vs. 1.01 for end-systolic and end-diastolic phases respectively). The end-systolic phase showed higher specificity and PPV (87% vs. 81% and 51% vs. 44% respectively) but similar sensitivity and NPV (67% vs. 71% and 93% vs. 93% respectively). Overall, DER showed similar accuracy in both end-systolic and end-diastolic phases, with areas under the curve of 0.81 (95% CI: 0.78 – 0.84) and 0.82 (95% CI: 0.79 – 0.85) respectively. Comparison of ROC curves showed no significant difference in accuracy (p=0.51, Figure 8.3).

	End-systole	End-diastole
Criterion	1.16	1.01
Sensitivity	67 (58 – 74)	71 (63 – 78)
Specificity	87 (84 – 89)	81 (78 – 84)
PPV	51 (44 – 59)	44 (39 – 51)
NPV	93 (90 – 94)	93 (91 – 95)
AUC	0.81 (0.78 – 0.84)	0.82 (0.79 – 0.85)

Table 8.9 *Accuracy of end-systolic and end-diastolic DE ratios for detection of transmural MI on MPS (prevalence 17.4%).*

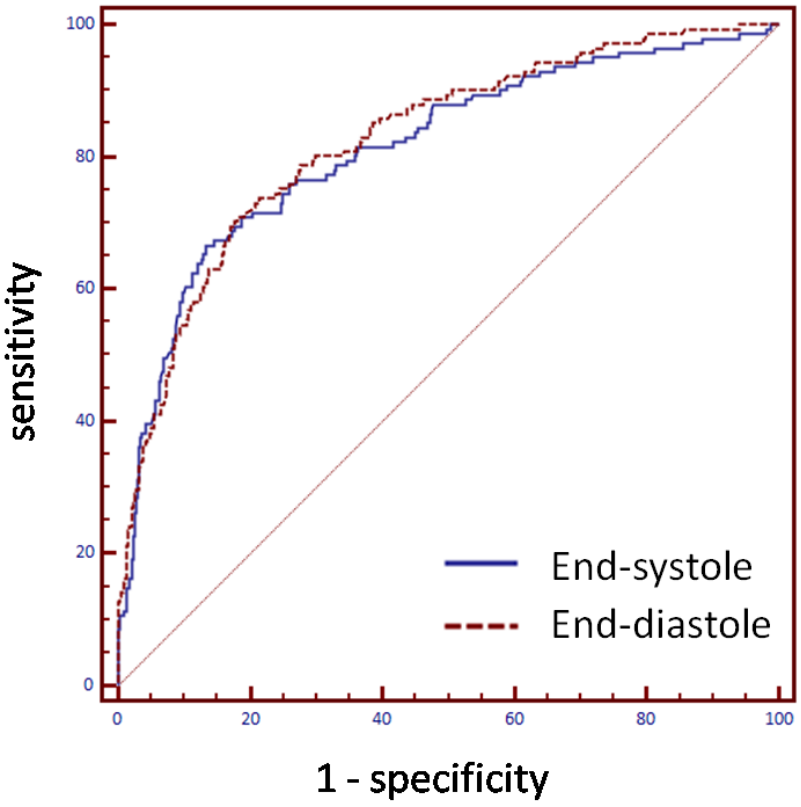


Figure 8.3 *Comparison of ROC curves for detection of transmural myocardial scarring in end-systole and end-diastole. There were no significant differences in AUC (p=0.51).*

8.4 DISCUSSION

These results show that there are no important overall differences between the end-systolic and end-diastolic phases for the assessment of myocardial scarring on CCT. Each of the permutations show slight variations in the sensitivity, specificity, PPV and NPV of CCT to discriminate normal myocardial segments, non-transmural and transmural MI, but overall accuracy is very similar for all strategies. At patient level, visual measures of MI transmurality on end-systolic eCCT show higher agreement and accuracy than end-diastolic eCCT. The importance of this finding is however questionable when results from eCCT in general are so modest – only fair accuracy and moderate agreement with MPS – when compared with dCCT. As shown for end-diastole in Chapter 6, dCCT is superior to eCCT for agreement and accuracy in the end-systolic phase. However, end-systolic and end-diastolic phases yield similar results on dCCT overall. The former is probably more specific at patient level but 95% confidence intervals are wide with significant overlap; overall accuracy is therefore no different between phases. Both phases show excellent and equivalent correlation with MPS summed rest scores, implying that CT summed scarring scores measured in end-systole and end-diastole share an similar linear relationship with MPS values.

At segment level, end-systolic and end-diastolic dCCT images show good agreement and accuracy on visual analysis for discriminating normal myocardial segments, non-transmural and transmural MI. However, an important difference between phases was identified when patients were sub-classified according to heart rate at the time of scan. Agreement was best on end-diastolic dCCT images in patients with heart rates under 65 beats per minute, with any other combination resulting in much

poorer segmental agreement. This is compatible with findings on CMR[125] and suggests that heart rate control plays an important role in image quality when evaluating myocardial enhancement patterns, much as it does for CT coronary angiography. However, there was no evidence from this study that the end-systolic phase performed better at high heart rates.

Quantitative parameters once again performed poorly compared to their qualitative counterparts. In particular (and regardless of phase), specificity and PPV of DER were far lower than for visual quantification of MI transmurality. There was better separation of end-systolic DER values across categories of MI transmurality on MPS, with significantly higher values compared to end-diastole. However, this did not result in better overall accuracy for discriminating normal myocardial segments, non-transmural and transmural MI, although end-systolic DER yielded marginally higher specificity and PPV compared to end-diastolic values. Higher specificity is to be expected from end-systolic DER as any rim of remaining viable myocardium will contract and render the overall contribution of the rim of infarcted myocardium to a given segment smaller. This leads to relative underestimation of scar transmurality compared to end-diastolic imaging and therefore identification of more true negative cases. Similarly, a 'positive' result on end-systolic images represents a larger absolute quantity of scarring and is therefore more likely to be a true positive result – hence higher PPV. The converse is true also – higher numbers of false negatives (hence lower sensitivity) and lower numbers of true positives (hence lower NPV). These points, demonstrated recently on late gadolinium-enhanced CMR evaluation of myocardial scarring[124], are to a certain extent borne out in the quantitative results

presented in this study. It should be noted that, although these issues arise on quantitative analysis of segmental MI on CCT, there is no such issue on visual analysis of the same images. As discussed in Chapter 7, there is therefore little to recommend quantification of myocardial enhancement patterns over expert visual scoring at the present time, irrespective of the phase of the cardiac cycle that is evaluated.

In conclusion, the clinical impact of choice of cardiac phase for evaluation of MI on dCCT is not likely to be very high. However, segmental agreement with MPS is clearly highest when evaluating end-diastolic images in patients with heart rates under 65bpm. Adequate heart rate control during imaging is therefore imperative and, provided this is achieved, the end-diastolic phase should be considered the appropriate phase for evaluation of delayed enhancement on CCT.

8.5 LIMITATIONS

Given that the differences in accuracy between end-systolic and end-diastolic phases may be subtle, it is possible that this small, single centre study was inadequately powered to detect a difference between them. However, one study evaluating the effects of phase on scar transmurality found a significant difference based only on 20 patients[124]. Assessment of quantitative parameters on delayed imaging is subject to the same limitations as described in Section 7.5.

8.6 SUMMARY FINDINGS

1. At patient level, end-systolic and end-diastolic phases show similar sensitivity and PPV for detection of patients with reduced resting MPS tracer uptake, with the latter >90% in all cases. Specificity and NPV are poor, although end-systole is superior to end-diastole.
2. Overall correlation between CT summed scarring score and MPS summed rest score is similar for both phases, with values on dCCT higher than on eCCT.
3. Overall segmental agreement is similar for both phases, with dCCT showing higher values than eCCT. No difference in overall accuracy was identified between phases for discrimination of normal from abnormal myocardial segments and non-transmural from transmural MI.
4. Heart rates >65bpm significantly reduce overall segmental agreement. The best segmental agreement is seen in end-diastole on dCCT with heart rates <65bpm.
5. DERs were higher on end-systolic images. The optimal DER cut-off for the end-systolic phase had marginally higher specificity and PPV than the optimal cut-off of the end-diastolic phase. Overall, there were no differences in accuracy of DER for discriminating normal segments or those with transmural MI.
7. Whilst the overall differences between the phases are relatively marginal, the excellent (and significantly higher) segmental agreement seen on end-diastolic dCCT in patients with heart rates <65bpm suggest that these are the most important factors in accurately identifying MI on CCT.

CHAPTER 9 EFFECT OF RECONSTRUCTION KERNEL ON AGREEMENT WITH SPECT MYOCARDIAL PERFUSION SCINTIGRAPHY

9.1 INTRODUCTION

Use of low X-ray tube voltages in delayed cardiac computed tomography (CCT) increases conspicuity of hyperenhancement in areas of myocardial scarring but has the unwanted effect of increasing image noise due to the lower mean energy of the primary X-ray beam. Although the signal to noise ratio (SNR) can be increased by increasing X-ray beam intensity, there is an upper limit above which tube current cannot be set without overheating the X-ray tube. Adjustment of X-ray tube current and voltage must also take into account X-ray dose. For a standard-sized 70kg patient on a Siemens Sensation 64 CT scanner, the effective radiation doses from retrospectively-gated CCT with tube voltage/current pairings of 120kV/250mAs and 80kV/825mAs are roughly equivalent (dose length product 600mGycm). Even if X-ray effective dose is reduced by prospectively gating, the tube current for the 80kV/825mAs pairing represents the maximum rated current for the tube, with no further increase possible to improve SNR. Given the relatively noisy image from this pairing, it is conceptually attractive to find alternative methods to improve image quality as this may improve diagnostic performance.

Image noise may be reduced by using different convolution filters (kernels) during image reconstruction. Kernels are mathematical algorithms that enhance or smooth

object boundaries by selectively altering the spatial frequency content of data during reconstruction. They therefore offer a balance between image noise and spatial resolution. Smooth filters blur image boundaries and reduce image noise at the expense of spatial resolution. Sharp filters increase presented spatial resolution (the spatial resolution of the *raw* data is unchanged) but the final image is noisier. Choice of appropriate kernel depends on the balance of spatial resolution and image noise that offers the best diagnostic yield.

CCT is usually reconstructed with medium-smooth filters for standard coronary angiography and medium-sharp filters for the evaluation of coronary stents. Smooth filters are rarely used for CCT applications, as the level by which they reduce image noise is usually unnecessary and the loss of spatial resolution unacceptable. However, imaging myocardium at low tube voltages results in reasonable image noise and the requirement for imaging fine detail is less strict. Cardiovascular magnetic resonance imaging (CMR) and SPECT myocardial perfusion scintigraphy (MPS), accepted techniques for evaluating myocardial scarring, have spatial resolutions of 1-2mm and 5-15mm respectively. CCT offers ~0.65mm near-isotropic spatial resolution, so there is scope to sacrifice some spatial resolution in order to reduce image noise.

The aim of this study was to compare delayed CCT (dCCT) reconstructions using medium-smooth (b35f in Siemens terminology) and smooth (b10f) kernels in patients with previous myocardial infarction (MI) and assess accuracy at detecting non-transmural and transmural MI using SPECT MPS as the gold standard.

9.2 METHODS

50 patients (39 male, mean age 66±8.8 years) with previous MI referred for clinical stress/rest SPECT MPS were recruited. Full demographics and recruitment criteria are described in Section 6.2. All patients were taking oral beta-blockade. The study was approved by the local research ethics committee and all patients gave written informed consent.

9.2.1 Cardiac computed tomography

Images were acquired using retrospectively-gated 64-slice CT (Sensation 64, Siemens AG Medical Solutions, Erlangen) as described in Sections 2.4, 5.2.2 and 6.2.2. Early and delayed CCT data were reconstructed using smooth (45 cases, b10f) and medium-smooth (50 cases, b35f) kernels in end-diastole (75% R-R interval). Delayed images were viewed using a window width and level of 150HU with manual adjustment as required and scored as described in Sections 2.5, 2.6 and 7.2.1.

9.2.3 SPECT Myocardial Perfusion Scintigraphy

All patients underwent pharmacological stress and rest MPS imaging as outlined in Section 2.3. MPS images were analysed using QPS/QGS software (Hermes Medical Systems). Segmental tracer uptake was scored as described in Chapter 6.2.1.

9.2.4 Statistics

For visual analysis, sensitivity, specificity, positive (PPV) and negative (NPV) predictive values and accuracy were calculated at patient and segment-level. Spearman's rank correlation was used to compare summed resting and CT summed

scarring scores. Segmental agreement was calculated using Cohen's kappa. Results for quantitative analysis are presented as median (interquartile range). Kruskal-Wallis testing was used to compare delayed enhancement ratios (DER) across categories with pairwise Mann-Whitney testing if indicated. ROC analysis was used to assess accuracy of DER for discriminating either normal from abnormal segments or non-transmural from transmural MI on MPS.

9.3 RESULTS OF VISUAL ANALYSIS

9.3.1 Patient Level

Results are summarised in Table 9.1. dCCT images reconstructed using the medium-smooth kernel agreed with MPS in 42/50 (84%) cases. Sensitivity, specificity, PPV, NPV and accuracy were 91%, 33%, 91%, 33% and 62% respectively. Those reconstructed with the smooth kernel agreed with MPS in 40/45 (89%) cases. Sensitivity, specificity, PPV, NPV and accuracy were 89%, 86%, 97%, 60% and 88% respectively. The smooth kernel showed higher overall accuracy at patient level (p=0.04). Correlation between MPS summed rest scores and CT summed scaring scores were excellent for both smooth and medium-smooth kernels (r=0.95 and 0.93 respectively; Table 9.2).

	Spearman's rank correlation	**95% Confidence Interval**
Smooth	0.95	0.91 – 0.97
Medium-smooth	0.93	0.88 – 0.96

Table 9.2 *Correlation between MPS summed rest scores and dCCT summed scarring scores for both reconstruction kernels.*

	Sensitivity	Specificity	PPV	NPV	AUC	p-value
Smooth	89 (75 – 97)	86 (42 – 100)	97 (85 – 100)	60 (25 – 89)	0.88 (0.74 – 0.96)	0.04
Medium-smooth	91 (78 – 97)	33 (4 – 78)	91 (78 – 98)	33 (4 – 78)	0.62 (0.47 – 0.76)	

Table 9.1 *Analysis of dCCT for patient-level sensitivity, specificity, positive (PPV) and negative predictive value (NPV) and accuracy (AUC: area under the curve) for detection of at least one segment of myocardial infarction on MPS.*

9.3.2 Segment level

Overall agreement

Results are shown in Table 9.3. Overall segmental agreement using the smooth kernel was very good (643/765 (84%) segments , κ=0.81) . Results using the medium-smooth kernel were similar (714/850 (84%) segments , κ=0.79).

	Kappa	**95% Confidence Interval**
Medium-smooth	0.79	0.75 – 0.83
Smooth	0.81	0.77 – 0.85

Table 9.3 *Comparison of overall segmental agreement for both kernels*

Discriminating normal and abnormal myocardium

Results are shown in Table 9.4. Overall segmental agreement for reconstructing delayed images using the smooth kernel was good (677/765 (88%) segments, κ=0.73). Results using the medium-smooth kernel were similar (753/850 (89%) segments , κ=0.73). Sensitivities, specificities, PPV and NPV are given in Table 9.6. Values were similar for both kernels, with no difference in overall accuracy.

	Kappa	**95% Confidence Interval**
Medium-smooth	0.73	0.68 – 0.78
Smooth	0.73	0.68 – 0.78

Table 9.4 *Segmental agreement between dCCT and MPS for normal and abnormal myocardial segments for each kernel.*

Detection of segmental transmural myocardial infarction

Results are shown in Table 9.5. Overall segmental agreement for reconstructing delayed images using the smooth kernel was good (717/765 (94%) segments, κ=0.76). Results using the medium-smooth kernel were similar (790/850 (93%) segments , κ=0.73). Sensitivities, specificities, PPV and NPV are given in Table 9.6. Values were similar for both kernels, with no difference in overall accuracy.

	Kappa	**95% Confidence Interval**
Medium-smooth	0.73	0.67 – 0.80
Smooth	0.76	0.70 – 0.83

Table 9.5 *Segmental agreement between dCCT and MPS for non-transmural and transmural myocardial infarction for each kernel.*

		Sensitivity	Specificity	PPV	NPV	AUC	p-value
Normal	**Smooth**	76 (70 – 81)	94 (92 – 96)	86 (81 – 91)	89 (87 – 92)	0.85 (0.83 – 0.88)	0.68
	Medium-smooth	75 (69 – 80)	95 (93 – 97)	88 (83 – 92)	89 (86 – 91)	0.85 (0.82 – 0.87)	
Transmural MI	**Smooth**	71 (62 – 78)	99 (97 – 99)	91 (84 – 96)	94 (92 – 96)	0.85 (0.82 – 0.87)	0.54
	Medium-smooth	70 (62 – 77)	98 (96 – 99)	87 (80 – 93)	94 (92 – 96)	0.84 (0.81 – 0.86)	

Table 9.6 *Analysis of dCCT for segment-level sensitivity, specificity, positive (PPV) and negative predictive value (NPV) and accuracy (AUC: area under the curve) for visual discrimination of normal from abnormal myocardial segments and non-transmural from transmural myocardial infarction (MI).*

9.4 RESULTS OF QUANTITATIVE ANALYSIS

9.4.1 Comparison of delayed enhancement ratios across MPS categories

Differences in DER were seen across MPS categories for both reconstruction kernels ($p<0.0001$ for both, Table 9.7). DERs were no different with either kernel in segments showing severely reduced or absent resting tracer uptake (1.18 vs. 1.43, $p=0.20$; 1.17 vs. 1.36, $p=0.18$ respectively), but all other within-group comparisons were significant. In particular, both kernels demonstrated differences in DER between segments with normal tracer uptake and those with mild reduction (smooth: 0.82 vs. 0.88, $p=0.005$; medium-smooth: 0.81 vs. 0.90, $p<0.0001$) and between those with mild and moderate reductions (smooth: 0.88 vs. 1.01, $p=0.004$; medium-smooth: 0.90 vs. 1.03, $p=0.003$) on SPECT MPS.

	Smooth	**Medium-smooth**
Normal uptake	0.82 (0.71 – 0.96)	0.81 (0.71 – 0.95)
Mild reduction	0.88 (0.75 – 1.05)	0.90 (0.76 – 1.12)
Moderate reduction	1.01 (0.87 – 1.16)	1.03 (0.86 – 1.28)
Severe reduction	1.18 (1.01 – 1.46) †	1.17 (1.03 – 1.53) †
Absent uptake	1.43 (1.09 – 2.10) †	1.36 (1.16 – 2.14) †
p-value	<0.0001	<0.0001

Table 9.7 *Comparison of DER across MPS categories for both reconstruction kernels. †no significant difference; all other pairwise comparisons significant.*

9.4.2 Comparison of DER values according to MI transmurality

Both reconstruction kernels resulted in similar DERs for normal, non-transmural and transmural MI (Table 9.8). There was a significant but clinically meaningless

difference between DERs of normal myocardial segments (p=0.003) but otherwise there were no differences between kernels.

	Smooth	Medium-smooth	p-value
Normal	0.82 (0.70 – 0.96)	0.81 (0.71 – 0.95)	0.003
Non-transmural	0.88 (0.75 – 1.05)	0.90 (0.76 – 1.12)	0.18
Transmural	1.12 (0.95 – 1.45)	1.16 (0.97 – 1.49)	0.66
p-value	<0.0001†	<0.0001†	

Table 9.8 *DER values for normal myocardium, non-transmural and transmural myocardial infarction after reconstruction using smooth and medium-smooth kernels. †all pairwise comparisons significant.*

9.4.3 Discrimination of normal and abnormal resting MPS uptake using DER

Results are summarised in Table 9.9. Images reconstructed using the medium-smooth kernel showed higher specificity and PPV than the smooth kernel (85% vs. 78%; and 63% vs. 54% respectively) for detecting normal myocardial segments. The medium-smooth kernel was marginally more accurate for discriminating normal segments on MPS (AUC 0.74 vs. 0.71, p=0.01, Figure 9.1).

9.4.4 Discrimination of non-transmural and transmural myocardial infarction using DER

Results are summarised in Table 9.10. Images reconstructed using the smooth kernel showed no important differences over the medium-smooth kernel for detection of transmural MI at segmental level. There was no difference in accuracy between either kernel (AUC 0.80 vs. 0.82 respectively, p=0.06, Figure 9.2).

	Smooth	Medium-smooth
Criterion	0.98	1.01
Sensitivity	55 (49 – 62)	55 (49 – 62)
Specificity	78 (74 – 82)	85 (82 – 88)
PPV	54 (48 – 61)	63 (57 – 69)
NPV	79 (75 – 82)	80 (77 – 83)
AUC	0.71 (0.68 – 0.74)	0.74 (0.71 – 0.77)
Comparison	p=0.01	

Table 9.9 *Accuracy of DER for each reconstruction kernel for discrimination of normal and abnormal myocardial segments.*

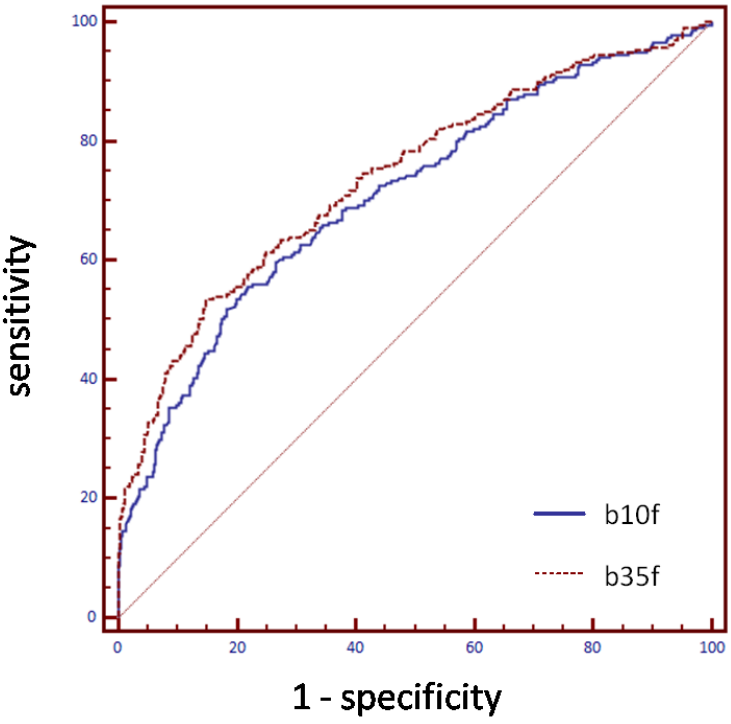


Figure 9.1 *Comparison of ROC curves of smooth (b10f) and medium-smooth (b35f) kernels for discrimination of normal and abnormal myocardial segments.*

	Smooth	Medium-smooth
Criterion	1.01	1.01
Sensitivity	68 (60 – 76)	71 (63 – 78)
Specificity	79 (76 – 82)	81 (78 – 84)
PPV	40 (34 – 47)	44 (37 – 50)
NPV	92 (90 – 94)	93 (91 – 95)
AUC	0.80 (0.78 – 0.83)	0.82 (0.79 – 0.85)
Comparison	p=0.06	

Table 9.10 *Accuracy of DER for each reconstruction kernel for discrimination of non-transmural and transmural myocardial infarction.*

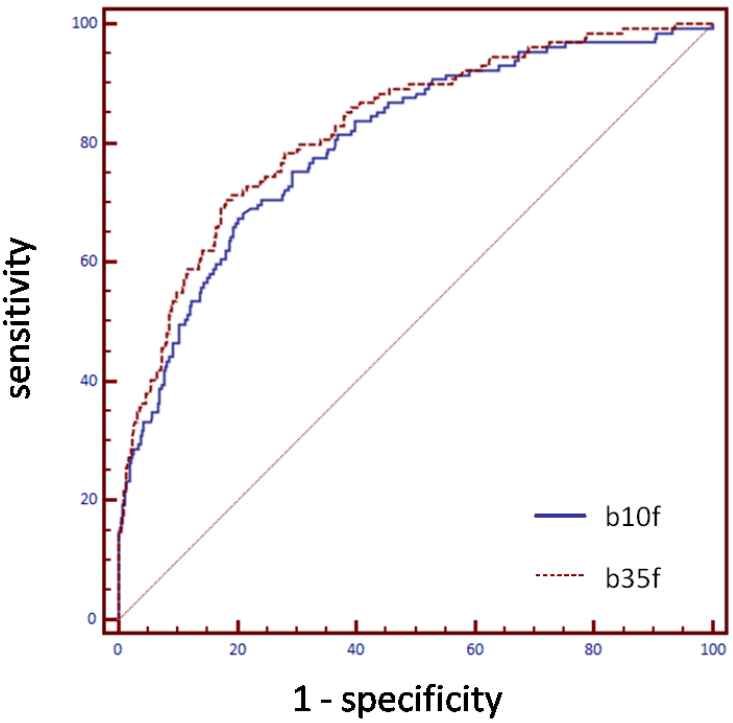


Figure 9.2 *Comparison of ROC curves of segment-level accuracy of smooth (b10f) and medium-smooth (b35f) kernels for discrimination of non-transmural and transmural myocardial infarction.*

9.5 DISCUSSION

Overall, the results demonstrate no clear benefits from using a smooth kernel to reconstruct delayed CCT images. Smooth kernels seem to offer clear benefits at patient level, with a roughly twofold increase in specificity and NPV. Accuracy is also significantly higher (88%). There are however very wide confidence intervals for patient-level parameters and it is interesting to see that there were only 4 disagreements in total at patient level between the two kernels. It is therefore difficult to take much that is meaningful away from the patient-level comparison, except that sensitivity and PPV (in a cohort with 86% disease prevalence at patient level) are excellent for both kernels. Correlation of CCT summed scarring and MPS summed rest scores is excellent and equal for both kernels. Segment-level visual analysis shows no benefits from using a smooth reconstruction kernel with regards to overall agreement, discrimination of normal from abnormal myocardium or transmural from non-transmural myocardial scarring. On quantitative analysis, the medium-smooth kernel resulted in marginally more specific (85% vs. 78% for smooth kernel) and accurate (74% vs. 71% for smooth kernel) DERs for discriminating normal from abnormal myocardial segments, although accuracy was still only fair overall. There were no differences between kernels for distinguishing transmural from non-transmural MI.

The effects of changing kernels have been measured in a variety of settings. Most compelling is the improvement in luminal assessment of coronary artery stents that accompanies the use of a sharper kernels[128-132]. This practice should therefore be considered routine. Data from evaluation of CT coronary angiography have shown

that using smooth kernels increases the measured attenuation values of coronary atherosclerotic plaque[133], whilst sharper kernels may increase the attenuation value of the calcified part of a mixed atherosclerotic plaque but reduce the attenuation value of the non-calcified part[134]. These phenomena may vary between different models of CT scanner[135]. In other settings, use of smoother kernels results in higher calcium scores when imaging the aortoiliac arteries[136] whilst in thoracic CT, smoother kernels have been shown to increase apparent bronchial wall thickness[137]. These findings reflect the reduction in spatial resolution and increase in blooming artefact that accompanies the use of kernels that selectively blur object boundaries. The impact of smooth reconstruction kernels on measured attenuation values is interesting but not reflected in the data collected in this study. Although only DERs are presented formally above, review of data shows no significant difference between early and delayed segmental wall intensity using either kernel ($p=0.24$ and 0.40 respectively). This is likely to be due to relatively unimportant effects of the smooth kernel on spatial resolution when averaging pixel intensity over an entire myocardial segment. Regardless, the effect would be systematic for both early and delayed imaging and the resultant DER would most likely render this systematic difference unimportant. In retrospect, it was unlikely that the smooth kernel would have any measurable difference in any quantitative parameter of myocardial scarring on CCT. The benefits of the smoothing effect ought therefore to be expected, if present, in the visual analysis of myocardial hypernehancement on dCCT. That this was not the case at segment level demonstrates that a medium-smooth kernel, as used for conventional CT coronary angiography, is sufficient for evaluating myocardial scaring on dCCT.

9.6 LIMITATIONS

The differences shown between the two reconstruction kernels are modest and rarely significant. This may be related to study power given the small sample size. Whilst this might explain patient-level results, the high number of segments under evaluation (850) and the high prevalence of myocardial infarction (271, 32%) should render study power adequate and the segmental findings accurate.

9.7 SUMMARY FINDINGS

1. At patient level, smooth kernels offer better specificity and accuracy, but negative predictive value remains relatively modest.
2. The use of smooth or medium-smooth kernels has no effect on the excellent linear relationship between CT summed scarring scores and MPS summed resting scores, overall segmental agreement or visual discrimination of either normal from abnormal myocardium or transmural from non-transmural MI.
3. Medium-smooth kernels lead to a small but significant increase in accuracy of DER for discriminating normal from abnormal myocardium. Neither kernel increases accuracy of DER for distinguishing transmural from non-transmural MI.

CHAPTER 10 SEGMENTAL MYOCARDIAL THICKNESS ON CARDIAC CT AS A PREDICTOR OF MYOCARDIAL INFARCTION ON SPECT MYOCARDIAL PERFUSION SCINTIGRAPHY

10.1 INTRODUCTION

Myocardial wall thickness correlates with depth of myocardial scarring and predicts likelihood of segmental recovery of function after revascularisation[70]. End-diastolic wall thickness (EDWT) is the most commonly quoted parameter, with values of 5.5mm – 6mm in dysfunctional segments considered the appropriate cut-off on cardiovascular magnetic resonance imaging (CMR) for predicting non-recovery of function after revascularisation[70, 138-140]. Similar values have been found for echocardiography[141, 142]. Whilst functional recovery is extremely unlikely below these values, the converse has rarely been demonstrated. It has been shown that CMR is unable to predict functional recovery when EDWT is between 6 and 15 mm[138]. Similarly, myocardial segments with EDWT >6mm on echocardiography may be non-viable in around a third of cases[142]. Cardiac computed tomography (CCT) has superior spatial resolution to CMR and echocardiography. The standard gated CCT dataset allows measurement of mean segmental myocardial thickness that, provided the scan is retrospectively gated, may be analysed in any phase of the cardiac cycle. The aim of this study is to measure mean segmental myocardial thickness in end-systole and end-diastole and assess usefulness of these parameters as predictors of

both transmural segmental myocardial infarction (MI) and segmental MI of any severity on SPECT myocardial perfusion scintigraphy (MPS).

10.2 METHODS

50 patients (39 male, mean age 66±8.8 years) with previous MI referred for clinical stress/rest SPECT MPS were recruited. Mean time since MI was 10±9.0 years (min 62 days, max 30 years). Full demographics and recruitment criteria are described in Section 6.2. All patients were taking oral beta-blockade. The study was approved by the local research ethics committee and all patients gave written informed consent.

10.2.1 Cardiac computed tomography

Images were acquired using retrospectively gated 64-slice CT (Sensation 64, Siemens AG Medical Solutions, Erlangen) as described in Sections 2.4, 5.2.2 and 6.2.2. Data from the initial arterial-phase acquisition were reconstructed using a medium-smooth kernel at 10% increments from 25-95% of the R-R interval.

10.2.2 Cardiac CT image analysis

End-systolic and end-diastolic phases (25% and 75% R-R interval respectively) were analysed. Images were loaded into a density threshold program (Time Volume Analysis) and the LV blood pool identified in semi-automated fashion, as described in Sections 2.5 and 2.6. The outer edge of the LV blood pool was defined as the endocardial contour, with manual adjustments made as necessary. The epicardial contour was defined as the boundary between the myocardial surface and epicardial fat. The endo- and epicardial contours defined the myocardial volume, which was

then divided into 17 segments and displayed on a polar plot, as described in Section 2.6. Mean myocardial thickness was recorded for each segment in the end-systolic and end-diastolic phases, to generate mean segmental end-systolic wall thickness (ESWT) and end-diastolic wall thickness (EDWT).

10.2.3 SPECT Myocardial Perfusion Scintigraphy

All patients underwent pharmacological stress and rest MPS imaging as outlined in Section 2.3. MPS images were analysed using QPS/QGS software (Hermes Medical Systems). Resting segmental uptake was scored as described in Section 6.2.1.

10.2.4 Statistics

Mean segmental wall thickness measurements on cardiac CT are presented as median (interquartile range). Values across MPS categories were analysed using the Kruskal-Wallis test, with pair-wise Mann-Whitney testing as appropriate. Ability of mean segmental wall thickness to discriminate normal from abnormal segments and non-transmural from transmural MI on MPS was assessed using ROC analysis.

10.3 RESULTS

10.3.1 Myocardial perfusion scintigraphy

As shown in Section 6.3.1, 43/50 (86%) patients demonstrated evidence of previous MI on perfusion images. Of 850 segments, 579 (68%) were normal whilst 123 (15%) and 148 (17%) segments showed non-transmural and transmural MI respectively.

10.3.2 Comparison of segmental wall thickness across MPS categories

Significant differences in segmental ESWT were seen across MPS categories ($p<0.0001$, Table 10.1), although segments with severely reduced uptake on MPS could not be distinguished from those with absent uptake (6mm vs. 5mm respectively, $p=0.08$). Significant differences were seen in EDWT ($p<0.0001$), although there was no measurable difference in segmental thickness between segments with mild and moderate reductions in resting tracer uptake on MPS (7mm vs. 7mm, $p=0.79$), or those with severely reduced or absent uptake (6mm vs. 5mm, $p=0.28$).

When defined according to transmurality of MI (Table 10.2), there were significant differences in both ESWT and EDWT between normal segments and those with non-transmural and transmural MI on MPS ($p<0.0001$ for both).

	End-systole	End-diastole
Normal	12 (10 – 14)	8 (6 – 9)
Mild reduction	10 (8 – 12)	7 (6 – 9) †
Moderate reduction	8 (7 – 10)	7 (6 – 8) †
Severe reduction	6 (4.5 – 8) †	6 (4 – 7)*
Absent uptake	5 (4 – 6) †	5 (4 – 6)*
p-value	<0.0001	<0.0001

Table 10.1 *Variation in end-systolic and end-diastolic segmental wall thickness according to resting MPS uptake categories (median [IQR]). †* no significant difference; all other pairwise comparisons significant*

	End-systole	End-diastole
Normal	12 (10 – 14)	8 (6 – 9)
Non-transmural	10 (8 – 12)	7 (6 – 9)
Transmural	7 (5 – 8)	6 (5 – 8)
p-value	<0.0001†	<0.0001†

Table 10.2 *End-systolic and end-diastolic wall thickness (median [IQR]) in segments with normal tracer uptake, non-transmural myocardial infarction and transmural myocardial infarction on resting MPS. †All pairwise comparisons significant*

10.3.3 Discrimination of normal from abnormal myocardial segments

Results are summarised in Table 10.3. Using a threshold of 10mm, ESWT had sensitivity, specificity, positive (PPV) and negative (NPV) predictive values of 66%, 82%, 63% and 84% respectively for discrimination of normal and abnormal myocardial segments. Using a threshold of 7mm, values for EDWT were poorer (38%, 89%, 42% and 88% respectively). ROC analysis showed good accuracy of ESWT (AUC 0.81 (95% CI 0.78 – 0.84)), whilst accuracy was poor for EDWT (AUC 0.60 (0.57 – 0.64)). Comparison of ROC curves showed a highly significant difference in favour of ESWT ($p<0.0001$, Figure 10.1).

10.3.4 Detection of segmental transmural myocardial infarction

Results are summarised in Table 10.4. Using a threshold of 9mm, ESWT had sensitivity, specificity, PPV and NPV of 77%, 87%, 54% and 95% respectively for detection of segmental transmural MI. Using a threshold of 6mm, EDWT was again poorer (41%, 75%, 47% and 76% respectively). ROC analysis showed good accuracy of ESWT (AUC 0.88 (0.86 – 0.90)), whilst accuracy was only fair for EDWT (AUC 0.70 (0.67 – 0.73)). Comparison of ROC curves again showed a highly significant difference in favour of ESWT ($p<0.0001$, Figure 10.2).

	End-systole	End-diastole
Threshold	10mm	7mm
Sensitivity	66 (61 – 72)	41 (33 – 51)
Specificity	82 (79 – 85)	75 (71 – 78)
PPV	63 (57 – 69)	47 (42 – 54)
NPV	84 (81 – 87)	76 (72 – 79)
AUC	0.81 (0.78 – 0.84)	0.60 (0.57 – 0.64)
Comparison	p<0.0001	

Table 10.3 *Accuracy of end-systolic and end-diastolic segmental wall thickness for detection of any MI on MPS (prevalence 31.9%).*

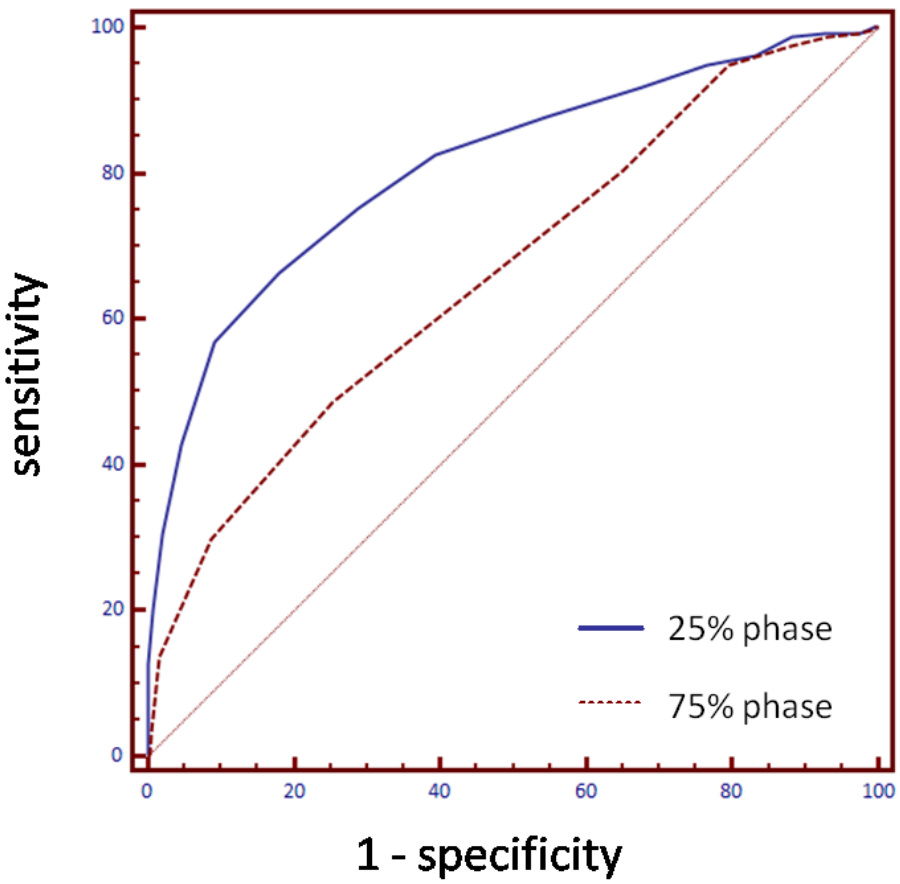


Figure 10.1 *ROC curves showing accuracy of end-systolic (25%) and end-diastolic (75%) segmental wall thickness for detection of any MI on MPS.*

	End-systole	End-diastole
Threshold	9mm	6mm
Sensitivity	77 (69 – 84)	38 (30 – 46)
Specificity	87 (84 – 89)	89 (87 – 91)
PPV	54 (47 – 61)	42 (33 – 51)
NPV	95 (93 – 96)	88 (85 – 90)
AUC	0.88 (0.86 – 0.90)	0.70 (0.67 – 0.73)
Comparison	p<0.0001	

Table 10.4 *Accuracy of end-systolic and end-diastolic segmental wall thickness for detection of transmural MI on MPS (prevalence 17.4%).*

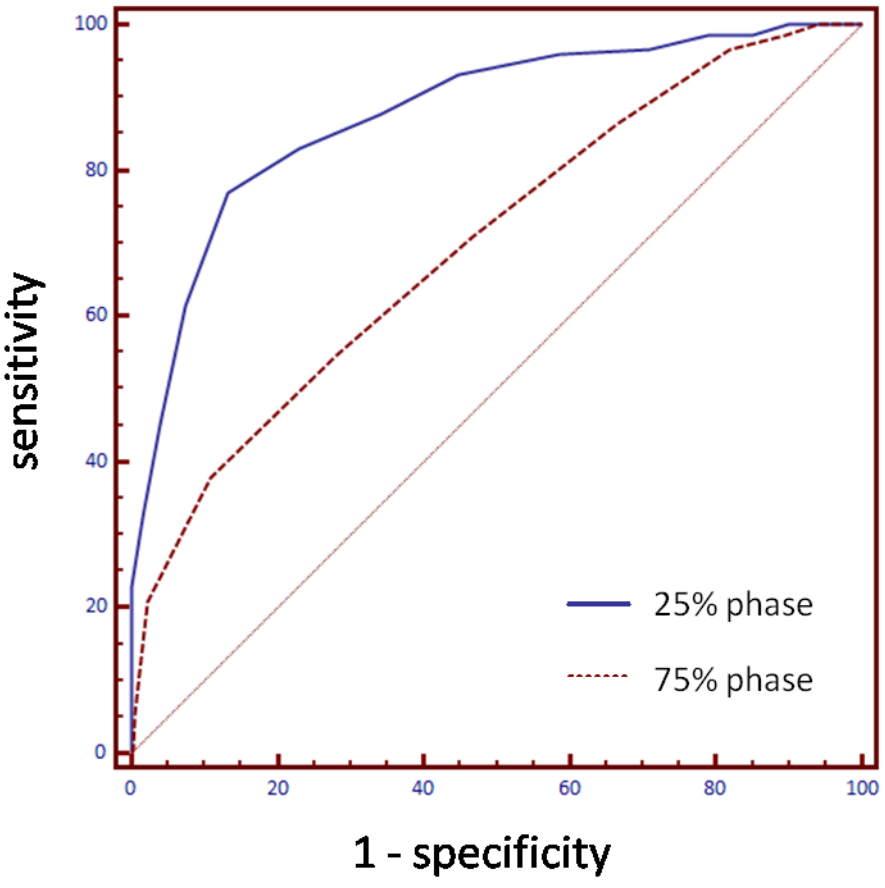


Figure 10.2 *ROC curves showing accuracy of end-systolic (25%) and end-diastolic (75%) segmental wall thickness for detection of transmural MI on MPS.*

10.4 DISCUSSION

These results show that end-systolic wall thickness (ESWT) on CCT is a better discriminator of MI than end-diastolic wall thickness (EDWT). There is no significant difference in EDWT between segments with mild and moderate reductions in resting tracer uptake on MPS. This results in an extremely poor sensitivity (38%) for detection of transmural MI (defined as <50% resting tracer uptake) when a threshold of 6mm is used. This seems at odds with equivalent data published for CMR, but it should be noted that EDWT is used on CMR to predict viability in segments already judged dysfunctional.. A recent meta-analysis of EDWT on CMR for prediction of segmental recovery after revascularisation showed mean weighted sensitivity, specificity, PPV and NPV of 96%, 38%, 71% and 85% respectively[143]. When only akinetic segments on CCT are considered in this study (see Chapter 10), EDWT<6mm has sensitivity, specificity, PPV and NPV of 83%, 70%, 84% and 68% respectively, suggesting that CCT EDWT has poorer sensitivity and NPV but better specificity and PPV in akinetic segments. Comparison of results should be made with caution, as this study compared power of EDWT to predict non-viability on MPS, which is itself imperfectly sensitive for segmental recovery after revascularisation. Furthermore, with increasing use of prospective gating, it is sensible to evaluate the predictive power of segmental wall thickness alone, without information on segmental function.

CCT EDWT >6mm carries a specificity and NPV in the region of 90%, which implies that such segments rarely show transmural MI. Regardless, it is clear from the current study that ESWT performs better than EDWT for excluding transmural

scarring on SPECT MPS, with ESWT ≤9mm generating a much higher area under the curve. This pattern has been demonstrated before in a small study comparing CMR and thallium-201 MPS[144]. The negative predictive value of ESWT when >9mm is 95%, suggesting that this value is most appropriate for excluding transmural MI on SPECT MPS. The number of myocardial segments with ESWT >9mm in this study was 66%, indicating that this is by no means a rare value in patients with previous MI. Unfortunately, ESWT ≤9mm had only 54% PPV, indicating that around half of segments with ESWT below this threshold will be viable on SPECT MPS. This reinforces the notion of ESWT as a rule-out test for transmural MI if used alone. When evaluated in akinetic segments only, ESWT <9mm has much better sensitivity and PPV – 95% and 81% respectively – implying that the combination is better at ruling in transmural MI.

The limiting factor in the application of these results to real world clinical practice is the need to acquire an end-systolic dataset. In Chapter 8, it was demonstrated that transmurality of MI was best demonstrated on delayed CCT (dCCT) in patients with heart rates under 65bpm. If heart rate is optimised to enable the highest accuracy from dCCT, it will also be in the range most acceptable for prospective ECG gating of the early CCT scan. This is a powerful manoeuvre for reducing X-ray dose and it is difficult to see the justification for either switching to retrospective gating (64-slice CT) or acquiring an additional, isolated end-systolic phase (higher specification CT scanners) when the yield from ESWT for predicting transmural MI is not especially high. On balance, it may therefore be more reasonable to accept the slightly poorer NPV offered by a threshold of 6mm on EDWT (88% NPV) for the sake of keeping X-

ray dose as low as reasonably practicable. However, if the clinical situation necessitates acquisition of early CCT images using retrospective gating (e.g. high heart rates or atrial fibrillation), it is clear that ESWT combined with analysis of regional function is the preferred marker for MI.

10.5 LIMITATIONS

The analysis would be strengthened by comparing ESWT and EDWT in patients before and after revascularisation, to assess their effects on predicting segmental recovery, along the lines of similar CMR data. However, validating accuracy in discriminating transmural MI (≤50% tracer uptake on resting MPS) is an important first step in predicting segmental hibernating myocardium.

10.6 SUMMARY FINDINGS

1. ESWT is a better differentiator of MPS resting uptake scores than EDWT.
2. Although both ESWT and EDWT vary with infarct transmurality, absolute differences between normal, non-transmural and transmural categories are larger for ESWT, suggesting again that it discriminates between these categories more effectively.
3. ESWT has all round better performance for discrimination of normal from abnormal myocardium and transmural from non-transmural MI.
4. Although ESWT shows good accuracy, it suffers from poor sensitivity and PPV, rendering it more useful for ruling out MI when used as a single marker.
5. ESWT >9mm excludes segmental transmural MI in 95% of cases.

CHAPTER 11 ASSESSMENT OF GLOBAL AND REGIONAL LEFT VENTRICULAR FUNCTION BY CARDIAC CT IN PATIENTS WITH PREVIOUS MYOCARDIAL INFARCTION: COMPARISON WITH SPECT MYOCARDIAL PERFUSION SCINTIGRAPHY

11.1 INTRODUCTION

Cardiac computed tomography (CCT) is recommended in current guidelines for non-invasive coronary angiography in patients with chest pain at low to intermediate likelihood of obstructive coronary artery disease[109]. Much of the validation data for CT coronary angiography has been collected using retrospectively gated 64-slice CCT[107, 108, 145, 146] and similar patient cohorts have also been used to validate global and regional functional assessment of the left ventricle[112, 147-149]. State-of-the-art high specification CT has better temporal resolution – particularly dual-source CT (DSCT) – and there is now substantial data for left ventricular (LV) assessment using these technologies[150-153]. The incidence of myocardial infarction (MI) in studied patient cohorts is typically rather low, so evidence for the utility of CCT for assessing global and regional LV function is strongest in relatively normal ventricles. There are little data assessing LV function by CCT in patients with documented previous MI, although patients with reperfused acute MI have been studied[154]. CT left ventriculography has been validated in other patient cohorts likely to have abnormal ventricular function, including those with pulmonary hypertension and congenital heart disease[155]. Given the potential of CCT to quantify myocardial scarring, as

shown in Chapters 5-10 and elsewhere[52, 63, 64, 96, 114-116, 156], it is clinically useful to measure the performance of CCT for assessment of global and regional LV function in patients with a high prevalence of MI.

The aim of the present study was to quantify LV volumes and ejection fraction (EF), score qualitative measures of regional LV function and calculate segmental EF and percentage thickening on CCT and compare them with similar functional parameters measured by SPECT myocardial perfusion scintigraphy (MPS).

11.2 METHODS

50 patients (39 male, mean age 66±8.8 years) with previous MI referred for clinical stress/rest SPECT MPS were recruited. Mean time since MI was 10±9.0 years (min 62 days, max 30 years). Full demographics and recruitment criteria are described in Section 6.2. All patients were taking oral beta-blockade. The study was approved by the local research ethics committee and all patients gave written informed consent.

11.2.1 SPECT Myocardial Perfusion Scintigraphy

All patients underwent pharmacological stress and MPS imaging as outlined in Section 2.3. MPS images were analysed using QPS/QGS software (Hermes Medical Systems). LV dilatation was defined as end-diastolic volume >125mL in females or >150mL in males. Qualitative scoring of wall motion and thickening was performed according to the 17-segment model as described in Section 2.3.7.

11.2.2 Cardiac computed tomography

Images were acquired using retrospectively gated 64-slice CT (Sensation 64, Siemens AG Medical Solutions, Erlangen) as described in Sections 2.4, 5.2.2 and 6.2.2. Data from the arterial phase acquisition were reconstructed using a medium-smooth kernel at 10% increments from 25-95% of the R-R interval.

11.2.3 Cardiac CT image analysis

Data from all phases were loaded into a density threshold program (Time Volume Analysis). LV volumes were identified in semi-automated fashion, as described in Sections 2.5 and 2.6. Segmental wall motion and thickening were analysed qualitatively using the same scoring categories as described for MPS in Section 2.3.7. Quantitative measurement of mean segmental EF and thickening was undertaken as described in Section 2.6.1.

11.2.4 Statistics

Left ventricular end-diastolic volume (EDV), end-systolic volume (ESV) and ejection fraction (EF) were compared using Bland Altman analysis. Values were distributed non-parametrically; Passing and Bablok regression was used to compare values for systematic and proportional differences. Segmental EF and percentage thickening were compared using the Kruskal-Wallis test, with pair-wise Mann-Whitney testing as appropriate. Sensitivity, specificity, positive and negative predictive values (PPV/NPV) and accuracy of segmental EF and percentage thickening to discriminate either normal from abnormal myocardial segments or non-transmural from transmural MI on MPS were assessed using ROC analysis.

11.3 RESULTS

11.3.1 Myocardial perfusion scintigraphy

As shown in Section 6.3.1, 43/50 (86%) patients demonstrated evidence of previous MI on MPS. The gated images from one patient suffered from irrecoverable artefact, leaving 49 patients in total for comparison. Global LV functional parameters are given in Table 11.2. 16/49 (33%) patients had LVEF <50%; 10/49 (20%) had LVEF <35%. 9/49 (18%) patients had LV dilatation according to gender-specific values (all EDV≥150mL). Regional wall motion and thickening abnormalities were present in 240/833 (29%) and 248/833 (30%) segments respectively (Table 11.1).

		Normal	Mild ↓	Mod ↓	Severe ↓	Absent	Dyskinetic
Wall Motion (%)	MPS	593 (71)	64 (8)	30 (4)	46 (5)	89 (11)	11 (1)
	CCT	582 (70)	57 (7)	45 (5)	39 (5)	98 (12)	12 (1)
Wall Thickening (%)	MPS	585 (70)	63 (8)	51 (6)	56 (7)	78 (9)	
	CCT	584 (70)	73 (9)	49 (6)	47 (6)	80 (10)	

Table 11.1 *Distribution of segmental wall motion and thickening on MPS and CCT*

11.3.2 Cardiac Computed Tomography

As shown in Section 6.3.2, 43/50 (86%) patients demonstrated evidence of previous MI on delayed CCT. Global LV functional parameters are given in Table 11.2. 18/49 (37%) patients had LVEF <50%; 9/49 (18%) had LVEF <35%. Regional wall motion and

thickening abnormalities were seen in 251/833 (30%) and 249/833 (30%) segments respectively (Table 11.1).

11.3.3 Comparison between techniques for global LV function

Left ventricular ejection fraction

Measurement of LVEF was similar for both CCT and MPS (52.9±14.7 vs. 53.6±17.3, mean difference -0.68±8.2, p=0.56; Table 11.2, Figure 11.1). 95% limits of agreement (LOA) were wide (15.4, -16.7). Regression revealed no systematic difference between techniques (Table11.3, Figure 11.2), with an ~6% overestimation of LVEF by CCT but 95% confidence intervals (CI) including zero difference (95% CI -2.00 – 13.6). There were no proportional differences or deviation from linearity (p=0.89).

Left ventricular end-diastolic volume

CCT overestimated LVEDV compared with MPS (157.2±54.7mL vs. 118.1±53.6mL, mean difference 39.1±23.7mL, p<0.001; Table 11.2, Figure 11.1). 95%LOA were wide (85.7mL, -7.4mL). Passing and Bablok regression revealed a marked systematic overestimation of LVEDV by CT (44mL; 95%CI: 25.5 – 58.1; Table 11.3, Figure 11.3) but no proportional differences or deviation from linearity (p=0.84).

EDV ≥160mL on CCT predicted LV dilatation on MPS with sensitivity, specificity, PPV, NPV and accuracy of 100%, 75%, 47%, 100% and 89% (Table 11.4, Figure 11.5). Increasing this value to 200mL increased specificity and PPV to 98% and 75% at the expense of sensitivity (33%) and NPV (87%).

Left ventricular end-systolic volume

CCT overestimated LVESV compared with MPS (79.2±55.3mL vs. 60.3±49.5mL, mean difference 18.9±16.8mL, p<0.001; Table 11.2, Figure 11.1). 95%LOA were wide (51.8mL, -14mL). Regression revealed a systematic overestimation of LVESV by CCT of 16.9mL (9.16 – 22.6; Table 11.3, Figure 11.4) but no proportional differences or deviation from linearity (p=0.88).

	MPS	CCT	Mean Difference	95%CI LOA	p-value
EF	53.6±17.3	52.9±14.7	-0.68±8.20	15.4. -16.7	0.56
EDV	118.1±53.6	157.2±54.7	39.1±23.7	85.7, -7.4	<0.0001
ESV	60.3±49.5	79.2±55.3	18.9±16.8	51.8, -14	<0.0001

Table 11.2 *Indices of global left ventricular function for MPS and CCT. 95%CI LOA: 95% confidence interval limits of agreement.*

	Systematic differences	Proportional differences	Random differences	Linear model validity (p-value)
EF	6.26 (-2.00 – 13.6)	0.84 (0.71 – 1.00)	7.39 (±14.5)	0.89
EDV	44.0 (25.5 – 58.1)	1.00 (0.84 – 1.16)	17.3 (±34.0)	0.84
ESV	16.9 (9.16 – 22.6)	1.08 (0.95 – 1.21)	11.5 (±22.5)	0.88

Table 11.3 *Comparison of CCT and MPS using Passing and Bablok regression. This demonstrates no systematic difference in ejection fraction (EF; 95% CI crosses zero difference) but systematic overestimation of end-diastolic volume (EDV) and end-systolic volume (ESV) by CCT. There are no proportional differences or deviation from linearity.*

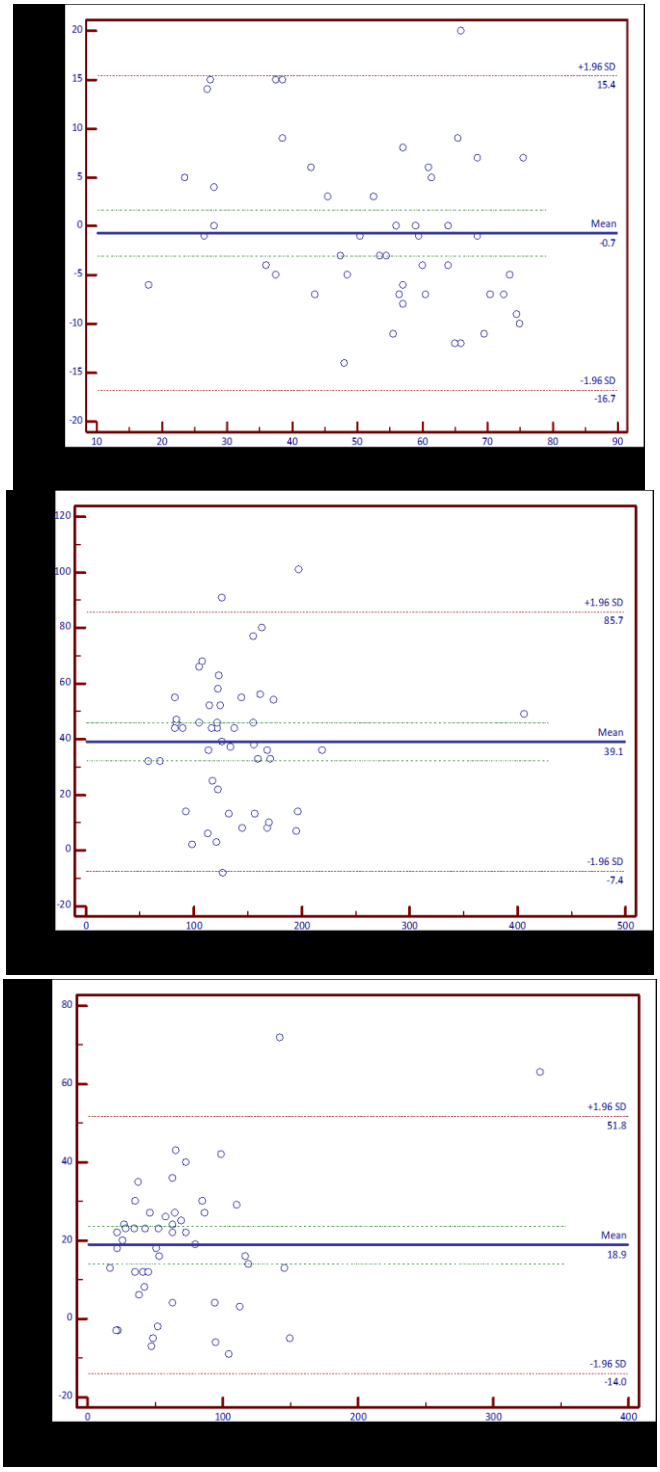


Figure 11.1 *Bland-Altman plots showing the relationship between CCT and MPS for measures of LV ejection fraction (top), end-diastolic volume (middle) and end-systolic volume (bottom).*

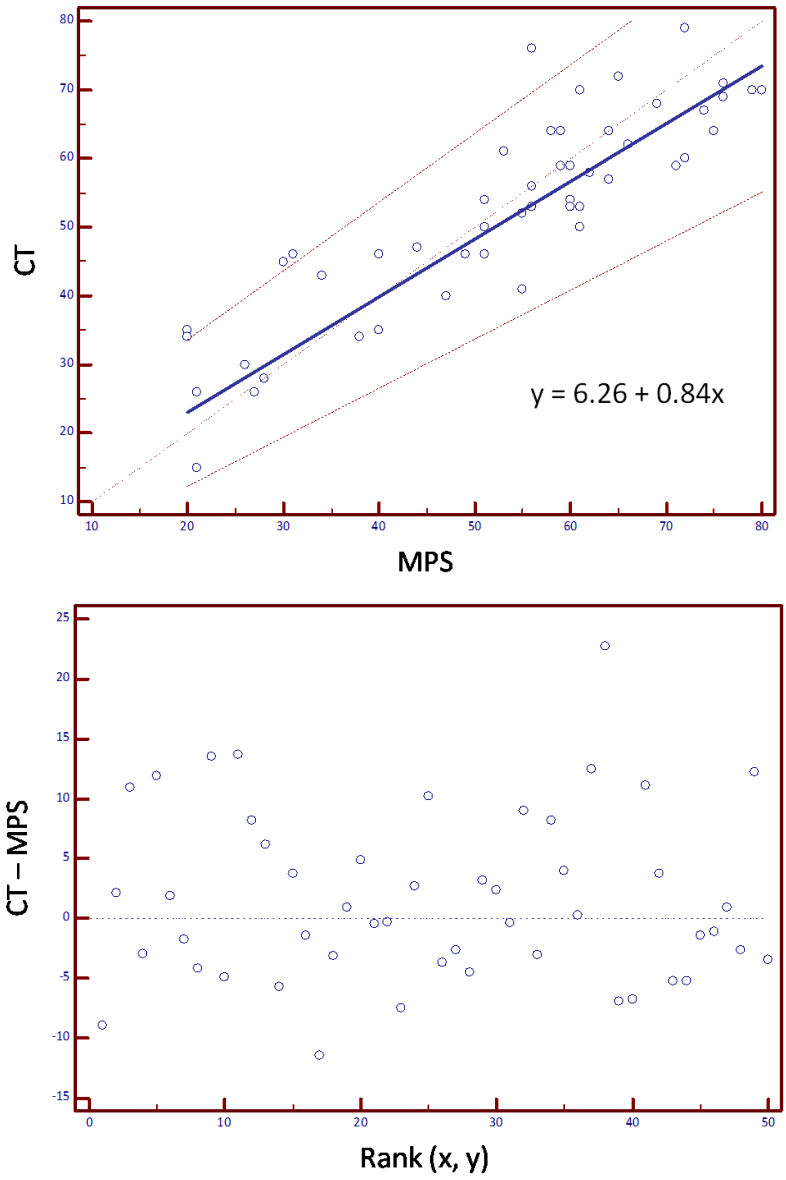


Figure 11.2 *Comparison of LV ejection fraction measurements, with the regression line (top) and residual plot (bottom).*

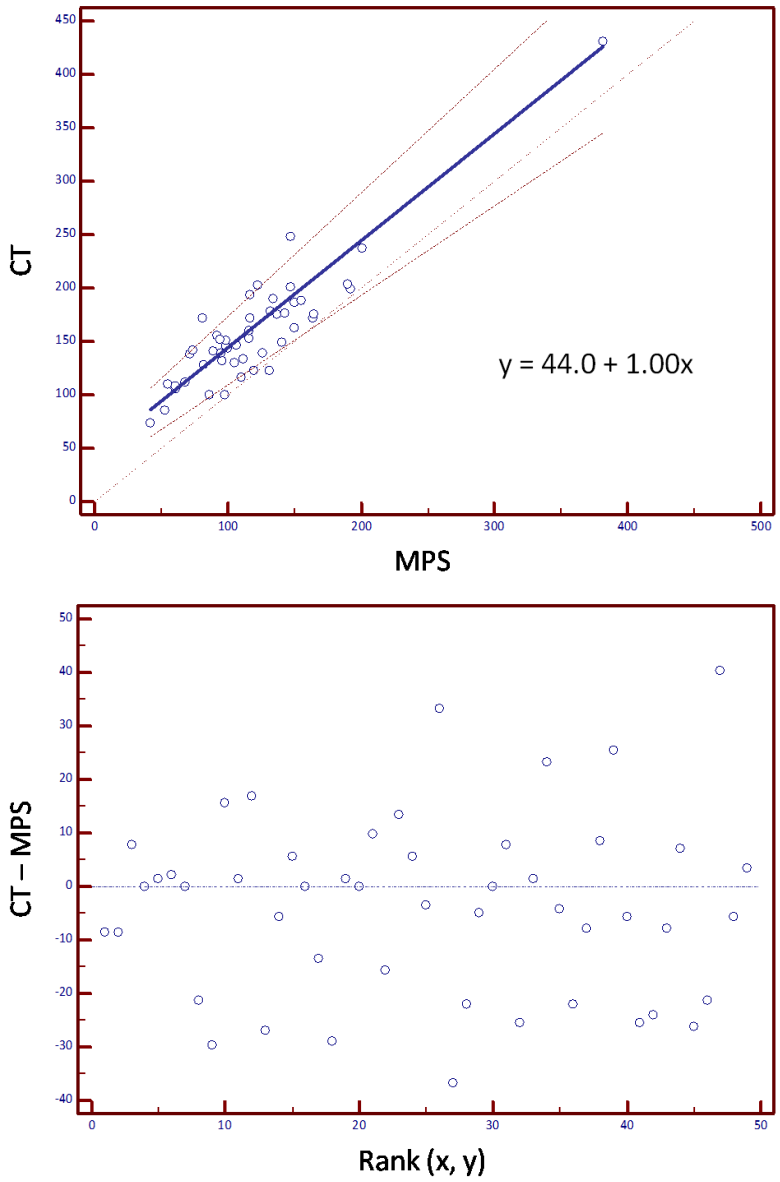


Figure 11.3 *Comparison of LV end-diastolic volume measurements, with the regression line (top) and residual plot (bottom).*

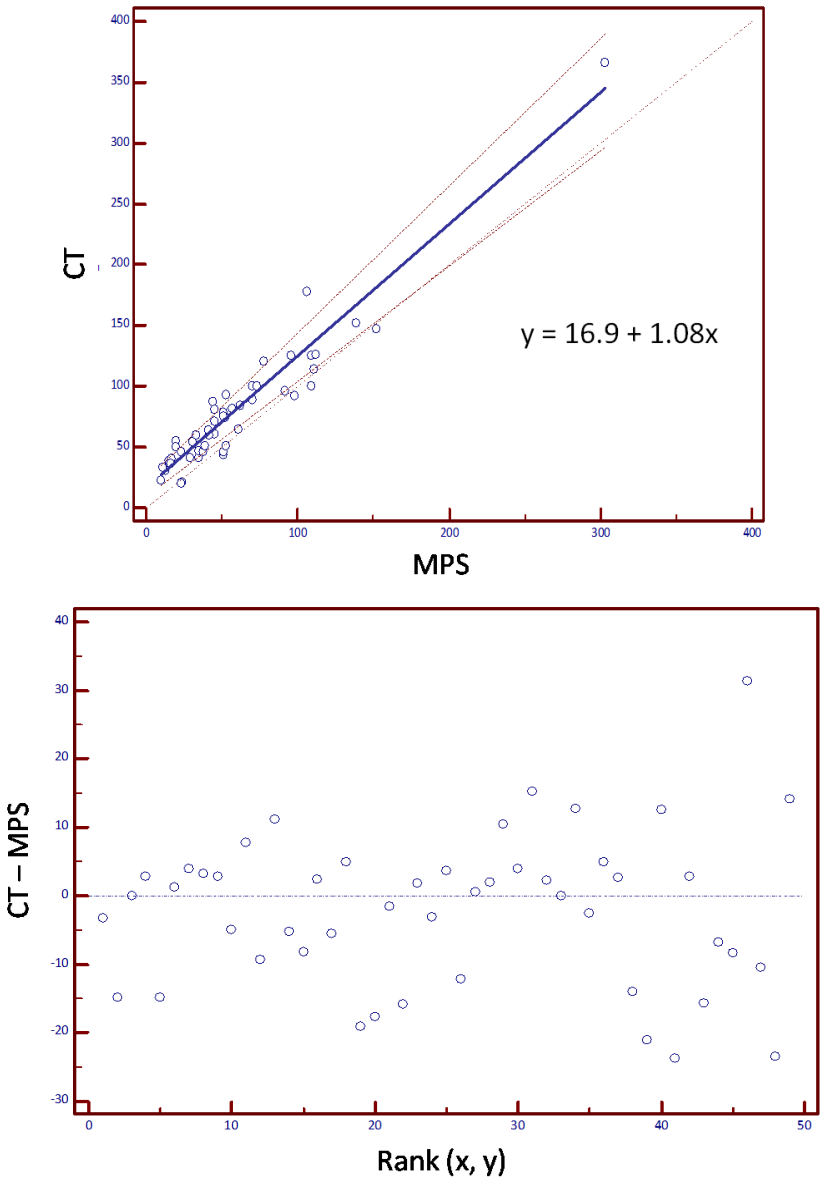


Figure 11.4 *Comparison of LV end-systolic volume measurements, with the regression line (top) and residual plot (bottom).*

Threshold	Sensitivity	Specificity	PPV	NPV
160mL	100 (66 – 100)	75 (59 – 87)	47 (23 – 71)	100 (88 – 100)
200mL	33 (8 – 70)	98 (87 – 100)	75 (13 – 100)	87 (74 – 95)
AUC	0.89 (0.76 – 0.96)			

Table 11.4 *Threshold values for end-diastolic volume on CCT to predict a dilated ventricle on MPS, using ROC analysis.*

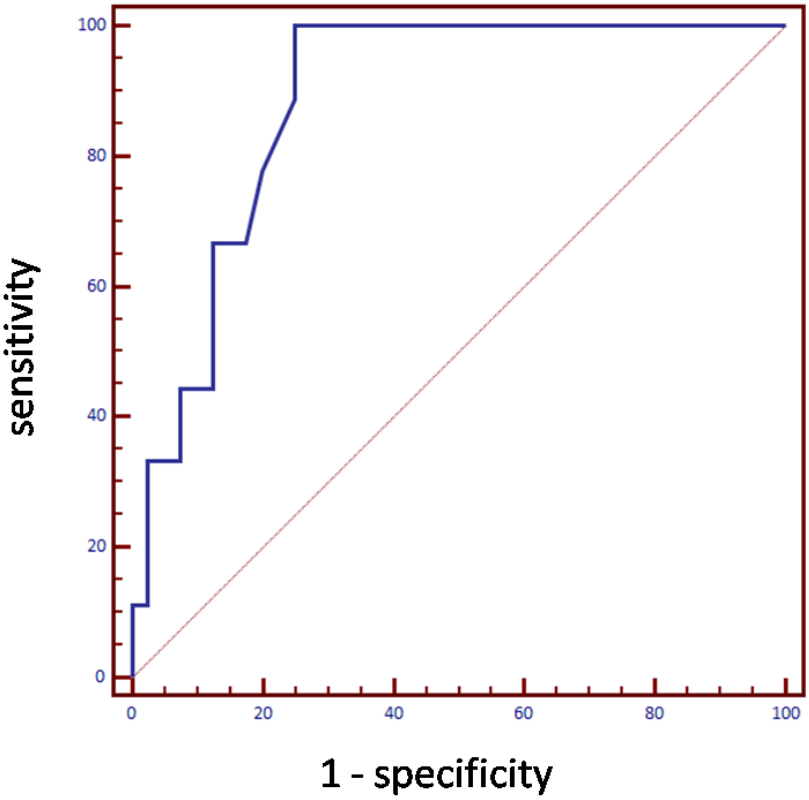


Figure 11.5 *ROC curve showing good accuracy of end-diastolic volume on CCT for predicting left ventricular dilatation on MPS.*

11.3.4 Qualitative measures of regional LV function

Results for agreement between CCT and MPS are shown in Table 11.5-7. There was excellent overall agreement between techniques for regional wall motion (83%, κ=0.88) and thickening (80%, κ=0.86).

Any degree of regional wall motion abnormality on CCT (i.e. mild reduction in wall motion or worse) predicted MI on MPS with sensitivity, specificity, PPV, NPV and accuracy of 75%, 91%, 81%, 88% and 83% respectively. Values for any abnormality in wall thickening were 75%, 91%, 82%, 89% and 85% respectively. CCT wall thickening was a better predictor (p=0.007).

Segments that were moderately impaired or worse on CCT had sensitivity, specificity, PPV, NPV and accuracy of 84%, 90%, 64%, 96% and 91% respectively for identification of transmural MI. Values for similarly abnormal wall thickening were 84%, 93%, 71%, 97% and 93% respectively. Once again, CCT wall thickening was a better predictor (p=0.048).

	Kappa	**95% Confidence Interval**
Wall Motion	0.88	0.85 – 0.91
Wall Thickening	0.86	0.82 – 0.89

Table 11.5 *Agreement between CCT and MPS regional wall motion and thickening.*

	Threshold	Sensitivity	Specificity	PPV	NPV	Accuracy	p-value
Wall Motion	≥ Mild ↓	75 (69 – 80)	91 (89 – 94)	81 (75 – 85)	88 (85 – 91)	83 (80 – 86)	0.007
Wall Thickening		75 (70 – 80)	92 (89 – 94)	82 (77 – 87)	89 (86 – 91)	85 (83 – 88)	

Table 11.6 *Analysis of CCT segmental wall motion and thickening (threshold: ≥mildly reduced) for sensitivity, specificity, positive and negative predictive value (PPV/NPV) and accuracy for detection of any myocardial infarction on MPS.*

	Threshold	Sensitivity	Specificity	PPV	NPV	Accuracy	p-value
Wall Motion	≥ Mod ↓	84 (78 – 90)	90 (87 – 92)	64 (57 – 71)	96 (95 – 98)	91 (89 – 93)	0.048
Wall Thickening		84 (78 – 90)	93 (90 – 94)	71 (64 – 78)	97 (95 – 98)	93 (91 – 94)	

Table 11.7 *Analysis of CCT segmental wall motion and thickening (threshold: ≥moderately reduced) for sensitivity, specificity, positive and negative predictive value PPV/(NPV) and accuracy for discrimination of transmural and non-transmural myocardial infarction on MPS.*

11.3.4 Quantitative measures of regional LV function

Segmental wall motion

Results are summarised in Table 11.8. Segmental EF was higher for normal segments than those that showed mild reduction in wall motion on MPS (66% (IQR 53.75 – 77%) vs. 44% (IQR 26 – 56.5%), p<0.0001). No differences were seen on CT between segments with mild and moderate reductions in wall motion on MPS (44% (IQR 26 – 56.5%) vs. 41% (IQR 31 – 50%), p=0.95), but segments with moderately reduced wall motion on MPS showed higher segmental EF values than those segments with severely reduced wall motion (41% (IQR 31 – 50%) vs. 26% (IQR 11 – 38%), p=0.0005). There were no differences between segments showing severely reduced or absent wall motion on MPS (26% (IQR 11 – 38%) vs. 21 (IQR 12 – 32.5%), p=0.47).

When reclassified according to transmurality (Table 11.9), segmental EF was higher in normal myocardial segments on MPS than in those that showed non-transmural or transmural MI (64% (IQR 50 – 77%) vs. 55 (IQR 38.25 – 69%) vs. 28.5 (IQR 14 – 40.5%) respectively, p<0.0001).

Segmental percentage wall thickening

Results are summarised in Table 11.10. Segmental percentage thickening was higher for normal segments than those that showed mild reduction in wall thickening on MPS (71% (IQR 44.5 – 95.5%) vs. 47% (IQR 21.25 – 69%), p<0.0001). No differences were seen on CT between segments with mild and moderate reductions in wall thickening on MPS (47% (IQR 21.25 – 69%), vs. 36% (IQR 17.25 – 64.5%), p=0.44), but segments with moderately reduced wall thickening on MPS showed higher segmental percentage thickening values

than those segments with severely reduced wall thickening (36% (IQR 17.25 – 64.5%) vs. 20% (IQR 4.5 – 50%), p=0.02). There were no differences between segments showing severely reduced or absent wall thickening on MPS (20% (IQR 4.5 – 50%) vs. 15.5% (IQR 0 – 38%), p=0.08).

When reclassified according to transmurality (Table 11.9), segmental percentage thickening was higher in normal myocardial segments on MPS compared to those that showed non-transmural and transmural MI (72% (IQR 47 – 95%) vs. 49% (IQR 22 – 72.75%) vs. 21% (4 – 41.5%) respectively, p<0.0001).

MPS Wall Motion	Segmental EF (%)
Dyskinesis	6 (0 – 10.75)†
Absent	21 (12 – 32.5)†
Severely reduced	26 (11 – 38)
Moderately reduced	41 (31 – 50)*
Mildly reduced	44 (26 – 56.5)*
Normal	66 (53.75 – 77)
p-value	<0.0001

Table 11.8 *Variation in CCT segmental EF across MPS wall motion categories. *† No differences between marked groups; all other pairwise differences significant.*

	Segmental EF (%)	Segmental % Thickening
Normal	64 (50 – 77)	72 (47 – 95)
Non-transmural	55 (38.25 – 69)	49 (22 – 72.75)
Transmural	28.5 (14 – 40.5)	21 (4 – 41.5)
p-value	<0.0001	<0.0001

Table 11.9 *Segmental EF and percentage wall thickening according to transmurality of myocardial infarction on MPS. All pairwise differences significant.*

MPS Wall Thickening	Segmental % Thickening
Absent	15.5 (0 – 38)†
Severely reduced	20 (4.5 – 50)†
Moderately reduced	36 (17.25 – 64.5)
Mildly reduced	47 (21.25 – 69)*
Normal	71 (44.5 – 95.5)*
p-value	<0.0001

Table 11.10 *CCT segmental percentage wall thickening across MPS wall motion categories. *† No differences between these groups; all other pairwise differences significant.*

11.3.5 Discrimination of normal and abnormal myocardium

Results are summarised in Table 11.11. Sensitivity, specificity, PPV and NPV of segmental EF for discriminating normal and abnormal myocardium were 69%, 73%, 51% and 85% respectively. Corresponding values for segmental percentage thickening were 75%, 70%, 52% and 87% respectively. Both parameters showed fair and equal accuracy for detecting normal myocardium (AUC 0.75 and 0.77 respectively, p=0.35, Figure 11.6) but neither were as accurate as their qualitative counterparts (AUC 0.75 vs. 0.83 for wall motion and 0.77 vs. 0.85 for wall thickening respectively, p<0.0001 for both).

11.3.6 Discrimination of non-transmural and transmural myocardial infarction

Results are summarised in Table 11.12. Sensitivity, specificity, PPV and NPV of segmental EF for detection of transmural MI (<50% resting MPS tracer uptake) were 83%, 76%, 58% and 92% respectively. Corresponding values for segmental percentage thickening were 85%, 68%, 54% and 91% respectively. Both parameters showed good and equal accuracy for detecting transmural MI (AUC 0.85 and 0.83 respectively, p=0.24, Figure 11.7) but neither were as accurate as their qualitative counterparts (AUC 0.85 vs. 0.91 for wall motion [p=0.0002] and 0.83 vs. 0.93 for wall thickening [p<0.0001] respectively).

	Segmental EF	Segmental % thickening
Threshold	51%	53%
Sensitivity	69 (63 – 74)	75 (70 – 80)
Specificity	73 (69 – 77)	70 (66 – 74)
PPV	51 (46 – 0 57)	52 (47 – 57)
NPV	85 (82 – 88)	87 (84 – 90)
AUC	0.75 (0.72 – 0.78)	0.77 (0.74 – 0.80)
Comparison	No difference (p=0.35)	

Table 11.11 *ROC analysis for CCT segmental EF and percentage thickening for discriminating normal and abnormal myocardium.*

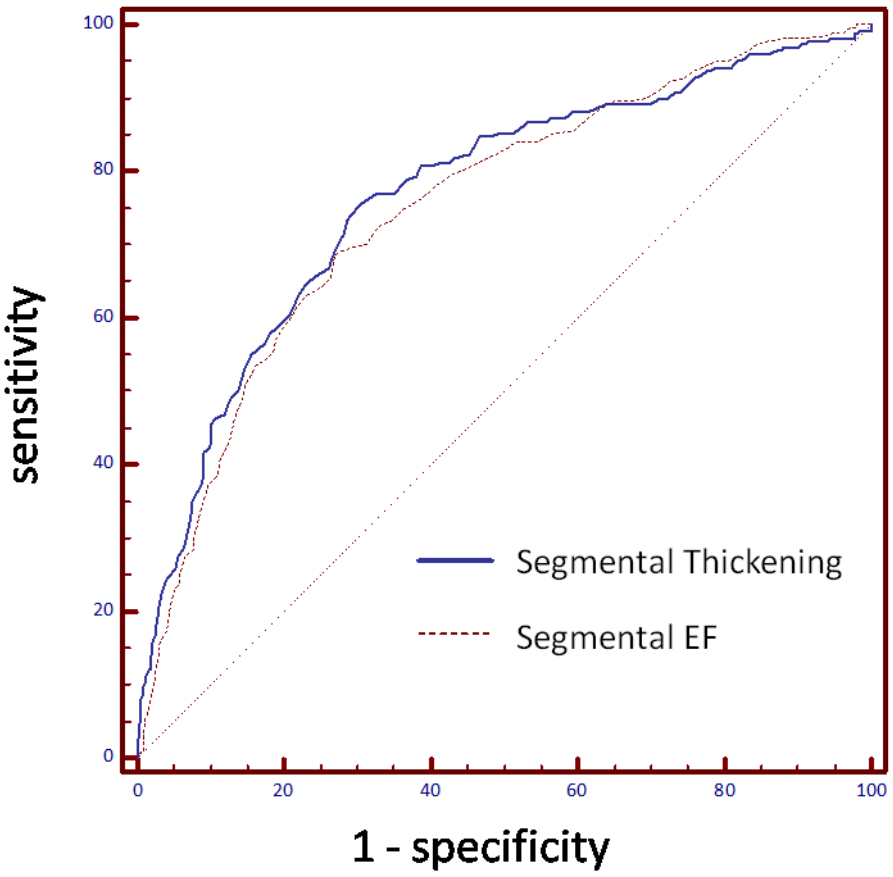


Figure 11.6 *ROC curves showing accuracy of quantitative CCT segmental ejection fraction (EF) and percentage thickening for discriminating normal and abnormal myocardium.*

	Segmental EF	Segmental % thickening
Threshold	46%	49%
Sensitivity	83 (76 – 89)	85 (78 – 90)
Specificity	76 (72 – 79)	68 (65 – 72)
PPV	58 (53 – 64)	54 (49 – 59)
NPV	92 (89 – 94)	91 (89 – 94)
AUC	0.85 (0.83 – 0.88)	0.83 (0.80 – 0.86)
Comparison	No difference (p=0.24)	

Table 11.12 *ROC analysis for CCT segmental EF and percentage thickening for discriminating non-transmural and transmural myocardial infarction.*

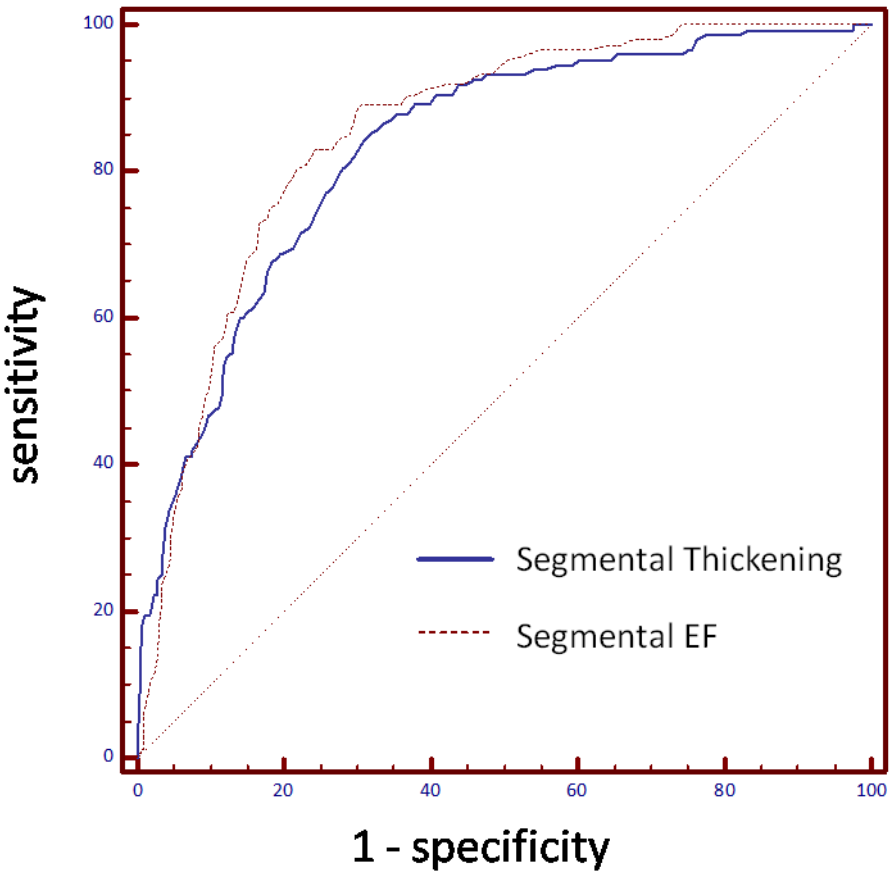


Figure 11.7 *ROC curves showing accuracy of quantitative CCT segmental ejection fraction (EF) and percentage thickening for discrimination of non-transmural and transmural myocardial infarction.*

11.4 DISCUSSION

Ventriculography by CCT has been extensively validated, mostly using 64-slice CCT[112, 157-160] but also, more recently, on higher specification CCT scanners[151-153, 161-165]. Comparisons with SPECT MPS have demonstrated consistently a systematic over-estimation of LV EDV and ESV but similar LVEF[112, 157, 158]. Overestimation of EDV compared to SPECT is typically in the 35 – 45mL range EDV for 64-slice CCT, but seems to be reduced on newer CT scanners[163]. Consistent overestimation of volumes has also been seen when CCT is compared to CMR[151, 161, 165] and echocardiography[151, 153], although for the large part this is in the range of 10-15mL for EDV and may be clinically irrelevant. Improved temporal resolution of newer generation CCT scanners also seems to improve comparisons with other techniques, particularly CMR. The present study, carried out using 64-slice CCT, reflects previously published results – systematic overestimation of LV volumes but no overall difference in LVEF. Most validation studies have been in either populations without confirmed CAD – low-to-intermediate likelihood patients under investigation for chest pain – or in patient populations with relatively low prevalence of segmental MI. In the present study, 86% of patients had demonstrable MI on SPECT MPS, with 32% prevalence of segmental MI and 36% prevalence of global LV dysfunction. The results therefore validate CCT in the setting of chronic MI. There were no proportional differences or deviation from linearity in global LV parameters when measured by CCT, suggesting that they can be used reliably provided the systematic error seen by CCT is accounted for by defining normal reference ranges. For example, a threshold for EDV of 160mL has 100% negative predictive value for the presence of a dilated left ventricle on MPS but the threshold above which end-diastolic LV dilatation can be confidently diagnosed is uncertain.

Qualitative measures of regional LV function on CCT show excellent agreement with those on MPS. Normal segmental wall motion or thickening on CCT excludes MI in ~90% of cases. This is reflected at patient level, with normal resting myocardial perfusion in all patients with normal regional LV function on CCT. PPV is somewhat lower, with ~80% of segments with abnormal regional function on CCT showing MI in the same segment on MPS. Segmental wall thickening appears to be a better predictor of segmental MI.

Quantitative values for regional function perform only moderately well. There are clear differences in segmental EF and percentage thickening across MPS categories and at different grades of MI transmurality. However, these quantitative measures have only modest sensitivity and specificity for discriminating normal from abnormal myocardial segments, mainly because mild abnormalities on CCT are normal on MPS. Only 13% of segments with abnormal thickening on MPS were normal on CCT, whilst 49% of abnormal segments on CCT were normal on MPS. Respective values for wall motion abnormalities were 9% and 39%. This may be the result of either overcalling abnormalities on CT or poor spatial and temporal resolution of MPS. ROC analysis shows only fair accuracy for detecting normal myocardial segments, although a cut-off value of around 50% for segmental EF and thickening has a negative predictive value of 85% and 87% for the presence of any MI. Quantitative CT fares better at detecting segments with transmural MI, with good accuracy of both segmental EF and thickening (AUC 0.85 and 0.83 respectively) and sensitivities in the mid-80% range. NPV for both parameters is >90%, suggesting that absence of quantitative wall motion and thickening abnormalities on CT effectively rules out transmural MI. However, much like quantitative assessment of delayed myocardial hyperenhancment, it is clear that quantitative measures of regional LV function on CCT are not yet good enough to replace expert visual scoring.

11.5 LIMITATIONS

The study was not adequately powered to determine the CCT EDV above which LV dilatation on MPS could be reliably predicted, although this was not the primary aim of the study. Sample size may also have limited power to detect differences between MPS and quantitative CCT measures of regional LV function. Although MPS was the gold standard, it has poorer spatial and temporal resolution than CCT and differences in quantitation might be expected without necessarily reflecting inadequacies of either technique.

11.6 SUMMARY FINDINGS

1. CCT systematically overestimates end-systolic and end-diastolic volumes compared with SPECT MPS, although there is no difference in calculated LV ejection fractions.
2. There were no proportional differences or deviations from linearity between CCT and MPS measures of global LV function, suggesting that CCT can be used reliably provided systematic errors are accounted for by defining normal reference ranges.
3. No patient with EDV <160mL on CCT had a dilated LV on MPS.
4. Qualitative measures of regional LV function on CCT (segmental wall motion and thickening) demonstrate excellent agreement with similar measures on MPS.
5. Moderate or greater reductions in segmental wall motion and thickening carry a 96-97% negative predictive value for transmural MI in that segment. Positive predictive value is poorer, however (64-71%).
6. Segmental wall thickening on CCT appears better than wall motion at discriminating normal from abnormal myocardium and non-transmural from transmural MI.
7. Quantitative measures of regional LV function on CCT (segmental EF and percentage wall thickening) are less accurate than qualitative measures and should not replace expert visual scoring.

SECTION THREE

CHAPTER 12 DELAYED DUAL SOURCE CARDIAC CT IN PATIENTS WITH PREVIOUS MYOCARDIAL INFARCTION: COMPARISON WITH CARDIOVASCULAR MAGNETIC RESONANCE IMAGING

12.1 INTRODUCTION

Extent and depth of myocardial scarring predicts prognosis[97-101] and quantification allows prediction of segmental recovery after revascularisation[102, 103]. Cardiovascular magnetic resonance imaging (CMR) is now considered the reference standard method for quantification of myocardial scarring[166], identifiable as late gadolinium enhancement (LGE) on delayed CMR acquisitions. As demonstrated in Chapters 5-7 and by other investigators[63, 96, 114-116], cardiac computed tomography (CCT) may be used to identify myocardial scarring through visualisation of myocardial hyperenhancement on delayed imaging (dCCT). CMR has several advantages over CCT, which include superior temporal resolution and the ability to null normal myocardium by selecting appropriate inversion times, exacerbating signal differences between hyperenhanced and normal myocardium. Dual-source CCT (DSCT) improves CCT temporal resolution twofold by doubling the number of X-ray tube/detector array pairs on the gantry, halving acquisition time. Alternatively, each X-ray source can be set to emit X-ray beams of different energies. Data are reconstructed using attenuation coefficients derived from the two X-ray beams, allowing better delineation of tissues with, for example, high iodine density. This may have benefits for visualisation of myocardial hyperenhancement on dCCT[65-67]. The aim of this study was to quantify visually myocardial enhancement patterns on single-energy and dual-energy

dCCT images (SE-dCCT and DE-dCCT respectively) in patients with previous MI and assess agreement with LGE on CMR.

12.2 METHODS

16 patients (12 male, mean age 66±8.7 years) with previous myocardial infarction (MI) referred for clinical CMR were recruited. Median time since MI was 1.25 years (IQR: 0.75 – 11 years, min 57 days, max 21 years). Patients were excluded if they had any of the following: NYHA class IV symptoms; contraindication to negative chronotropic agents; severe renal dysfunction (creatinine >150μmol/L); pregnancy or childbearing potential; allergy or previous intolerance of iodinated contrast. The study was approved by the local research ethics committee and all patients gave written informed consent.

12.2.1 Cardiovascular Magnetic Resonance Imaging

CMR images were acquired on a 1.5T Siemens Sonata CMR system (Siemens Medical Systems, Erlangen, Germany) as described in Section 2.5. Images were reconstructed and analysed as described in Section 2.7.3.

12.2.2 Cardiac Computed Tomography

Scans were performed on a dual source 128-slice CT scanner with oscillating z-axis focal spot (Somatom Definition Flash, Siemens Medical Systems). A test bolus technique was used to time scan delay, as described in Section 2.4.4. Intravenous iodinated contrast (Ultravist 370, Bayer Healthcare Pharmaceuticals Inc) was administered using the triphasic protocol described in Chapter 5.2.2. Early acquisitions used identical parameters for each X-ray source, as follows: retrospective ECG gating, tube voltage 100kVp, tube current 120 quality reference mAs/rot, 128x0.6 mm collimation, 0.28s rotation time, pitch 0.23 for 60

bpm, and CareDose 4D on. Delayed acquisitions used different tube voltages and currents for each X-ray source (Tube A: 100kVp, 120 quality reference mAs/rot; Tube B: 140kVp with Sn filter, 102 quality reference mAs/rot) but were otherwise unchanged from early acquisitions. Dose constraints were DLP 900mGycm and effective radiation dose 18mSv. 10/16 (63%) patients had resting heart rates of <70 beats per minute (range 41 – 77bpm). One patient (HR 77bpm) received intravenous metoprolol. Median heart rates during the early and delayed CCT scans were 63bpm (IQR 53 – 71bpm) and 66bpm (IQR 57.5 – 75bpm), with the latter higher than the former (p=0.02).

12.2.3 Image Analysis

Images were reconstructed in the end-diastolic phase (75% R-R interval). 3 datasets were created: early CCT (eCCT) images, 100kVp single-energy delayed CCT (SE-dCCT) images and dual-energy dCCT (DE-dCCT) images based on a 50/50 combination of 100kVp and 140kVp acquisitions. Images were analysed using proprietary cardiac software (TeraRecon Inc) as 5mm thick multiplanar reformatted images oriented into horizontal long, vertical long and short axis views and scored as described in Sections 2.2 and 6.2.3.

12.2.4 Statistics

Data were analysed using MedCalc statistical software (version 12.2.1.0, MedCalc Software). Values are presented as mean±SD or median (interquartile range) as appropriate. Patient and segment level agreement were compared using Cohen's kappa. Where appropriate, sensitivities, specificities, positive (PPV) and negative (NPV) predictive values were calculated. CMR summed rest scores and CCT summed scarring scores were correlated using Spearman's rank correlation. Inter- and intraobserver agreement was calculated using Cohen's kappa.

12.3 RESULTS

12.3.1 Cardiovascular Magnetic Resonance Imaging

11/16 (69%) patients showed evidence of previous MI, of which 9/16 (56%) had at least one segment of transmural MI. Median late gadolinium enhancement (LGE) score was 57.5 (IQR 43.5 – 68). Of 272 segments, 200 (74%) were normal, while 3 (1%), 17 (6%), 13 (5%) and 39 (14%) showed mild, moderate or severe reduction or absent uptake respectively. These were grouped into 200 (74%), 20 (7%) and 52 (19%) segments showing either no MI, non-transmural or transmural MI respectively.

12.3.2 Computed Tomography

Early CCT

9/16 (56%) patients demonstrated MI. Median summed scarring score was 1.5 (IQR 0 – 9.5). Of 272 segments, 227 (84%) were considered normal, whilst 17 (6%) and 28 (10%) showed non-transmural or transmural MI respectively.

Single-energy delayed CCT

12/16 (75%) patients demonstrated MI. Median summed scarring score was 3.5 (IQR 0.5 – 11). Of 272 segments, 206 (76%) were considered normal, whilst 31 (11%) and 35 (13%) showed non-transmural or transmural MI respectively.

Dual-energy delayed CCT

12/13 (92%) patients demonstrated MI. Median summed scarring score was 2 (IQR 0 – 15.25). Of 221 segments, 160 (72%) were considered normal, whilst 30 (14%) and 31 (14%) showed non-transmural or transmural MI respectively.

Comparison between images

Both SE-dCCT and DE-dCCT showed higher summed scarring scores (p=0.05 and 0.01 respectively) and greater number of segments demonstrating MI (p=0.0008 and 0.0001 respectively) than eCCT. No differences were observed between dCCT (SSS: p=0.58; segmental MI: p=0.14).

12.3.3 Patient level agreement between CMR and CCT

Discrimination of patients with and without late gadolinium enhancement

Results are summarised in Table 12.1. eCCT agreed with CMR in 12/16 (75%) cases. Sensitivity, specificity, PPV and NPV were 73%, 80%, 89% and 57% respectively, with false positive and false negative results in 1/9 (11%) and 3/7 (43%) respectively. Overall accuracy was fair (AUC 0.76). SE-dCCT agreed with CMR in 15/16 (94%) cases. Sensitivity, specificity, PPV and NPV were 100%, 80%, 92% and 100% respectively, with false positive results in 1/12 (8%) cases; no scans were false negative. Overall accuracy was excellent (AUC 0.90). DE-dCCT agreed with CMR in 10/13 (77%) cases. Sensitivity, specificity, PPV and NPV were 88%, 60%, 78% and 75% respectively, with false positive and false negative results in 2/9 (22%) and 1/4 (25%) respectively. Overall accuracy was fair (AUC 0.74).

Detection of patients with ≥50% late gadolinium enhancement

Results are summarised in Table 12.2. eCCT agreed with CMR in 14/16 (88%) cases. Sensitivity, specificity, PPV and NPV were 78%, 100%, 100% and 78% respectively. eCCT was false positive and false negative in 0/7 (0%) and 2/9 (22%) cases respectively. Overall accuracy was good (AUC 0.89). SE-dCCT and DE-dCCT agreed with CMR in all cases. Sensitivity, specificity, PPV and NPV were thus 100% and accuracy was perfect (AUC 1.00).

	Sensitivity	Specificity	PPV	NPV	AUC
eCCT	73 (39 – 94)	80 (28 – 100)	89 (49 – 100)	57 (18 – 90)	0.76 (0.49 – 0.94)
SE-dCCT	100 (72 – 100)	80 (28 – 100)	92 (60 – 100)	100 (40 – 100)	0.90 (0.65 – 0.99)
DE-dCCT	88 (47 – 100)	60 (15 – 95)	78 (40 – 97)	75 (13 – 100)	0.74 (0.43 – 0.93)

Table 12.1 *Analysis of CCT at patient level for sensitivity, specificity, positive predictive value (PPV), negative predictive value (NPV) and accuracy (AUC, area under the curve) for the detection of patients with any LGE on CMR.*

	Sensitivity	Specificity	PPV	NPV	AUC
eCCT	78 (40 – 97)	100 (59 – 100)	100 (59 – 100)	78 (40 – 97)	0.89 (0.63 – 0.99)
SE-dCCT	100 (66 – 100)	100 (59 – 100)	100 (66 – 100)	100 (59 – 99)	1.00 (0.79 – 1.00)
DE-dCCT	100 (54 – 100)	100 (59 – 100)	100 (54 – 100)	100 (59 – 100)	1.00 (0.75 – 1.00)

Table 12.2 *Analysis of CCT at patient level for sensitivity, specificity, positive predictive value (PPV), negative predictive value (NPV) and accuracy (AUC, area under the curve) for the detection of patients with at least one segment of ≥50% LGE on CMR.*

Correlation between CCT and CMR summed scores

Correlation was strong between CMR LGE scores and CCT summed scaring scores (Table 12.3; r=0.78, 0.92 and 0.86 for eCCT, SE-dCCT and DE-dCCT respectively). SE-dCCT summed scaring scores showed the strongest linear relationship with CMR LGE scores, although there was significant overlap in confidence intervals.

	Spearman's rank correlation	**95% Confidence Interval**
eCCT	0.78	0.45 – 0.92
SE-dCCT	0.92	0.79 – 0.97
DE-dCCT	0.86	0.58 – 0.96

Table 12.3 *Correlation between CMR summed LGE scores and CCT summed scarring scores.*

12.3.4 Segment level agreement between CMR and CCT

Results for overall segmental agreement are shown in Table 12.4. Agreement was good for eCCT (84%, κ=0.65), and excellent for SE-dCCT (85%, κ=0.80) and DE-dCCT (83%, κ=0.79).

	Kappa	**95% Confidence Interval**
eCCT	0.65	0.53 – 0.76
SE-dCCT	0.80	0.72 – 0.87
DE-dCCT	0.79	0.71 – 0.87

Table 12.4 *Segment level agreement between CCT and CMR for the presence of normal myocardium, non-transmural and transmural MI.*

For discriminating normal from abnormal myocardium, sensitivity, specificity, PPV and NPV were 56%, 98%, 89% and 86% respectively for eCCT; 76%, 95%, 83% and 92% respectively for SE-dCCT; and 85%, 90%, 74% and 95% for DE-dCCT (Table 12.5). Overall accuracy was fair for eCCT (AUC 0.77), good for SE-dCCT (AUC 0.87) and excellent for DE-dCCT (AUC 0.90). SE-dCCT and DE-dCCT showed equal accuracy (p=0.73) and both were more accurate than eCCT (p=0.02 and 0.008 for SE-dCCT and DE-dCCT respectively).

For the discrimination of segments with transmural MI, sensitivity, specificity, PPV and NPV were 52%, 100%, 96% and 90% respectively for eCCT; 63%, 99%, 94% and 92% respectively for SE-dCCT; and 67%, 97%, 84% and 93% for DE-dCCT (Table 12.6). Overall accuracy was good for eCCT (AUC 0.79) and excellent for SE-dCCT (AUC 0.92) and DE-dCCT (AUC 0.93). SE-dCCT and DE-dCCT showed equal accuracy (p=0.54) and both were more accurate than eCCT (p=0.005 and 0.01 for SE-dCCT and DE-dCCT respectively).

	Sensitivity	Specificity	PPV	NPV	AUC
eCCT	56 (43 – 67)	98 (94 – 99)	89 (76 – 96)	86 (81 – 90)	0.77 (0.72 – 0.82)
SE-dCCT	76 (65 – 86)	95 (90 – 97)	83 (83 – 92)	92 (87 – 95)	0.87 (0.82 – 0.90)†
DE-dCCT	85 (72 – 93)	90 (85 – 95)	74 (61 – 84)	95 (90 – 98)	0.90 (0.85 – 0.93)†

Table 12.5 *Analysis of CCT at segment level for sensitivity, specificity, positive predictive value (PPV), negative predictive value (NPV) and accuracy AUC, area under the curve) for the detection of any LGE on CMR. †No difference; other comparisons significant.*

	Sensitivity	Specificity	PPV	NPV	AUC
eCCT	52 (38 – 66)	100 (98 – 100)	96 (81 – 100)	90 (85 – 93)	0.79 (0.74 – 0.84)
SE-dCCT	63 (49 – 76)	99 (97 – 100)	94 (81 – 99)	92 (88 – 95)	0.92 (0.88 – 0.95)†
DE-dCCT	67 (50 – 81)	98 (94 – 99)	84 (66 – 95)	93 (89 – 96)	0.93 (0.88 – 0.96)†

Table 12.6 *Analysis of CCT at segment level for sensitivity, specificity, positive predictive value (PPV), negative predictive value (NPV) and accuracy (AUC, area under the curve) for the detection of ≥50% LGE on CMR. †No difference; other comparisons significant.*

12.3.5 Interobserver and intraobserver agreement

Results are summarised in Table 12.7. Segmental inter- and intraobserver agreement for categorising normal myocardium, non-transmural and transmural MI on DE-dCCT were both excellent (κ=0.84 and 0.94 respectively).

		Observer 1		
		Normal	**Non-transmural MI**	**Transmural MI**
Observer 2	**Normal**	184	14	2
	Non-transmural MI	15	17	3
	Transmural MI	0	5	32
		Observed agreement 86% Kappa = 0.84 [0.78 – 0.90]		

		Observation 1		
		Normal	**Non-transmural MI**	**Transmural MI**
Observation 2	**Normal**	195	7	0
	Non-transmural MI	4	25	1
	Transmural MI	0	4	36
		Observed agreement 94% Kappa = 0.94 [0.92 – 0.97]		

Table 12.7 *Interobserver (top) and intraobserver (bottom) agreement for DE-dCCT detection of normal myocardium, non-transmural and transmural MI*

12.4 DISCUSSION

These results demonstrate that, as in Chapter 6, dCCT is a promising technique for the evaluation of myocardial scarring in patients with previous MI. Confidence intervals for these preliminary results are wide. Nonetheless, several statements may be put forward on the basis of these results. First, dCCT has better sensitivity and NPV for myocardial scarring at patient-level than eCCT. In this regard, both single-energy and dual-energy dCCT images showed perfect performance at discriminating patients with ≥1 segment of full thickness MI on CMR. Interestingly, SE-dCCT outperformed DE-dCCT at patient-level when discriminating between patients with and without MI. Indeed, overall accuracy of DE-dCCT for detecting patients without MI was similar to that shown by eCCT (AUC 0.74 vs 0.76 respectively), which were both inferior to SE-dCCT (AUC 0.90). With only 16 patients recruited to this initial study, patient-level data should be interpreted with caution. However, it is reassuring that patient-level comparisons (of SE-dCCT at least) with CMR generate results similar to those seen when compared with SPECT myocardial perfusion scintigraphy (MPS, Chapter 6) – namely excellent sensitivity, PPV and accuracy. This is reflected in the correlation of CCT summed scarring scores with CMR LGE summed scores. SE- and DE-dCCT show better linear relationships with CMR LGE summed scores than those generated by eCCT, suggesting that, although no account is made for systematic errors, dCCT shows at least the same proportional changes in analysis of scarring severity as CMR LGE summed scores.

Segment-level agreement was better for dCCT than eCCT, with no difference observed between single- and dual-energy images. Once again, kappa values were

similar to those seen between CCT and SPECT MPS in Chapter 6, helping to corroborate these findings. There was significant overlap of confidence intervals, limiting the validity of segmental comparisons as truly representative findings. Bearing this in mind, DE-dCCT shows better sensitivity and NPV than either SE-dCCT or eCCT for discriminating patients with normal myocardium, non-transmural LGE and transmural LGE. It is intuitively sensible that any manoeuvre designed to increase the conspicuity of contrast-enhanced tissue (dual-energy imaging) ought to improve sensitivity. This consequence has been suggested by others[167] and is the basis for the implied benefit of dual-energy imaging in dCCT. However, our data suggest the trade-off for DE-dCCT is lower specificity and PPV. Indeed, eCCT shows the highest specificity and PPV for discriminating patients with and without LGE, a finding contrary to that demonstrated in Chapter 6 when compared with SPECT MPS. The reason for this is not immediately apparent – temporal resolution may be an issue, with a twofold improvement for eCCT imaging in this study – and confirmation is required from a larger prospective analysis. Regardless, as an overall result, both SE-dCCT and DE-dCCT show excellent and equivalent accuracy for discriminating patients with normal myocardium, non-transmural LGE and transmural LGE and perform better than eCCT. This result again corroborates those seen in comparisons with SPECT MPS (Chapter 6). Finally, it is reassuring to see that inter- and intraobserver segmental agreement for DE-dCCT is excellent. Reproducibility is paramount for any technique and is a requirement for validation and, ultimately, acceptance in clinical practice. A summary conclusion of these results is therefore that, given the wide confidence intervals resulting from small sample size, there is probably no significant difference between SE-dCCT and DE-dCCT for the detection

of myocardial scarring when compared to CMR and the reproducibility of DE-dCCT renders it suitable for clinical use.

12.5 LIMITATIONS

As stated, numbers recruited to this preliminary study were small, limiting the interpretability of some findings – for example, perfect patient-level accuracy of dCCT for detecting patients with ≥1 segment with ≥50% LGE. There were wide confidence intervals for virtually all patient-level values, reducing the likelihood of finding between-group differences where they existed. Regardless, these promising initial results may be used to inform future prospective analyses of dCCT.

12.6 SUMMARY FINDINGS

1. SE-dCCT and DE-dCCT result in higher summed scarring scores when compared to eCCT. SE-dCCT scores show the strongest linear relationship with CMR LGE scores.
2. SE-dCCT is most accurate at identifying patients with LGE on CMR, whilst both SE-dCCT and DE-dCCT show perfect accuracy for determining patients with ≥50% LGE in at least one segment. Small patient numbers limits the significance of this result.
3. SE-dCCT and DE-dCCT perform equally well at segment level, showing excellent overall agreement with CMR and accuracy for discriminating patients with any LGE or ≥50% LGE on CMR. DE-dCCT may be more sensitive but both are superior to eCCT
4. Inter- and intraobserver agreement for visual analysis of DE-dCCT are excellent.
5. Results suggest that, despite the small number of patients studies, DE-dCCT reproducibly identifies partial- and full-thickness myocardial scarring on CMR.

CHAPTER 13 SEGMENTAL MYOCARDIAL THICKNESS ON DUAL SOURCE CARDIAC CT AS A PREDICTOR OF MYOCARDIAL INFARCTION ON CARDIOVASCULAR MAGNETIC RESONANCE IMAGING

13.1 INTRODUCTION

Cardiovascular magnetic resonance imaging (CMR) is considered the reference standard for quantification of myocardial scarring[166]. Myocardial wall thickness correlates with depth of myocardial scarring and predicts likelihood of segmental recovery of function after revascularisation[70]. End-diastolic wall thickness (EDWT) is the most commonly quoted parameter, with values of 5.5mm – 6mm in dysfunctional segments considered the appropriate cut-off on CMR for predicting non-recovery of function after revascularisation[70, 138-140]. Whilst functional recovery is extremely unlikely below this value, predictive power above it is poor[138]. Although guidelines suggest that basal septal and inferolateral left ventricular (LV) EDWT should be reported routinely on CMR, reporting of values for all 17 myocardial segments is not recommended in a standard clinical report[168]. Cardiac computed tomography (CCT) has superior spatial resolution to CMR. The standard CCT dataset allows measurement of mean segmental myocardial thickness in any acquired cardiac phase. The aim of this study is to measure EDWT on CCT and compare values with those measured on CMR. As shown in Chapter 10, end-systolic wall thickness (ESWT) is a better predictor of depth of segmental myocardial infarction on SPECT

myocardial perfusion scintigraphy. The power of ESWT and EDWT to predict transmurality of segmental late gadolinium enhancement (LGE) on CMR is also therefore assessed.

13.2 METHODS

16 patients (12 male, mean age 66±8.7 years) with previous myocardial infarction referred for clinical CMR were recruited. Median time since myocardial infarction was 1.25 years (IQR: 0.75 – 11 years, min 57 days, max 21 years). Exclusion criteria are listed in Section 12.2. The study was approved by the local research ethics committee and all patients gave written informed consent.

13.2.1 Cardiac computed tomography

Early and delayed CCT acquisitions (eCCT and dCCT respectively) were performed on a dual source 128-slice CT scanner with oscillating z-axis focal spot (Somatom Definition Flash, Siemens Medical Systems) as described in Sections 2.4, 5.2.2 and 12.2.2. Data from both acquisitions were reconstructed using a medium-smooth kernel at 10% increments from 25-95% of the R-R interval.

13.2.2 Cardiac CT image analysis

Myocardial hyperenhancement on dCCT was assessed as described in Section 2.6.1. EDWT and ESWT were calculated from end-systolic and end-diastolic phases (25% and 75% R-R interval respectively) on eCCT. Datasets were loaded into a density threshold program (Time Volume Analysis) and the LV blood pool identified in semi-automated fashion, as described in Sections 2.5 and 2.6. The outer edge of the LV

blood pool was defined as the endocardial contour, with manual adjustments made as necessary. The epicardial contour was defined as the boundary between the myocardial surface and epicardial fat. The endo- and epicardial contours defined the myocardial volume, which was then fitted to the 17-segment model and displayed as a polar plot, as described in Section 2.6. EDWT and ESWT were recorded for each segment.

13.2.3 Cardiovascular Magnetic Resonance Imaging

CMR images were acquired on a 1.5T Siemens Sonata CMR system (Siemens Medical Systems, Erlangen, Germany) as described in Section 2.5. Images were reconstructed and analysed as described in Section 2.6.3.

13.2.4 Statistics

Mean segmental wall thicknesses are presented as mean±standard deviation. CCT and CMR values were compared using the paired t-test and Bland-Altman analysis. Values across CMR late gadolinium enhancement (LGE) categories were analysed using one-way analysis of variance, with pair-wise t-testing as appropriate. Threshold mean segmental wall thicknesses for discriminating normal segments and those with ≥50% LGE were calculated using ROC analysis.

13.3 RESULTS

13.3.1 Cardiovascular Magnetic Resonance Imaging

11/16 (69%) patients showed evidence of previous myocardial infarction, of which 9/16 (56%) had at least one segment of transmural myocardial scarring. Median LGE score was 57.5 (43.5–68). Mean EDWT was 6.6±2.11mm. Of 272 segments, 210 (74%), 20 (7%) and 42 (19%) segments showed 0%, 1-49% or ≥50% transmural LGE respectively, which in turn had mean thicknesses of 6.6±2.08mm, 8.1±1.61mm and 6.0±2.14mm respectively.

13.3.2 Cardiac Computed Tomography

Mean EDWT was 7.3±1.59mm. Of 272 segments, 206 (76%), 31 (11%) and 42 (19%) segments showed 0%, 1-49% or ≥50% transmural delayed enhancement on dCCT respectively, which in turn had mean EDWT of 7.5±1.53mm, 7.1±1.40mm and 6.0±1.48mm respectively. EDWT was a poor discriminator of normal myocardium from non-transmural MI ($p=0.10$), but segments with transmural MI were thinner than other segments ($p=0.02$ vs. non-transmural MI; $p<0.0001$ vs. normal).

Mean ESWT was 11.7±3.66mm. Segments with 0%, 1-49% or ≥50% transmural delayed enhancement on dCCT had mean ESWT of 12.7±3.25mm, 9.91±3.16mm and 7.4±2.35mm respectively. ESWT was a good discriminator of normal myocardium, non-transmural and transmural MI ($p<0.001$).

13.3.3 Comparison of CCT and CMR end-diastolic wall thickness

Results are summarised in Table 13.1 and Figure 13.1. CCT overestimated EDWT ($p<0.0001$), with a mean difference of -0.71±1.95mm. Cumulative sum linearity testing showed that the relationship between CCT and CMR values deviated significantly from linearity ($p<0.01$).

	CCT	CMR	Mean Difference	95% LOA	p-value
EDWT/mm	7.3±1.59	6.6±2.11	-0.7±1.95	-4.5, 3.1	<0.0001

Table 13.1 *Comparison of end-diastolic wall thickness (EDWT) on cardiac CT (CCT) and cardiovascular magnetic resonance imaging (CMR). 95% LOA: 95% confidence interval limits of agreement.*

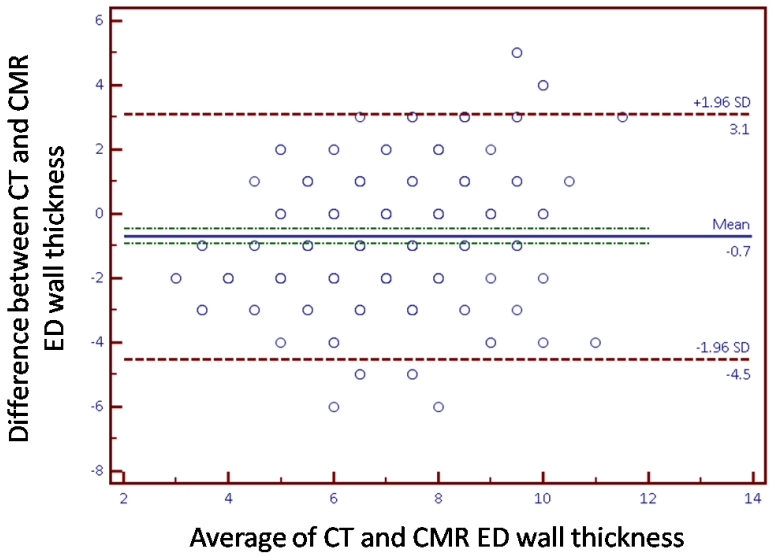


Figure 13.1 *Bland-Altman plot of CCT and CMR end-diastolic wall thickness.*

13.3.4 CCT wall thickness and transmurality of late gadolinium enhancement on CMR

Results are summarised in Table 13.2. There was no difference in EDWT between segments with 0% and 1-49% LGE on CMR (p=1.0) but segments with ≥50% LGE were significantly thinner (p<0.05). Differences in ESWT were observed across all CMR LGE categories (p<0.001).

	ESWT	EDWT
Normal	12.7±3.28†	7.5±1.54
1-49% LGE	11.1±3.27†	7.5±1.28
≥50% LGE	8.11±2.79†	6.4±1.60†
p-value	<0.001	<0.001

Table 13.2 *End-systolic and end-diastolic wall thickness (ESWT/EDWT) according to transmurality of late-gadolinium enhancement (LGE) on CMR (mean±SD). †p<0.05 versus other categories*

13.3.5 Discrimination of normal from abnormal myocardial segments

Results are summarised in Table 13.3. Using a threshold of 9mm, ESWT had sensitivity, specificity, PPV and NPV of 65%, 82%, 56% and 87% respectively for the discrimination of normal segments from those with LGE on CMR. Using a threshold of 6mm, values for EDWT were poorer (46%, 74%, 39% and 79% respectively. ROC analysis showed good accuracy of ESWT (AUC 0.80), whilst accuracy was poor for EDWT (AUC 0.63). Comparison of ROC curves showed a highly significant difference in favour of ESWT (p<0.0001, Figure 13.2).

13.3.6 Detection of ≥50% segmental late gadolinium enhancement on CMR

Results are summarised in Table 13.4. Using a threshold of 9mm, ESWT had sensitivity, specificity, PPV and NPV of 71%, 79%, 44% and 92% respectively for the discrimination of segments with <50% and ≥50% transmural LGE on CMR. Using a threshold of 6mm, values for EDWT were again poorer (54%, 74%, 33% and 87% respectively). ROC analysis showed good accuracy of ESWT (AUC 0.84), whilst accuracy was poor for EDWT (AUC 0.68). Comparison of ROC curves again showed a highly significant difference in favour of ESWT ($p<0.0001$, Figure 13.3).

	End-systole	End-diastole
Threshold	9mm	6mm
Sensitivity	65 (53 – 76)	46 (34 – 58)
Specificity	82 (75 – 87)	74 (67 – 80)
PPV	56 (45 – 67)	39 (28 – 50)
NPV	87 (81 – 91)	79 (73 – 85)
AUC	0.80 (0.74 – 0.84)	0.63 (0.57 – 0.69)
Comparison	p<0.0001	

Table 13.3 *Accuracy of end-systolic and end-diastolic segmental wall thickness for the detection of any late gadolinium enhancement on CMR (prevalence 27%).*

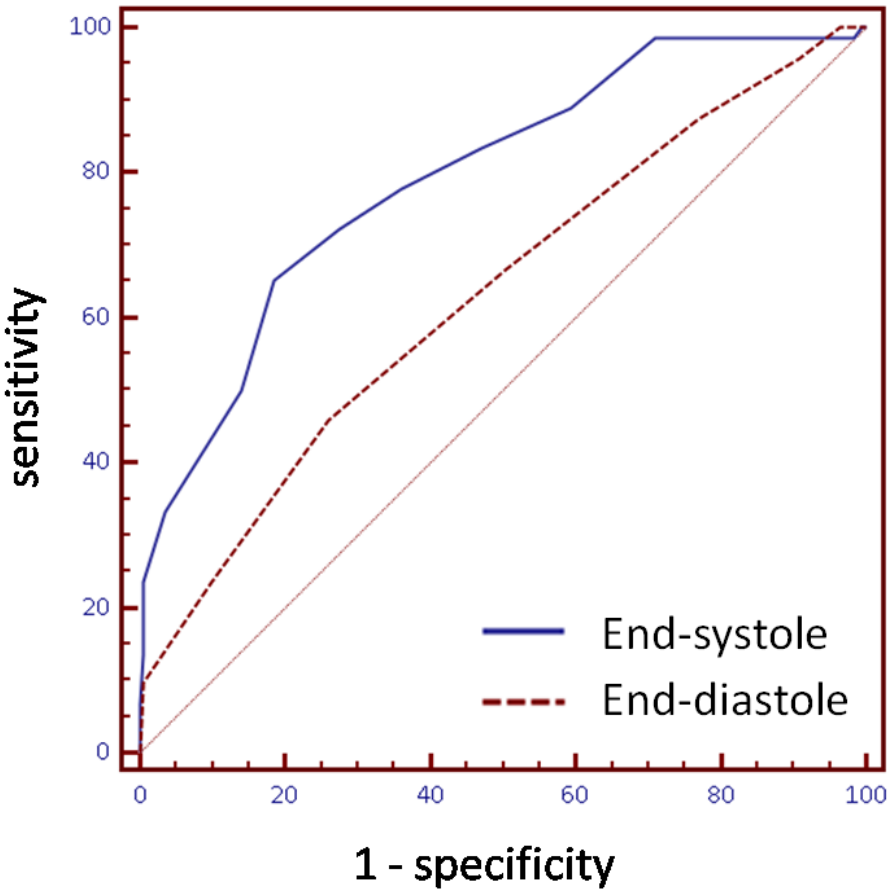


Figure 13.2 *ROC curves showing accuracy of end-systolic and end-diastolic segmental wall thickness for the detection of any late gadolinium enhancement on CMR.*

	End-systole	End-diastole
Threshold	9mm	6mm
Sensitivity	71 (57 – 83)	54 (40 – 68)
Specificity	79 (73 – 84)	74 (68 – 80)
PPV	44 (33 – 55)	33 (23 – 44)
NPV	92 (87 – 96)	87 (82 – 92)
AUC	0.84 (0.79 – 0.88)	0.68 (0.62 – 0.74)
Comparison	p<0.0001	

Table 13.4 *Accuracy of end-systolic and end-diastolic segmental wall thickness for the detection of ≥50% late gadolinium enhancement on CMR (prevalence 19%).*

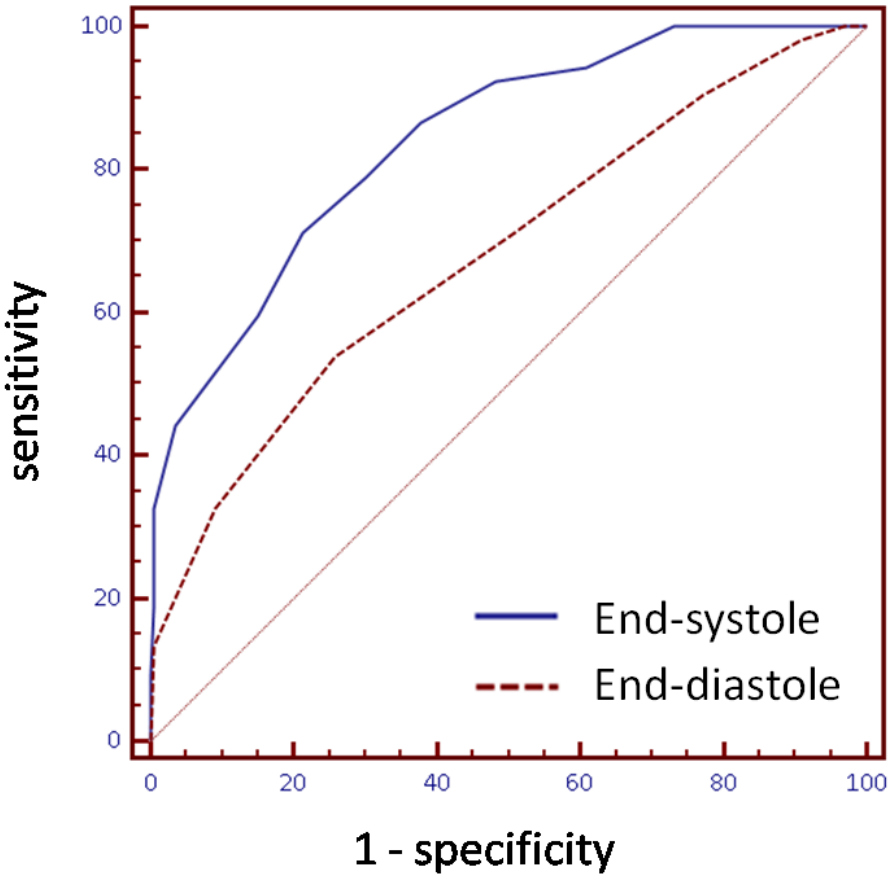


Figure 13.3 *ROC curves showing accuracy of end-systolic and end-diastolic segmental wall thickness for the detection of ≥50% late gadolinium enhancement on CMR.*

13.4 DISCUSSION

These results demonstrate that end-systolic wall thickness (ESWT) on CCT is superior to end-diastolic wall thickness (EDWT) as a discriminator of segmental late gadolinium enhancement (LGE) categories on CMR. This is in line with findings in Chapter 10 when segmental wall thickness was compared with viability on SPECT MPS. Performance of ESWT at discriminating segments with and without myocardial scarring on CMR is similar to that seen when compared with MPS – namely relatively poor sensitivity (65-66%) and PPV (56-63%) but reasonable specificity, NPV and accuracy (80-87%). ESWT>9mm carries 92% NPV for transmural LGE, which is similar to the NPV for predicting >50% reduction in resting tracer uptake on MPS (95%). CMR and SPECT MPS assess different aspects of the same pathology. LGE on CMR is a direct marker of scarring, with unenhanced myocardium therefore presumed viable. Radiotracer uptake on MPS is a direct marker of viability, with reduction in uptake presumed to indicate scarring. It is reassuring, therefore, that wall thickness on CCT performs identically when compared to both CMR and MPS. Unfortunately, this means that the same weaknesses of the technique apply. ESWT is regardless a poor predictor of scarring; the defined threshold values are useful only for excluding segmental MI. As expected, NPV is highest for the exclusion of transmural segmental LGE (92%). Transmural (>50%) LGE is an imperfect predictor of segmental recovery after revascularisation when considered in akinetic segments. Absence of LGE predicts functional recovery in only 78%; for >75% segmental LGE the value is below 2%[59]. Predictive value in between is much poorer. In this cohort, only 17% of segments with ≤75% LGE had ESWT <9mm, whilst this was true in 69% of segments with >75% LGE. Clearly the most important parameter to predict from

measurements of wall thickness is the likelihood of recovery after revascularisation. Formal evaluation of CCT in this domain has not been performed, probably because the technique is currently used mainly in patients at low to intermediate likelihood of significant coronary artery disease rather than in those under consideration for revascularisation after invasive coronary angiography. Given that severe hypo-/akinesis is a pre-requisite for segmental myocardial hibernation, it is interesting to note that, in segments with these wall motion abnormalities on CCT (as assessed in Chapter 14), EDWT≤7mm carried sensitivity, specificity, PPV and NP of 90%, 50%, 90% and 50% respectively for transmural LGE on CMR. This data is much more in keeping with published comparisons of CMR EDWT with SPECT[141] for prediction of functional recovery after revascularisation, where only segments with severe wall motion abnormalities are considered for analysis.

A disappointing result in this study was the lack of linear relationship between CMR and CCT measurements of EDWT. This result is unexpected, and presumably relates to the small sample size. Mean difference between segmental values is less than 1mm but limits of agreement are wide (~±4mm), suggesting analysis of a larger sample is necessary before conclusions can be drawn. The lack of linear relationship precluded estimation of systematic and proportional differences between the techniques.

13.5 LIMITATIONS

This is a single centre study with small recruitment numbers and so results should be seen as hypothesis-generating rather than proof of utility. Only 8/16 patients had

stress CMR and therefore relationship of wall thickness to segmental hibernation (viable but ischaemic and dysfunctional myocardium) was not assessed. The majority of comparative data for wall thickness have come from evaluation of dysfunctional segments for irreversible scarring but validation of EDWT for predicting lack of hibernation requires demonstration of ischaemia.

13.6 SUMMARY FINDINGS

1. EDWT on CCT differed from CMR values by less than 1mm on average. However, limits of agreement were wide and EDWT on CCT and CMR were non-linearly related, possibly as a result of small sample size.
2. ESWT is superior to EDWT at discriminating normal myocardium, non-transmural and transmural MI on both dCCT and CMR.
3. Although ESWT shows good accuracy, it suffers from poor sensitivity and PPV, rendering it more useful for ruling out MI.
4. ESWT >9mm excludes ≥50% segmental LGE on CMR in 92% of cases.

CHAPTER 14 ASSESSMENT OF LEFT VENTRICULAR FUNCTION BY DUAL SOURCE CARDIAC CT IN PATIENTS WITH PREVIOUS MYOCARDIAL INFARCTION: COMPARISON WITH CARDIOVASCULAR MAGNETIC RESONANCE IMAGING

14.1 INTRODUCTION

Single-source multislice cardiac CT (CCT) has been validated as a tool for assessment of global and regional left ventricular (LV) function against a variety of techniques, including SPECT myocardial perfusion scintigraphy (MPS)[112, 157, 169], echocardiography[149, 169-172], cardiovascular magnetic resonance imaging (CMR)[149, 154, 159, 169, 172] and invasive left ventriculography[149]. Higher-specification CT scanners are now commonplace, with competition in the market between dual-source CT (DSCT) and 256-slice+ CCT. As only a quarter-rotation of the gantry is required to acquire a single axial image, DSCT offers superior temporal resolution and potentially more accurate assessment of global and regional LV function. DSCT has been mainly validated in animals[173], normal patients[165], patients with suspected or known coronary artery disease[150, 152, 162, 163, 174, 175] and patients with valvular heart disease[151] but to a lesser extent in chronic myocardial infarction (MI) and ischaemic LV dysfunction. The aim of the present study was to quantify LV volumes and ejection fraction, score qualitative measures of regional LV function and calculate segmental ejection fraction (EF) and percentage thickening on CCT and compare them with LV functional parameters measured by CMR in patients with previous MI.

14.2 METHODS

16 patients (12 male, mean age 66±8.7 years) referred for clinical CMR were recruited. Median time since MI was 1.25 years (IQR: 0.75 – 11 years, min 57 days, max 21 years). Exclusion criteria ar elisted in Section 12.2. All patients were on oral beta-blockade. The study was approved by the local research ethics committee and all patients gave written informed consent.

14.2.1 Cardiovascular magnetic resonance imaging

CMR images were acquired on a 1.5T Siemens Sonata CMR system (Siemens Medical Systems, Erlangen, Germany) as described in Section 2.5. Images were reconstructed and analysed as described in Section 2.6.3.

14.2.2 Cardiac computed tomography

Scans were acquired using a dual source 128-slice CT scanner with oscillating z-axis focal spot (Somatom Definition Flash, Siemens Medical Systems). A test bolus technique was used to time scan delay, as described in Section 2.4.4. Intravenous iodinated contrast (Ultravist 370, Bayer Healthcare Pharmaceuticals Inc) was administered using the triphasic protocol described in Chapter 5.2.2. CCT data were acquired using parameters as follows: retrospective ECG gating, tube voltage 100kVp, tube current 120 quality reference mAs/rot, 128x0.6 mm collimation, 0.28s rotation time, pitch 0.23 for 60 bpm, and CareDose 4D on. Patient heart rates were as described in Section 12.2.2.

14.2.3 Cardiac CT image analysis

Images were reconstructed using a medium-smooth kernel at 10% increments from 25-95% of the R-R interval. All phases of the cardiac cycle were analysed. Images were loaded into a density threshold program (Time Volume Analysis) and the LV volumes for each phase calculated in semi-automated fashion, as described in Sections 2.5 and 2.6. Segmental wall motion and thickening were analysed qualitatively according to the 17-segment model, as being normal; mildly, moderately or severely reduced; or absent. A further category of wall motion – dyskinesis – was also scored.

14.2.4 Statistics

Left ventricular end-diastolic volume (EDV), end-systolic volume (ESV) and ejection fraction (EF) were compared using Bland Altman analysis. Values were distributed non-parametrically, rendering linear regression unsuitable. Passing and Bablok regression was therefore used to compare values for systematic and proportional differences. Sensitivity, specificity, positive and negative predictive values (PPV/NPV) and accuracy of regional LV function parameters for discriminating either normal from abnormal myocardial segments or non-transmural from transmural myocardial scarring on MPS were assessed using ROC analysis. Inter- and intraobserver variability was calculated using Cohen's kappa.

14.3 RESULTS

14.3.1 Cardiovascular magnetic resonance imaging

As shown in Section 12.3.1, 11/16 (69%) patients demonstrated evidence of previous MI on CMR. Global LV functional parameters are given in Table 14.2. 6/16 (38%) patients had LVEF <50%; 1/16 (6%) had LVEF <35%. 10/16 (63%) patients had LV dilatation according to BSA-indexed, gender-specific values. Regional wall motion and thickening abnormalities were present in 68/272 (25%) and 68/272 (25%) segments respectively. Breakdown of regional abnormalities is shown in Table 14.1.

		Normal	Mild ↓	Mod ↓	Severe ↓	Absent	Dyskinetic
Wall Motion (%)	CMR	204 (75)	8 (3)	9 (3)	11 (4)	29 (11)	11 (4)
	CCT	204 (75)	21 (8)	12 (4)	3 (1)	30 (11)	2 (1)
Wall Thickening (%)	CMR	204 (75)	12 (4)	12 (4)	11 (4)	33 (12)	
	CCT	204 (75)	22 (8)	15 (6)	4 (2)	27 (10)	

Table 14.1 *Distribution of segmental wall motion and thickening on CMR and CCT*

14.3.2 Cardiac Computed Tomography

As shown in Section 12.3.2, 12/16 (75%) patients demonstrated evidence of previous MI on delayed CT images. Global LV functional parameters are given in Table 14.2. 8/16 (50%) patients had LVEF <50%; 4/16 (25%) had LVEF <35%. Regional wall motion and thickening abnormalities were seen in 68/272 (25%) and 68/272 (25%) segments respectively; these are summarised in Table 14.1.

14.3.3 Comparison between techniques for global LV function

Left ventricular ejection fraction

LVEF was lower on CCT than CMR (51.4±14.3 vs. 56.3±13.4, mean difference -4.9±6.1, p=0.006; Table 14.2, Figure 14.1). 95% limits of agreement (LOA) were wide (7.1, -16.8). Regression revealed no systematic (4%, 95%CI -24.9 – 5.3, Table14.3, Figure 14.2) or proportional differences or deviation from linearity (p=0.95).

Left ventricular end-diastolic volume

CCT and CMR generated similar LVEDV (184.4±70.0mL vs. 177.5±63.2mL, mean difference 6.88±23.7mL, p=0.26; Table 14.2, Figure 14.1). 95% LOA were wide (53.3mL, -39.6mL). Regression revealed no systematic (15.3mL, 95%CI -57.0 – 27.5, Table 14.3, Figure 14.3) or proportional differences or deviation from linearity (p=0.95) between techniques.

LVEDV ≥126mL (BSA-indexed value 69mL) in men predicted a dilated LV on CMR with sensitivity, specificity, PPV, NPV and accuracy of 100%, 75%, 89%, 100% and 91% (Table 14.4, Figure 14.5). Sample size was too small to estimate values for women.

Left ventricular end-systolic volume

CCT overestimated LVESV compared with CMR (95.5±56.0mL vs. 84.4±52.7mL, mean difference 11.1±14.4mL, p=0.008; Table 14.2, Figure 14.1). 95% LOA were wide (39.3mL, -17.2mL). Regression revealed no systematic (1.62mL, 95%CI -17.3 – 8.94;

Table 14.3, Figure 14.4) or proportional differences or deviation from linearity (p=0.95) between techniques.

	CCT	CMR	Mean Difference	95%CI LOA	p-value
EF	51.4±14.3	56.3±13.4	-4.9±6.09	7.1, -16.8	0.006
EDV	184.4±70.0	177.5±63.2	6.9±23.7	53.3, -39.6	0.26
ESV	95.5±56.0	84.4±52.7	11.1±14.4	39.3, -17.2	0.008

Table 14.2 *Indices of global LV function for CMR and CCT. EF, EDV and ESV: LV ejection fraction, end-diastolic and end-systolic volumes respectively; 95%CI LOA: 95% confidence interval limits of agreement.*

	Systematic differences	Proportional differences	Random differences	Linear model validity (p-value)
EF	-4.0 (-24.9 – 5.25)	1.03 (0.88 – 1.36)	4.8 (±9.41)	0.95
EDV	15.3 (-57.0 – 27.5)	1.10 (0.86 – 1.35)	17.2 (±33.7)	0.95
ESV	1.6 (-17.3 – 8.94)	1.05 (0.96 – 1.34)	10.9 (±21.5)	0.95

Table 14.3 *Comparison of CT and CMR using Passing and Bablok regression. EF, EDV and ESV: LV ejection fraction, end-diastolic and end-systolic volumes respectively.*

Threshold	Sensitivity	Specificity	PPV	NPV
126mL	100 (63 – 100)	75 (19 – 99)	89 (52 – 100)	100 (29– 100)

Accuracy	91 (60 – 100)

Table 14.4 *Male threshold values for end-diastolic volume on CCT to predict a dilated ventricle on CMR (BSA indexed EDV of 80mL).*

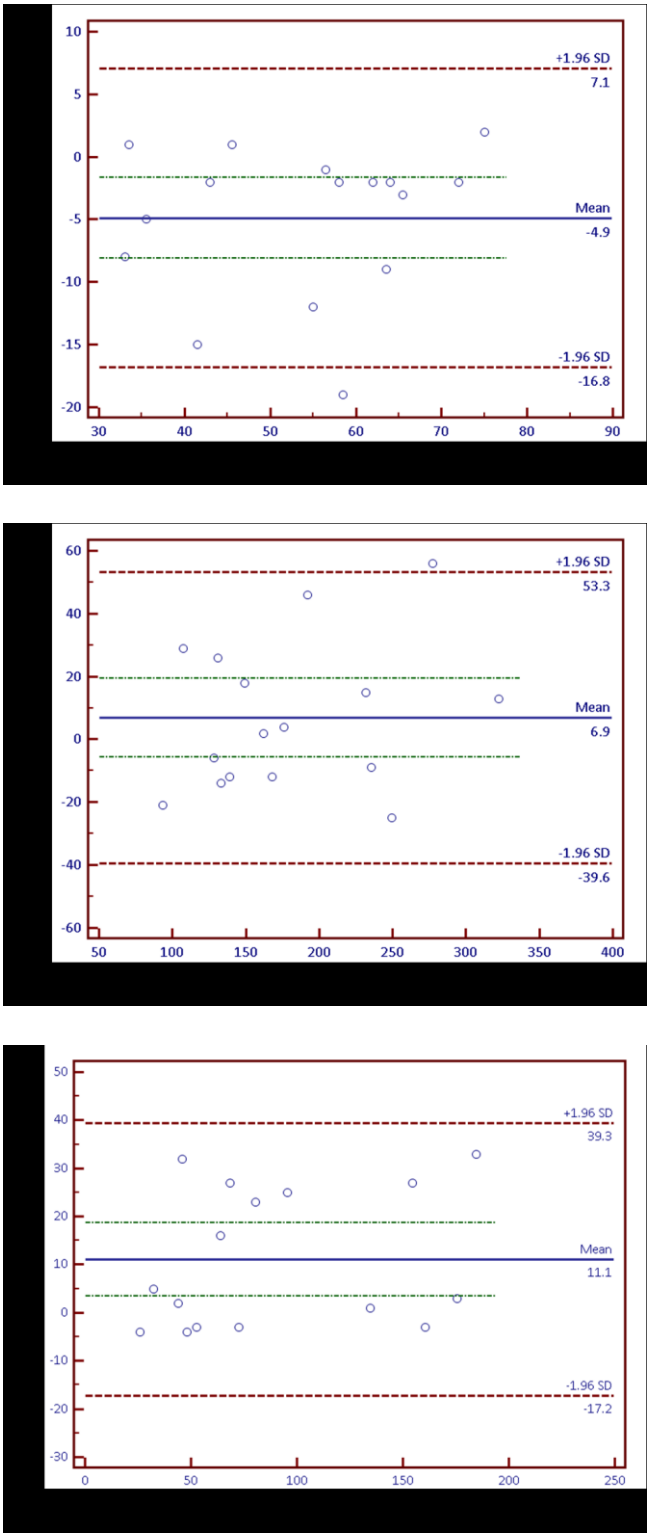


Figure 14.1 *Bland-Altman plots showing the relationship between CCT and CMR for measures of LV ejection fraction (LVEF, top), end-diastolic volume (LVEDV, middle) and end-systolic volume (LVESV, bottom).*

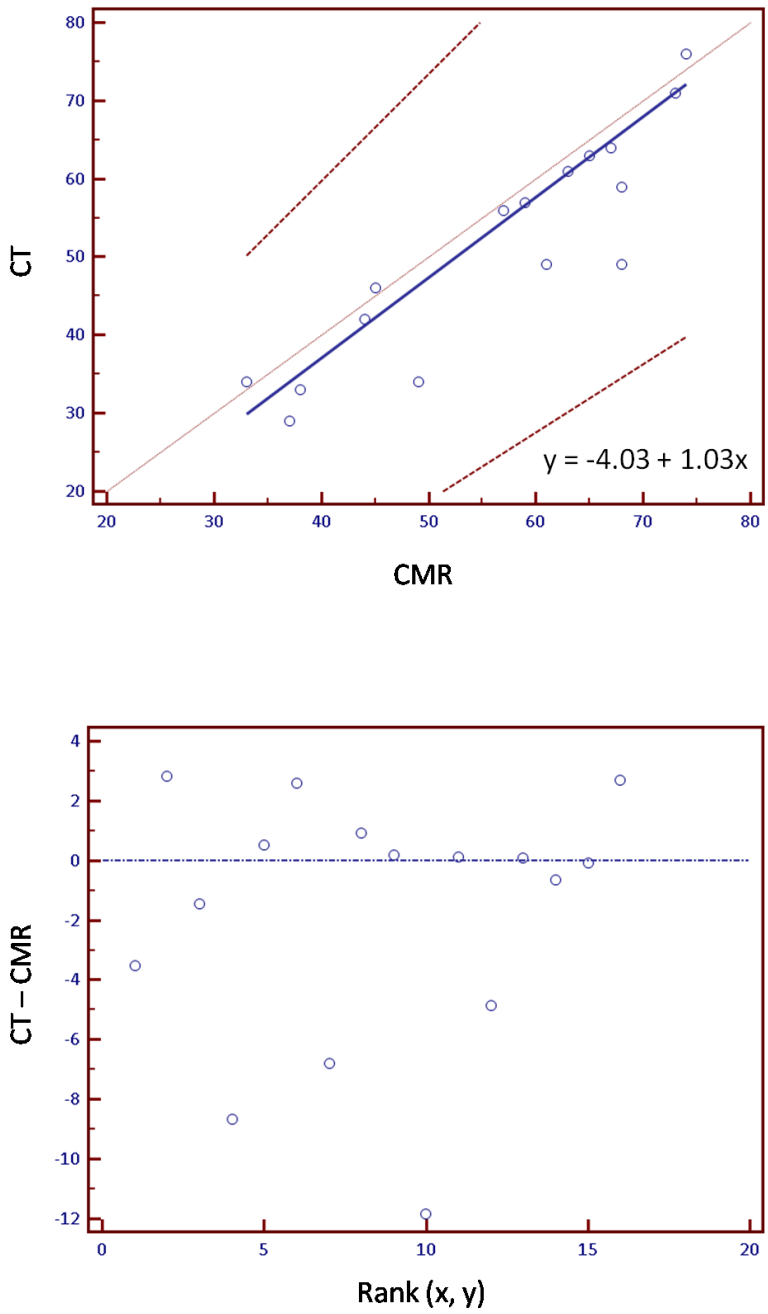


Figure 14.2 *Comparison of CCT and CMR LV ejection fraction measurements, with regression line (top) and residual plot (bottom).*

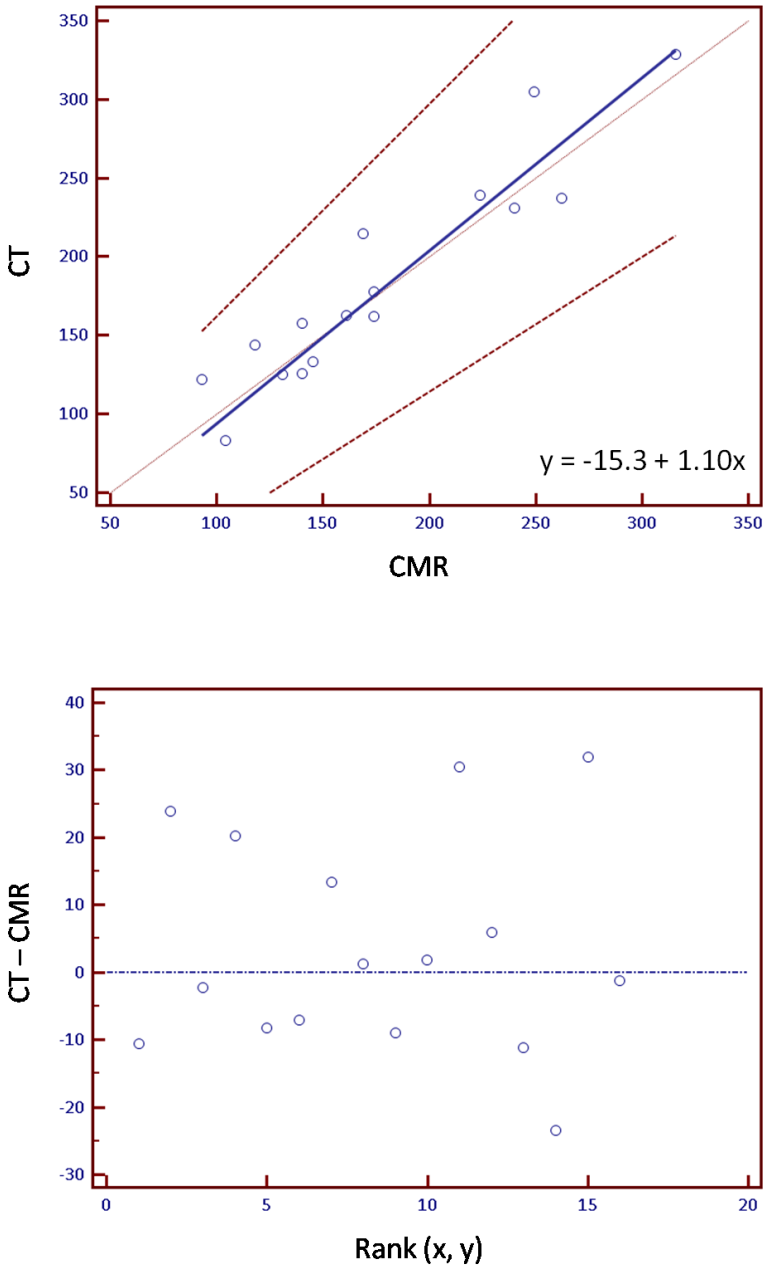


Figure 14.3 *Comparison of CCT and CMR LV end-diastolic volume measurements, with regression line (top) and residual plot (bottom).*

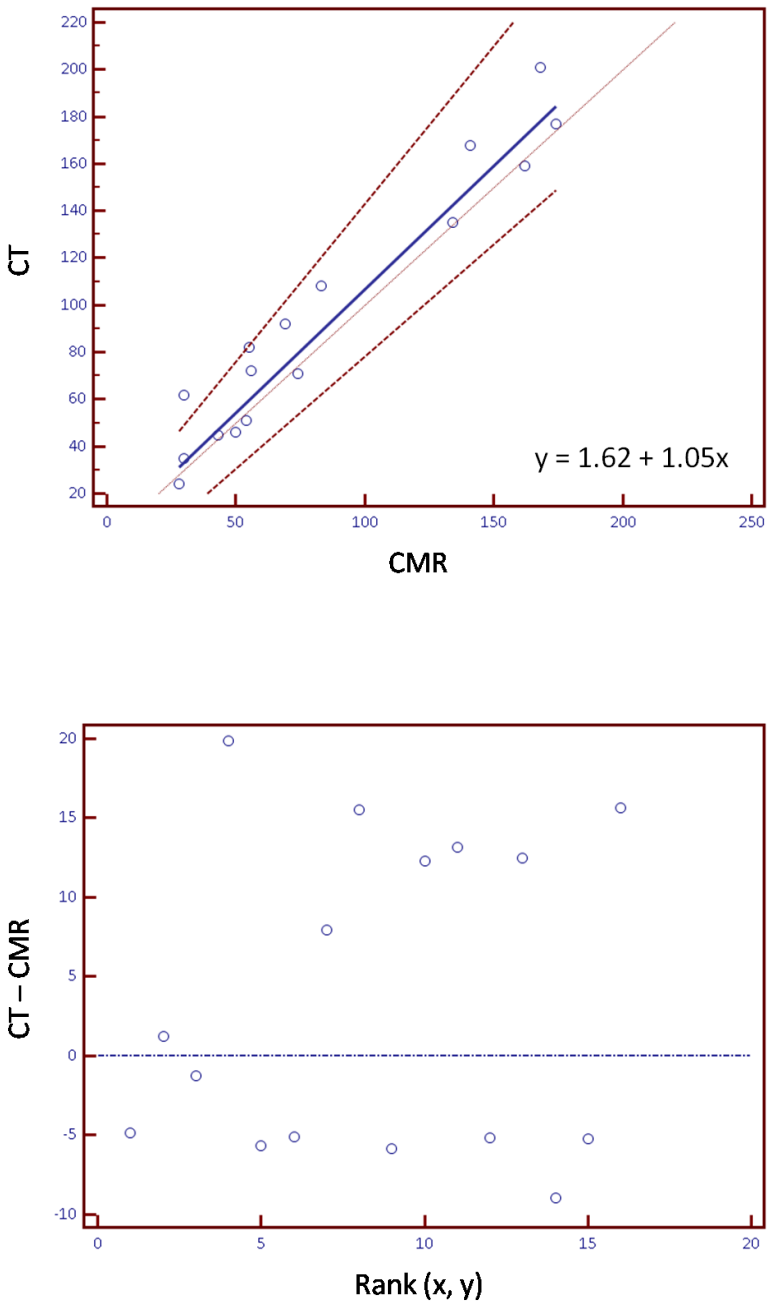


Figure 14.4 *Comparison of CCT and CMR LV end-systolic volume measurements, with regression line (top) and residual plot (bottom).*

14.3.4 Regional LV function

Results are summarised in Tables 14.5-7. There was good agreement between CCT and CMR for regional wall motion (78%, κ=0.80) and thickening (76%, κ=0.76).

Any degree of regional wall motion abnormality on CCT (i.e. mild reduction in wall motion or worse) predicted MI on CMR with sensitivity, specificity, PPV, NPV and accuracy of 72%, 92%, 77%, 90% and 83% respectively. Values for any abnormality in wall thickening were 71%, 92%, 75%, 90% and 83% respectively. Wall motion and thickening were equally accurate at predicting MI on CMR (p=0.64).

Segments that were moderately impaired or worse on CCT had sensitivity, specificity, PPV, NPV and accuracy of 63%, 94%, 70%, 92% and 82% respectively for identification of transmural MI. Values for similarly abnormal wall thickening were 65%, 95%, 74%, 92% and 82% respectively. CCT wall motion and thickening were equally accurate at predicting transmural MI on CMR (p=0.44).

	Kappa	**95% Confidence Interval**
Wall Motion	0.80	0.72 – 0.88
Wall Thickening	0.76	0.67 – 0.85

Table 14.5 *Agreement between CCT and CMR for regional wall motion and thickening.*

	Threshold	Sensitivity	Specificity	PPV	NPV	Accuracy	p-value
Wall Motion	≥ Mild ↓	72 (60 – 82)	92 (87 – 95)	77 (65 – 86)	90 (85 – 94)	83 (78 – 87)	0.64
Wall Thickening		71 (59 – 81)	92 (87 – 95)	75 (63 – 85)	90 (85 – 94)	83 (78 – 88)	

Table 14.6 *Analysis of CCT segmental wall motion and thickening for sensitivity, specificity, positive predictive value (PPV), negative predictive value (NPV) and accuracy for the detection of any myocardial infarction on CMR.*

	Threshold	Sensitivity	Specificity	PPV	NPV	Accuracy	p-value
Wall Motion	≥ Mod ↓	63 (49 – 76)	94 (90 – 97)	70 (55 – 83)	92 (87 – 95)	82 (76 – 86)	0.44
Wall Thickening		65 (51 – 78)	95 (91 – 97)	74 (59 – 86)	92 (88 – 95)	82 (77 – 87)	

Table 14.7 *Analysis of CCT segmental wall motion and thickening for sensitivity, specificity, positive predictive value (PPV), negative predictive value (NPV) and accuracy for the discrimination of transmural and non-transmural myocardial infarction on CMR.*

14.3.4 Interobserver and intraobserver agreement for regional LV function

Results are summarised in Tables 14.8 – 9. Interobserver agreement for regional wall motion and thickening was excellent (κ=0.85 and 0.82 respectively); intraobserver agreement was much higher (κ=0.96 and 0.97 respectively).

		Observer 1					
		Dyskinesia	**Absent**	**Severely reduced**	**Moderately reduced**	**Mildly reduced**	**Normal**
Observer 2	**Dyskinesia**	2	0	0	0	0	0
	Absent	0	2	0	0	0	0
	Severely reduced	0	23	2	4	1	1
	Moderately reduced	0	3	0	4	3	3
	Mildly reduced	0	0	1	0	6	2
	Normal	0	2	0	4	11	198
		Observed agreement 79% Kappa=0.85 [0.78 – 0.91]					

		Observer 1				
		Absent	**Severely reduced**	**Moderately reduced**	**Mildly reduced**	**Normal**
Observer 2	**Absent**	2	0	0	0	0
	Severely reduced	22	3	4	1	1
	Moderately reduced	1	0	4	5	3
	Mildly reduced	0	1	2	4	2
	Normal	2	0	5	12	198
		Observed agreement 78% Kappa=0.82 [0.75 – 0.90]				

Table 14.8 *Interobserver agreement for CCT regional wall motion (top) and thickening (bottom).*

		Observation 1					
		Dyskinesia	Absent	Severely reduced	Moderately reduced	Mildly reduced	Normal
Observation 2	Dyskinesia	2	2	0	0	0	0
	Absent	0	24	2	0	0	0
	Severely reduced	0	3	1	1	0	0
	Moderately reduced	0	0	0	10	5	0
	Mildly reduced	0	0	0	1	12	1
	Normal	0	1	0	0	4	203
		Observed agreement 93% Kappa=0.97 [0.93 – 0.99]					

		Observation 1				
		Absent	Severely reduced	Moderately reduced	Mildly reduced	Normal
Observation 2	Absent	25	2	1	0	0
	Severely reduced	1	2	0	0	0
	Moderately reduced	0	0	13	5	0
	Mildly reduced	0	0	1	13	1
	Normal	1	0	0	4	203
		Observed agreement 94% Kappa=0.96 [0.93 – 0.99]				

Table 14.9 *Intraobserver agreement for CCT regional wall motion (top) and thickening (bottom).*

14.4 DISCUSSION

These results demonstrate good agreement between DSCT and CMR for measures of global and regional LV function. Bland-Altman analysis shows that CCT underestimates LVEF (mean difference -4.9±6.1%, p=0.0006), although regression suggests no systematic difference as the 95% confidence interval for LVEF includes zero difference. Wide limits of agreement imply that small sample size may have an effect here. For reference, LVEF reproducibility by CMR in normal subjects is 0.5-1%[176]; 64-slice CCT values are similar[177]. Wider variability is expected in the present patient cohort, given the high prevalence of previous MI and abnormal LV volumes. A reassuring result is that LV volumes are similar between DSCT and CMR, with no significant difference in EDV and a 10mL difference in ESV (p=0.008), with the latter explaining the underestimation of LVEF by DSCT. No systematic or proportional differences are identified on regression, in contrast to comparisons of CCT and SPECT MPS (Chapter 11). Again, this is to be expected as the spatial and temporal resolutions of CCT are, in contrast to MPS, similar to CMR, which itself overestimates LV volumes on MPS by as much as 20-30%[178]. Systematic errors compared to MPS are therefore likely to be fundamentally issues of resolution. The absence of proportional differences in LVEF on DSCT and CMR indicate that DSCT values are valid provided systematic differences are accounted for by CCT-specific normal reference ranges.

Agreement for regional function is good, suggesting that DSCT is also a valid method of assessing segmental wall motion and thickening in patients with previous MI. Agreement with CMR was slightly poorer than has been described previously for 64-

slice CCT (κ=0.80 vs. 0.91 [Wu et al.[169]]), although the prevalence of wall motion and thickening abnormalities on CMR in this cohort was lower (25% vs. 52%). The main sources of disagreement were in the categorisation of hypokinetic segments, with absolute agreement with CMR poorer compared with akinetic and normal segments (39% vs. 70% and 92% respectively). This result has been demonstrated previously in patients with reperfused acute myocardial infarction[154]. Segmental wall motion and thickening show good accuracy and excellent specificity and NPV for discriminating normal segments and those with transmural LGE on CMR, although sensitivity and PPV are relatively poor. These findings are almost identical to those demonstrated in Chapter 11 for comparisons with MPS, suggesting that normal wall motion and thickening on CCT reliably excludes myocardial infarction on both SPECT MPS and CMR but that abnormal regional function is less reliable. Pathology unrelated to myocardial scarring may lead to abnormalities of regional function – left bundle branch block, for example – and so perfect accuracy at predicting LGE on CMR is neither expected nor required. Inter- and intraobserver agreement for regional abnormalities is excellent and similar to published values in patients with low prevalence of regional abnormalities[177], confirming the reproducibility of the technique in patients with chronic MI. Again, main sources of disagreement were in the classification of hypokinesis, particularly of mild and moderate severity. 11/17 and 12/16 mild reductions respectively in segmental wall motion and thickening, as classified by Observer 1, were judged normal by Observer 2. These segments alone accounted for ~20% of disagreements, findings similar to other published interobserver comparisons for CCT regional function[177]. Visual estimation of regional abnormalities of myocardial function is subject to significant variability, regardless of

imaging modality[179] and it is for this reason that quantitative methods are sought. As demonstrated in Chapter 11, potential parameters on CCT are not yet better than expert visual scoring but improvements in software may change this.

Despite the relatively small sample size, findings in this study are supportive of DSCT as an accurate and reproducible method for quantifying global and regional left ventricular function in patients with previous myocardial infarction.

14.5 LIMITATIONS

The sample size is small, with wide confidence intervals and limits of agreement, particularly for patient-level measurements of global LV function. This may impact on the validity of these initial findings for DSCT in patients with previous MI. For example, Bland-Altman analysis suggests a ~5% underestimation of LVEF by CCT but Passing and Bablok regression demonstrates that this systematic difference is statistically insignificant. Larger samples are required for further validation.

14.6 SUMMARY FINDINGS

1. On Bland-Altman analysis, CCT shows ~5% underestimation of LVEF compared to CMR; this is mediated by ~10mL overestimation of LVESV. EDV is not significantly different between the techniques.
2. Passing and Bablok regression yields no systematic or proportional differences between techniques for any measure of global LV function.
3. Although sample size was too small to allow estimation for women, no man with LVEDV <126mL (BSA-indexed 69mL) had LV dilatation on CMR.

4. Agreement between CCT and CMR for measures of regional LV function is good.
5. CCT segmental wall motion and thickening shows good accuracy for detection of segments with absent or ≥50% LGE on CMR.
6. Inter- and intraobserver agreement for CCT segmental wall motion and thickening are excellent.

CHAPTER 15 FINAL CONCLUSIONS

15.1 GENERAL COMMENTS

X-ray computed tomography (CT) scanners have revolutionised medical practice – there is no NHS Acute Trust in the UK without one. The National Audit Office estimates that, as of March 2011, 426 CT scanners were installed in NHS Trusts, of which 376 were installed within the last 11 years. Many of these are 64-slice+ scanners and are at least cardiac-capable (if not cardiac-enabled), particularly if recently procured. All Acute Trusts with a cardiology service require access to cardiac CT (CCT) given recent recommendations by NICE for the investigation of stable chest pain[109]. As Trusts look to tighten budgets, it is increasingly likely that business cases for replacement CT scanners will incorporate the need to fulfil a cardiac CT service, rather than require patients to be referred to potentially more expensive external providers. With this in mind, it is sensible to explore how far CCT capabilities extend. This is not limited to stand-alone high-end CCT. Many nuclear medicine departments have gamma cameras with some form of CT – even if single-slice – as it allows anatomical localisation of abnormalities detected at scintigraphy. It is thus pertinent to ask whether this technology ought to be used in MPS for attenuation correction.

15.2 REVIEW OF FINDINGS

15.2.1 Single-slice CT

Presented results suggest that AC has undeniable technical effects on MPS images, namely increasing apparent tracer uptake inferiorly and variably affecting apparent tracer uptake anteroapically (Chapter 3). Whilst this improves reporter confidence (although does not change the report itself) prior to knowledge of clinical details – as demonstrated in several prior trials[29, 87, 89] – this benefit is lost as soon as clinical information is known (Chapter 4). As discussed, reporting images blind necessarily disadvantages non-corrected strategies as clinical information provides an estimation of disease prevalence. Test results allow estimation of posterior probability of disease (relative likelihood of true versus false positives, for instance) but only if prior probability (prevalence) is known. AC images provide insight into prior probability but their value is trumped by clinical information, as has been demonstrated. Report and reporter confidence are therefore similar whether or not AC is used provided clinical information is known – as is the case for any MPS study reported in clinical practice (rather than for research purposes).

15.2.2 Multi-slice CT

Several important results have been demonstrated in this thesis: end-diastolic delayed CCT (dCCT) best identifies segmental myocardial infarction (MI), showing good agreement and high specificity, negative predictive value and accuracy compared with SPECT MPS (Chapters 6-8) and CMR (Chapter 12); choice of smooth or medium-smooth reconstruction kernel appears relatively unimportant (Chapter

9); dual-energy dCCT (DE-dCCT) may be more sensitive for segmental MI on CMR (Chapter 12); CCT end-systolic wall thickness is a better predictor of myocardial scarring on MPS and CMR than end-diastolic wall thickness (Chapters 10 and 13); CCT overestimates end-systolic and end-diastolic volumes on MPS but LV ejection fraction is equivalent (Chapter 11); CCT shows no systematic differences in measures of global LV function when compared to CMR (Chapter 14); measures of regional ventricular function on CCT show excellent and good agreement with MPS and CMR respectively (Chapters 11 and 14); inter- and intraobserver agreement for dCCT myocardial enhancement patterns and regional LV function is excellent (Chapters 12 and 14). Ultimately, findings support the use of CCT to detect chronic MI and assess global and regional LV function reliably and reproducibly. DE-dCCT seems to be more sensitive and probably represents the future of myocardial assessment by CCT. The major weakness of CCT compared to CMR – the gold standard method for evaluating myocardial scarring – is radiation exposure. CCT radiation exposures used in this thesis were relatively high as all scans were retrospectively ECG-gated; tube current was therefore applied throughout the cardiac cycle. Although only end-diastolic images were analysed for the main comparisons of dCCT and SPECT MPS/CMR, analysis of myocardial enhancement patterns in end-systole and end-diastole (Chapter 8) and predictive power of end-systolic and end-diastolic wall thickness for MI (Chapters 10 and 13) required retrospective gating. Clinical dCCT should be performed using prospective gating in end-diastole to minimise radiation dose.

15.3 AREAS FOR FURTHER STUDY

15.3.1 Attenuation correction

As discussed in Chapter 4, the purpose of this thesis is not to suggest that attenuation correction (AC) has no value, only that its role in improving recognition of attenuation artefacts in stress/rest MPS is limited for experienced observers. This thesis does not examine the role of attenuation correction in enabling stress-only MPS imaging in order to reduce radiation exposure and it is in this domain, and in absolute quantification of MPS tracer uptake, that AC is likely to add value.

15.3.2 Myocardial scarring on CCT

The major difficulties in identifying delayed myocardial hyperenhancement on CCT are distinguishing scarred myocardium from LV blood pool and detecting relatively subtle differences in enhancement visually. The major strength of CMR, other than being radiation-free, is the ability to set inversion times to null signal from normal myocardium. Preferential accumulation of gadolinium contrast in scarred myocardial segments results in faster T1 relaxation on CMR and thus brighter signal. Thus normal myocardium looks black whilst scarred myocardium appears bright. CCT currently has nothing that can match this phenomenon, relying solely instead on differences in attenuation coefficient between normal and scarred myocardium. As shown in Chapter 7, the difference in segmental wall intensity (SWI) between normal myocardial segments and those with non-transmural scarring was only 8HU. Domains for future work are development of, first, dual-energy CT and detector element technology and, second, specific software for analysing images. DE-dCCT

allows better detection of MI as primary signals from X-ray beams of different energies are compared, allowing better distinction of enhanced and unenhanced tissues. Improved detector technology would allow better discrimination of subtle differences in the primary signals, one of which is generated by low X-ray tube voltages. Most importantly, software development should allow much of what was done manually in this thesis to be done automatically. For example, virtually all dCCT studies required manual tracing of endo- and epicardial contours as the software used was designed to evaluate contrast-enhanced left ventricles rather than the relatively unopacified LV seen on dCCT. The ability to port contours over from an early CCT dataset, with manual adjustments only if required, would substantially reduce processing time. It would also be useful to colour code the myocardium on dCCT, rather than retain greyscale values. This has been demonstrated in a porcine model to increase the conspicuity of enhancement, potentially improving accuracy[180].

15.3.3 Regional LV function on CCT

Quantitative measures of regional LV function performed poorly in this study when compared to expert visual scoring. New methods under development are likely to improve automated quantitative performance. One method, demonstrated in the porcine model against CMR, involves tracking endocardial surface trabeculations during myocardial contraction[181]. Regional values compare well with CMR and the technique is promising.

CHAPTER 16 REFERENCES

(1) Almquist H, Arheden H, Arvidsson AH, Pahlm O, Palmer J. Clinical implication of down-scatter in attenuation-corrected myocardial SPECT. *J Nucl Cardiol* 1999 July;6(4):406-11.

(2) Goetze S, Wahl RL. Prevalence of misregistration between SPECT and CT for attenuation-corrected myocardial perfusion SPECT. *J Nucl Cardiol* 2007 April;14(2):200-6.

(3) Fricke H, Fricke E, Weise R, Kammeier A, Lindner O, Burchert W. A method to remove artifacts in attenuation-corrected myocardial perfusion SPECT Introduced by misalignment between emission scan and CT-derived attenuation maps. *J Nucl Med* 2004 October;45(10):1619-25.

(4) Chouraqui P, Livschitz S, Sharir T et al. Evaluation of an attenuation correction method for thallium-201 myocardial perfusion tomographic imaging of patients with low likelihood of coronary artery disease. *J Nucl Cardiol* 1998 July;5(4):369-77.

(5) Gallowitsch HJ, Sykora J, Mikosch P et al. Attenuation-corrected thallium-201 single-photon emission tomography using a gadolinium-153 moving line source: clinical value and the impact of attenuation correction on the extent and severity of perfusion abnormalities. *Eur J Nucl Med* 1998 March;25(3):220-8.

(6) Kluge R, Sattler B, Seese A, Knapp WH. Attenuation correction by simultaneous emission-transmission myocardial single-photon emission tomography using a technetium-99m-labelled radiotracer: impact on diagnostic accuracy. *Eur J Nucl Med* 1997 September;24(9):1107-14.

(7) Prvulovich EM, Lonn AH, Bomanji JB, Jarritt PH, Ell PJ. Effect of attenuation correction on myocardial thallium-201 distribution in patients with a low likelihood of coronary artery disease. *Eur J Nucl Med* 1997 March;24(3):266-75.

(8) Gallowitsch HJ, Unterweger O, Mikosch P et al. Attenuation correction improves the detection of viable myocardium by thallium-201 cardiac tomography in patients with previous myocardial infarction and left ventricular dysfunction. *Eur J Nucl Med* 1999 May;26(5):459-66.

(9) Ficaro EP, Fessler JA, Shreve PD, Kritzman JN, Rose PA, Corbett JR. Simultaneous transmission/emission myocardial perfusion tomography. Diagnostic accuracy of attenuation-corrected 99mTc-sestamibi single-photon emission computed tomography. *Circulation* 1996 February 1;93(3):463-73.

(10) Thompson RC, Heller GV, Johnson LL et al. Value of attenuation correction on ECG-gated SPECT myocardial perfusion imaging related to body mass index. *J Nucl Cardiol* 2005 March;12(2):195-202.

(11) Fricke E, Fricke H, Weise R et al. Attenuation correction of myocardial SPECT perfusion images with low-dose CT: evaluation of the method by comparison with perfusion PET. *J Nucl Med* 2005 May;46(5):736-44.

(12) Hendel RC, Berman DS, Cullom SJ et al. Multicenter clinical trial to evaluate the efficacy of correction for photon attenuation and scatter in SPECT myocardial perfusion imaging. *Circulation* 1999 June 1;99(21):2742-9.

(13) Links JM, Becker LC, Rigo P et al. Combined corrections for attenuation, depth-dependent blur, and motion in cardiac SPECT: a multicenter trial. *J Nucl Cardiol* 2000 September;7(5):414-25.

(14) Links JM, DePuey EG, Taillefer R, Becker LC. Attenuation correction and gating synergistically improve the diagnostic accuracy of myocardial perfusion SPECT. *J Nucl Cardiol* 2002 March;9(2):183-7.

(15) Shotwell M, Singh BM, Fortman C, Bauman BD, Lukes J, Gerson MC. Improved coronary disease detection with quantitative attenuation-corrected Tl-201 images. *J Nucl Cardiol* 2002 January;9(1):52-62.

(16) Masood Y, Liu YH, Depuey G et al. Clinical validation of SPECT attenuation correction using x-ray computed tomography-derived attenuation maps: multicenter clinical trial with angiographic correlation. *J Nucl Cardiol* 2005 November;12(6):676-86.

(17) Grossman GB, Garcia EV, Bateman TM et al. Quantitative Tc-99m sestamibi attenuation-corrected SPECT: development and multicenter trial validation of myocardial perfusion stress gender-independent normal database in an obese population. *J Nucl Cardiol* 2004 May;11(3):263-72.

(18) Dondi M, Fagioli G, Salgarello M, Zoboli S, Nanni C, Cidda C. Myocardial SPECT: what do we gain from attenuation correction (and when)? *Q J Nucl Med Mol Imaging* 2004 September;48(3):181-7.

(19) Slart RH, Bax JJ, Sluiter WJ, van Veldhuisen DJ, Jager PL. Added value of attenuation-corrected Tc-99m tetrofosmin SPECT for the detection of myocardial viability: comparison with FDG SPECT. *J Nucl Cardiol* 2004 November;11(6):689-96.

(20) Heller GV, Links J, Bateman TM et al. American Society of Nuclear Cardiology and Society of Nuclear Medicine joint position statement: attenuation correction of myocardial perfusion SPECT scintigraphy. *J Nucl Cardiol* 2004 March;11(2):229-30.

(21) Malkerneker D, Brenner R, Martin WH et al. CT-based attenuation correction versus prone imaging to decrease equivocal interpretations of rest/stress Tc-99m tetrofosmin SPECT MPI. *J Nucl Cardiol* 2007 May;14(3):314-23.

(22) Utsunomiya D, Tomiguchi S, Shiraishi S et al. Initial experience with X-ray CT based attenuation correction in myocardial perfusion SPECT imaging using a combined SPECT/CT system. *Ann Nucl Med* 2005 September;19(6):485-9.

(23) Baghdasarian SB, Noble GL, Ahlberg AW, Katten D, Heller GV. Risk stratification with attenuation corrected stress Tc-99m sestamibi SPECT myocardial perfusion imaging in the absence of ECG-gating due to arrhythmias. *J Nucl Cardiol* 2009 July;16(4):533-9.

(24) Slomka PJ, Fish MB, Lorenzo S et al. Simplified normal limits and automated quantitative assessment for attenuation-corrected myocardial perfusion SPECT. *J Nucl Cardiol* 2006 September;13(5):642-51.

(25) Wolak A, Slomka PJ, Fish MB, Lorenzo S, Berman DS, Germano G. Quantitative diagnostic performance of myocardial perfusion SPECT with attenuation correction in women. *J Nucl Med* 2008 June;49(6):915-22.

(26) Vashist A, Collins D, Prasad Y, Blum S, Heller EN. Does cardiac SPECT using attenuation and scatter correction accurately predict coronary artery disease in a minority women population? *Med Sci Monit* 2007 September;13(9):CR386-CR390.

(27) Genovesi D, Giorgetti A, Gimelli A et al. Impact of attenuation correction and gated acquisition in SPECT myocardial perfusion imaging: results of the multicentre SPAG (SPECT Attenuation Correction vs Gated) study. *Eur J Nucl Med Mol Imaging* 2011 October;38(10):1890-8.

(28) Gibson PB, Demus D, Noto R, Hudson W, Johnson LL. Low event rate for stress-only perfusion imaging in patients evaluated for chest pain. *J Am Coll Cardiol* 2002 March 20;39(6):999-1004.

(29) Heller GV, Bateman TM, Johnson LL et al. Clinical value of attenuation correction in stress-only Tc-99m sestamibi SPECT imaging. *J Nucl Cardiol* 2004 May;11(3):273-81.

(30) Bateman TM, Heller GV, McGhie AI et al. Multicenter investigation comparing a highly efficient half-time stress-only attenuation correction approach against standard rest-stress Tc-99m SPECT imaging. *J Nucl Cardiol* 2009 June 23.

(31) Leschka S, Alkadhi H, Plass A et al. Accuracy of MSCT coronary angiography with 64-slice technology: first experience. *Eur Heart J* 2005 August;26(15):1482-7.

(32) Mollet NR, Cademartiri F, van Mieghem CA et al. High-resolution spiral computed tomography coronary angiography in patients referred for diagnostic conventional coronary angiography. *Circulation* 2005 October 11;112(15):2318-23.

(33) Raff GL, Gallagher MJ, O'Neill WW, Goldstein JA. Diagnostic accuracy of noninvasive coronary angiography using 64-slice spiral computed tomography. *J Am Coll Cardiol* 2005 August 2;46(3):552-7.

(34) Miller JM, Rochitte CE, Dewey M et al. Diagnostic performance of coronary angiography by 64-row CT. *N Engl J Med* 2008 November 27;359(22):2324-36.

(35) Meijboom WB, Meijs MF, Schuijf JD et al. Diagnostic accuracy of 64-slice computed tomography coronary angiography: a prospective, multicenter, multivendor study. *J Am Coll Cardiol* 2008 December 16;52(25):2135-44.

(36) Reant P, Brunot S, Lafitte S et al. Predictive value of noninvasive coronary angiography with multidetector computed tomography to detect significant coronary stenosis before valve surgery. *Am J Cardiol* 2006 May 15;97(10):1506-10.

(37) Hamon M, Biondi-Zoccai GG, Malagutti P et al. Diagnostic performance of multislice spiral computed tomography of coronary arteries as compared with conventional invasive coronary angiography: a meta-analysis. *J Am Coll Cardiol* 2006 November 7;48(9):1896-910.

(38) Dewey M, Zimmermann E, Deissenrieder F et al. Noninvasive coronary angiography by 320-row computed tomography with lower radiation exposure and maintained diagnostic accuracy: comparison of results with cardiac catheterization in a head-to-head pilot investigation. *Circulation* 2009 September 8;120(10):867-75.

(39) Lima RS, Watson DD, Goode AR et al. Incremental value of combined perfusion and function over perfusion alone by gated SPECT myocardial perfusion imaging for detection of severe three-vessel coronary artery disease. *J Am Coll Cardiol* 2003 July 2;42(1):64-70.

(40) Schepis T, Gaemperli O, Koepfli P et al. Comparison of 64-slice CT with gated SPECT for evaluation of left ventricular function. *J Nucl Med* 2006 August;47(8):1288-94.

(41) Belge B, Coche E, Pasquet A, Vanoverschelde JL, Gerber BL. Accurate estimation of global and regional cardiac function by retrospectively gated multidetector row computed tomography: comparison with cine magnetic resonance imaging. *Eur Radiol* 2006 July;16(7):1424-33.

(42) Beanlands RS, Ruddy TD, deKemp RA et al. Positron emission tomography and recovery following revascularization (PARR-1): the importance of scar and the development of a prediction rule for the degree of recovery of left ventricular function. *J Am Coll Cardiol* 2002 November 20;40(10):1735-43.

(43) Lee KS, Marwick TH, Cook SA et al. Prognosis of patients with left ventricular dysfunction, with and without viable myocardium after myocardial infarction. Relative efficacy of medical therapy and revascularization. *Circulation* 1994 December;90(6):2687-94.

(44) Yoshida K, Gould KL. Quantitative relation of myocardial infarct size and myocardial viability by positron emission tomography to left ventricular ejection fraction and 3-year mortality with and without revascularization. *J Am Coll Cardiol* 1993 October;22(4):984-97.

(45) Hurrell DG, Milavetz J, Hodge DO, Gibbons RJ. Infarct size determination by technetium 99m sestamibi single-photon emission computed tomography predicts

survival in patients with chronic coronary artery disease. *Am Heart J* 2000 July;140(1):61-6.

(46) Henneman MM, Schuijf JD, Jukema JW et al. Comprehensive cardiac assessment with multislice computed tomography: evaluation of left ventricular function and perfusion in addition to coronary anatomy in patients with previous myocardial infarction. *Heart* 2006 December;92(12):1779-83.

(47) Ko SM, Seo JB, Hong MK et al. Myocardial enhancement pattern in patients with acute myocardial infarction on two-phase contrast-enhanced ECG-gated multidetector-row computed tomography. *Clin Radiol* 2006 May;61(5):417-22.

(48) Lardo AC, Cordeiro MA, Silva C et al. Contrast-enhanced multidetector computed tomography viability imaging after myocardial infarction: characterization of myocyte death, microvascular obstruction, and chronic scar. *Circulation* 2006 January 24;113(3):394-404.

(49) Dawson P. Pharmacokinetics of watersoluble iodinated Xray contrast agents. In: Dawson P, Cosgrove DO, Grainger RG, editors. *Textbook of Contrast Media*. Taylor & Francis Group; 1999. p. 61-74.

(50) van der Laan AM, Piek JJ, van RN. Targeting angiogenesis to restore the microcirculation after reperfused MI. *Nat Rev Cardiol* 2009 August;6(8):515-23.

(51) Lardo AC, Cordeiro MA, Silva C et al. Contrast-enhanced multidetector computed tomography viability imaging after myocardial infarction: characterization of myocyte death, microvascular obstruction, and chronic scar. *Circulation* 2006 January 24;113(3):394-404.

(52) Gerber BL, Belge B, Legros GJ et al. Characterization of acute and chronic myocardial infarcts by multidetector computed tomography: comparison with contrast-enhanced magnetic resonance. *Circulation* 2006 February 14;113(6):823-33.

(53) Brodoefel H, Reimann A, Klumpp B et al. Assessment of myocardial viability in a reperfused porcine model: evaluation of different MSCT contrast protocols in acute and subacute infarct stages in comparison with MRI. *J Comput Assist Tomogr* 2007 March;31(2):290-8.

(54) Kim RJ, Fieno DS, Parrish TB et al. Relationship of MRI delayed contrast enhancement to irreversible injury, infarct age, and contractile function. *Circulation* 1999 November 9;100(19):1992-2002.

(55) Ramani K, Judd RM, Holly TA et al. Contrast magnetic resonance imaging in the assessment of myocardial viability in patients with stable coronary artery disease and left ventricular dysfunction. *Circulation* 1998 December 15;98(24):2687-94.

(56) Ingkanisorn WP, Rhoads KL, Aletras AH, Kellman P, Arai AE. Gadolinium delayed enhancement cardiovascular magnetic resonance correlates with clinical measures of myocardial infarction. *J Am Coll Cardiol* 2004 June 16;43(12):2253-9.

(57) Wu KC, Zerhouni EA, Judd RM et al. Prognostic significance of microvascular obstruction by magnetic resonance imaging in patients with acute myocardial infarction. *Circulation* 1998 March 3;97(8):765-72.

(58) Gerber BL, Rochitte CE, Melin JA et al. Microvascular obstruction and left ventricular remodeling early after acute myocardial infarction. *Circulation* 2000 June 13;101(23):2734-41.

(59) Kim RJ, Wu E, Rafael A et al. The use of contrast-enhanced magnetic resonance imaging to identify reversible myocardial dysfunction. *N Engl J Med* 2000 November 16;343(20):1445-53.

(60) Selvanayagam JB, Kardos A, Francis JM et al. Value of delayed-enhancement cardiovascular magnetic resonance imaging in predicting myocardial viability after surgical revascularization. *Circulation* 2004 September 21;110(12):1535-41.

(61) Leyva F, Foley PW, Chalil S et al. Cardiac resynchronization therapy guided by late gadolinium-enhancement cardiovascular magnetic resonance. *J Cardiovasc Magn Reson* 2011;13:29.

(62) Adelstein EC, Tanaka H, Soman P et al. Impact of scar burden by single-photon emission computed tomography myocardial perfusion imaging on patient outcomes following cardiac resynchronization therapy. *Eur Heart J* 2011 January;32(1):93-103.

(63) Sato A, Hiroe M, Nozato T et al. Early validation study of 64-slice multidetector computed tomography for the assessment of myocardial viability and the prediction of left ventricular remodelling after acute myocardial infarction. *Eur Heart J* 2008 February;29(4):490-8.

(64) Habis M, Capderou A, Ghostine S et al. Acute myocardial infarction early viability assessment by 64-slice computed tomography immediately after coronary angiography: comparison with low-dose dobutamine echocardiography. *J Am Coll Cardiol* 2007 March 20;49(11):1178-85.

(65) Kerl JM, Deseive S, Tandi C et al. Dual energy CT for the assessment of reperfused chronic infarction - a feasibility study in a porcine model. *Acta Radiol* 2011 October 1;52(8):834-9.

(66) Deseive S, Bauer RW, Lehmann R et al. Dual-energy computed tomography for the detection of late enhancement in reperfused chronic infarction: a comparison to magnetic resonance imaging and histopathology in a porcine model. *Invest Radiol* 2011 July;46(7):450-6.

(67) Bauer RW, Kerl JM, Fischer N et al. Dual-energy CT for the assessment of chronic myocardial infarction in patients with chronic coronary artery disease: comparison with 3-T MRI. *AJR Am J Roentgenol* 2010 September;195(3):639-46.

(68) Cerqueira MD, Weissman NJ, Dilsizian V et al. Standardized myocardial segmentation and nomenclature for tomographic imaging of the heart: a statement for healthcare professionals from the Cardiac Imaging Committee of the Council on Clinical Cardiology of the American Heart Association. *Circulation* 2002 January 29;105(4):539-42.

(69) Hesse B, Tagil K, Cuocolo A et al. EANM/ESC procedural guidelines for myocardial perfusion imaging in nuclear cardiology. *Eur J Nucl Med Mol Imaging* 2005 July;32(7):855-97.

(70) Schinkel AF, Poldermans D, Elhendy A, Bax JJ. Assessment of myocardial viability in patients with heart failure. *J Nucl Med* 2007 July;48(7):1135-46.

(71) Moon JC, McKenna WJ, McCrohon JA, Elliott PM, Smith GC, Pennell DJ. Toward clinical risk assessment in hypertrophic cardiomyopathy with gadolinium cardiovascular magnetic resonance. *J Am Coll Cardiol* 2003 May 7;41(9):1561-7.

(72) O'Hanlon R, Grasso A, Roughton M et al. Prognostic significance of myocardial fibrosis in hypertrophic cardiomyopathy. *J Am Coll Cardiol* 2010 September 7;56(11):867-74.

(73) Bland JM, Altman DG. Statistical methods for assessing agreement between two methods of clinical measurement. *Lancet* 1986 February 8;1(8476):307-10.

(74) Bland JM, Altman DG. Comparing methods of measurement: why plotting difference against standard method is misleading. *Lancet* 1995 October 21;346(8982):1085-7.

(75) Cohen J. Weighted kappa: nominal scale agreement with provision for scaled disagreement or partial credit. *Psychol Bull* 1968 October;70(4):213-20.

(76) Swets JA. ROC analysis applied to the evaluation of medical imaging techniques. *Invest Radiol* 1979 March;14(2):109-21.

(77) Altman DG, Bland JM. Diagnostic tests 2: Predictive values. *BMJ* 1994 July 9;309(6947):102.

(78) Altman DG, Bland JM. Diagnostic tests 3: receiver operating characteristic plots. *BMJ* 1994 July 16;309(6948):188.

(79) Xu Y, Fish M, Gerlach J et al. Combined quantitative analysis of attenuation corrected and non-corrected myocardial perfusion SPECT: Method development and clinical validation. *J Nucl Cardiol* 2010 August;17(4):591-9.

(80) Giubbini RM, Gabanelli S, Lucchini S et al. The value of attenuation correction by hybrid SPECT/CT imaging on infarct size quantification in male patients with previous inferior myocardial infarct. *Nucl Med Commun* 2011 November;32(11):1026-32.

(81) Tonge CM, Manoharan M, Lawson RS, Shields RA, Prescott MC. Attenuation correction of myocardial SPECT studies using low resolution computed tomography images. *Nucl Med Commun* 2005 March;26(3):231-7.

(82) Graf S, Khorsand A, Stix G et al. Attenuation correction for myocardial perfusion imaging. A comparison between SPECT and PET imaging by polar map analysis. *Nuklearmedizin* 2006;45(4):171-6.

(83) Tonge CM, Ellul G, Pandit M et al. The value of registration correction in the attenuation correction of myocardial SPECT studies using low resolution computed tomography images. *Nucl Med Commun* 2006 November;27(11):843-52.

(84) Banzo I, Pena FJ, Allende RH, Quirce R, Carril JM. Prospective clinical comparison of non-corrected and attenuation- and scatter-corrected myocardial perfusion SPECT in patients with suspicion of coronary artery disease. *Nucl Med Commun* 2003 September;24(9):995-1002.

(85) Garcia EV. SPECT attenuation correction: an essential tool to realize nuclear cardiology's manifest destiny. *J Nucl Cardiol* 2007 January;14(1):16-24.

(86) Lee DS, So Y, Cheon GJ et al. Limited incremental diagnostic values of attenuation-noncorrected gating and ungated attenuation correction to rest/stress myocardial perfusion SPECT in patients with an intermediate likelihood of coronary artery disease. *J Nucl Med* 2000 May;41(5):852-9.

(87) Taneja S, Mohan HK, Blake GM, Livieratos L, Clarke SE. Synergistic impact of attenuation correction and gating in routine myocardial SPECT reporting: 2 year follow-up study. *Nucl Med Commun* 2008 April;29(4):390-7.

(88) Johansen A, Grupe P, Veje A, Braad PE, Hoilund-Carlsen PF. Scatter and attenuation correction changes interpretation of gated myocardial perfusion imaging. *Eur J Nucl Med Mol Imaging* 2004 August;31(8):1152-9.

(89) Noble GL, Ahlberg AW, Kokkirala AR et al. Validation of attenuation correction using transmission truncation compensation with a small field of view dedicated cardiac SPECT camera system. *J Nucl Cardiol* 2009 March;16(2):222-32.

(90) Flotats A, Knuuti J, Gutberlet M et al. Hybrid cardiac imaging: SPECT/CT and PET/CT. A joint position statement by the European Association of Nuclear Medicine (EANM), the European Society of Cardiac Radiology (ESCR) and the European Council of Nuclear Cardiology (ECNC). *Eur J Nucl Med Mol Imaging* 2011 January;38(1):201-12.

(91) Reyes E, Wiener S, Underwood SR. Myocardial perfusion scintigraphy in Europe 2007: a survey of the European Council of Nuclear Cardiology. *Eur J Nucl Med Mol Imaging* 2012 January;39(1):160-4.

(92) Cerqueira MD, Allman KC, Ficaro EP et al. Recommendations for reducing radiation exposure in myocardial perfusion imaging. *J Nucl Cardiol* 2010 August;17(4):709-18.

(93) Gerber BL, Belge B, Legros GJ et al. Characterization of acute and chronic myocardial infarcts by multidetector computed tomography: comparison with contrast-enhanced magnetic resonance. *Circulation* 2006 February 14;113(6):823-33.

(94) Bondarenko O, Beek AM, Nijveldt R et al. Functional outcome after revascularization in patients with chronic ischemic heart disease: a quantitative late gadolinium enhancement CMR study evaluating transmural scar extent, wall thickness and periprocedural necrosis. *J Cardiovasc Magn Reson* 2007;9(5):815-21.

(95) Krittayaphong R, Saiviroonporn P, Boonyasirinant T, Udompunturak S. Prevalence and prognosis of myocardial scar in patients with known or suspected coronary artery disease and normal wall motion. *J Cardiovasc Magn Reson* 2011;13(1):2.

(96) Sato A, Nozato T, Hikita H et al. Prognostic value of myocardial contrast delayed enhancement with 64-slice multidetector computed tomography after acute myocardial infarction. *J Am Coll Cardiol* 2012 February 21;59(8):730-8.

(97) Kwon DH, Halley CM, Carrigan TP et al. Extent of left ventricular scar predicts outcomes in ischemic cardiomyopathy patients with significantly reduced systolic function: a delayed hyperenhancement cardiac magnetic resonance study. *JACC Cardiovasc Imaging* 2009 January;2(1):34-44.

(98) Klem I, Shah DJ, White RD et al. Prognostic value of routine cardiac magnetic resonance assessment of left ventricular ejection fraction and myocardial damage: an international, multicenter study. *Circ Cardiovasc Imaging* 2011 November;4(6):610-9.

(99) Bello D, Einhorn A, Kaushal R et al. Cardiac magnetic resonance imaging: infarct size is an independent predictor of mortality in patients with coronary artery disease. *Magn Reson Imaging* 2011 January;29(1):50-6.

(100) Scott PA, Morgan JM, Carroll N et al. The extent of left ventricular scar quantified by late gadolinium enhancement MRI is associated with spontaneous ventricular arrhythmias in patients with coronary artery disease and implantable cardioverter-defibrillators. *Circ Arrhythm Electrophysiol* 2011 June;4(3):324-30.

(101) Perrone-Filardi P, Pace L, Dellegrottaglie S et al. Rest-redistribution 201-Thallium single photon emission computed tomography predicts myocardial infarction and cardiac death in patients with ischemic left ventricular dysfunction. *J Cardiovasc Med (Hagerstown)* 2009 February;10(2):122-8.

(102) Hachamovitch R, Rozanski A, Shaw LJ et al. Impact of ischaemia and scar on the therapeutic benefit derived from myocardial revascularization vs. medical therapy among patients undergoing stress-rest myocardial perfusion scintigraphy. *Eur Heart J* 2011 April;32(8):1012-24.

(103) Camici PG, Prasad SK, Rimoldi OE. Stunning, hibernation, and assessment of myocardial viability. *Circulation* 2008 January 1;117(1):103-14.

(104) Kwong RY, Chan AK, Brown KA et al. Impact of unrecognized myocardial scar detected by cardiac magnetic resonance imaging on event-free survival in patients presenting with signs or symptoms of coronary artery disease. *Circulation* 2006 June 13;113(23):2733-43.

(105) Sciagra R, Leoncini M, Marcucci G, Dabizzi RP, Pupi A. Technetium-99m sestamibi imaging to predict left ventricular ejection fraction outcome after revascularisation in patients with chronic coronary artery disease and left ventricular dysfunction: comparison between baseline and nitrate-enhanced imaging. *Eur J Nucl Med* 2001 June;28(6):680-7.

(106) La CG, Alfieri O, Giubbini R, Gargano M, Ferrari R, Visioli O. Echocardiography during infusion of dobutamine for identification of reversibly dysfunction in patients with chronic coronary artery disease. *J Am Coll Cardiol* 1994 March 1;23(3):617-26.

(107) Miller JM, Rochitte CE, Dewey M et al. Diagnostic performance of coronary angiography by 64-row CT. *N Engl J Med* 2008 November 27;359(22):2324-36.

(108) Meijboom WB, Meijs MF, Schuijf JD et al. Diagnostic accuracy of 64-slice computed tomography coronary angiography: a prospective, multicenter, multivendor study. *J Am Coll Cardiol* 2008 December 16;52(25):2135-44.

(109) Skinner JS, Smeeth L, Kendall JM, Adams PC, Timmis A. NICE guidance. Chest pain of recent onset: assessment and diagnosis of recent onset chest pain or discomfort of suspected cardiac origin. *Heart* 2010 June;96(12):974-8.

(110) Kim RJ, Chen EL, Lima JA, Judd RM. Myocardial Gd-DTPA kinetics determine MRI contrast enhancement and reflect the extent and severity of myocardial injury after acute reperfused infarction. *Circulation* 1996 December 15;94(12):3318-26.

(111) Gerber BL, Belge B, Legros GJ et al. Characterization of acute and chronic myocardial infarcts by multidetector computed tomography: comparison with contrast-enhanced magnetic resonance. *Circulation* 2006 February 14;113(6):823-33.

(112) Nicol ED, Stirrup J, Reyes E et al. Comparison of 64-slice cardiac computed tomography with myocardial perfusion scintigraphy for assessment of global and regional myocardial function and infarction in patients with low to intermediate likelihood of coronary artery disease. *J Nucl Cardiol* 2008 July;15(4):497-502.

(113) Lessick J, Dragu R, Mutlak D et al. Is functional improvement after myocardial infarction predicted with myocardial enhancement patterns at multidetector CT? *Radiology* 2007 September;244(3):736-44.

(114) Ko SM, Seo JB, Hong MK et al. Myocardial enhancement pattern in patients with acute myocardial infarction on two-phase contrast-enhanced ECG-gated multidetector-row computed tomography. *Clin Radiol* 2006 May;61(5):417-22.

(115) Ghoshhajra BB, Maurovich-Horvat P, Techasith T et al. Infarct detection with a comprehensive cardiac CT protocol. *J Cardiovasc Comput Tomogr* 2012 January;6(1):14-23.

(116) Goetti R, Feuchtner G, Stolzmann P et al. Delayed enhancement imaging of myocardial viability: low-dose high-pitch CT versus MRI. *Eur Radiol* 2011 October;21(10):2091-9.

(117) Gosling O, Loader R, Venables P, Rowles N, Morgan-Hughes G, Roobottom C. Cardiac CT: are we underestimating the dose? A radiation dose study utilizing the 2007 ICRP tissue weighting factors and a cardiac specific scan volume. *Clin Radiol* 2010 December;65(12):1013-7.

(118) Buderer NM. Statistical methodology: I. Incorporating the prevalence of disease into the sample size calculation for sensitivity and specificity. *Acad Emerg Med* 1996 September;3(9):895-900.

(119) Gosalia A, Haramati LB, Sheth MP, Spindola-Franco H. CT detection of acute myocardial infarction. *AJR Am J Roentgenol* 2004 June;182(6):1563-6.

(120) Paul JF, Wartski M, Caussin C et al. Late defect on delayed contrast-enhanced multi-detector row CT scans in the prediction of SPECT infarct size after reperfused acute myocardial infarction: initial experience. *Radiology* 2005 August;236(2):485-9.

(121) Baks T, Cademartiri F, Moelker AD et al. Multislice computed tomography and magnetic resonance imaging for the assessment of reperfused acute myocardial infarction. *J Am Coll Cardiol* 2006 July 4;48(1):144-52.

(122) Rubinshtein R, Miller TD, Williamson EE et al. Detection of myocardial infarction by dual-source coronary computed tomography angiography using quantitated myocardial scintigraphy as the reference standard. *Heart* 2009 September;95(17):1419-22.

(123) Berman DS, Kang X, Gransar H et al. Quantitative assessment of myocardial perfusion abnormality on SPECT myocardial perfusion imaging is more reproducible than expert visual analysis. *J Nucl Cardiol* 2009 January;16(1):45-53.

(124) Schuster A, Chiribiri A, Ishida M et al. End-systolic versus end-diastolic late gadolinium enhanced imaging for the assessment of scar transmurality. *Int J Cardiovasc Imaging* 2012 April;28(4):773-81.

(125) Matsumoto H, Matsuda T, Miyamoto K et al. Late gadolinium-enhanced cardiovascular MRI at end-systole: feasibility study. *AJR Am J Roentgenol* 2010 November;195(5):1088-94.

(126) Nieman K, Rensing BJ, van Geuns RJ et al. Non-invasive coronary angiography with multislice spiral computed tomography: impact of heart rate. *Heart* 2002 November;88(5):470-4.

(127) Chartrand-Lefebvre C, White CS, Bhalla S et al. Comparison of the effect of low- and iso-osmolar contrast agents on heart rate during chest CT angiography: results of a prospective randomized multicenter study. *Radiology* 2011 March;258(3):930-7.

(128) Cademartiri F, Schuijf JD, Pugliese F et al. Usefulness of 64-slice multislice computed tomography coronary angiography to assess in-stent restenosis. *J Am Coll Cardiol* 2007 June 5;49(22):2204-10.

(129) Pugliese F, Weustink AC, van MC et al. Dual source coronary computed tomography angiography for detecting in-stent restenosis. *Heart* 2008 July;94(7):848-54.

(130) Oncel D, Oncel G, Tastan A, Tamci B. Evaluation of coronary stent patency and in-stent restenosis with dual-source CT coronary angiography without heart rate control. *AJR Am J Roentgenol* 2008 July;191(1):56-63.

(131) Rixe J, Achenbach S, Ropers D et al. Assessment of coronary artery stent restenosis by 64-slice multi-detector computed tomography. *Eur Heart J* 2006 November;27(21):2567-72.

(132) Ehara M, Kawai M, Surmely JF et al. Diagnostic accuracy of coronary in-stent restenosis using 64-slice computed tomography: comparison with invasive coronary angiography. *J Am Coll Cardiol* 2007 March 6;49(9):951-9.

(133) Achenbach S, Boehmer K, Pflederer T et al. Influence of slice thickness and reconstruction kernel on the computed tomographic attenuation of coronary atherosclerotic plaque. *J Cardiovasc Comput Tomogr* 2010 March;4(2):110-5.

(134) Cademartiri F, Runza G, Mollet NR et al. Influence of increasing convolution kernel filtering on plaque imaging with multislice CT using an ex-vivo model of coronary angiography. *Radiol Med* 2005 September;110(3):234-40.

(135) Birnbaum BA, Hindman N, Lee J, Babb JS. Multi-detector row CT attenuation measurements: assessment of intra- and interscanner variability with an anthropomorphic body CT phantom. *Radiology* 2007 January;242(1):109-19.

(136) Komen N, Klitsie P, Hermans JJ et al. Calcium scoring in unenhanced and enhanced CT data of the aorta-iliacal arteries: impact of image acquisition, reconstruction, and analysis parameter settings. *Acta Radiol* 2011 November 1;52(9):943-50.

(137) Dettmer S, Entrup J, Schmidt M, de WC, Wacker F, Shin H. Bronchial wall thickness measurement in computed tomography: Effect of intravenous contrast agent and reconstruction kernel. *Eur J Radiol* 2012 June 4.

(138) Klow NE, Smith HJ, Gullestad L, Seem E, Endresen K. Outcome of bypass surgery in patients with chronic ischemic left ventricular dysfunction. Predictive value of MR imaging. *Acta Radiol* 1997 January;38(1):76-82.

(139) Baer FM, Theissen P, Schneider CA et al. Dobutamine magnetic resonance imaging predicts contractile recovery of chronically dysfunctional myocardium after successful revascularization. *J Am Coll Cardiol* 1998 April;31(5):1040-8.

(140) Schmidt M, Voth E, Schneider CA et al. F-18-FDG uptake is a reliable predictory of functional recovery of akinetic but viable infarct regions as defined by magnetic resonance imaging before and after revascularization. *Magn Reson Imaging* 2004 February;22(2):229-36.

(141) Cwajg JM, Cwajg E, Nagueh SF et al. End-diastolic wall thickness as a predictor of recovery of function in myocardial hibernation: relation to rest-redistribution T1-201 tomography and dobutamine stress echocardiography. *J Am Coll Cardiol* 2000 April;35(5):1152-61.

(142) Schinkel AF, Bax JJ, Elhendy A et al. Assessment of viable tissue in Q-wave regions by metabolic imaging using single-photon emission computed tomography in ischemic cardiomyopathy. *Am J Cardiol* 2002 May 15;89(10):1171-5.

(143) Romero J, Xue X, Gonzalez W, Garcia MJ. CMR Imaging Assessing Viability in Patients With Chronic Ventricular Dysfunction Due to Coronary Artery Disease: A Meta-Analysis of Prospective Trials. *JACC Cardiovasc Imaging* 2012 May;5(5):494-508.

(144) Lawson MA, Johnson LL, Coghlan L et al. Correlation of thallium uptake with left ventricular wall thickness by cine magnetic resonance imaging in patients with acute and healed myocardial infarcts. *Am J Cardiol* 1997 August 15;80(4):434-41.

(145) Meijboom WB, van Mieghem CA, Mollet NR et al. 64-slice computed tomography coronary angiography in patients with high, intermediate, or low pretest probability of significant coronary artery disease. *J Am Coll Cardiol* 2007 October 9;50(15):1469-75.

(146) Meijboom WB, Weustink AC, Pugliese F et al. Comparison of diagnostic accuracy of 64-slice computed tomography coronary angiography in women versus men with angina pectoris. *Am J Cardiol* 2007 November 15;100(10):1532-7.

(147) Husmann L, Leschka S, Desbiolles L et al. Thick maximum intensity projections for the assessment of left ventricular function with 64-slice computed tomography. *Invest Radiol* 2006 October;41(10):746-52.

(148) Schepis T, Gaemperli O, Koepfli P et al. Comparison of 64-slice CT with gated SPECT for evaluation of left ventricular function. *J Nucl Med* 2006 August;47(8):1288-94.

(149) Greupner J, Zimmermann E, Grohmann A et al. Head-to-Head Comparison of Left Ventricular Function Assessment with 64-Row Computed Tomography, Biplane Left Cineventriculography, and Both 2- and 3-Dimensional Transthoracic Echocardiography: Comparison With Magnetic Resonance Imaging as the Reference Standard. *J Am Coll Cardiol* 2012 May 22;59(21):1897-907.

(150) Puesken M, Fischbach R, Wenker M et al. Global left-ventricular function assessment using dual-source multidetector CT: effect of improved temporal resolution on ventricular volume measurement. *Eur Radiol* 2008 October;18(10):2087-94.

(151) Bak SH, Ko SM, Jeon HJ, Yang HS, Hwang HK, Song MG. Assessment of global left ventricular function with dual-source computed tomography in patients with valvular heart disease. *Acta Radiol* 2012 April 1;53(3):270-7.

(152) Takx RA, Moscariello A, Schoepf UJ et al. Quantification of left and right ventricular function and myocardial mass: comparison of low-radiation dose 2nd generation dual-source CT and cardiac MRI. *Eur J Radiol* 2012 April;81(4):e598-e604.

(153) Nasis A, Moir S, Seneviratne SK, Cameron JD, Mottram PM. Assessment of left ventricular volumes, ejection fraction and regional wall motion with retrospective electrocardiogram triggered 320-detector computed tomography: a comparison with 2D-echocardiography. *Int J Cardiovasc Imaging* 2012 April;28(4):955-63.

(154) Sarwar A, Shapiro MD, Nasir K et al. Evaluating global and regional left ventricular function in patients with reperfused acute myocardial infarction by 64-slice multidetector CT: a comparison to magnetic resonance imaging. *J Cardiovasc Comput Tomogr* 2009 May;3(3):170-7.

(155) Nicol ED, Kafka H, Stirrup J et al. A single, comprehensive non-invasive cardiovascular assessment in pulmonary arterial hypertension: combined computed tomography pulmonary and coronary angiography. *Int J Cardiol* 2009 August 21;136(3):278-88.

(156) Lardo AC, Cordeiro MA, Silva C et al. Contrast-enhanced multidetector computed tomography viability imaging after myocardial infarction: characterization of myocyte death, microvascular obstruction, and chronic scar. *Circulation* 2006 January 24;113(3):394-404.

(157) Schepis T, Gaemperli O, Koepfli P et al. Comparison of 64-slice CT with gated SPECT for evaluation of left ventricular function. *J Nucl Med* 2006 August;47(8):1288-94.

(158) Mehta A, Travin MI, Levsky JM, Jain VR, Burton WB, Haramati LB. Ejection fractions determined by cardiac computed tomographic angiography and single photon emission computed tomographic myocardial perfusion imaging are not

interchangeable: evidence of significant and sex-associated disparities. *J Comput Assist Tomogr* 2009 July;33(4):489-97.

(159) Fischbach R, Juergens KU, Ozgun M et al. Assessment of regional left ventricular function with multidetector-row computed tomography versus magnetic resonance imaging. *Eur Radiol* 2007 April;17(4):1009-17.

(160) Cury RC, Nieman K, Shapiro MD et al. Comprehensive assessment of myocardial perfusion defects, regional wall motion, and left ventricular function by using 64-section multidetector CT. *Radiology* 2008 August;248(2):466-75.

(161) van der Vleuten PA, de Jonge GJ, Lubbers DD et al. Evaluation of global left ventricular function assessment by dual-source computed tomography compared with MRI. *Eur Radiol* 2009 February;19(2):271-7.

(162) Pflederer T, Ho KT, Anger T et al. Assessment of regional left ventricular function by dual source computed tomography: interobserver variability and validation to laevocardiography. *Eur J Radiol* 2009 October;72(1):85-91.

(163) Uthamalingam S, Gurm GS, Sidhu MS et al. Comparison of dual-source 64-slice adenosine stress CT perfusion with stress-gated SPECT-MPI for evaluation of left ventricular function and volumes. *J Cardiovasc Comput Tomogr* 2012 January;6(1):24-30.

(164) de Graaf FR, Schuijf JD, van Velzen JE et al. Assessment of global left ventricular function and volumes with 320-row multidetector computed tomography: A comparison with 2D-echocardiography. *J Nucl Cardiol* 2010 April;17(2):225-31.

(165) Busch S, Johnson TR, Wintersperger BJ et al. Quantitative assessment of left ventricular function with dual-source CT in comparison to cardiac magnetic resonance imaging: initial findings. *Eur Radiol* 2008 March;18(3):570-5.

(166) Schuster A, Morton G, Chiribiri A, Perera D, Vanoverschelde JL, Nagel E. Imaging in the management of ischemic cardiomyopathy: special focus on magnetic resonance. *J Am Coll Cardiol* 2012 January 24;59(4):359-70.

(167) Arnoldi E, Lee YS, Ruzsics B et al. CT detection of myocardial blood volume deficits: dual-energy CT compared with single-energy CT spectra. *J Cardiovasc Comput Tomogr* 2011 November;5(6):421-9.

(168) Hundley WG, Bluemke D, Bogaert JG et al. Society for Cardiovascular Magnetic Resonance guidelines for reporting cardiovascular magnetic resonance examinations. *J Cardiovasc Magn Reson* 2009;11:5.

(169) Wu YW, Tadamura E, Yamamuro M et al. Estimation of global and regional cardiac function using 64-slice computed tomography: a comparison study with echocardiography, gated-SPECT and cardiovascular magnetic resonance. *Int J Cardiol* 2008 August 1;128(1):69-76.

(170) Lim SJ, Choo KS, Park YH et al. Assessment of left ventricular function and volume in patients undergoing 128-slice coronary CT angiography with ECG-based maximum tube current modulation: a comparison with echocardiography. *Korean J Radiol* 2011 March;12(2):156-62.

(171) Butler J, Shapiro MD, Jassal DS et al. Comparison of multidetector computed tomography and two-dimensional transthoracic echocardiography for left ventricular assessment in patients with heart failure. *Am J Cardiol* 2007 January 15;99(2):247-9.

(172) Guo YK, Yang ZG, Ning G et al. Sixty-four-slice multidetector computed tomography for preoperative evaluation of left ventricular function and mass in patients with mitral regurgitation: comparison with magnetic resonance imaging and echocardiography. *Eur Radiol* 2009 September;19(9):2107-16.

(173) Mahnken AH, Bruners P, Bornikoel CM et al. Dual-source CT assessment of ventricular function in healthy and infarcted myocardium: an animal study. *Eur J Radiol* 2011 March;77(3):443-9.

(174) Stolzmann P, Scheffel H, Trindade PT et al. Left ventricular and left atrial dimensions and volumes: comparison between dual-source CT and echocardiography. *Invest Radiol* 2008 May;43(5):284-9.

(175) Drosch T, Tsiflikas I, Brodoefel H et al. Semi-automatic assessment of global left ventricular function and left ventricular parameters with dual-source computed tomography: comparison with invasive angiography. *Heart Vessels* 2010 January;25(1):57-62.

(176) Grothues F, Smith GC, Moon JC et al. Comparison of interstudy reproducibility of cardiovascular magnetic resonance with two-dimensional echocardiography in normal subjects and in patients with heart failure or left ventricular hypertrophy. *Am J Cardiol* 2002 July 1;90(1):29-34.

(177) Nicol ED, Stirrup J, Roughton M, Padley SP, Rubens MB. 64-Channel cardiac computed tomography: intraobserver and interobserver variability, part 2: global and regional ventricular function, mass, and first pass perfusion. *J Comput Assist Tomogr* 2009 March;33(2):169-74.

(178) Hedeer F, Palmer J, Arheden H, Ugander M. Gated myocardial perfusion SPECT underestimates left ventricular volumes and shows high variability compared to cardiac magnetic resonance imaging -- a comparison of four different commercial automated software packages. *BMC Med Imaging* 2010;10:10.

(179) Hoffmann R, von BS, Kasprzak JD et al. Analysis of regional left ventricular function by cineventriculography, cardiac magnetic resonance imaging, and unenhanced and contrast-enhanced echocardiography: a multicenter comparison of methods. *J Am Coll Cardiol* 2006 January 3;47(1):121-8.

(180) Yim NY, Kim YH, Choi S et al. Multidetector-row computed tomographic evaluation of myocardial perfusion in reperfused chronic myocardial infarction: value of color-coded perfusion map in a porcine model. *Int J Cardiovasc Imaging* 2009 April;25 Suppl 1:65-74.

(181) Pourmorteza A, Schuleri KH, Herzka DA, Lardo AC, McVeigh ER. A new method for cardiac computed tomography regional function assessment: stretch quantifier for endocardial engraved zones (SQUEEZ). *Circ Cardiovasc Imaging* 2012 March;5(2):243-50.

APPENDIX 1 PUBLICATIONS

PUBLICATIONS ARISING DURING THE COURSE OF THIS THESIS

1. Jabbour A, Boshell D, Sesel K, Silverstone E, Muller D, **Stirrup J**, Rubens M, Hayward CS, Wright SP. Inducible myocardial ischaemia diagnosed using computed tomography dipyridamole stress myocardial perfusion technique. *Journal of Medical Imaging and Radiation Oncology* 2012 doi: 10.1111/j.1754-9485.2012.02363.x
2. **Stirrup J**. What would the number needed to examine be? BMJ 2011 Jun 28;342:d3992.
3. Sá MI, Nicol ED, **Stirrup J**, Crean A, Roughton M, Padley SP, Rubens MB. Implications for Single Phase Prospective CT Coronary Angiography for the Diagnosis of Significant Coronary Stenoses in Clinical Practice. *Int J Cardiol* 2011 Mar 17;147(3):393-7.
4. Nicol ED, **Stirrup J**, Leatham E, Roughton M, Underwood SR, Padley SPG, Rubens MB. Clinical Management and Short-term Cost - 64-slice MDCT vs. Myocardial Perfusion Scintigraphy. *Int J Cardiol* 2010 144(2):248-50.
5. Nicol E, Schultz C, **Stirrup J**, Roughton M, Padley SP, Rubens MB, Davies SW, di Mario C. Defining the appropriate CTA stenosis threshold for gatekeeping to invasive angiography: 50% or 70%? *Int J Cardiol* 2010 144(2):297-8.
6. Reyes E, **Stirrup J**, Roughton M, D'Souza S, Davies SW, Underwood SR, Anagnostopoulos C. Reduction of Adenosine-Induced Myocardial Perfusion Heterogeneity by Atenolol and other Commonly Prescribed Beta1-Selective Adrenoceptor Blockers. *Journal of Nuclear Medicine* 2010; 51(7):1036-43.
7. **Stirrup J**, Maenhout A, Wechalekar K, Anagnostopoulos C. Radionuclide imaging in ischaemic heart failure. *British Medical Bulletin* 2009; 92:43-59.

8. Nicol ED, Kafka H, **Stirrup J**, Padley SP, Rubens MB, Kilner PJ, Gatzoulis MA. A single, comprehensive non-invasive cardiovascular assessment in pulmonary arterial hypertension: Combined computed tomography pulmonary and coronary angiography. *Int J Cardiol*. 2009 Aug 21;136(3):278-88.
9. Nicol ED, **Stirrup J**, Padley SP, Rubens MB. Diagnostic Accuracy of 64-Slice Computed Tomography Coronary Angiography – A flawed comparison. *JACC* 2009 May 12;53(19):1824-5.
10. Nicol E, **Stirrup J**, Roughton M, Padley SPG, Rubens MB. 64-Channel Cardiac Computed Tomography: Intraobserver and Interobserver Variability (Part 1): Coronary Angiography. *Journal of Computer Assisted Tomography* 2009 33(2); 161-168.
11. Nicol E, **Stirrup J**, Roughton M, Padley SPG, Rubens MB. 64-Channel Cardiac Computed Tomography: Intraobserver and Interobserver Variability (Part 2): Global and Regional Ventricular Function, Mass and First Pass Perfusion. *Journal of Computer Assisted Tomography* 2009 33(2); 169-174.
12. Nicol ED, **Stirrup J**, Lyne JC. Multimodality imaging of myocardial infarction. *Br J Cardiol* 2009 16:43.
13. **Stirrup J**, Wechalekar K, Maenhout A, Anagnostopoulos C. Cardiac Radionuclide Imaging in Stable Coronary Artery Disease and Acute Coronary Syndromes. *British Medical Bulletin* 2009; 89: 63-78.
14. **Stirrup J**, Nicol E, Underwood SR. Defining myocardial infarction by cardiac computed tomography. *Int J Cardiovasc Imaging* 2008 24(8):891-3.
15. Nicol E, **Stirrup J**, Underwood SR. CT coronary angiography: the continuing challenges of validating and optimizing a new and rapidly developing technique. *Int J Cardiovasc Imaging* 2008 24(8):905-6

16. Nicol E, **Stirrup J**. Severe interscapular pain: Limitations of multidetector computed tomography (MDCT). *BMJ* 2008 Aug 27;337:a1402.
17. Nicol E, **Stirrup J**, Reyes E, Roughton M, Padley SP, Rubens MB, Underwood SR. Comparison of 64-slice Cardiac Computed Tomography with Myocardial Perfusion Scintigraphy for Assessment of Global and Regional Myocardial Function and Infarction in Patients with Low to Intermediate Likelihood of Coronary Artery Disease. *J Nucl Cardiol* 2008 15(4):497-502.
18. Nicol E, **Stirrup J**, Reyes E, Roughton M, Padley SP, Rubens MB, Underwood SR. 64-slice Computed Tomography Coronary Angiography Compared with Myocardial Perfusion Scintigraphy for Diagnosis of Functionally Significant Coronary Stenoses in Patients with Low to Intermediate Likelihood of Coronary Artery Disease. *J Nuc Cardiol* 2008 15(3):311-8.

INVITED PUBLICATIONS ARISING DURING THE COURSE OF THIS THESIS

1. Nicol ED, **Stirrup J**, Padley SP, Kelion A (editors). *Cardiovascular Computed Tomography: Oxford Specialist Handbooks in Cardiology*. Oxford University Press, Oxford, August 2011.
2. **Stirrup J**, Nicol E, Rubens M. Cardiac computed tomography in adult congenital heart disease. In *Diagnosis and Management of Adult Congenital Heart Disease* 2nd edition; Gatzoulis MA, Webb GD, Daubeney PEF, Eds.; Churchill Livingstone, 2010; pp59-67.
3. **Stirrup J**, Anagnostopoulos C. Cardiac radionuclide imaging in the assessment of patients with heart failure. In *Heart Failure in Clinical Practice* Henein M, Ed.; Springer-Verlag: London, 2010; pp231-240.

4. **Stirrup J**, Underwood SR. Nuclear cardiology and detection of coronary artery disease. In *European Society of Cardiology Textbook of Cardiovascular Imaging* Zamarano J-L, Bax J, Rademakers F, Knuuti J, Eds.; Springer-Verlag: London, 2010; pp249-266.
5. Nicol E, **Stirrup J**, Rubens M. Cardiac evaluation of the patient with advanced heart failure – computed tomography. In *International Society of Heart and Lung Transplantation Monograph Series Volume 2: Advanced Heart Failure* Banner N, Jessup M, Eds.; Elsevier: Philapdelphia, 2009; Vol 3.1, pp141-161.
6. **Stirrup J**, Underwood SR. Non-invasive imaging of coronary artery disease. *Br J Hosp Med* 2008 69(3):152-7.
7. Nicol E, **Stirrup J**. Functional cardiac assessment with MDCT. *MIMS Cardiovascular* 2007 2(3):44-45.

ABSTRACTS

1. **Stirrup J**, Nicol E, Reyes E, Castellano I, Rubens R, Padley S, Underwood SR. Early and delayed-pass 64-slice cardiac computed tomography in patients with chronic myocardial infarction: comparison of visual and quantitative segmental myocardial enhancement patterns with SPECT myocardial perfusion scintigraphy. *Oral Abstract Session 1, Society of Cardiovascular Computed Tomography 8th Annual Meeting 2013.*
2. **Stirrup J**, Nicol E, Reyes E, Castellano I, Rubens R, Padley S, Underwood SR. Segmental myocardial thickness on cardiac computed tomography as a predictor of myocardial infarction on SPECT myocardial perfusion scintigraphy. *Poster, Society of Cardiovascular Computed Tomography 8th Annual Meeting 2013:226 .*
3. **Stirrup J**, Nicol E, Reyes E, Castellano I, Rubens R, Padley S, Underwood SR. Qualitative and quantitative assessment of global and regional left ventricular function by 64-slice

cardiac CT in patients with previous myocardial infarction: comparison with SPECT myocardial perfusion scintigraphy. *Poster, Society of Cardiovascular Computed Tomography 8th Annual Meeting 2013:227.*

4. **Stirrup J**, Nicol E, Reyes E, Castellano I, Rubens R, Padley S, Underwood SR. Assessment of myocardial scarring by delayed pass 64 slice cardiac computed tomography: effect of reconstruction kernel on agreement with SPECT myocardial perfusion scintigraphy. *Poster, European Society of Cardiac Radiology Annual Meeting 2013:52.*
5. **Stirrup J**, Nicol E, Reyes E, Castellano I, Rubens R, Padley S, Underwood SR. Effects of cardiac phase and heart rate on accuracy of delayed cardiac computed tomography for detection of myocardial scarring on SPECT myocardial perfusion scintigraphy. *Poster, Radiological Society of North America 99th Scientific Assembly and Annual Meeting 2013*.
6. Price J, **Stirrup J**, Bailey J, Underwood SR, Wechalekar K. Planar versus tomographic radionuclide ventriculography: ready for primetime? *British Nuclear Cardiology Society Annual General Meeting* Dec 2010:3 and *British Nuclear Medicine Society Spring Meeting* May 2011:14.
7. **Stirrup J**, Reyes E, Roughton M, Bailey J, Benson K, Gregg S, Underwood SR. Attenuation correction of myocardial perfusion scintigraphy has no clear benefits on report, reporter confidence or interobserver agreement when clinical information is known. *British Nuclear Cardiology Society Annual General Meeting* Dec 2009:2 and *UK Radiological Congress* Jun 2010:p1603.
8. Chandrasekaran B, Sharma R, Donovan J, **Stirrup J**, Wechalekar K, Hooper J, Underwood SR, Cowie MR, McDonagh, T. The Effect of Cardiac Resynchronisation therapy on Plasma Apelin. *ESC Congress 2009:*831.

9. Nicol ED, **Stirrup J**, Underwood SR, Padley SPG, Rubens MB. Cost and clinical management of patients with low to intermediate likelihood of coronary artery disease using 64-MDCT vs MPS. *9th International Conference of Non-Invasive Cardiovascular Imaging* May 2009:395
10. Wechalekar K, Chandrasekaran B, **Stirrup J**, Benson K, Bailey J, Duncan A, Mohiaddin R, Sharma R, McDonagh T, Underwood R. SPECT Radionuclide Ventriculography in the Assessment of Advanced Heart Failure Patients: A Comparison of Planar Radionuclide Ventriculography, Transthoracic Echocardiography and Cardiac Magnetic Resonance Imaging. *EANM Annual Congress* 2008:300.
11. Nicol E, **Stirrup J**, Reyes E, Roughton M, Padley SP, Rubens MB, Underwood SR. 64-slice Computed Tomography Coronary Angiography Compared with Myocardial Perfusion Scintigraphy for Diagnosis of Functionally Significant Coronary Stenoses in Patients with Low to Intermediate Likelihood of Coronary Artery Disease. *BCS Scientific Conference* 2008:151
12. Chandrasekaran B, Sharma R, **Stirrup J**, Dar O, Wechalekar K, Clague J, Underwood SR, Cowie MR, McDonagh, T. Left ventricular remodelling following cardiac resynchronisation therapy in a contemporary heart failure population. *BCS Scientific Conference* 2008:196
13. Nicol E, **Stirrup J**, Padley S, Rubens M. Functional Cardiac Analysis by 64-MDCT: Beyond the Coronary Arteries. *UK Radiological Congress* 2007:47